WESTERN SYDNEY
UNIVERSITY

Hawkesbury Institute
for the Environment

CARBON ISOTOPE DISCRIMINATION AND STOMATAL FUNCTION IN C_4 GRASSES

WALTER KRYSTLER DELA CRUZ ISRAEL

BSc. Biology

MSc. Molecular Biology and Biotechnology

A thesis submitted in fulfilment of the requirements for the degree of

Doctor of Philosophy

Hawkesbury Institute for the Environment

Western Sydney University

Australia

November 2019

Through hardships to the stars, this thesis is dedicated to my earthly and heavenly families.

Per aspera ad astra, opus hoc dedicatur familae meae in terra et in caelo.
(Latin)

Mula sa pakikibaka patungo sa tagumpay, inaalay ko ang akdang pang-agham na ito para sa aking makalupa at makalangit na pamilya
(Filipino)

ACKNOWLEDGEMENTS

Firstly, I would like to acknowledge and pay respect to the Aboriginal people of the Dharug nation, past and present, as traditional owners of the land to which this research was conducted and where the Western Sydney University was built upon.

Secondly, I wish to acknowledge the following people who were instrumental to the completion of the longest academic examination I have ever had. My deepest gratitude goes primarily to my principal supervisor, **A/Prof Oula Ghannoum,** for the opportunity to work on this exciting project and for her unfathomable support throughout my candidature. Completion of this thesis would be impossible without her valuable insights and constant optimism. I owe the success of this research for her unwavering generosity and encouraging supervision.

I likewise thank my associate supervisor, **Prof Zhong-Hua Chen** and the whole Chen laboratory of the School of Sciences and Health-WSU for the immense support, especially on teaching me valuable techniques on stomatal assays and electrophysiology. More than this, I acknowledge the great friendships from **Celymar Angela Solis, Dr Chenchen Zhao, Dr Shenguan Cai, Dr Michelle Mak, David Randall,** and **Miing Yong**.

I am also incredibly grateful to my associate supervisor, **Dr Hilary Stuart-Williams** and the whole Farquhar laboratory for the mentorship and guidance on stable isotope analyses and HPLC assays. I also could not remise the kindness and immense help of **Haydon Siiteri** during EA-IRMS assay and to **Dr Ross Deans** for his helpful insights on stomatal kinetics. I also acknowledge the support, expertise, and the valuable pieces of advice from **Dr Charles Hocart, Dr Guillaume Tcherkez, Prof Susanne von Caemmerer,** and **Prof Robert Furbank**. I am thankful to the von Caemmerer laboratory, especially to **Soumi Bala** and **Dr Florence Danila** for the assistance during my experiments at ANU.

I am immensely grateful to the vibrant and incredibly supportive research environment at the Hawkesbury Institute for the Environment and the ARC Centre of Excellence for Translational Photosynthesis especially to **Prof Ian Anderson, Dr David Harland, Patricia Hellier, Lisa Davison, Jenny Harvey, Gavin McKenzie**, and **David Thompson**. A heartfelt thanks to my research group, **Fiona Koller, Urs Benning, Yazen Al-Salman,**

Yogesh Chaudari, Dr Julius Sagun, Dr Sachin Chavan, Dr Bala Sonawane, Dr Clémence Henry, Dr Alex Watson-Lazowski, Dr Christie Foster, and **Dr Javier Cano Martin** for the great friendship.

Most importantly, I also could not help but mention the unwavering love, support, and motivation of my family **(Papa, Mama, Korryne, Don, Darell, Macky and Quine), Tito Tony and Tita Grace Esquillon, Abigail Tuddao, Vegielene Lazo, Mark Christophere Tarculas, Bro. Francis Xavier Ma. Esquillon, Laurice Aiko Guillermo, Lhia Amor Roma,** and **The UPLB Lisieux Music Ministry**. A big chunk of this PhD candidature was because of your fervent love and prayers.

Finally, to the Almighty, who had blessed me with all the necessary virtues, graces, and blessings to complete a degree which has thought me so much about humility (ταπεινότητα), sacrifice (θυσία), and love (αγάπη). I give this back to You. In Christo per Mariam, Consummatus est, Deo omnis gloria!

STATEMENT OF AUTHENTICATION

The work presented in this thesis is, to the best of my knowledge and belief, original except as acknowledged in the text. I hereby declare that I have not submitted this material, either in full or in part, for a degree at this or any other institution.

Author's Signature

TABLE OF CONTENTS

LIST OF FIGURES

LIST OF TABLES

LIST OF SUPPLEMENTARY FIGURES

LIST OF APPENDICES

ABBREVIATIONS

$\Delta^{13}C$	-	Carbon isotope discrimination (‰)
$\delta^{13}C$	-	Carbon isotope signature/composition (‰)
ΔC	-	Forgone photosynthesis (mmol m^{-2})
ΔW	-	Excess transpiration (mol m^{-2})
ϕ	-	Leakiness
a	-	Kinetic fractionation of stomata (4.4 ‰)
A^-	-	Anion
ABA	-	Abscisic acid
a_{max}	-	Maximum stomatal aperture (μm^2)
A_{net}	-	net CO_2 assimilation rate (µmol CO_2 m^{-2} s^{-1})
A_{sat}	-	saturated CO_2 assimilation rate (µmol CO_2 m^{-2} s^{-1})
AL	-	Aperture length (µm)
AlaAT	-	Alanine aminotransferase
Asp	-	Aspartate
AspAT	-	Aspartate aminotransferase
ANOVA	-	Analysis of variance
ANU	-	The Australian National University
ATP	-	Adenosine triphosphate
AW	-	Aperture width (µm)
b	-	Fractionation of Rubisco (29 ‰)
b_4	-	Net fractionation of PEPC
BSC	-	Bundle-sheath cell
C_3	-	C_3 photosynthetic pathway
C_4	-	C_4 photosynthetic pathway
CA	-	Carbonic anhydrase
$[Ca^{2+}]_{cyt}$	-	cytoplasmic $[Ca^{2+}]$
$CaCl_2$	-	Calcium chloride
C_a	-	Atmospheric CO_2
CelSyn	-	Cellulose synthase
Chl	-	chloroplast
C_i	-	Intercellular CO_2

C_i/ C_a	-	Ratio of intercellular CO_2 to atmospheric CO_2
CCM	-	Carbon concentrating mechanism
CSIA	-	Compound-specific isotope analysis
d	-	Diffusivity of water vapour at 25°C (0.0000249 m^{-2} s^{-1})
DC	-	Decarboxylating enzyme
df	-	Degrees of freedom
E	-	Transpiration rate
EA	-	Elemental analyser
[eCO_2]	-	Elevated [CO_2]
E_m	-	Membrane potential
G-1-P	-	Glucose-1-phosphate
GC	-	Gas chromatography
GCL	-	Guard cell length (μm)
GCW	-	Guard cell width (μm)
[gCO_2]	-	Glacial [CO_2]
g_s	-	Stomatal conductance (mol H_2O m^{-2} s^{-1})
g_{s_amax}	-	Maximum theoretical conductance (mol H_2O m^{-2} s^{-1})
H_2SO_4	-	Sulfuric acid
Hex-P	-	Hexose phosphate
HK	-	Hexokinase
HL	-	High light
HPLC	-	High performance liquid chromatography
IAEA	-	International atomic energy agency
INV	-	Invertase
IRMS	-	Isotope ratio mass spectrometry
iWUE		Intrinsic water-use efficiency (A_{net}/g_s; μmol [CO_2] (mol H_2O)$^{-1}$)
k	-	Time constant
K^+_{in}	-	Inward rectifying K^+ channels
KCl	-	Potassium chloride
l	-	Stomatal pore depth (μm)
LL	-	Low light
lm	-	Linear models
LSD	-	Least significant difference

MAL	-	Malate
MDH	-	Malate dehydrogenase
MIFE	-	Microelectrode ion flux estimation
MM	-	*Megathyrsus maximus*
NAD-ME	-	Nicotinamide adenine dinucleotide malic enzyme
NADP-ME	-	Nicotinamide adenine dinucleotide phosphate malic enzyme
NO	-	Nitrous oxide
OAA	-	Oxaloacetic acid
OST1	-	Open stomata 1
PA	-	*Panicum antidotale*
PAR	-	Photosynthetically active radiation
PB	-	*Panicum bisulcatum*
PCK	-	Phosphoenolpyruvate carboxykinase
PCR	-	Photosynthetic carbon reduction
PEPC	-	Phosphoenolpyruvate carboxylase
pH_{cyt}	-	Cytoplasmic pH
phot	-	phototropins
PGA	-	Phosphoglyceraldehyde
PGI	-	Phosphoglucoisomerase
PGM	-	Phosphoglucomutase
PM	-	*Panicum miliaceum*
PPDK	-	Pyruvate phosphate dikinase
ppm	-	Parts per million
PWUE	-	Photosynthetic water-use efficiency (A_{sat}/g_s)
PYR	-	Pyruvate
RH	-	Relative humidity (%)
RID	-	Refractive index detector
R_{sample}	-	$^{13}C/^{12}C$ isotope ratio of the sample
R_{std}	-	$^{13}C/^{12}C$ isotope ratio of the standard
Rubisco	-	Ribulose-1, 5-bisphosphate carboxylase/ oxygenase
RuBP	-	Ribulose-1, 5-bisphosphate
s	-	Fractionation due to CO_2 leakage out of the BSC
SA	-	Stomatal aperture (μm^2)

SC	-	Subsidiary cells
SCW	-	Subsidiary cell width (μm)
SD	-	Stomatal density (mm^{-2})
SE	-	Standard error
SI	-	Stomatal index (%)
SLAC1	-	Slow anion channel 1
SPP	-	Sucrose phosphate phosphatase
SPS	-	Sucrose phosphate synthase
SS	-	Stomatal size (μm^2)
OD	-	Density of open stomata (mm^{-2})
$\mathbf{t_{1/2}}$	-	Half-time response
TAG	-	triacylglycerol
TDL	-	Tuneable diode laser
TE	-	Transpiration efficiency
TP	-	Triosphosphate
$\boldsymbol{v}$	-	molar volume of air (0.0224 m^3 mol^{-1})
UV	-	Ultraviolet spectrum
VPD	-	Vapour pressure deficit
VPDB	-	Vienna Pee-Dee Belemnite
WCO	-	Wet chemical oxidation
WUE	-	Water-use efficiency
$\mathbf{WUE_i}$	-	Instantaneous water-use efficiency (A_{net}/E; μmol [CO_2] mol H_2O^{-1})
$\mathbf{WUE_{plant}}$	-	Plant water-use efficiency

GENERAL ABSTRACT

Water scarcity is projected to intensify over the next fifty years due to the increasing population and changing climate. Hence, efforts are channelled towards breeding crops with improved water-use efficiency (WUE) to mitigate the negative impact of the future insecurity of food, feed, and biofuel. Leaf-level crop improvement is one key target, but to reach maximal improvements, we will need to exploit the physiological, anatomical, and biochemical diversity of grasses, the family which includes the all-important cereal crops. The success of grass productivity can be partly attributed to a finely-regulated balance between CO_2 assimilation (A_{net}) and transpiration through highly responsive stomata, as well as the evolution of a CO_2 concentrating mechanism (CCM) - the C_4 cycle. The CCM of C_4 photosynthesis endows C_4 grasses with higher leaf-level instantaneous (WUE_i) and intrinsic water use efficiency (iWUE) than C_3 counterparts. In C_3 plants, iWUE is directly correlated with the carbon isotope composition ($\delta^{13}C$) of the leaf dry matter through their separate relationships with a common parameter, the ratio of intercellular to ambient CO_2 (C_i/C_a). However, leaf $\delta^{13}C$ and iWUE in C_4 plants are not consistently correlated because of the CCM and factors including post-photosynthetic carbon isotope fractionation.

The two main objectives of this thesis were to (1) investigate how stomatal responses regulate leaf iWUE by exploring the physiological mechanisms underpinning the highly responsive C_4 grass stomata, and (2) elucidate the impact of post-photosynthetic fractionation, particularly carbohydrate metabolism, on leaf $\delta^{13}C$. The two objectives serve the overall goal of better understanding the physiological factors that control leaf $\delta^{13}C$, iWUE and their relationship in C_4 plants. I utilised C_3 and C_4 grasses with different photosynthetic types and C_4 biochemical subtypes (NADP-ME, NAD-ME, PCK) grown under different environmental conditions. The outcomes from this study will provide fundamental knowledge and understanding of stomatal and photosynthetic regulation of iWUE in C_4 grasses, allowing for the development of screening tools for breeding crops with improved iWUE.

In the first growth chamber experiment (Chapter 2), two C_3 and six C_4 (two of each subtype) grasses were grown at ambient or glacial [CO_2] ([aCO_2] = 400 µl l^{-1}, [gCO_2] = 180 µl l^{-1}) and high or low light (HL = 1000 µmol m^{-2} s^{-1}, LL = 200 µmol m^{-2} s^{-1}). Leaf gas

exchange at growth conditions and saturating conditions and stomatal morphology were measured in four growth chambers (HL+[aCO_2], [control]; HL+[gCO_2]; LL+[aCO_2]; and LL+[gCO_2]). Glacial [CO_2] increased stomatal conductance (g_s), and stomatal aperture (SA) and reduced stomatal size (SS) and iWUE of C_3 more than C_4 grasses. LL reduced g_s of C_4 more than C_3 grasses, iWUE of C_3 grasses, and stomatal aperture and density of all species. Overall, g_s and iWUE strongly correlated with SA but not with measures of stomatal frequency (stomatal density and stomatal index). On the other hand, the response of stomatal conductance under [CO_2]-limited and light-saturated conditions (g_{s_sat}), a surrogate measure for stomatal acclimation (Maherali *et al.*, 2002; Vogan & Sage, 2012; Pinto *et al.*, 2014), was highly species-specific. Overall, variations in gas exchange traits depended on the C_4 subtypes, but this did not apply to stomatal morphology. *Chapter 2 highlights that [gCO_2] elicited a trade-off between SA and SS while LL reduced both SA and SD; and that iWUE is dependent on a dynamic stomatal trait, stomatal aperture, during CO_2 and light limitation.*

In the second growth chamber experiment (Chapter 3), four species from the Panicoideae lineage representing C_3, NAD-ME, NADP-ME, and PCK types were grown in conditions similar to the first growth chamber experiment in Chapter 2 to assess the speed of stomatal response to short-term light transitions (1000 ⇆ 100 µmol m^{-2} s^{-1}), as well as guard cell K^+ flux using electrophysiology. There was a negative correlation between opening and closing $t_{1/2}$ among the four species under control conditions (HL+[aCO_2]) and a positive relationship under single [CO_2] and light limitation conditions. However, no correlation was observed under both LL+[gCO_2] conditions. Faster stomatal closure reduced potential water loss during low light transitions and faster opening stomata reduced forgone CO_2 assimilation during transitions to high light. Glacial [CO_2] increased K^+ influx in all species but to a greater extent in the C_3 species, while, LL reduced ion fluxes relative to control conditions only in the C_3 species. Stomatal conductance and iWUE strongly correlated with SA and K^+ influx while g_s weakly correlated with stomatal opening $t_{1/2}$. *In Chapter 3, novel mechanistic links between SA, g_s, iWUE, opening $t_{1/2}$ and K^+ influx were revealed, highlighting potential molecular targets (genes that regulate stomatal opening and guard cell K^+ uptake) for breeding crops with high iWUE.*

In the first glasshouse experiment (Chapter 4), a new method using wet chemical oxidation system (WCO) coupled to high-performance liquid chromatography (HPLC), and isotope ratio mass spectrometry (IRMS) was developed for measuring carbon isotope signature ($\delta^{13}C$) of three key soluble sugars (glucose, fructose and sucrose). Sugars from

two standards and extracted from leaves of a C_3 (*Oryza sativa*) and C_4 (*Zea mays*) cereal crop species were used. Analysis of the two known sucrose standards showed that $\delta^{13}C$ was similar when measured using the classical EA-IRMS or the new HPLC-WCO-IRMS systems, confirming the accuracy of the newly developed method. The HPLC-WCO-IRMS system also showed that it was able to detect soluble sugars for as low 0.1 mg ml^{-1}. Analysis of leaf soluble sugars in *O. sativa* (C_3) showed that sucrose is ^{13}C-enriched while fructose is depleted with ^{13}C relative to whole leaf and glucose. In contrast, *Z. mays* (C_4) showed enrichment in fructose $\delta^{13}C$ followed by glucose then sucrose and whole leaf being the most depleted. *Chapter 4 demonstrates the capability of the new system to resolve sugar metabolites both in leaves and known standards in an aqueous solution which could aid in high throughput analysis of metabolite carbon isotope signatures.*

In the second glasshouse experiment (Chapter 5), four C_3, five C_4/NAD-ME, and four C_4/NADP-ME grasses were grown in a glasshouse under the ambient [CO_2], 28°C/22°C day/night temperature, and 16 h photoperiod from December 2017 to February 2018. Whole leaf and cellulose carbon isotope composition ($\delta^{13}C$) were measured using the classical EA-IRMS. Specific post-photosynthetic sugars (sucrose, fructose and glucose) were assayed using the newly developed HPLC-WCO-IRMS method in Chapter 4. Overall, sucrose $\delta^{13}C$ deviated the most and cellulose $\delta^{13}C$ deviated the least relative to the bulk leaf. Among C_3 grasses, the $\delta^{13}C$ of soluble sugars did not differ but were positively correlated with each other, reflecting the simpler carbon metabolism in C_3 leaves. Fructose $\delta^{13}C$ was 1.6 ‰ more ^{13}C-enriched in NADP-ME relative to NAD-ME species. In addition, leaf and cellulose $\delta^{13}C$ correlated well with stomatal conductance (but not with iWUE) in C_4 (but in C_3) grasses, highlighting the dominant role played by stomata in determining leaf $\delta^{13}C$ and iWUE of C_4 species. *This chapter demonstrates variations in sugar $\delta^{13}C$ between C_4 subtypes. Outcomes of this chapter could aid in understanding the underlying causes of the long-known differences in leaf $\delta^{13}C$ between the NAD-ME and NADP-ME C_4 variations and ultimately help develop a tool for high throughput screening of iWUE among C_4 plants.*

All data taken together (**Chapter 6**), this project demonstrated the significant role of stomatal aperture dynamics, speed of stomatal responses, and guard cell K^+ influx as potential targets for the improvement of iWUE in C_3 and C_4 grasses. Between C_4 subtypes, stomatal acclimation to glacial [CO_2] and low light in NAD-ME grasses was less than that in NADP-ME. The project also established a method employing wet chemical oxidation system coupled to HPLC and IRMS in measuring carbon isotope composition of sugar

standards and leaf samples. Employing this method, this project highlights a significant discrepancy in $\delta^{13}C$ signature of leaf fructose in NAD-ME and NADP-ME but not in glucose and sucrose.

CHAPTER 1

GENERAL INTRODUCTION

1.1 Water Limitation and Crop Water-Use Efficiency

About 70% of global accessible water supply is allocated in agricultural irrigation and will not be sufficient in the near future's water supply considering the projected population increase, drought frequency, and unsustainable water withdrawal (FAO, 2017). IPCC (2018) predicts a 1.5°C increase in global temperature, which will negatively impact crop production, especially in the semi-arid regions. Meeting global food demand due to rising population is also an inevitable concern as the global food demand is forecasted to increase by 100-110% (in the years 2005-2050) based on per capita caloric demand (Tilman *et al.*, 2011). To address both challenges (climate change impact and food sustainability), crop production needs to be increased in two ways: (1) agricultural intensification, involving land clearing to expand crop production, and (2) intensification, by crop variety improvements such as yield, resource use efficiency and tolerance to stresses (Tilman *et al.*, 2011).

Water-use efficiency (WUE) is one key trait in crops that are usually affected by drought. Efforts of applied and fundamental research have been channelled in order to improve water use in crops (Medrano *et al.*, 2015). WUE can be defined and assessed at various levels (**Figure 1. 1**). Crop-level WUE is defined as the ratio between grain yield and water utilised (either irrigated or rain-fed). Plant-level WUE is the total plant biomass divided by evapotranspiration (water loss). Plant-level WUE, interchangeably referred to as transpiration efficiency (TE), is an important factor in determining crop-level WUE. WUE definition at the leaf-level is termed as instantaneous WUE (or instantaneous TE) which is the ratio of instantaneous CO_2 assimilation (A_{net}) and transpiration (E) rates. Since transpiration is greatly affected by temperature, humidity, and vapour pressure deficit (VPD), another term 'intrinsic WUE' [which is the ratio of A_{net} and stomatal conductance (g_s)] is an additional term used as a stable indicator of genotypic variations (Xu & Hsiao, 2004; Vadez *et al.*, 2014; Ellsworth & Cousins, 2016; Ghannoum, 2016). While crop level WUE is seen as an ultimate target, leaf-level iWUE improvement is of physiological significance as it could eventually translate to the crop level. For this study, I am investigating leaf-level WUE with a particular focus on iWUE.

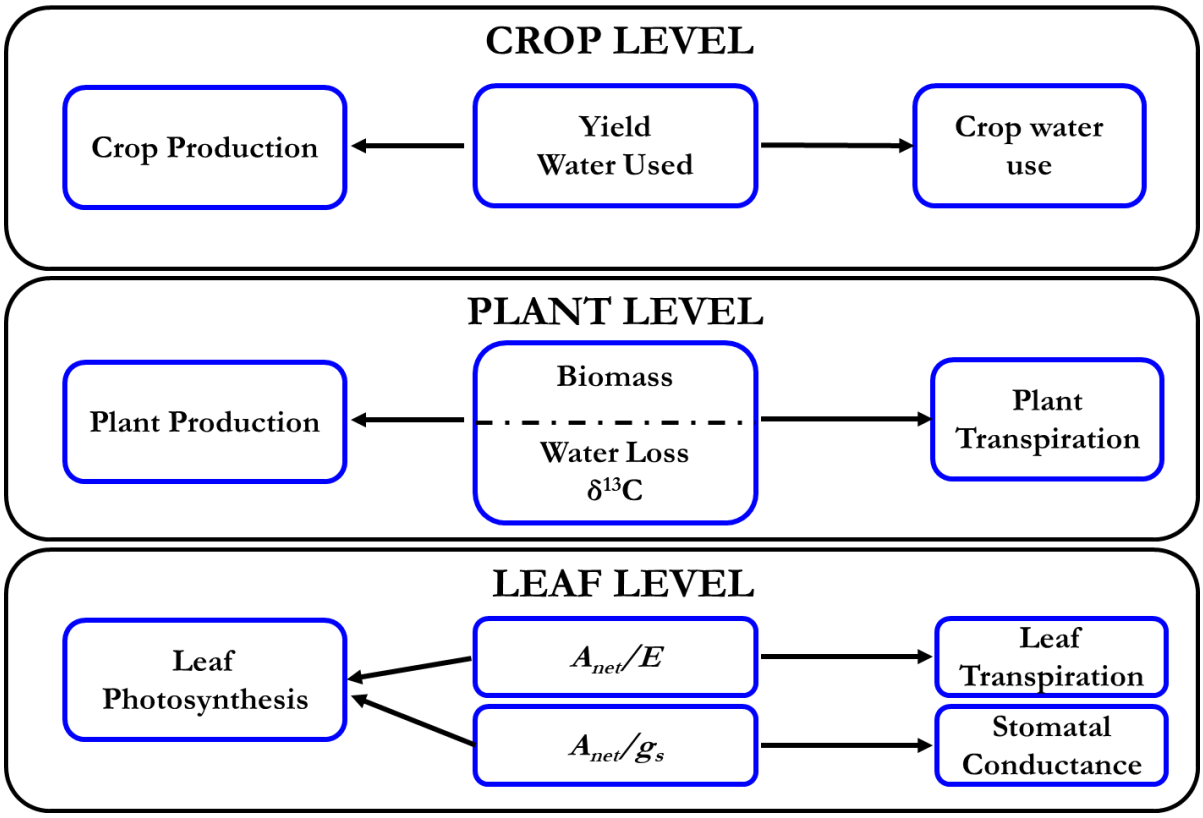

Figure 1. 1 Different levels and scales of WUE depending on the capacity and purpose of the study.

Crop level WUE is the ratio of harvestable yield to the amount of water used. At the plant level, it is the ratio between the biomass and water loss. While at the leaf-level, it is the ratio of photosynthetic rate (A_{net}) and transpiration rate (E) or stomatal conductance (g_s). The figure was adapted from Medrano *et al.* (2015).

1.2 WUE in C_4 Leaves

1.2.1 C_4 photosynthesis

Plants can be classified according to the mode of CO_2 assimilation during photosynthesis. The most prevalent is the C_3 type wherein atmospheric [CO_2] is directly fixed by the major carboxylating enzyme, ribulose-1,5-bisphosphate carboxylase/oxygenase (Rubisco) (Ehleringer *et al.*, 1997; Ehleringer & Cerling, 2014). The dual function of the enzyme has a drawback, particularly the oxygenase reaction. O_2 around the enzyme is a substrate, and the resulting reaction produces phosphoglycolate during RuBP oxygenation. Eventually, it is detoxified in the peroxisome using additional ATP (Ehleringer *et al.*, 1977; Pearcy & Ehleringer, 1984; Ehleringer & Cerling, 2014). This is termed as photorespiration and can

lead to loss of fixed CO_2, thus become an inefficient process. Photorespiration reduces photosynthetic efficiency of C_3 plants and hence can impact WUE. For example, WUE increases at elevated CO_2 in C_3 plants because CO_2 assimilation rates increase as well as g_s decrease. In C_4 plants, photorespiration in ambient air is negligible and hence will have a minor effect on WUE (Ghannoum *et al.*, 2000). Important crops included in this photosynthetic type are rice, barley, and wheat (Sage *et al.*, 2012).

An adaptation to conditions that promote high rates of photorespiration is the C_4 (Hatch-Slack) cycle (Sage *et al.*, 2012). The C_4 cycle is a series of anatomical and biochemical modifications that isolate Rubisco in a two-celled structure (**Figure 1. 2**), allowing the concentration of high amounts of CO_2 and thereby suppressing photorespiration (Sage, 2004). The C_4 pathway independently evolved over 66 times in 19 families of angiosperms and first arose in grasses, around 24–35 million years ago during the Oligocene epoch (**Figure 1. 3A**) with periods of low atmospheric [CO_2] concentration (**Figure 1. 3**) and high temperature (Sage, 2004; Christin *et al.*, 2008; Sage *et al.*, 2012).

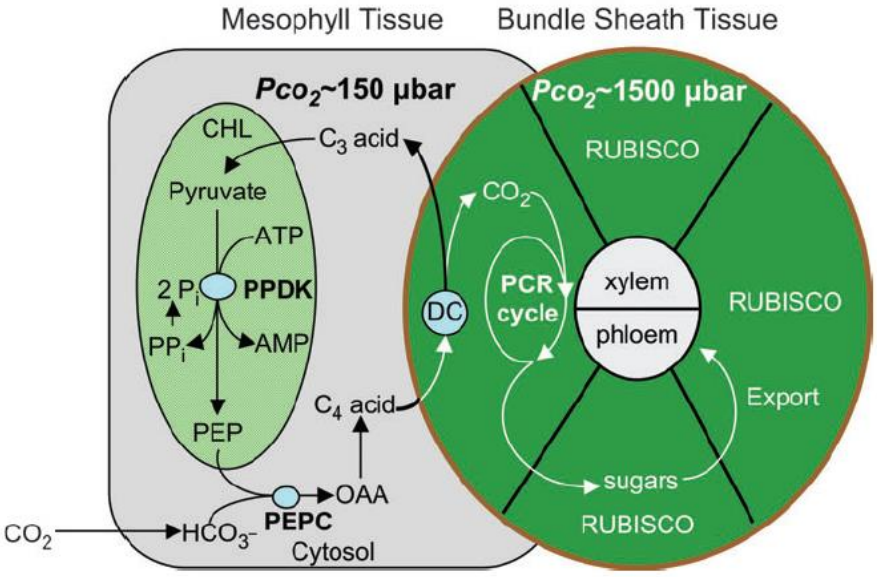

Figure 1. 2 The mechanism of CO_2 concentration in C_4 tissues during photosynthetic carbon dioxide assimilation.

CO_2 is initially fixed by PEPC into a C_4 acid which is transported to the bundle sheath cells (BSC) where a specific decarboxylase releases CO_2 which enters a typical C_3 cycle. The concentration of [CO_2] inside the BSC exceeds that in the atmospheric. Abbreviations: DC, decarboxylating enzyme; PEPC, phosphoenolpyruvate carboxylase; PCR, photosynthetic carbon reduction; PPDK, pyruvate, phosphate dikinase. Figure source: Sage & McKown (2006).

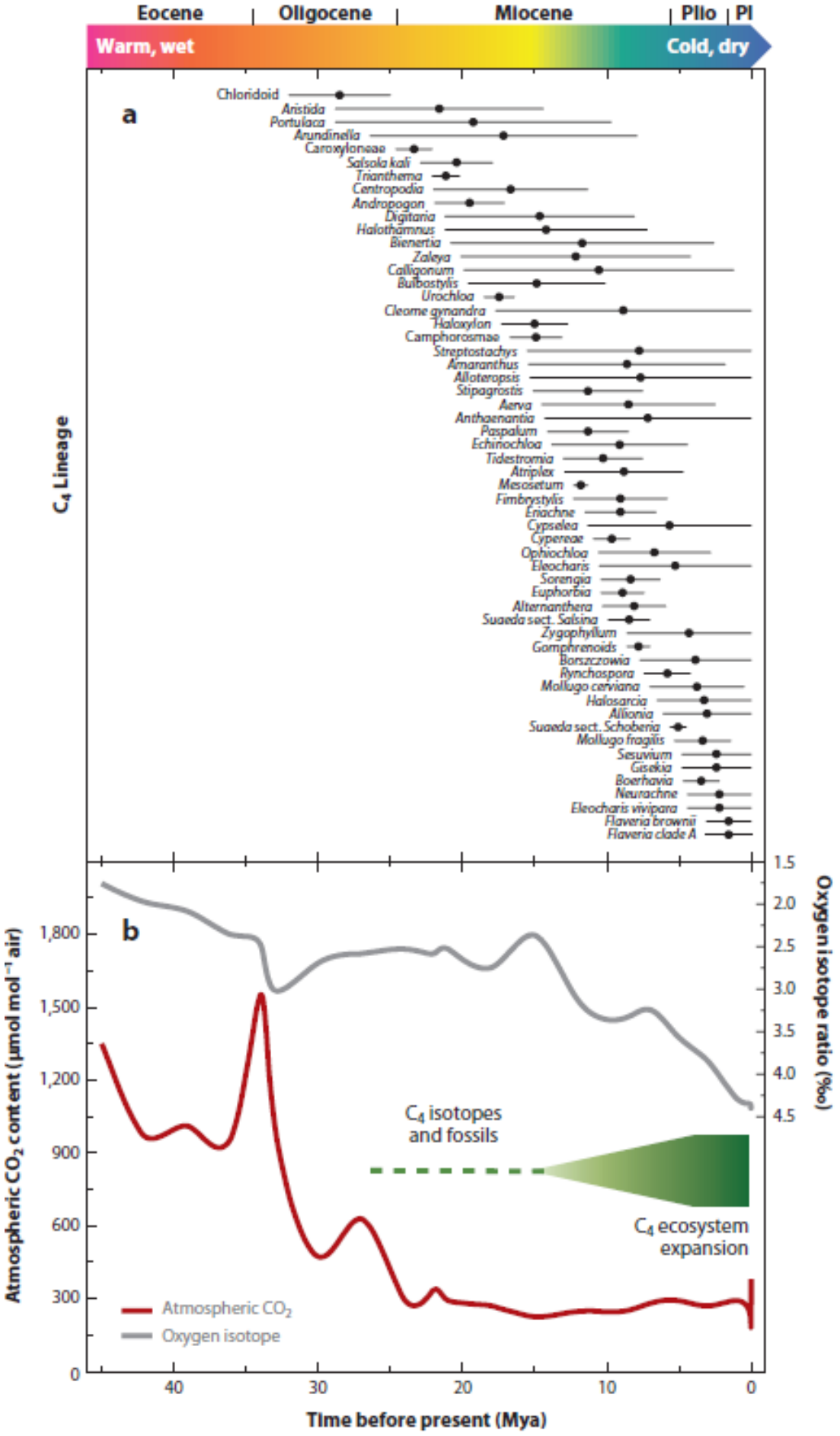
Eocene
Oligocene
Miocene
Plio
Pl
Warm, wet
Cold, dry
a
C4 Lineage
Chloridoid
Aristida
Portulaca
Arundinella
Caroxyloneae
Salsola kali
Trianthema
Centropodia
Andropogon
Digitaria
Halothamnus
Bienertia
Zaleya
Calligonum
Bulbostylis
Urochloa
Cleome gynandra
Haloxylon
Camphorosmae
Streptostachys
Amaranthus
Alloteropsis
Stipagrostis
Aerva
Anthaenantia
Paspalum
Echinochloa
Tidestromia
Atriplex
Mesosetum
Fimbristylis
Eriachne
Cypselea
Cypereae
Ophiochloa
Eleocharis
Sorengia
Euphorbia
Alternanthera
Suaeda sect. Salsina
Zygophyllum
Gamphrenoids
Borszczowia
Rynchaspora
Mollugo cerviana
Halosarcia
Allionia
Suaeda sect. Schoberia
Mollugo fragilis
Sesuvium
Gisekia
Boerhavia
Neurachne
Eleocharis vivipara
Flaveria brownii
Flaveria clade A
b
Atmospheric CO2 content (µmol mol−1 air)
Oxygen isotope ratio (‰)
1,800
1,500
1,200
900
600
300
0
1.5
2.0
2.5
3.0
3.5
4.0
4.5
C4 isotopes and fossils
C4 ecosystem expansion
Atmospheric CO2
Oxygen isotope
40
30
20
10
0
Time before present (Mya)

Figure 1. 3 Evolutionary lineages of C_4 monocots and dicots over the geologic timescale.

The glacial period during the Oligocene promoted the evolution and diversification of C_4 photosynthesis. Circles in **(A)** represent median age and **(B)** shows the atmospheric [CO_2] decline over time. Figure source: Sage *et al.* (2012).

1.2.2 C_4 subtypes

C_4 photosynthesis can be further subdivided into three subtypes according to the major decarboxylating enzyme used to release CO_2 in the bundle sheath cells (BSC): nicotinamide adenine dinucleotide phosphate malic enzyme (NADP-ME), NAD malic enzyme (NAD-ME), and phosphoenolpyruvate carboxykinase (PCK) (Hatch, 1987; Kanai & Edwards, 1999). Each biochemical subtype differs in anatomy, biochemistry, and physiology (Hatch, 1987). **Figure 1. 4** outlines the simplified differences among the C_4 subtypes.

In NADP-ME subtype (**Figure 1. 4A)**, CO_2 is released in the BSC chloroplast while decarboxylation in NAD-ME (**Figure 1. 4B)** and PCK (**Figure 1. 4C)** occurs in the BSC mitochondria and cytosol respectively (Hatch, 1987; Kanai & Edwards, 1999). The PCK type is not exclusive as both NAD-ME, and NADP-ME could utilise mixed decarboxylases which could confer advantages during fluctuating conditions (Wingler *et al.*, 1999; Bellasio & Griffiths, 2014; Wang *et al.*, 2014; Watson-Lazowski *et al.*, 2018).

In terms of anatomy, NADP-ME and PCK species have suberized BSC walls while NAD-ME species do not possess suberized BSC wall (Hatch, 1987; Hattersley, 1992; Christin *et al.*, 2013). BSC chloroplasts in NADP-ME and PCK are arranged centrifugally relative to the vascular bundles whilst NAD-ME has centripetal chloroplast organisation (Kanai & Edwards, 1999). Granal stacks in thylakoid membranes are well developed in NAD-ME and PCK while it is reduced in NADP-ME (Kanai & Edwards, 1999) thus having lower PSII activities among NADP-ME subtypes (Kanai & Edwards, 1999; Ghannoum *et al.*, 2011). From an ecophysiological perspective, the NAD-ME subtype occurs predominantly in environments receiving comparatively lower average rainfall, whereas the NADP-ME and the PCK subtypes are dominant in regions with relatively higher rainfall (Fravolinil *et al.*, 2002).

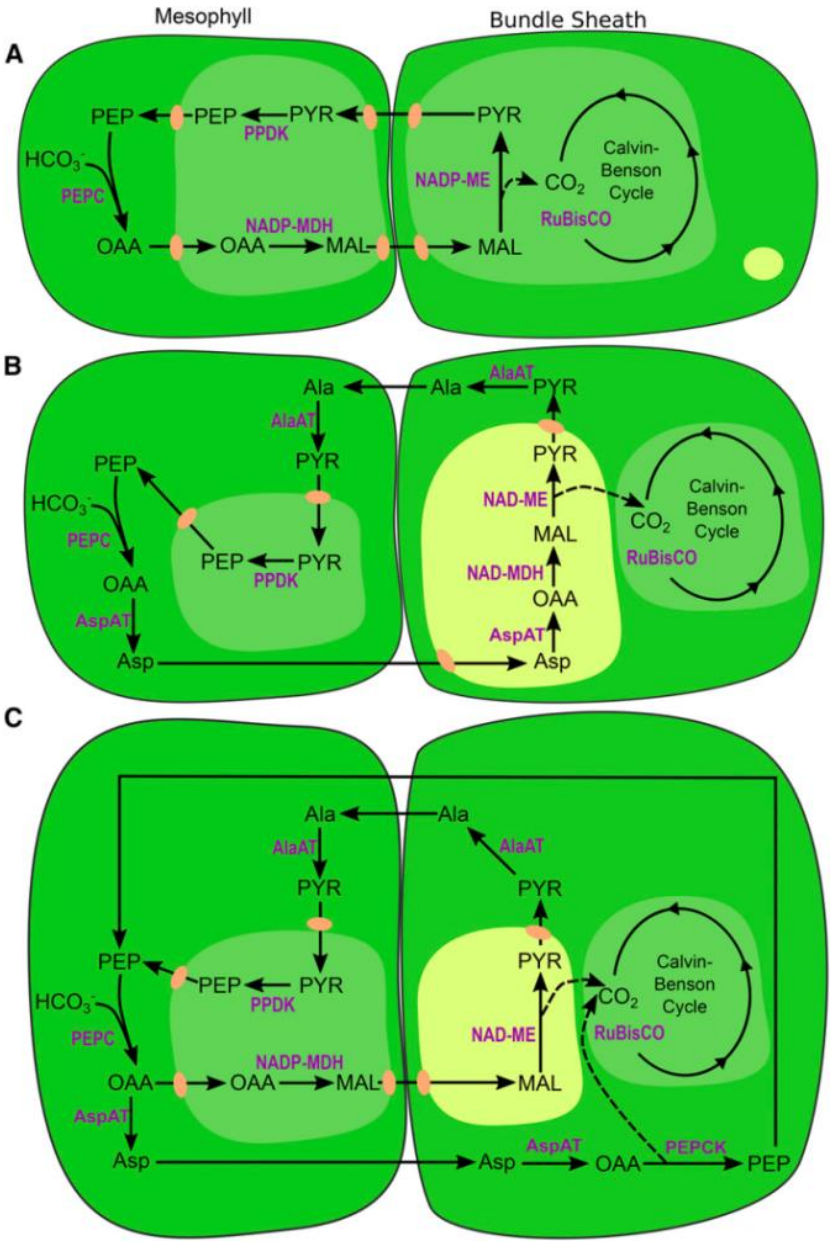

Figure 1. 4. Diagram showing differences in leaf biochemistry amongst three C_4 subtypes.

(**A**) NADP-ME subtype, in which decarboxylation occurs in the BSC chloroplast. PEP is carboxylated to a C_4 acid OAA and converted to AL which is decarboxylated by NADP-ME to release CO_2 and PYR. NAD-ME decarboxylation (**B**) on the other hand takes place in BSC mitochondria whereby PEP is carboxylated to OAA and transaminated to Asp, which is then transported to the BSC mitochondria for decarboxylation. (**C**) In the third PEPCK or PCK type, decarboxylation occurs in the BSC cytosol, whereby Asp from mesophyll cells is deaminated to OAA in BSC and decarboxylated to PEP by PEPCK. Abbreviations: Ala, alanine; AlaAT, Ala aminotransferase; Asp, aspartate; AspAT, Asp aminotransferase; MAL, malate; NAD-MDH, NAD-malate; NADP-MDH, NADP-malate dehydrogenase; OAA, oxaloacetate; PEP, phosphoenolpyruvate; PEPC, phosphoenolpyruvate carboxylase; PPDK, pyruvate, orthophosphate dikinase; PYR, pyruvate. Figure source: Covshoff *et al.* (2016).

1.2.3 Variations in iWUE in C_3 and C_4 species and among the C_4 subtypes under glacial [CO_2] and low light

A well-established effect of CCM endows C_4 species with higher WUE_i than their C_3 counterparts (Morison & Gifford, 1983; Huxman & Monson, 2003; Vogan & Sage, 2012). C_4 species tend to operate at a lower stomatal conductance (g_s) and intercellular CO_2 (C_i) while achieving higher photosynthetic rates (A_{net}) compared to C_3 counterparts (Taylor *et al.*, 2010a, 2012).

Several environmental conditions affect iWUE responses. When grown at a range of [CO_2] concentrations (200, 400, and 640 ppm) Taylor *et al.*, (2012), reported a superior iWUE (A_{net}/g_s) due to higher A_{net} and lower g_s among four C_3 and four C_4 grasses **(Figure 1. 5)**. Under low light, Sonawane *et al.*, (2018) showed that CCM is more efficient in NADP-ME grasses compared to NAD-ME and PCK subtypes due to higher photosynthetic quantum yield, decrease in carbon isotope discrimination, and reduced bundle sheath CO_2 leakiness. Superior CCM efficiency in NADP-ME subtype may be linked to the presence of suberin lamella in the BSC wall (Hatch, 1987) or the superior Rubisco kinetics of this subtype (Sharwood *et al.*, 2016). Results from Pinto *et al.*, (2014) showed higher CO_2 assimilation rates in C_4 relative to C_3 species in both glacial (180 ppm) and ambient [CO_2] (400 ppm) growth conditions, which translated to higher photosynthetic WUE (PWUE, A_{sat}/g_s). Considerable variations in PWUE were also observed with NAD-ME having the highest PWUE, followed by PCK and then NADP-ME, respectively (**Figure 1. 6**). Meanwhile, under drought conditions, Ghannoum *et al.* (2002) showed that NAD-ME grasses have higher whole-plant water-use efficiency than NADP-ME grasses. Recently Watson-Lazowski *et al.*, (2019) showed that NADP-ME species had reduced biomass when acclimated to glacial [CO_2] and were least affected when acclimated low light acclimation (200 µmol m^{-2} s^{-1}). Stomatal conductance also increased by 74% in NADP-ME compared to NAD-ME and PCK subtypes during growth at glacial [CO_2] (Watson-Lazowski *et al.*, 2019).

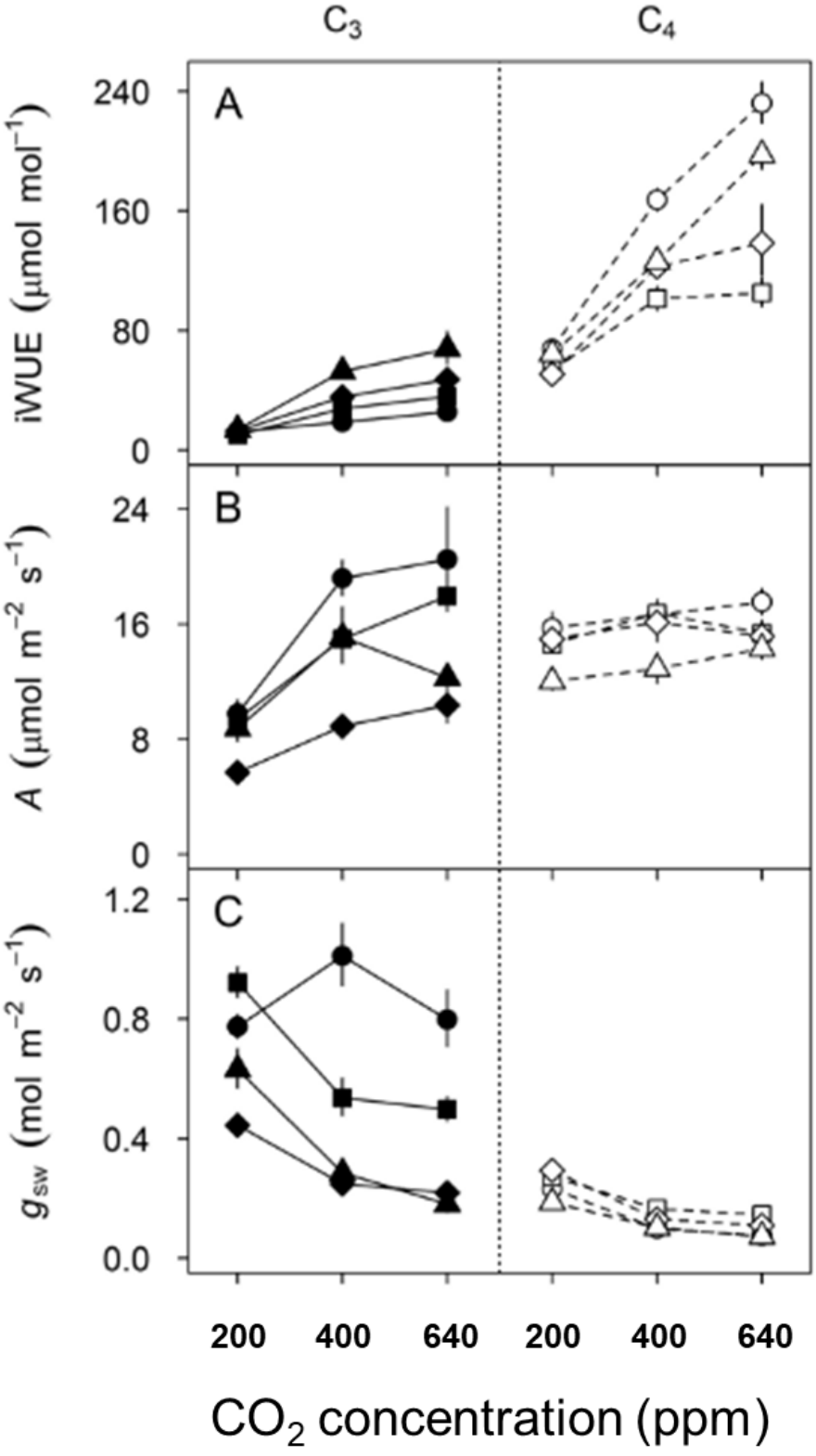

Figure 1. 5 C_4 grasses have higher iWUE when grown at a range of CO_2 concentrations.

(**A**) Intrinsic water-use efficiency (iWUE), (**B**) net CO_2 assimilation rate (*A*), and (**C**) stomatal conductance to water (g_{sw}) in four C_3 and four C_4 grasses (n=5-6) grown at glacial

(200 ppm), ambient (400 ppm) and elevated (640 ppm) [CO_2]. Figure source: Taylor *et al.* (2012).

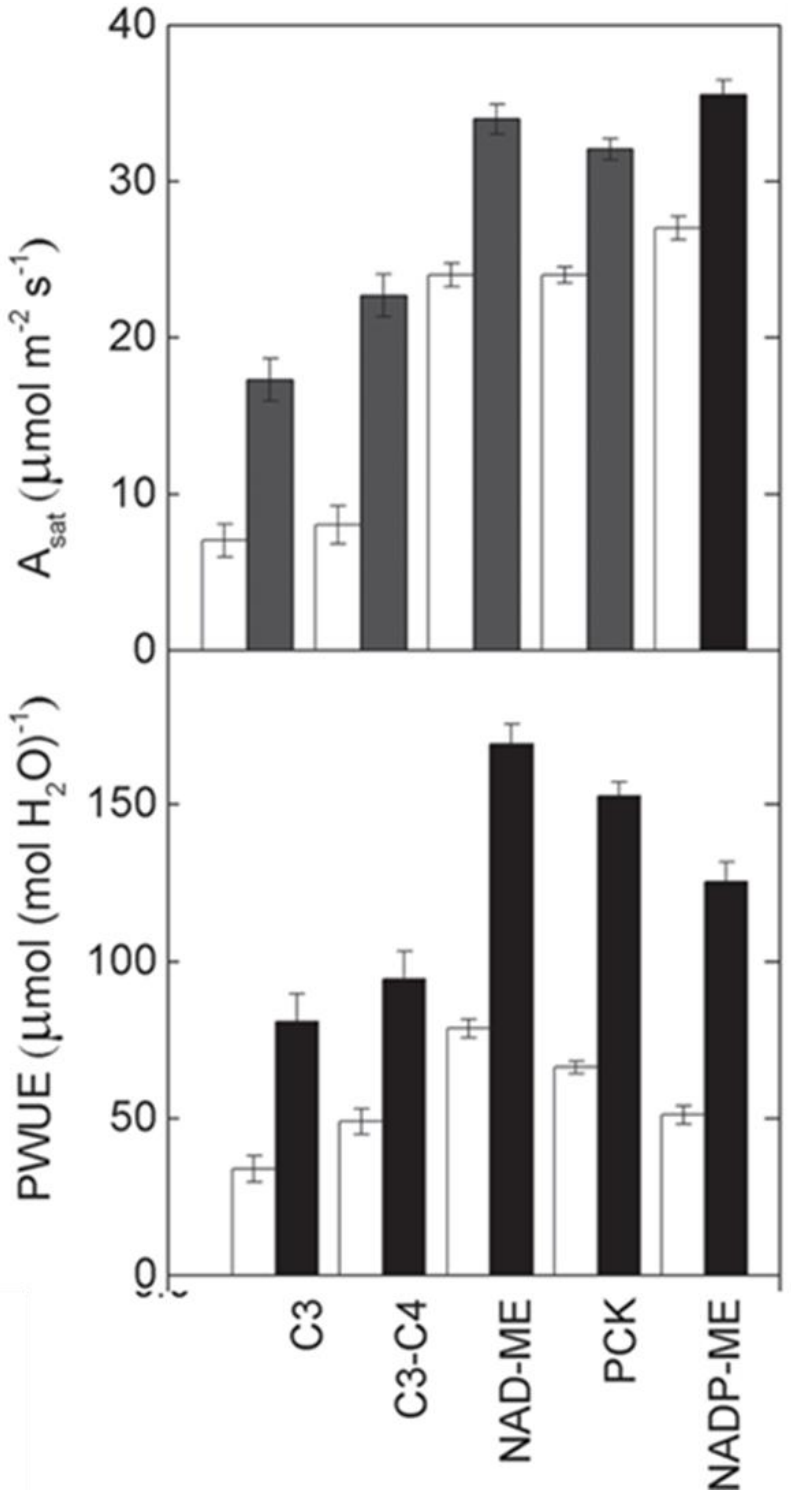

Figure 1. 6 C_4 species have greater A_{sat} and PWUE while NAD-ME subtype confers the highest PWUE among the other subtypes.

Light saturated assimilation rate (A_{sat}), and photosynthetic WUE (A_{sat}/g_s) of grasses with different photosynthetic types (C_3, C_3-C_4 intermediate, and C_4 biochemical subtypes)

acclimated at glacial [CO_2] (white bars) and ambient [CO_2] (dark bars). Figure source: Pinto *et al.* (2014).

1.3 Grass Stomata and WUE

In addition to the photosynthetic capacity, iWUE is greatly affected by stomatal performance. Stomata are structures located in the leaf epidermis that allow gas exchange (mainly CO_2 and H_2O) and permit the optimisation of carbon fixation and water loss (Raven, 2002). Compared to other plant lineages, the grass family have evolved a unique stomata morphology allowing faster response and tighter closure in comparison to stomata of eudicots during fluctuating environmental conditions such as [CO_2] limitation, light, shade, sun flecks, humidity, and temperature (Kollist *et al.*, 2014a; Chen *et al.*, 2017). Thus, having a C_4 photosynthetic system and highly responsive stomata allows optimum WUE_i regulation in grasses.

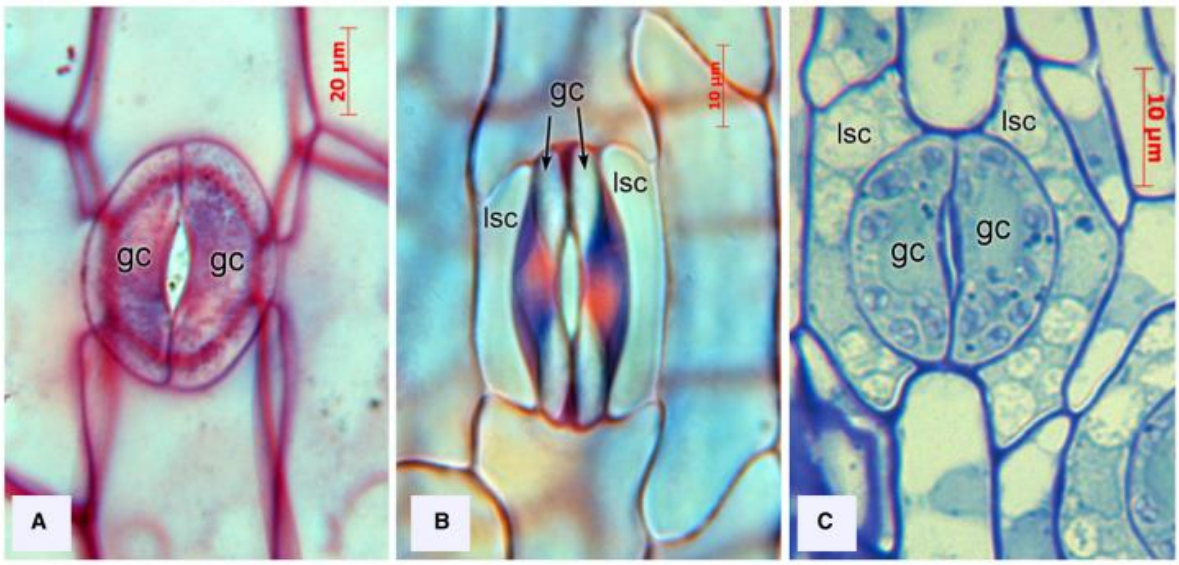

Figure 1. 7 Stomatal diversity in monocots.

Illustration of anomocytic (**A**), paracytic- non-oblique (**B**), and paracytic-oblique conditions (**C**) among mature monocot stomata. Abbreviations: guard cells (gc), lateral subsidiary cells (lsc). Figure source: Rudall *et al.* (2017).

1.3.1 The monocot stomata

Grasses belong to the monocot group which possess a typical linear venation pattern on the leaf. Within monocots, there is diversity in stomatal morphology (**Figure 1. 7,** Rudall *et al.*, 2017). According to the morphological definition of Rudall *et al.*, (2017), mature stomata could have the presence (paracytic) or absence (anomocytic, **Figure 1. 7**) of lateral subsidiary cells. Among those possessing lateral subsidiary cells (**Figure 1. 7B-C**), a non-oblique condition (**Figure 1. 7B**) is characterised to have smaller subsidiary cells and oriented parallel to the guard cells (Rudall *et al.*, 2017). In contrast, the oblique phenomenon (**Figure 1. 7C**) is characterised by morphologically oblique subsidiary cells almost covering all the guard cells. In other cases, subsidiary cells may also be located on polar ends of the guard cells and classified as tetracytic stomata (Rudall *et al.*, 2017). For grasses, especially those belonging to Poales, the paracytic, non-oblique condition is present (Rudall *et al.*, 2017). Meanwhile, members of the subfamilies Araceae, Petrosaviceae, Dioscoreacea; family Liliales and Asparagales possess anomocytic stomata (Rudall *et al.*, 2017). Hence, the paracytic phenomenon is not exclusive to the monocot group and would be interesting to study the stomatal dynamics among different stomatal morphologies in the monocot clade.

In addition, the stomatal location on the leaf surface, though not exclusive to monocots, could be classified as amphistomatous, hypostomatous, epistomatous, or heterostomatous (Kirkham, 2014). When stomata are located in lower (abaxial) or upper (adaxial) surface of the leaf, it is amphistomatic stomata (Kirkham, 2014). Stomata that are exclusively located on the upper leaf surface is epistomatous while hypostomatic stomata occur on the abaxial surface. The heterostomatic state is characterised by higher stomatal density in the abaxial surface compared to the adaxial surface (Kirkham, 2014).

1.3.2 Stomatal morphology in grasses

Fundamental to grass stomata are the functional guard cells and subsidiary cells that open and close to permit the balance between [CO_2] and [H_2O] exchange in the whole plant (**Figure 1. 8**). This gaseous exchange is operated by membrane transport mechanisms (mediated by ion, solute and water transport across the membranes) that allow guard cells to inflate and deflate, thereby opening and closing the stomatal aperture. Gas exchange is

not only regulated by stomatal pore size but also the stomatal density and stomatal index in the epidermis (Hetherington & Woodward, 2003). In general, C_4 grasses operate at a relatively lower stomatal conductance (g_s) compared to C_3 counterparts due to the regulation of stomatal aperture and decreased stomatal density (Taylor *et al.*, 2012).

Grass stomata are characteristically dumbbell-shaped (**Figure 1. 8A**), as opposed to regular kidney-shaped stomata (**Figure 1. 8B**) found in other plants. It is widely supported that the former kind is more advanced than the latter, as evidenced by the fact that during stomatal development in timothy grass (*Phleum pratense*), the guard cells assume the kidney-shaped form before transitioning to the final dumbbell-shaped morphology (Hetherington & Woodward, 2003). From an evolutionary perspective, the origins of a highly responsive grass stomata could be traced to the moss stomata as the nearest precursor to the stomata of vascular plants and went on to progress to more complex and functional stomata that could respond faster to environmental stimuli such as [CO_2], light, and water stress (Chen *et al.*, 2017). It was postulated that a passive stomatal regulation from mosses rather than a divergence from ferns, was the culprit for the emergence of active stomatal regulation (Chen *et al.*, 2017). On the other hand, in kidney-shaped stomata, it was proposed that during drought, ABA is synthesised and transported to the guard cells through ATP-binding cassette transporters (ABC) and nitrate transporters NRT1.2 (Kuromori *et al.*, 2010; Kanno *et al.*, 2012; Chen *et al.*, 2017). This process, in turn, activates the production of hydrogen peroxide and nitric oxide which is thought to activate Ca^{2+} channels and other anionic channels responsible for stomatal closing (Grabov & Blatt, 1998; Garcia-Mata *et al.*, 2003; Chen *et al.*, 2017). Active stomatal regulation also coincides with the acquisition and interaction of Slow Anion Channel 1 (SLAC1) which is activated by ancient drought/ABA signalling kinase Open Stomata 1 (OST1) leading to active stomatal closure only present in mosses and vascular plants with stomata, but absent in non-stomata-bearing liverworts and algae (Lind *et al.*, 2015).

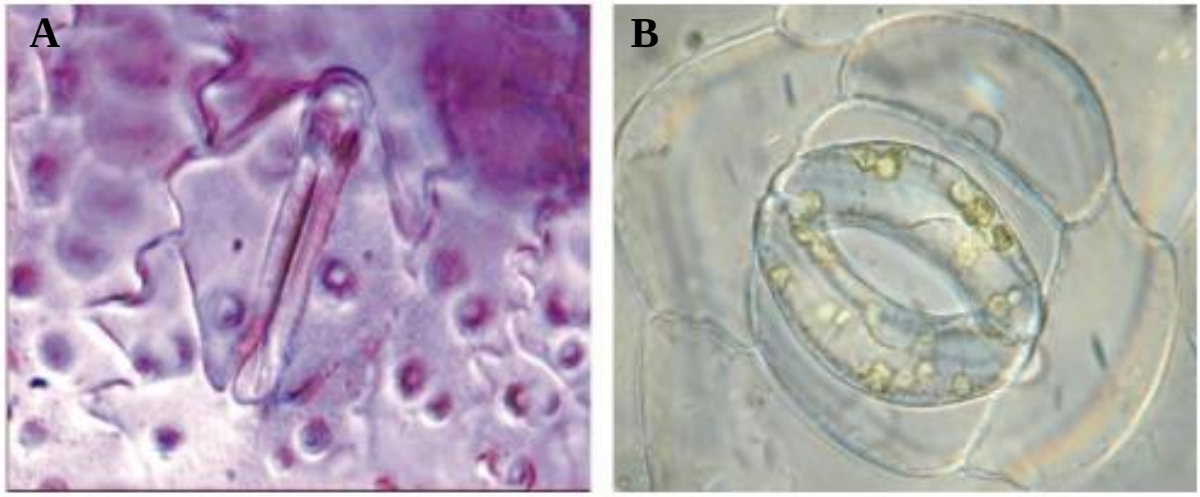

Figure 1. 8 Contrasting stomatal morphology showing dumbbell and kidney-shaped stomata.

Typical dumbbell-shaped stomata in grasses (**A**) and kidney-shaped stomata amongst dicots (**B**). Figure source: Hetherington & Woodward (2003).

Exploring further, Franks & Farquhar, (2006) examined the morphology of open stomata (A) brought about by high light and high humidity in a scanning electron cryomicroscopy (cryoSEM) section of *Triticum aestivum* (**Figure 1. 9**). Compared to the kidney-shaped stomata, the swelling of the guard cells (G) pushes the subsidiary cells toward the neighbouring epidermal cells to allow for higher and faster rates of gas exchange. Conversely, the lateral displacement of the guard cells is reversed (B) when turgor pressure in the guard cells decreases. The fast exchange of osmolytes and the rapid interaction between guard cells and subsidiary cells in grasses allowed for faster stomatal control which is advantageous in maximising water loss and CO_2 absorption during unfavourable conditions (Franks & Farquhar, 2007; Chen *et al.*, 2017; Vialet-Chabrand *et al.*, 2017a). In addition, stomata have no plasmodesmata. Hence, an individual stoma functions as a solitary unit which explains their responsiveness even in isolated epidermal peels (Willmer & Sexton, 1979).

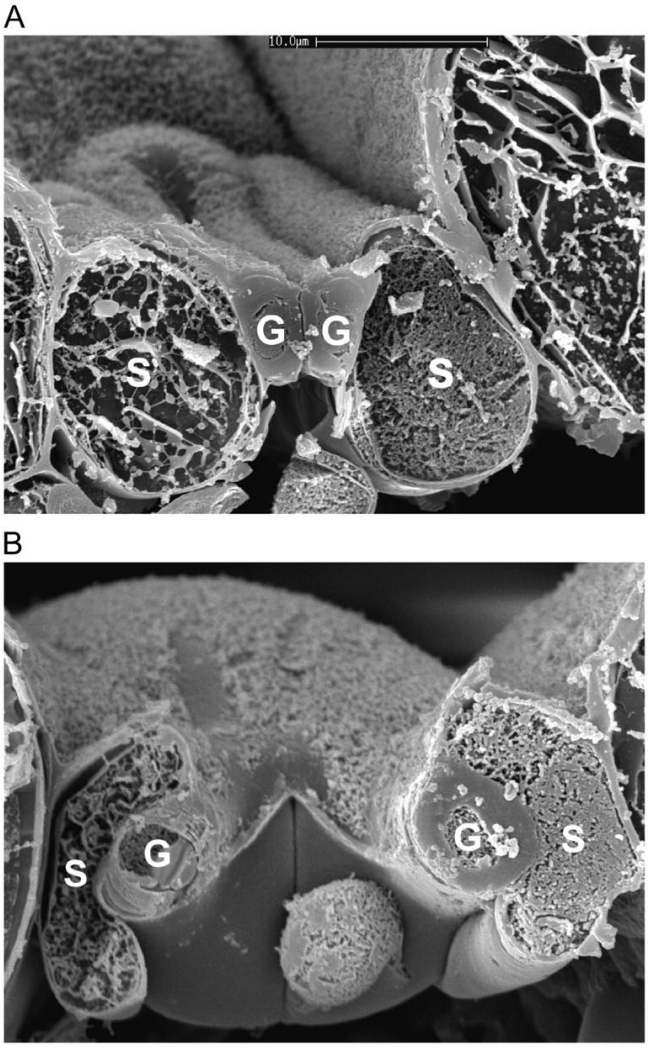

Figure 1. 9 A transverse section of a cryoSEM prepared stomata of *Triticum aestivum* intact leaf.

Open stomata (**A**) is observed during high irradiance and humidity. Low humidity closes the stomata aperture (**B**). G, Guard cell; S, subsidiary cell. Figure source: Franks & Farquhar (2007).

1.3.3 CO_2 sensing in guard cells

Guard cells respond to changes in [CO_2] in order to regulate assimilation and transpiration. Stomatal aperture generally closes when exposed to short-term high [CO_2] and opens under [CO_2] starvation both in darkness and light (Lawson, von Caemmerer, & Baroli, 2011). Engineer *et al.*, (2016) summarised that there are several studies (Webb *et al.*, 1996; Brearley *et al.*, 1997) that show the ability of guard cells to react to several environmental signals, most notably [CO_2]. They proposed that the components for guard cell sensing and

signalling reside in the guard cells *per se*. Furthermore, they presented a plethora of putative proteins that exert function in guard cells during CO_2 sensing. This proteins include carbonic anhydrases CA1 and CA4, high leaf temperature protein kinase HT1, the slow anion channel SLAC1 and the protein kinase OST1 (Engineer *et al.*, 2016). Hashimoto *et al.* (2006) demonstrated that HT1 kinase in *Arabidopsis* is responsible for the regulation of CO_2 responses. Down-regulation of HT1 kinase reduced the sensitivity of *Arabidopsis* mutants to changing [CO_2] conditions. Young *et al.*, (2006) demonstrated the participation of transient fluxes of cytosolic Ca^{2+} during induced stomatal closure and opening brought about by [CO_2]. The addition of Ca^{2+} chelator attenuated the closing of *Arabidopsis* stomata as well as its induced opening under low [CO_2].

Stomatal conductance is regulated by C_i rather than C_a (Mott, 1988). However, it is still unclear whether C_i is directly sensed by guard cells or responds to signals due to mesophyll photosynthesis (Lawson *et al.*, 2012; Azoulay-Shemer *et al.*, 2015). Several reviews have summarised the involvement of small diffusible molecules derived from the mesophyll cells (Engineer *et al.*, 2016; Chen *et al.*, 2017; Lawson & Matthews, 2020). Candidates include sucrose, malate and ABA (Engineer *et al.*, 2016; Chen *et al.*, 2017; Lawson & Matthews, 2020). However, the precise signalling interaction between mesophyll and stomata is still yet to be elucidated.

1.3.4 Stomatal responses to light

Spectral quality promotes guard cell movement and could be classified as direct (blue) and indirect (red) effects (Assmann & Jegla, 2016; Inoue & Kinoshita, 2017; Babla *et al.*, 2019). Blue light induces stomatal opening (**Figure 1. 10**) by directly activating the phototropins, *phot1* and *phot2*, in guard cells through a series of phosphorylation reactions (Christie, 2007; Shimazaki *et al.*, 2007; Inoue & Kinoshita, 2017; Babla *et al.*, 2019). This results to the rapid activation of protein kinase BLUE LIGHT SIGNALLING1 (BLUS1) which conveys the signal to type 1 protein phosphatase (PP1) (Takemiya *et al.*, 2006; Takemiya & Shimazaki, 2016; Babla *et al.*, 2019). This cascade of reaction activates the guard cell plasma membrane H^+ ATPase pump leading to H^+ extrusion and membrane hyperpolarisation (Shimazaki *et al.*, 2007; Marten *et al.*, 2010) which consequently activates the inward rectifying K^+ channels (K^+_{in}) (Kim *et al.*, 2010). K^+ accumulation follows resulting to water

uptake and finally, stomatal opening (Schroeder *et al.*, 1987; Shimazaki *et al.*, 2007; Kim *et al.*, 2010; Marten *et al.*, 2010; Inoue & Kinoshita, 2017; Babla *et al.*, 2019). This phenomenon is often referred to as blue-light induced stomatal opening (**Figure 1. 10**).

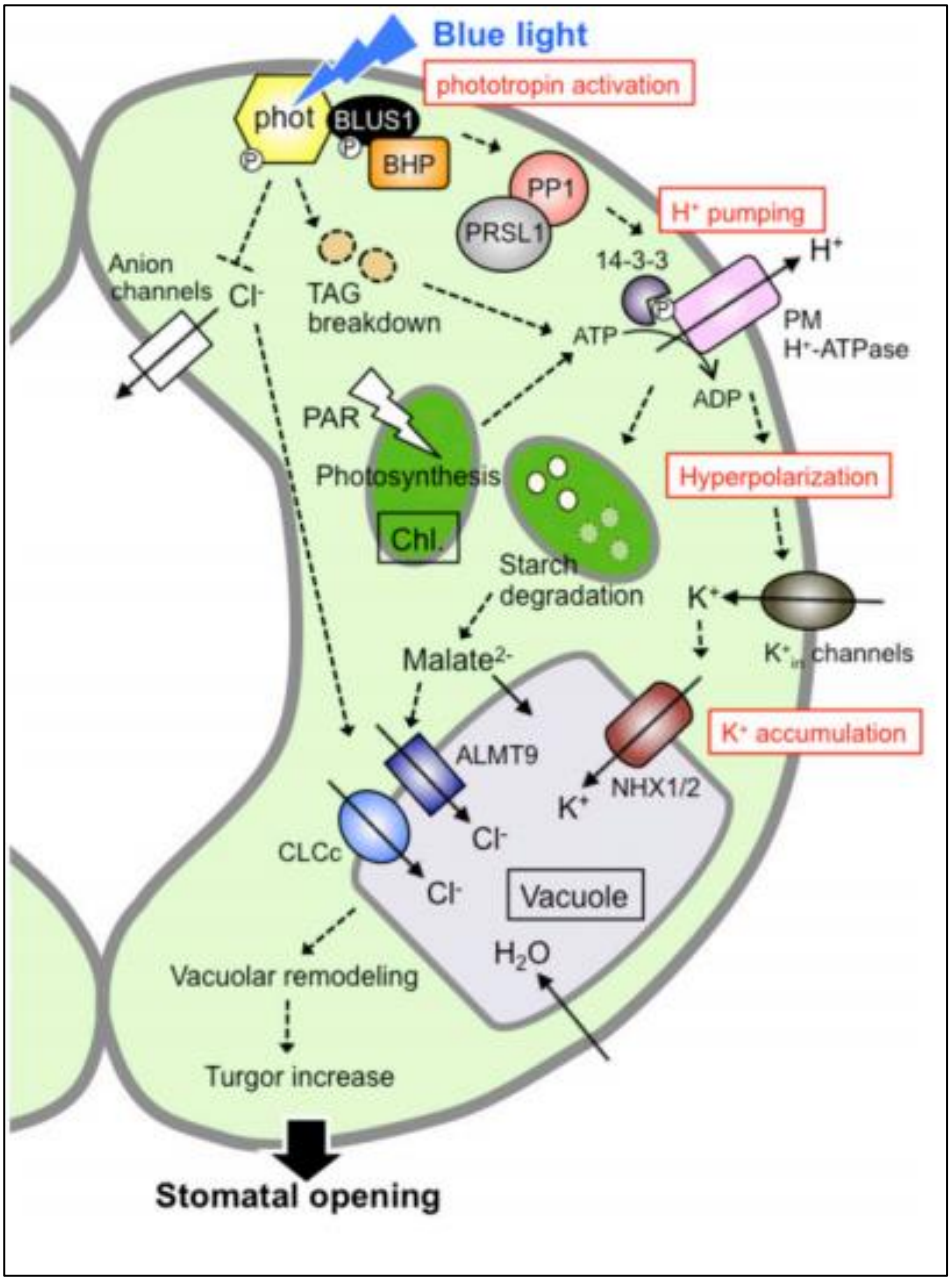

Figure 1. 10 The mechanism of blue-light activated stomatal opening

A cascade of reactions leading to stomatal opening via blue-light induction. Blue light and PAR also activate starch degradation and malate signalling in guard cell vacuoles leading to stomatal opening. Broken T bars represent negative regulation while arrows represent positive regulation. Abbreviations: phot, Phototropin; 14-3-3, 14-3-3 protein; Chl.,

chloroplast; PAR, photosynthetically active radiation; TAG, triacylglycerol. Figure source: Inoue & Kinoshita (2017).

The red light response (photosynthetically active radiation response) is an indirect response driven by mesophyll photosynthesis which lowers C_i and ultimately stimulating stomatal opening (Huxman & Monson, 2003; Roelfsema & Hedrich, 2005; Lawson *et al.*, 2012; Matrosova *et al.*, 2015; Chen *et al.*, 2017). The decreased C_i was postulated to deactivate anion channels in guard cell plasma membrane, thereby activating H^+ ATPase pump, then K^+ influx, and eventually stomatal opening (Roelfsema & Hedrich, 2005). It was also shown that tandem of weak blue light under a background of strong red light stimulated rapid stomatal opening in *Arabidopsis,* but stomatal opening was not triggered without red light (Shimazaki *et al.*, 2007). It was also shown that photosynthesis in guard cell chloroplast is essential in maintaining efficient turgor control (Azoulay-Shemer *et al.*, 2015). Hence, the red light-induced stomatal opening is more complex.

On the other hand, C_4 photosynthesis is efficiently coordinated with its light phase; hence, greater C_i response during light fluctuations. The indirect response elicits a substantial effect on *Zea mays* stomata and becomes increasingly sensitive to changes in C_i when exposed to different irradiances, particularly at low light (Sharkey & Raschke, 1981). Similar responses were observed in C_4 *Amaranthus sp.* (Huxman & Monson, 2003).

1.3.5 Responses of stomatal conductance and morphology to the environment

The primary driver for the evolution of C_4 photosynthesis is thought to be a period of low (glacial) atmosphere [CO_2] during the Oligocene (**Figure 1. 3**; Ehleringer *et al.*, 1997; Sage, 2004; Christin *et al.*, 2008). Growth under glacial [CO_2] (gCO_2) conditions promoted increased in stomatal numbers compared to the current atmospheric [CO_2] (Woodward, 1987; Woodward & Kelly, 1995). Under [CO_2] limitation, stomata generally open while elevated [CO_2] ([eCO_2]) stimulates stomatal closure both under the presence or absence of light (Assmann, 1999; Lawson *et al.*, 2011). For both C_3 and C_4 leaves, [gCO_2] elicits increased g_s but to a greater extent in C_3 leaves (Sage & Coleman, 2001; Maherali *et al.*, 2002; Pinto *et al.*, 2014; Watson-Lazowski *et al.*, 2019). In *Arabidopsis* leaves, [gCO_2] increased stomatal density by 42% (Li *et al.*, 2014). O the other hand, acclimation to [eCO_2]

resulted to lower stomatal numbers, stomatal conductance, and sensitivity to [CO_2] (Woodward & Kelly, 1995; Medlyn *et al.*, 2001; Maherali *et al.*, 2002; Leakey, 2009; Lawson *et al.*, 2011; Xu *et al.*, 2016).

Growth under high light stimulated an increase in stomatal density (SD) in tomato (Gay & Hurd, 1975) and tobacco (Thomas *et al.*, 2004) while both SD and g_s in *Arabidopsis* SSD-1 mutants (Schlüter *et al.*, 2003). Similarly, tree species like *Eucalyptus globulus* leaves exposed to full sun had higher SD and stomatal pore lengths than leaves under 10% sunlight (James & Bell, 2000). Exposure to shade in tobacco leaves (Thomas *et al.*, 2004; Gerardin *et al.*, 2018) and *Coffea arabica* (Pompelli *et al.*, 2010) led to decreased stomatal density and index, but not stomatal size. *In this project, I seek to elucidate how stomatal morphology and function control iWUE in C_3 and C_4 grasses acclimated to low light and [CO_2]* (***Knowledge Gap 1***).

1.3.6 Guard cell ion fluxes

The fluxes of a multitude of ions between the guard cells and subsidiary cells are the cardinal feature of rapid stomatal control in grasses. Most studies were focused in three grass crops, *Z. mays, O. sativa,* and *H. vulgare* in determining the role of ions and respective transporters towards understanding the ion fluxes in grass stomata (Chen *et al.*, 2017). In mature paracytic stomata, the subsidiary cells act as a reservoir of ions which are exchanged between the two cell types (Mumm *et al.*, 2011). This sophisticated morphology allows for the observation of stomatal opening and closure in isolated epidermal leaves (Pallaghy, 1971). In both dumbbell and kidney-shaped stomata, the main osmolyte implicated for stomatal movement is K^+ (Mumm *et al.*, 2011; Chen *et al.*, 2017). The mechanisms of light-induce stomatal opening involving the uptake of K^+ ions were discussed above (**Section 1.3.4**).

In addition to light, phytohormones also play a role in light-induced stomatal opening. The most studied of which is abscisic acid (ABA). During drought and water stress, ABA from chloroplasts and those synthesised in the roots accumulate in the guard cell and activates a cascade of ion and solute reaction that promotes stomata closure (Garcia-Mata & Lamattina, 2007). Recently, it has been found out that nitrous oxide (NO) and Ca^{2+} accumulate and interact upstream of ABA reaction in order to inhibit light-induced stomatal opening

(Garcia-Mata & Lamattina, 2007). In the same way, it also acts as a signal for inwardly rectifying K^+ channels to close, thereby inhibiting K^+ influx and activates channels for anion efflux (Chen *et al.*, 2010a). This anion efflux channels include S-type and R-type anion channels that promote passive efflux of anions, causing membrane depolarisation and coordinated efflux of K^+ through outward-rectifying K^+ channels (Chen & Blatt, 2010). Here the role of Ca^{2+} acts as a secondary ionic messenger during ABA-mediated stomatal closure (Schroeder & Hagiwara, 1989). The purpose of cytosolic Ca^{2+} is to down-regulate inward rectifying K^+ channel activity which then reduces water uptake and thus functions for stomatal closure (Laanemets *et al.*, 2013a,b). The interactions between ions and transporters are illustrated in **Figure 1. 11.**

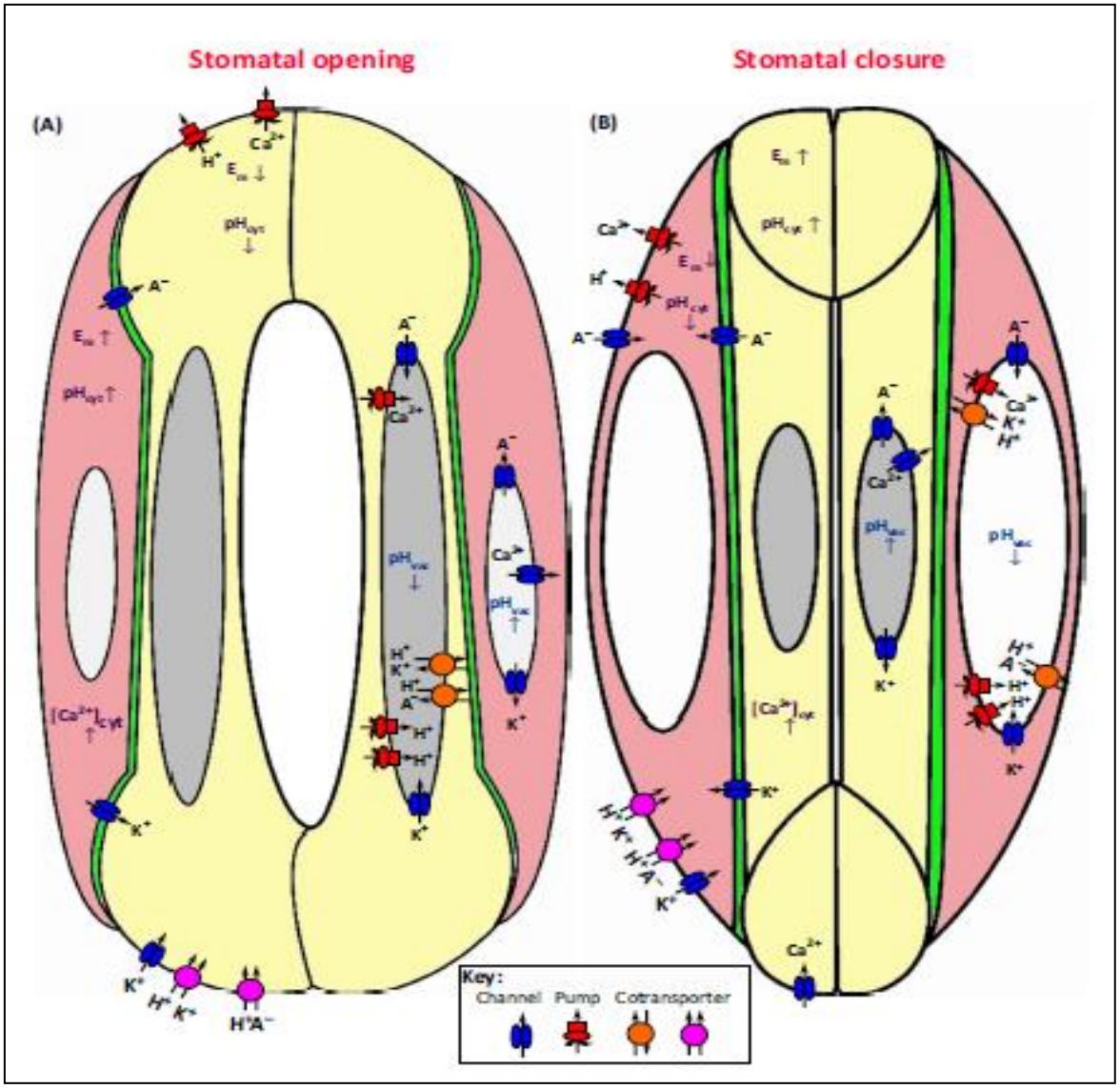

Figure 1. 11 Ion flux mechanisms and interactions in grass stomata during stomatal opening (A) and closing (B).

The process of stomatal opening involves H^+ extrusion, K^+ influx, reduced membrane potential and cytoplasmic Ca^{2+}, and pH drop in subsidiary cells (SC). Conversely, stomatal closure involves increased cytoplasmic $Ca^{2+,}$ thereby increasing K^+ efflux and elevated pH and membrane potential in SC. Subsidiary cells are coloured pink while guard cells are in yellow. Figure source: Chen *et al.* (2017). Abbreviations: A^-, anion; $[Ca^{2+}]$cyt, cytoplasmic $[Ca^{2+}]$; E_m, membrane potential; pH_{cyt}, cytoplasmic pH; pH_{vac}, vacuolar pH.

1.3.7 Microelectrode ion flux estimation (MIFE)

MIFE is a non-invasive ion-specific electrophysiological technique that allows measurement of ion fluxes in single cells or tissues (Cuin *et al.*, 2011; Shabala *et al.*, 2012). The technique measures real-time fluxes of specific ions across membranes on intact plants, tissues, and cells. Microelectrodes are filled with respective ion-selective ionophores that permit the passage of specific ions. It is then focused on the cell or tissue of interest and measures two specific positions: one near the cell and one away from the cell (**Figure 1. 12**). The difference in the ion concentration is registered, and ion flux is calculated using basic planar geometry by Newman, (2001). Several studies have utilised the MIFE technique such as the examination of sodium fluxes in barley roots under salinity stress (Chen *et al.*, 2005), leakiness of different ions in soybean leaf mesophyll subjected to drought stress (Mak *et al.*, 2014), and fluxes of major stomatal ions in *Arabidopsis* guard cells (Pornsiriwong *et al.*, 2017; Zhao *et al.*, 2019).

The MIFE assay utilised by Chen *et al.*, (2012), Pornsiriwong *et al.*, (2017), and Zhao *et al.*, (2019) was adapted for examining grass stomatal K^+ fluxes. Utilising this electrophysiological technique in studying stomata of grasses acclimated to $[CO_2]$ and light perturbations will give insights on the responses of major ions brought about by acclimation. Importantly, this technique has not been used before to compare the guard cell fluxes across photosynthetic types. *Employing this technique will give insights into whether C_3 or C_4 stomata possess different ion flux responses (**Knowledge Gap 2**).*

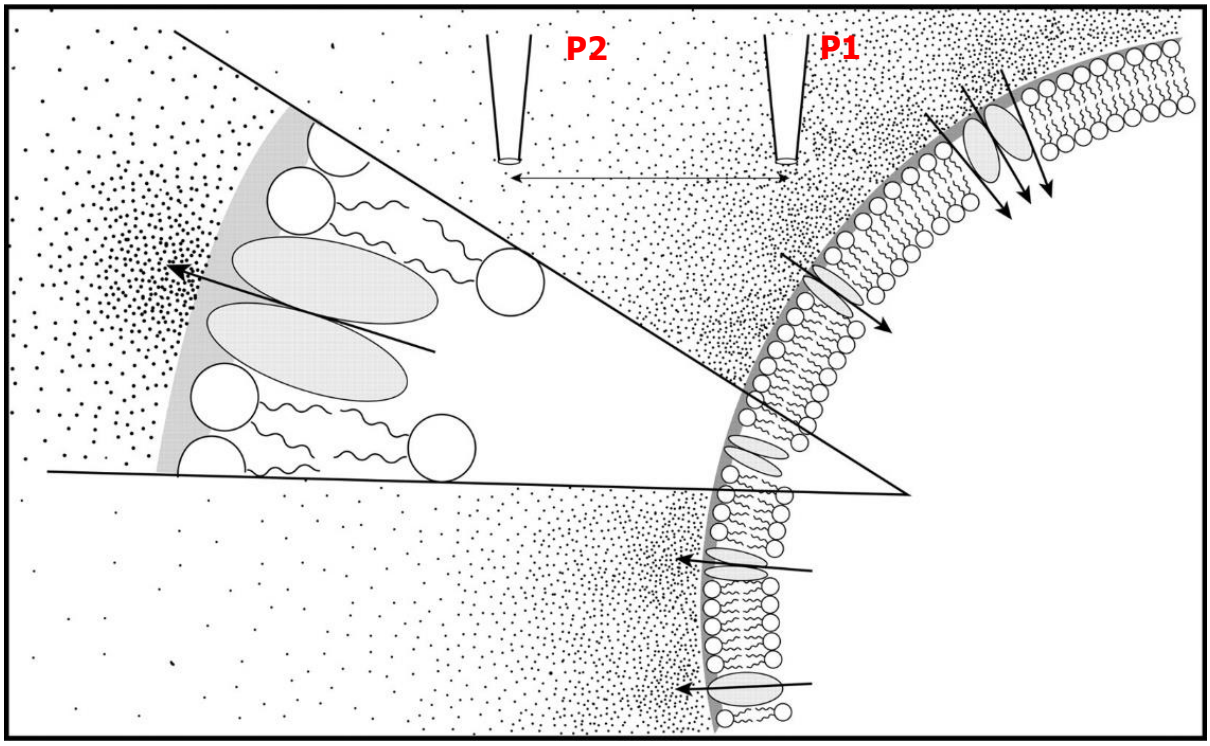

Figure 1. 12 The non-invasive mechanism of microelectrode ion flux estimation.

Microelectrodes are precisely focused near the cell (P1) and further away (P2) where the difference in ion concentration is measured. During ion uptake, the ionic concentration in P1 is usually lower compared to the concentration at P2. The reverse is true when observing ion extrusion from the cell. This difference is calculated, and ion uptake or extrusion is determined. Figure source: Smith & Trimarchi (2001).

1.3.8 Stomatal kinetics and iWUE

Stomata constantly respond to changing light intensity on a scale of seconds through to seasons (Lawson & Vialet-Chabrand, 2018). Stomatal opening and closing usually occur at a slower rate than photosynthetic activation (**Figure 1. 13)**, creating asynchrony between [CO_2] uptake and [H_2O] loss which to an extent, compromises iWUE (Vialet-Chabrand *et al.*, 2017a; Deans *et al.*, 2018; Lawson & Vialet-Chabrand, 2018). The speed of g_s and A_{net} response could be described and quantified using a sigmoidal model (Vico *et al.*, 2011; Elliott-Kingston *et al.*, 2016; McAusland *et al.*, 2016; Deans *et al.*, 2018) and the amount of excessive transpiration and forgone photosynthesis during transient light fluctuations could be estimated (**Figure 1. 13;** (Deans *et al.*, 2018; Lawson & Vialet-Chabrand, 2018). During periods of short and long term light perturbations, the rate of photosynthesis decreases following stomatal closure and deactivation of photosynthetic enzymes (Lawson & Blatt,

2014; Vialet-Chabrand *et al.*, 2017a; Deans *et al.*, 2018; Lawson & Vialet-Chabrand, 2018). While there is little gain in photosynthesis during low light, slower closing stomata thus tend to lose more water via transpiration. Conversely, during periods of illumination, faster stomatal opening decreases potential forgone photosynthesis (Deans *et al.*, 2018; Lawson & Vialet-Chabrand, 2018). Speedy stomatal dynamics is therefore advantageous during periods of environmental stress such as drought and transient light fluctuations in the open environment (McAusland *et al.*, 2016; Qu *et al.*, 2017; Vialet-Chabrand *et al.*, 2017b; Deans *et al.*, 2018).

Between plant groups possessing kidney-shaped stomata and possessing C_3 photosynthetic type, Deans *et al.*, (2018) demonstrated that shade-adapted leaves have a faster stomatal opening but slower stomatal closure speeds due to the ecological adaptation for maximal light-use. On the other hand, ferns and gymnosperms were also shown to have faster stomatal opening compared to angiosperms (Deans *et al.*, 2018; Xiong *et al.*, 2018). Between stomatal sizes, Elliott-Kingston *et al.*, (2016) showed that there was no relationship between stomatal size and stomatal speed during light transitions in a broader range of species but rather those that diversified during the glacial [CO_2] period possessed faster stomatal response. Comparing between stomatal morphologies, the dumbbell-shaped stomata showed faster stomatal opening and closing while between photosynthetic types, C_4 stomata showed faster stomatal closure than C_3 stomata (McAusland *et al.*, 2016).

Hence, dynamic stomatal responses are also critical for the optimisation of iWUE, in addition to advanced stomatal morphology and patterning (Cai *et al.*, 2017b; Vialet-Chabrand *et al.*, 2017b; Lawson & Vialet-Chabrand, 2018; Slattery *et al.*, 2018). *In this project, I investigate how stomatal opening and closing rates in response to light transition differ between C_3 and C_4 grasses acclimated to low light and [CO_2] (**Knowledge Gap 2**).*

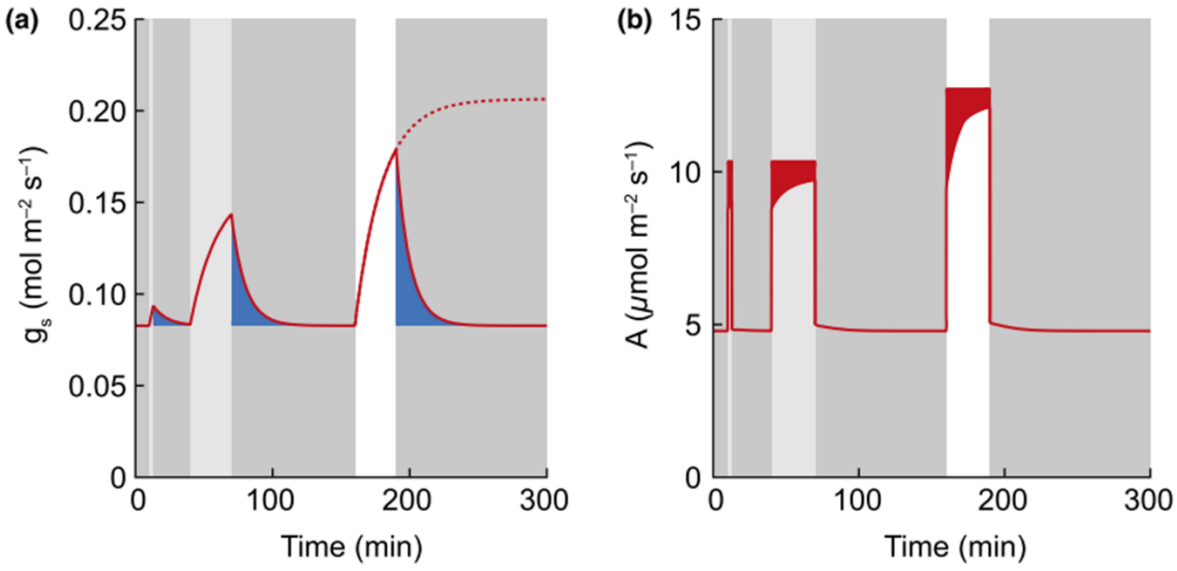

Figure 1. 13 Non-synchronous behaviour of g_s and A_{net} during transitions from high light to low light.

Grey shading shows when irradiance is decreased, and white shade represents periods of illumination. Blue shading represents water loss due to g_s being slower than A_{net} (**A**) while red shading represents forgone photosynthesis due to g_s limitation (**B**). Red dashed lines represent possible steady-state values if the light was not decreased. Figure source: Lawson & Vialet-Chabrand (2018).

1.4 Carbon Isotope Discrimination and WUE

The carbon from the major photosynthetic substrate, CO_2, exists in two stable carbon isotopes, ^{13}C and ^{12}C each with a slight difference in atomic mass and abundance. This variation results in different physical properties, including kinetics (i.e. diffusion) and thermodynamics (Brüggemann *et al.*, 2011; Tcherkez *et al.*, 2011; Cernusak *et al.*, 2013). During leaf biochemical reactions, the lighter carbon isotopologue, $^{12}CO_2$, is preferentially used hence fractionation or $^{13}CO_2$ discrimination occurs (Brüggemann *et al.*, 2011). This fractionation phenomenon alters the isotopic composition of the plant such that it contains lesser proportions of ^{13}C compared to the original proportions from the atmosphere (source).

1.4.1 Carbon isotope composition

The carbon isotope composition or carbon isotope signature (denoted as small Greek delta: $\delta^{13}C$), expressed in per mil (‰), is the molar abundance ratio of the sample tested (R_{sample}) and the standard (R_{std}). That is, $\delta^{13}C = (R_{sample}-R_{std})/(R_{std})$, where $R = {}^{13}C/{}^{12}C$ of either the sample or standard (Farquhar *et al.*, 1989; Tcherkez *et al.*, 2011). The international standard for carbon isotope measurement is the carbonate Vienna Pee Dee Belemnite (VPDB) with an *R*-signature of 0.0112372 (Werner & Brand, 2001). The current atmospheric $\delta^{13}C$ is estimated to be -8‰ with respect to VPDB. During photosynthesis, the two carbon isotopologues are differentially integrated into different metabolic pools such as structural compounds, storage metabolites or respired back to the atmosphere (Cernusak *et al.*, 2013). Plant synthetic processes (the source of almost all reduced carbon in nature) thus pass their reduced signature on, and biogenic materials have a negative $\delta^{13}C$ compared to the atmosphere (Craig, 1957; Tcherkez *et al.*, 2011; Ehleringer & Cerling, 2014). In this thesis, I described ^{13}C-enriched compounds as having 'heavier' $\delta^{13}C$ and ^{13}C-depleted compounds as having 'lighter' $\delta^{13}C$.

Another term that describes the degree of depletion of the heavier isotopologue is the photosynthetic carbon isotope discrimination (denoted as big Greek delta: $\Delta^{13}C$). Farquhar & Richards, (1984) defined $\Delta^{13}C$ as R_a-R_p/R_p where R_a is the $^{13}C/^{12}C$ of the atmosphere, and R_p is the $^{13}C/^{12}C$ of the plant photosynthetic product. The advantage of using $\Delta^{13}C$ over $\delta^{13}C$ is that the former takes into account the $^{13}C/^{12}C$ of the source. $\Delta^{13}C$ has been used as a

screening tool for leaf-level WUE_i as Farquhar & Richards, (1984) developed a model relating it to the integrated C_i/C_a of the leaf among C_3 leaves.

Assay for $\delta^{13}C$ is traditionally carried out using elemental analysers (EA) coupled to isotope ratio mass spectrometry (IRMS) (De Laeter & Peiser, 2003; Godin & McCullagh, 2011; Elsner *et al.*, 2012; Zhang, 2013). In this technique, bulk samples such as whole leaves, are converted to gases (H_2, CO_2, CO, N_2, and SO_2) via combustion (1000°C) through oxidation and reduction reactions (**Figure 1. 14**). Gases are carried through the separation chambers using an inert gas such as helium while sulphur-containing gases are trapped in a column containing silver (**Figure 1. 14**). Water is separated from the other gases using a magnesium perchlorate trap while the rest of the gases are separated using a gas chromatography (GC) column by virtue of their different molecular size and adsorption kinetics (**Figure 1. 14**). CO_2 isotopologues are then introduced to IRMS via an open split (Zhang, 2013; **Figure 1. 14**). The high throughput capacity of this method allows for screening a large number of samples (Cernusak *et al.*, 2013). On the other hand, the development of tuneable diode laser adsorption spectroscopy (TDL) is a recent advancement of the traditional IRMS assay whereby concurrent measurements of $\Delta^{13}C$ during gas exchange measurement could be achieved. Gases going in and out of the infrared gas analysers are measured, and this provides instantaneous measurements of carbon fluxes during CO_2 assimilation (von Caemmerer *et al.*, 2014). This TDL measurement is interchangeably referred to as on-line/concurrent isotope assay.

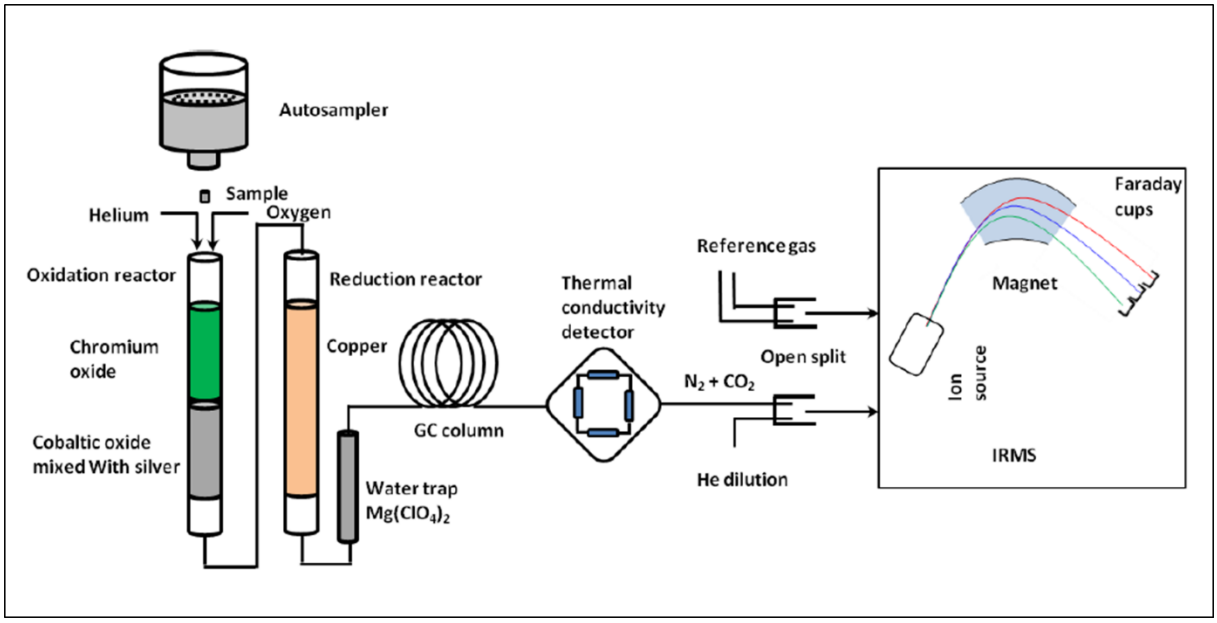

Figure 1. 14 The schematic diagram for elemental analyser (EA) coupled to isotope ratio mass spectrometry (IRMS)

Samples in tin capsules are individually placed in an autosampler carousel and undergo combustion/oxidation/reduction reactions and water separation. Gases enter through an open split unto the IRMS and Faraday cups detect different isotopologues. Figure source: Zhang (2013).

1.4.2 Carbon isotope discrimination in C_3 plants

In a simplified manner, C_3 carbon isotope discrimination can be expressed as:

$$\Delta = a + (b-a)\frac{Ci}{Ca} \qquad \text{equation 1.1}$$

Where a represents the kinetic fractionation brought about by stomata (4.4‰), b is the fractionation exerted by Rubisco (29‰), and $\frac{C_i}{C_a}$ represents the ratio of intercellular CO_2 to atmospheric CO_2. Recently, a ternary correction proposed by Farquhar & Cernusak, (2012) to take into account the effect of transpiration on the diffusion of CO_2 between the atmosphere and intercellular spaces (See Farquhar & Cernusak, 2012) for the detailed explanation about the ternary impact). Leaf dry matter $\delta^{13}C$ of C_3 plants falls on a wide range between -23 to -32‰, reflecting the significant influence of Rubisco on carbon metabolism in this photosynthetic type (**Figure 1. 15**). Carbon isotope discrimination in C_3 plants has

been straightforward in reflecting the integrated $\frac{C_i}{C_a}$ of the leaf (**Figure 1. 16**). Thus, it has been used as a tool in selecting lines with improved water use efficiency, most notably the selection of the Australian wheat varieties, Drysdale and Reese (Farquhar & Richards, 1984; Condon *et al.*, 2004).

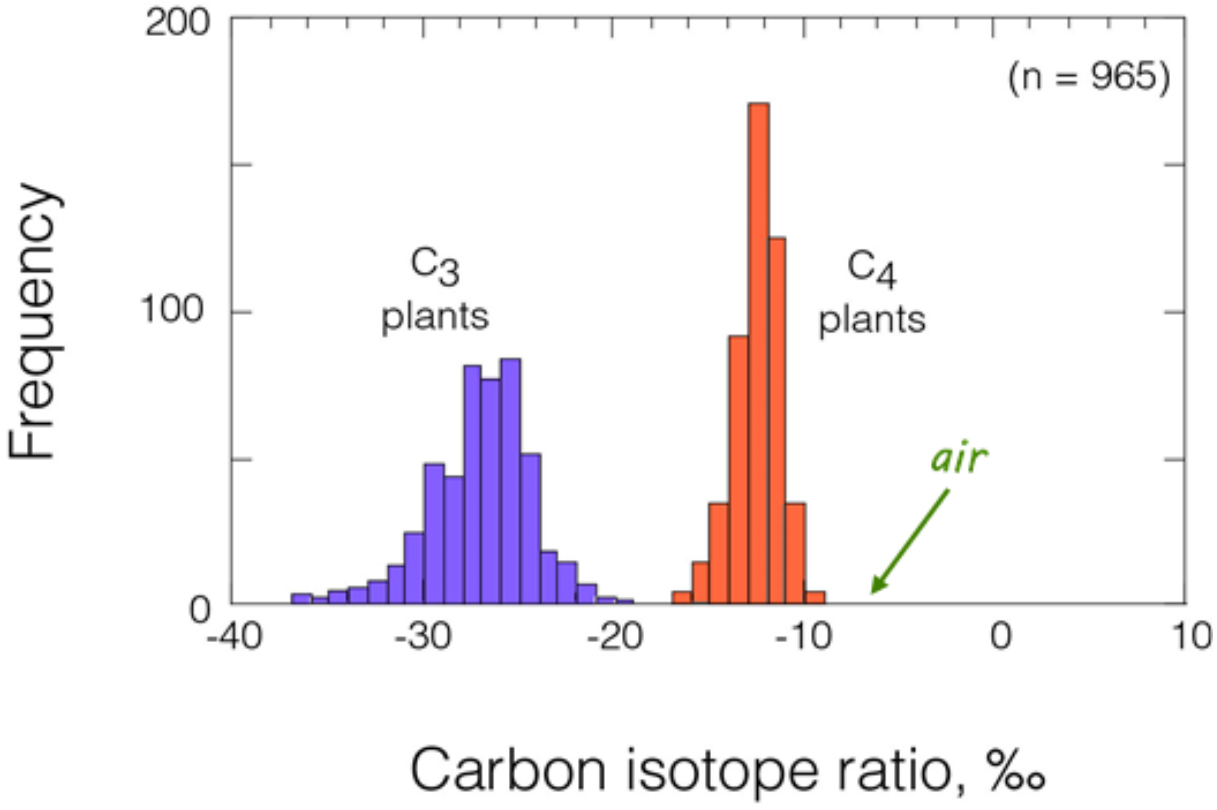

Figure 1. 15 Variations in carbon isotope composition ($\delta^{13}C$) in C_3 and C_4 plants.

The histogram depicts wider variations and more negative $\delta^{13}C$ in C_3 plants compared to C_4 plants and in comparison, with the atmospheric $\delta^{13}C$ (green arrow). The figure was adapted from Ehleringer & Cerling (2014).

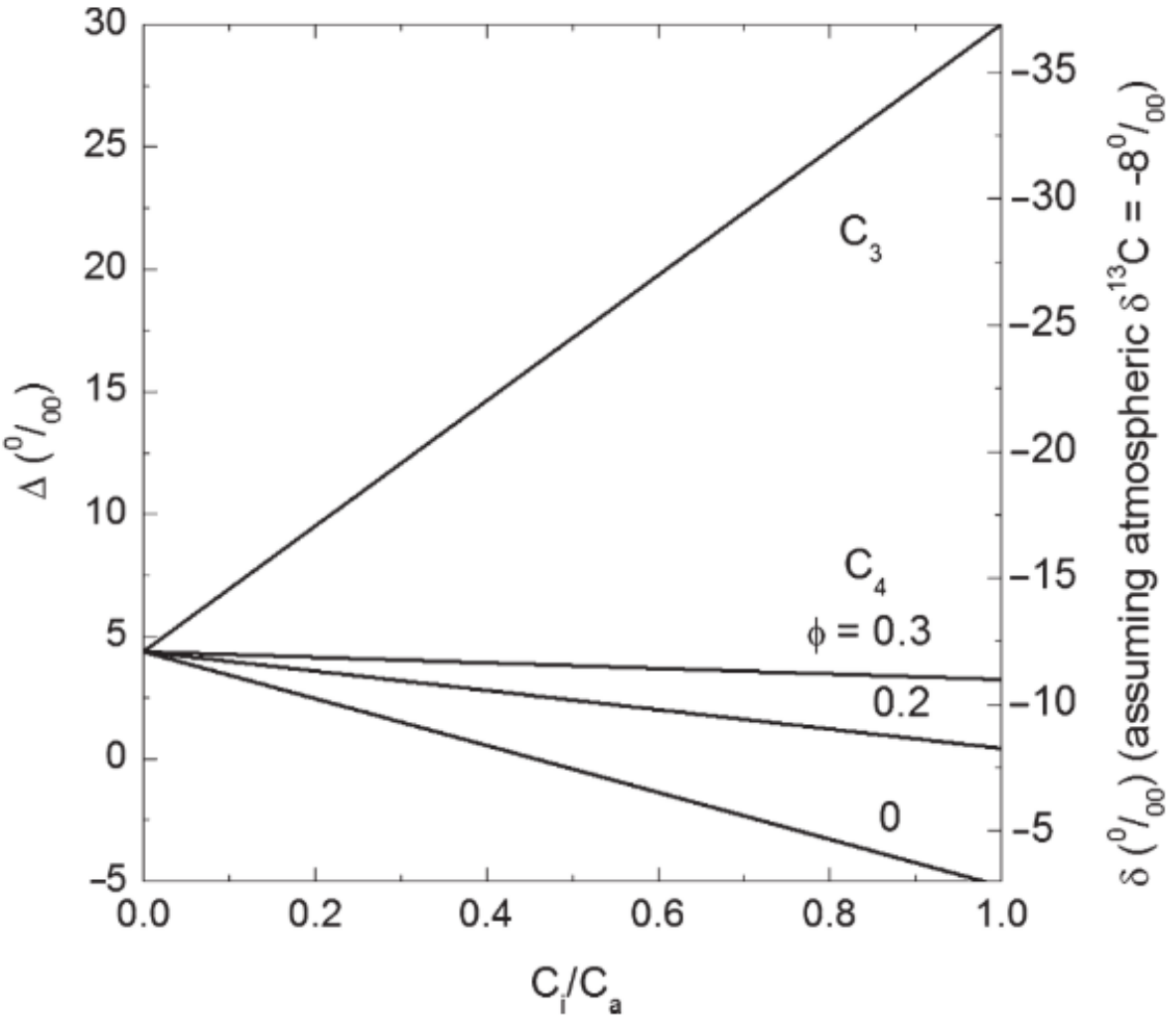

Figure 1. 16 A modelled relationship between Δ and C_i/C_a in both C_3 and C_4.

The positive linear relationship in C_3 makes it simpler to screen for genotypes with improved WUE as the main driver for Δ is C_i/C_a. In C_4 species, there is a varied negative linear response depending upon the extent of leakiness (ϕ) Figure source: Ghannoum *et al.* (2011).

1.4.3 Carbon isotope discrimination in C_4 plants

An expression of carbon isotope discrimination in C_4 plants was developed by Farquhar (1983) as follows:

$$\Delta^{13}C = a + (b_4 + (b_3 - s)\phi - a)\frac{C_i}{C_a} \qquad \text{equation 1.2}$$

where: *a* (4.4 ‰) is the fractionation during diffusion of CO_2 in the air; b_4 (-5.7 ‰) is the net fractionation contributed by PEPC discrimination (2.2‰) and conversion and dissolution of CO_2 to bicarbonate at equilibrium (-7.9 ‰); b_3 (29-30 ‰) is the fractionation due to Rubisco discrimination; *s* (1.8 ‰) is the fractionation due to CO_2 leakage out of BSC, and ϕ is bundle sheath leakiness (varies). Leakiness (ϕ) is the proportion of CO_2 fixed by PEPC that leaks back to the mesophyll tissues. It is a measure of the extent to which PEPC rate exceeds Rubisco (Henderson *et al.*, 1992a), and hence a proxy measure of CCM efficiency (von Caemmerer & Furbank, 1999). Leakiness also reflects the balance between the C_3 and C_4 cycle activities. For example, reduction of Rubisco by an antisense technology in transgenic *Flaveria bidentis* (a C_4 species) leads to reduced CO_2 assimilation rates, increased bundle-sheath CO_2 concentration, and leakiness (Von Caemmerer *et al.*, 1997). In transgenic *Flaveria* plants with less than 40% of wild-type NADP-ME activity, CO_2 assimilation rates at high intercellular CO_2 were significantly reduced, whereas the in vitro activities of both PEPC and Rubisco were increased. Consequently, Δ and calculated leakiness were lower (Pengelly *et al.*, 2012). Leakiness can be estimated by combining leaf gas exchange measurements with stable carbon isotope discrimination during photosynthesis using mass spectrometry (Henderson *et al.*, 1992a,b) or tuneable diode laser (Sonawane *et al.*, 2017). Leakiness can also be estimated from leaf dry matter carbon isotope composition (Cano *et al.*, 2019).

The CCM in C_4 species leads to a narrow range in leaf dry matter $\delta^{13}C$ values (-12 to -15‰), allowing the differentiation between photosynthetic types (**Figure 1. 15**). ϕ is one of the significant sources that drive variations in C_4 $\Delta^{13}C$. However, it is shown to be relatively constant (0.2) under various conditions except during low light conditions (Henderson *et al.*, 1992a; Cousins *et al.*, 2008; Sonawane *et al.*, 2017, 2018). Importantly, Hattersley (1982) identified a 1.35‰ difference in leaf $\delta^{13}C$ across C_4 grasses representing three biochemical subtypes grown in controlled conditions (**Figure 1. 17**). This pattern has been observed when (Ghannoum *et al.*, 2001a, 2002) compared leaf dry matter $\delta^{13}C$ of NAD-ME and NADP-ME grasses across different growth treatments (**Figure 1. 18**). Moreover, the variations observed were reflected in leaf cellulose $\delta^{13}C$ regardless of growth conditions.

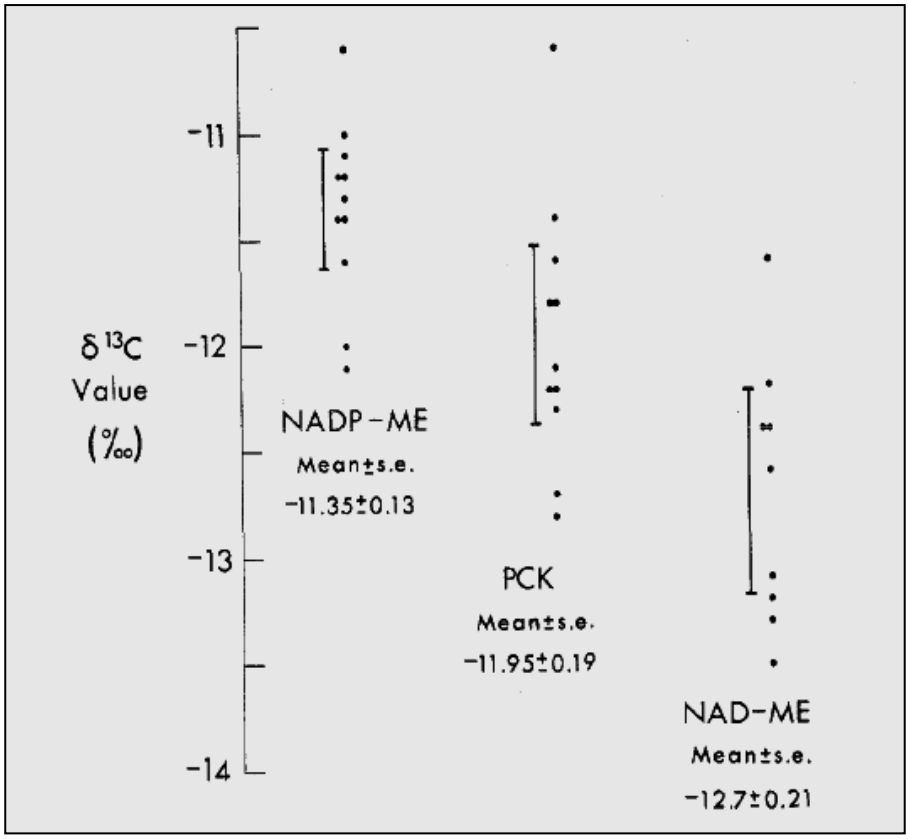

Figure 1. 17 Variations in whole leaf dry matter $\delta^{13}C$ among C_4 biochemical subtypes.

NADP-ME shows more enriched $\delta^{13}C$ than NAD-ME species. Figure source: Hattersley (1982).

Early studies by Henderson *et al.,* (1992a) revealed that carbon isotope discrimination in C_4 species was greater in leaf dry matter than short-term online measurements. Interestingly, Cousins *et al.,* (2008) found no difference in photosynthetic $\Delta^{13}C$ between NAD-ME and NADP-ME using concurrent measurements of gas exchange coupled with a tuneable diode laser (TDL), while differences in dry matter leaf $\delta^{13}C$ remained between the two C_4 subtypes. Furthermore, $\Delta^{13}C$ responded similarly between the C_4 subtypes to a range of leaf temperatures and only showed a difference between NAD-ME and NADP-ME at very low light intensities (Sonawane *et al.,* 2017, 2018). Taken together, these observations suggest that non-photosynthetic factors (i.e., post-photosynthetic fractionation) contribute to the observed variations of leaf dry matter $\delta^{13}C$ among the C_4 subtype.

It is essential to understand the impact of post-photosynthetic fractionation on leaf $\delta^{13}C$ for a number of reasons. For example, this will help us elucidate the differences between the C_4 subtypes and hence better understand C_4 photosynthesis. In addition, if leaf $\delta^{13}C$ will be

*used as a tool for screening species with improved WUE, the fractions that have significant impacts on dry matter carbon isotope composition can be used as a more reliable proxy to leaf $\delta^{13}C$ (**Knowledge Gap 4**).*

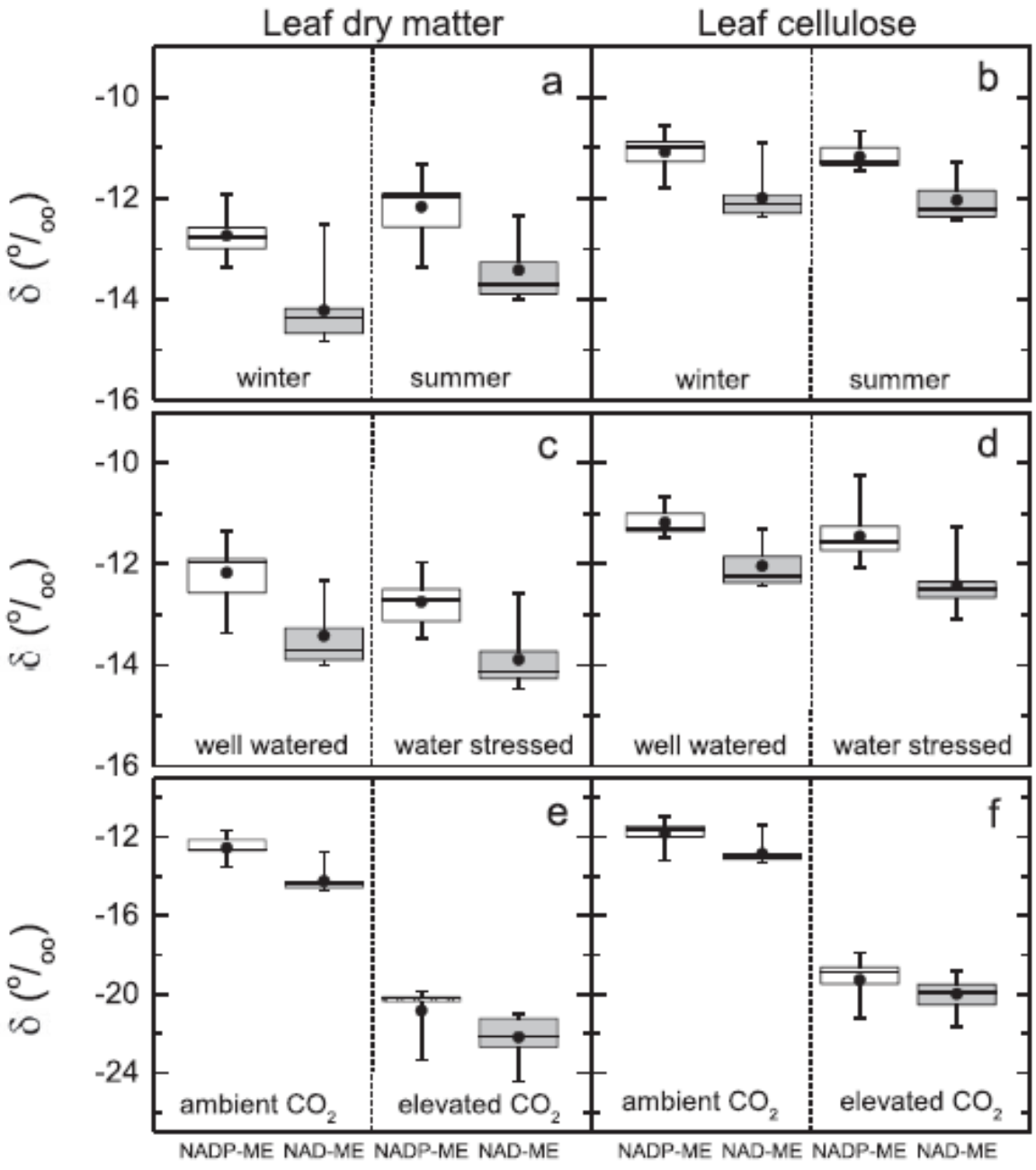

Figure 1. 18 Variations in leaf dry matter $\delta^{13}C$ between NAD-ME and NADP-ME grasses subjected to several growth conditions.

Marked differences in $\delta^{13}C$ of NADP-ME and NAD-ME are evident from the whole leaf dry matter and carried through at the cellulose level under different growth conditions. Figure source: von Caemmerer *et al*. (2014).

1.4.4 Post-photosynthetic fractionation

Post-photosynthetic fractionation is a general term which refers to the fractionation steps after Rubisco carboxylation. This type of fractionation includes post-carboxylation fractionation, respiratory fractionation and transport (Brüggemann et al., 2011). These processes alter the isotopic signatures imprinted on the newly assimilated metabolite during the downstream metabolic process (Werner et al., 2011). In this study, I focused on short-term sugar metabolism as immediate post-carboxylation products.

1.4.5 Post-carboxylation fractionation

Post-carboxylation fractionation involves the fractionation steps right after Rubisco carboxylation. The first step during post-carboxylation takes place during aldol condensation of triose phosphates yielding fructose 1,6, bisphosphate and ultimately starch (**Figure 1. 19**). This reaction favours ^{13}C to be incorporated in the third and fourth carbon atoms of the hexoses by 3-4‰ (Tcherkez *et al.*, 2011) while leaving behind light triose phosphates (Brüggemann *et al.*, 2011). As a consequence, the aldolase and transketolase fractionation enriches ^{13}C in chloroplastic fructose-phosphate and glucose-6-phosphate compared to dihydroxyacetone phosphate, thereby enriching transitory starch and depleting the remaining triose phosphate molecules (Tcherkez *et al.*, 2011). These triose-phosphate molecules are transported back to the cytosol to produce sucrose. Hence day-sucrose becomes depleted with ^{13}C. In addition, enzymes that consume glucose as a substrate (i.e. pentose phosphate pathway and glycolysis) can cause variations in ^{13}C. By virtue of mass balance, the preferential selection of ^{12}C should lead to an enrichment in ^{13}C in different carbon positions within the molecule (Tcherkez *et al.*, 2011) and within different metabolic pools.

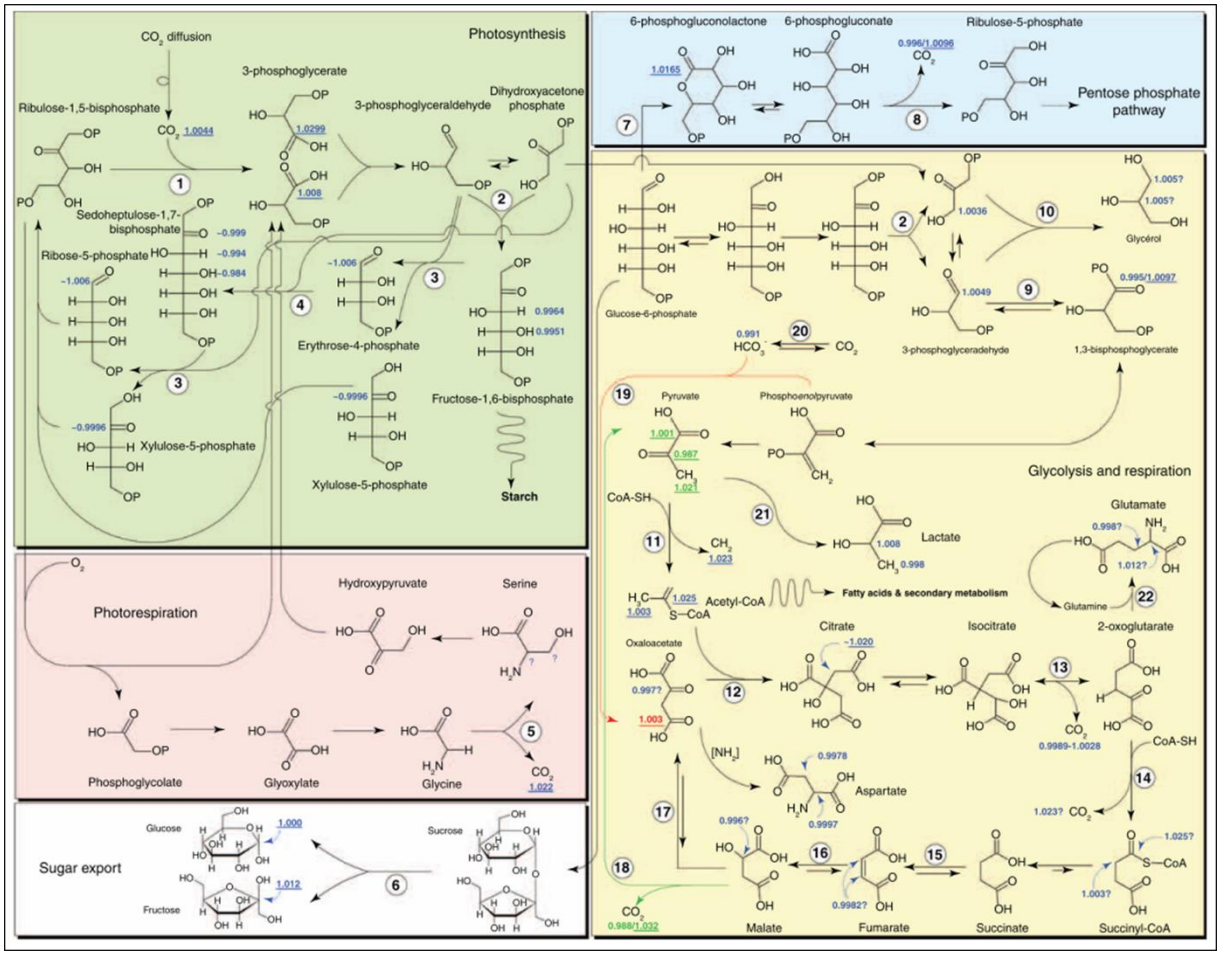

Figure 1. 19 A schematic summary of initial post-carboxylation fractionation during aldolase condensation to starch synthesis (light green box).

Pathways that feed glucose such as pentose phosphate pathway are highlighted in the light blue section. Reactions proceeding to glycolysis and respiration are highlighted in the yellow box. Underlined blue values indicate known isotope effects involved in plant primary metabolism. Figure Source: Tcherkez *et al.* (2011).

*The C_4 subtypes vary in biochemistry, hence contrast in primary metabolites utilised during the C_4 cycle. This would translate to differences in ^{13}C integration within the metabolites and eventually to target structural compound or storage compounds. To my knowledge, no study has considered the impact of post-carboxylation fractionation on the variations of leaf carbon isotope composition among C_4 grasses (**Knowledge Gap 4**).*

1.4.6 A method for measuring carbon isotope composition of soluble sugars

The traditional technique for measuring carbon isotope signature is through the combustion of bulk plant material by an elemental analyser (EA) coupled to isotope ratio mass spectrometry (IRMS; **Figure 1. 14**) (De Laeter & Peiser, 2003; Godin & McCullagh, 2011; Elsner *et al.*, 2012; Zhang, 2013). However, the disadvantage of this method is that it cannot assay the isotope composition of targeted compounds from the bulk sample directly.

Compound-specific isotope analysis (CSIA) is a developing field in stable isotope studies that endeavours in measuring $\delta^{13}C$ of separate metabolites in a complex mixture (Godin & McCullagh, 2011; Elsner *et al.*, 2012). The principle of CSIA assays is based on the separation of metabolites using chromatography (gas or liquid chromatography) followed by gas conversion through chemical oxidation; and then measurements of the carbon isotope composition of individual metabolites using IRMS (blue box, **Figure 1. 20**).

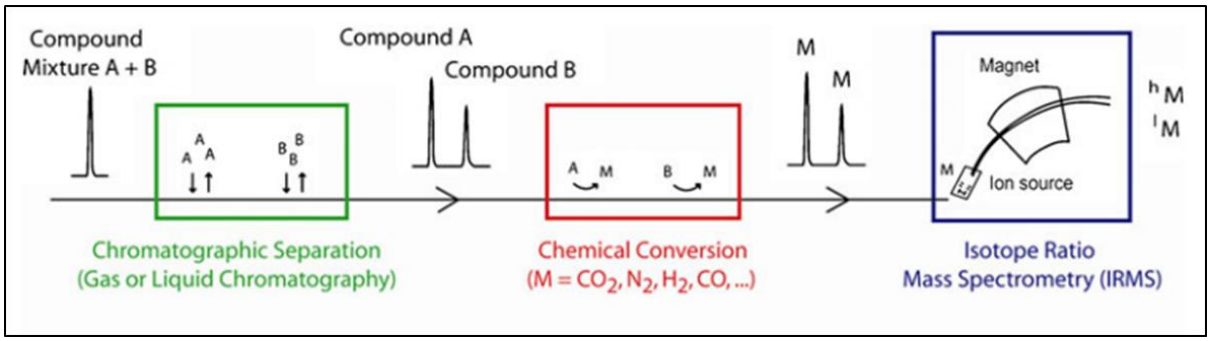

Figure 1. 20 The schematic diagram of GC/LC-based compound-specific isotope analysis

Individual compounds (green box) are separated and converted to gases via oxidation (red box) and enters through the IRMS system carried by helium gas. Figure source: Elsner *et al.* (2012).

In GC-based CSIA (**Figure 1. 21A**), samples are injected using an autosampler and volatilised into the gaseous phase and carried by helium gas. Compounds undergo separation using a long coil of capillary GC column. Individual compounds are converted to CO_2, N_2, and H_2O via oxidation/reduction reactors at very high temperatures (600-950°C); and water is removed using Nafion™ membrane allowing for CO_2 and N_2 to pass through. Consequently, CO_2 is introduced to the IRMS interface via an open split (Hettmann *et al.*,

2005; Elsner *et al.*, 2012; Zhang, 2013). The advantage of GC-based CSIA is a lower detection limit, less laborious preparation, and analysis of several compounds in one run (Zhang, 2013). On the other hand, the drawback of GC-based assays is that non-volatile organic compounds must be derivatised (converted to gaseous metabolites) by silylation, alkylation, acylation, esterification or other methods in order to volatilise the compounds and improve chromatographic separation (Meier-Augenstein, 2004; Morrison *et al.*, 2010; Godin & McCullagh, 2011; Elsner *et al.*, 2012). This derivatisation process means that addition of carbon molecules will complicate the estimation of carbon isotope signatures due to ^{13}C dilution (Gross & Glaser, 2004; Krummen *et al.*, 2008; Godin & McCullagh, 2011)

Meanwhile, the development of LC-based CSIA came in later because the compounds to be separated are in the liquid phase while IRMS requires gaseous detection of CO_2 (Krummen *et al.*, 2004; Boschker *et al.*, 2008; Godin & Fay, 2008; Godin & McCullagh, 2011; Elsner *et al.*, 2012; Zhang, 2013). The LC-based CSIA will aid in the measurement of $\delta^{13}C$ in non-volatile, polar, and thermally-labile compounds such as amino acids and sugars (Godin & McCullagh, 2011). To solve this dilemma, Krummen *et al.*, (2004) introduced an interface that quantitatively converts carbon from separated analytes to CO_2 via an oxidation agent, ammonium peroxodisulfite aided by a weak acid catalyst (dilute phosphoric acid) at high temperature (**Figure 1. 21B**). Similar to GC-based assays, the mixture of compounds is separated in a suitable LC column, and individual baseline-separated peaks is individually oxidised in a wet-chemical oxidiser (WCO) interface (**Figure 1. 21B**). Water is also trapped using Nafion™, and CO_2 is carried by helium gas to the IRMS interface (Krummen *et al.*, 2004; Godin & Fay, 2008; Zhang, 2013). There are several requirements for a successful LC-based CSIA. First, the mobile phase and analytical solutions should be free of contaminating carbons, hence the need to de-gas the solution and exclusive use of ultrapure water carbon-free buffers (Godin & McCullagh, 2011; Zhang, 2013). Second, baseline separation (suitable LC column) of individual analyte peaks should be endeavoured as overlapping peaks leads to inaccurate $\delta^{13}C$ due to mixture of carbons from compound overlap (Godin & McCullagh, 2011). Finally, sample-to-sample carryover contamination (memory) should be examined to obtain accurate results if the sample number is large (Godin & McCullagh, 2011; Skrzypek & Ford, 2018). Currently, there are two commercially available WCO interface in the market, the LC-IsoLink® system (Thermo Electron, Bremen,

Germany) and the Liquiface® interface (Isoprime Ltd., Cheadle Hulme, UK) with the latter having utilised less commonly (See Godin & McCullagh, 2011 review).

For this thesis, the method using wet chemical oxidation system (WCO, Liquiface®) coupled to high-performance liquid chromatography (HPLC), and isotope ratio mass spectrometry (IRMS) was optimised for measuring carbon isotope signature ($\delta^{13}C$) of three key soluble sugars (glucose, fructose and sucrose). *The new system can resolve sugar metabolites both in leaves and known standards in an aqueous solution which could aid in high throughput analysis of metabolite carbon isotope signatures (**Knowledge Gap 3**).*

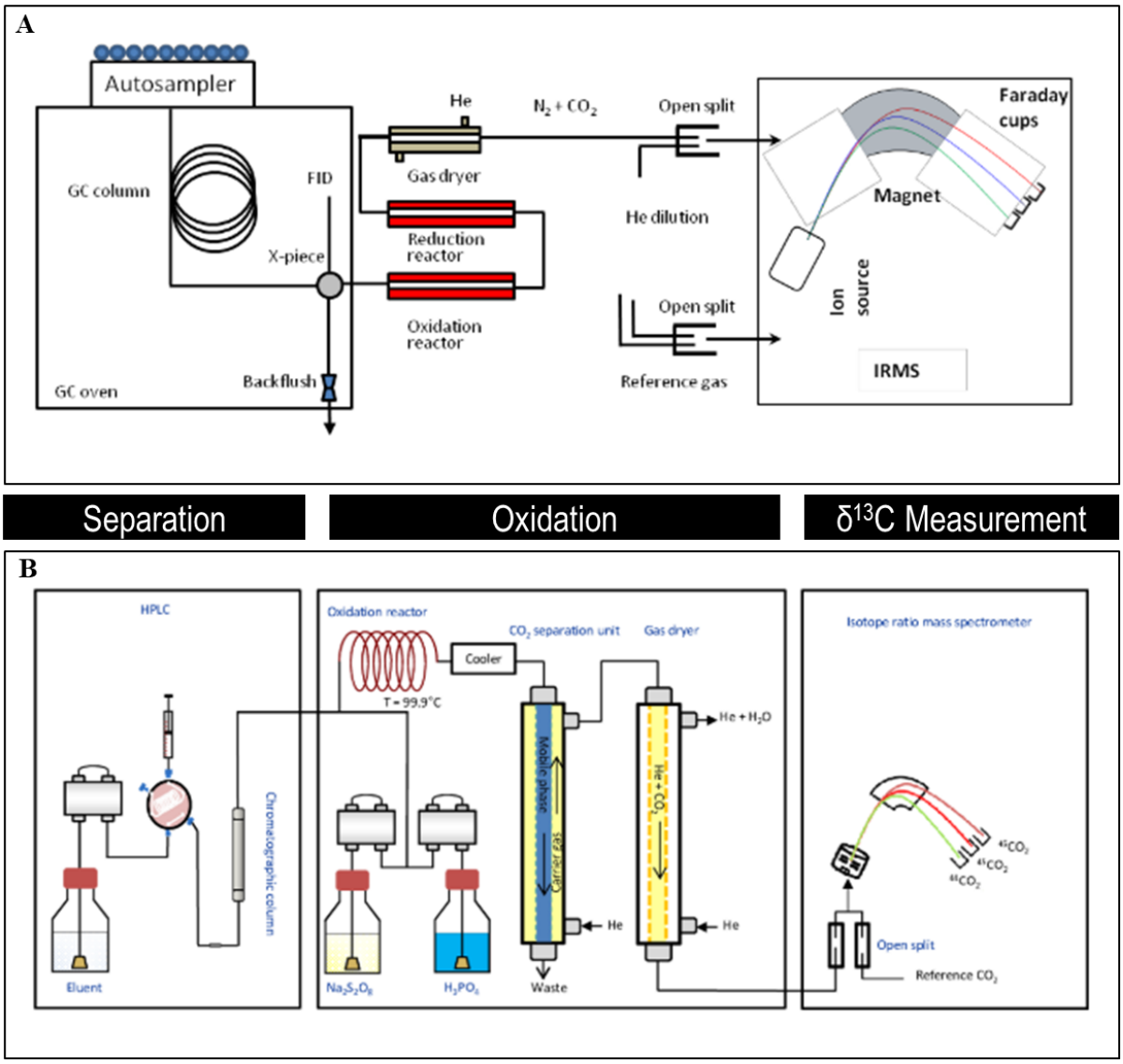

Figure 1. 21 The schematic interface of GC-based (A) and LC-based (B) CSIA

In both CSIA systems, targeted compounds are separated using chromatography followed by heated oxidation then $\delta^{13}C$ assay using IRMS. CO_2 is carried by helium gas. Figure source: Zhang (2013).

1.5 Linking iWUE, Stomata Function, and Carbon Isotope Discrimination in C_4 crops

The ultimate goal of the knowledge generated from studies of grass stomatal function and of the impact of post-photosynthetic fractionation on leaf carbon isotope discrimination in C_4 grasses is to better understand the link between leaf $\delta^{13}C$ and WUE in C_4 crops, such as sorghum. Several studies have utilised $\Delta^{13}C$ as a screening tool to several agronomically important traits, most notably WUE (Farquhar & Richards, 1984; Hubick *et al.*, 1986). Monneveux *et al.*, (2007) used $\Delta^{13}C$ to screen for *Zea mays* lines with tolerance to drought and found out that susceptible lines showed lower $\Delta^{13}C$ than the tolerant inbred lines.

Focusing on sorghum, earlier studies by Hubick *et al.*, (1990) revealed intraspecific variations in $\Delta^{13}C$ among twelve field-grown sorghum genotypes which may indicate differences in transpiration efficiency. They further showed that grain yield was negatively correlated to $\Delta^{13}C$. On the other hand, Henderson *et al.*, (1998), screened 30 lines of sorghum grown in glasshouse and eight lines grown in the field and found a positive correlation between WUE and $\Delta^{13}C$ in both growth conditions (**Figure 1. 22**). A similar positive relationship between $\Delta^{13}C$ and C_i/C_a was also found in two sugarcane (*Saccharum* spp. hybrid) cultivars supplied with water or with NaCl solutions (Meinzer *et al.*, 1994).

A recent study showed that a genomic segment on maize Chromosome 7 influences both carbon isotope composition and water use efficiency, possibly by affecting stomatal properties (Avramova *et al.*, 2019). A genomic link between leaf carbon isotope composition and plant water use efficiency has also been established for a recombinant inbred population of the C_4 grass *Setaria viridis* grown under well-watered and water-stressed conditions (Feldman *et al.*, 2018). Within the same *Setaria viridis* population, leaf $\delta^{13}C$ showed a good relationship with plant WUE (Ellsworth *et al.*, 2019).

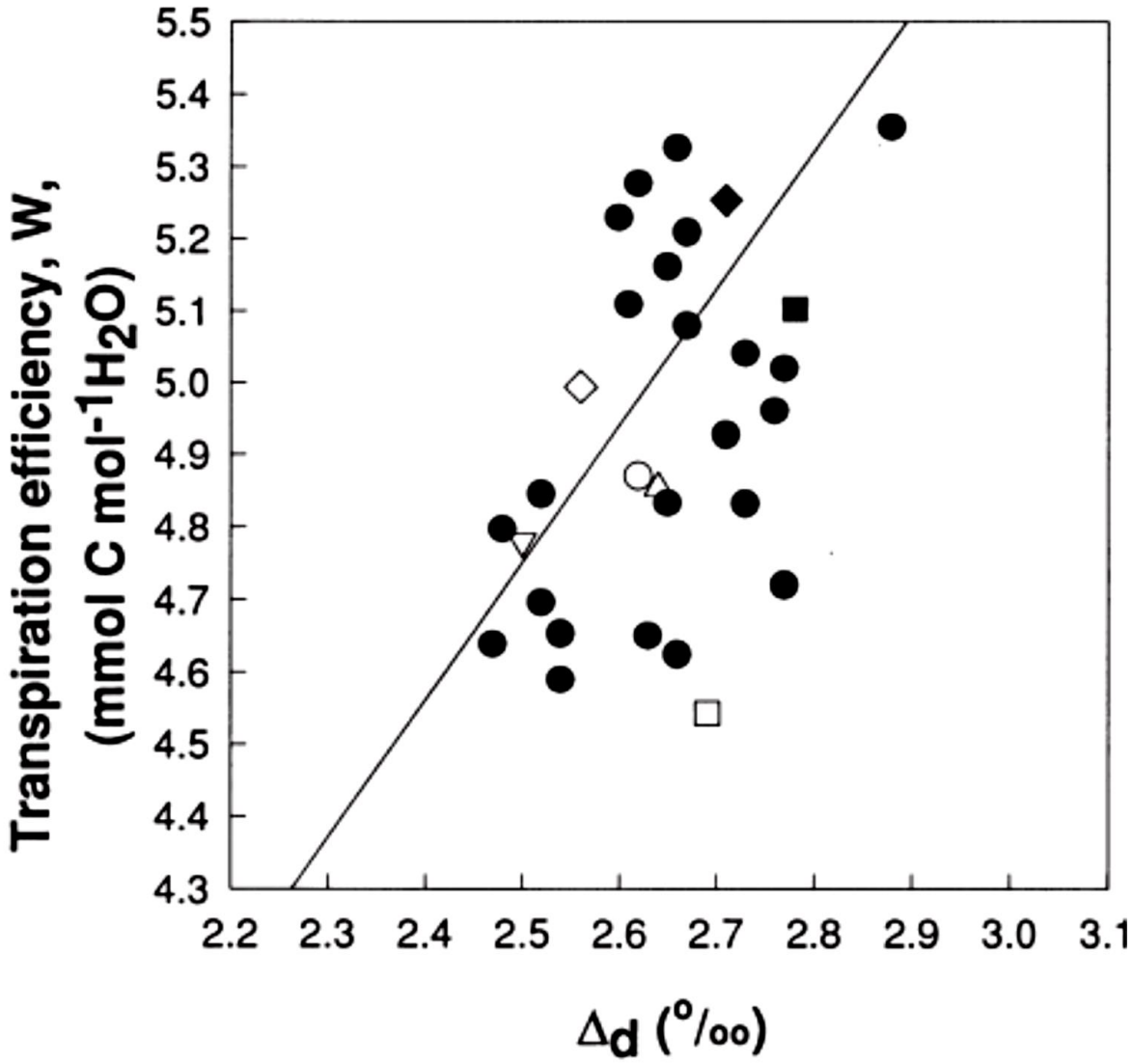

Figure 1. 22 The relationship of leaf dry matter discrimination (Δd) and transpiration efficiency in 30 lines of glasshouse-grown sorghum.

Linear regression equation is as follows: $W = 1.0\Delta_d + 1.93 \times 10^{-3}$; $r^2 = 0.18$, $p<0.05$. Figure source: Henderson *et al.* (1998).

1.6 Knowledge Gaps

Based on the above literature review, the project was designed to address the following knowledge gaps:

Knowledge Gap 1 (Chapter 2)*:* The operation of a CO_2 concentrating mechanism in C_4 grasses endows them with higher iWUE than their C_3 counterparts. However, it is unclear how this relates to underlying stomatal function or varies among the three C_4 biochemical subtypes with growth conditions, especially the two major photosynthetic factors: [CO_2] and light. A better understanding of stomatal responses will allow the exploration and development of molecular targets for breeding crops with high iWUE.

Knowledge Gap 2 (Chapter 3)*:* It remains unclear whether the speed of stomatal responses and guard cell K^+ fluxes in grass leaves differ between photosynthetic pathways (C_3 and C_4) and C_4 subtypes, or how these differences are influenced by the environment (e.g., [CO_2] and light).

Knowledge Gap 3 (Chapter 4)*:* This chapter identified a significant gap in developing an efficient method to analyse the $\delta^{13}C$ of leaf sugars extracted from C_3 and C_4 grasses using a wet chemical oxidiser (WCO) coupled to high-performance liquid chromatography (HPLC) and isotope ratio mass spectrometer (IRMS). Such a method will avoid the extensive chemical derivations required to volatilise the compounds prior to analysis using the traditional elemental analyser IRMS (EA-IRMS) system.

Knowledge Gap 4 (Chapter 5)*:* The contribution of post-carboxylation fractionation, particularly carbohydrate metabolism, to leaf carbon isotope composition ($\delta^{13}C$) is still unresolved among C_4 plants. In particular, it is not well understood why NAD-ME and NADP-ME leaves have different leaf $\delta^{13}C$. Resolving this long-standing puzzle will allow us to better understand how leaf $\delta^{13}C$ varies and how it can be used as a high throughput screen for leaf-level water use efficiency in C_4 plants.

1.7 Aims and Objectives

The overall aim of this PhD project was to investigate the relationship between the superior stomatal control and leaf iWUE in C_3 and C_4 grasses and investigate the impact of post-photosynthetic fractionation, particularly carbohydrate metabolism, on leaf carbon isotope signatures among these grasses to develop screening tools for improved iWUE.

The specific objectives of Chapter 2 were to:

I. Determine the interactive effects of glacial [CO_2] and low light on leaf gas exchange traits at growth and saturating conditions in C_3 grasses and C_4 grasses with different biochemical subtype;
II. Determine the acclimation response of stomatal morphology to growth at glacial [CO_2] and low light in C_3 grasses and C_4 grasses with different biochemical subtype.

The specific objectives of Chapter 3 were to:

I. Investigate the responses of stomatal kinetics to light transitions in C_3 and C_4 grasses acclimated to glacial [CO_2] and low light;
II. Investigate the responses of guard cell K^+ fluxes in C_3 and C_4 grasses acclimated to glacial [CO_2] and low light.

The specific objectives of Chapter 4 were to:

I. Develop a method for the optimal resolution of sugar standards using HPLC and wet chemical oxidation system coupled to IRMS;
II. Compare the carbon isotope composition of sugar standards measured using traditional EA-IRMS versus newly optimised HPLC-WCO-IRMS methods;
III. Apply the newly developed method to analyse the carbon isotope composition of a C_3 and a C_4 grass crop.

The specific objectives of Chapter 5 were to:

I. Determine the impact of post-photosynthetic fractionation, particularly carbohydrate metabolites, on the leaf carbon isotope composition of C_3 and C_4 grasses;

II. Compare the carbon isotope composition of whole leaf, cellulose and soluble sugars between C_4/NADP-ME and C_4/NAD-ME species.

1.8 Thesis Format and Structure

Research undertaken during my PhD project is presented herein as a series of four experimental chapters submitted or prepared for submission to peer-reviewed journals. The thesis is comprised of six chapters. Four chapters (2, 3, 4, and 5) describe four separate experiments whilst two Chapters (1 and 6) were designated as a general Introduction and Discussions for the whole Thesis.

Chapters	Title
Chapter 1	General introduction and literature review
Chapter 2	How do stomatal traits control leaf-level iWUE in grasses representing different photosynthetic type and biochemical subtypes to growth at glacial [CO_2] and low light?
Chapter 3	Faster stomatal opening half-times in grasses link to smaller stomatal aperture and guard cell K^+ influx providing targets for improving leaf-level iWUE
Chapter 4	Wet chemical oxidation system as a tool for analysing carbon isotope composition of sugars extracted from leaves of C_3 and C_4 grasses.
Chapter 5	Carbon isotope composition of soluble sugars in leaves of C_3 and C_4 grasses with different biochemical subtypes
Chapter 6	General discussion and prospects
References	

CHAPTER 2

HOW DO STOMATAL TRAITS CONTROL LEAF-LEVEL iWUE IN GRASSES REPRESENTING DIFFERENT PHOTOSYNTHETIC AND BIOCHEMICAL SUBTYPES UNDER GLACIAL [CO_2] AND LOW LIGHT?

ABSTRACT

The sophisticated morphology and molecular regulation of grass stomata provide an advantage that allowed grasses to dominate and diversify in the open environment. On the other hand, the acquisition of CO_2 concentrating mechanism amongst C_4 grasses endows them with higher leaf-level water use efficiency (iWUE) than their C_3 counterparts. However, it is unclear how this relates to underlying stomatal function or varies among the three C_4 biochemical subtypes with growth conditions, especially the two major photosynthetic factors: $[CO_2]$ and light. Two C_3 and six C_4 (two of each subtypes: NADP-ME, NAD-ME, and PCK) grasses were grown at ambient or glacial $[CO_2]$ ($[aCO_2]$ = 400, $[gCO_2]$ = 180 µl l^{-1}) and high or low light (HL = 1000, LL = 200 µmol m^{-2} s^{-1}). Leaf gas exchange and stomatal morphology were examined at growth and common conditions (2,000 µmol m^{-2} s^{-1} light and 180 µl l^{-1} $[CO_2]$). It was found that growth at glacial $[CO_2]$ increased stomatal conductance (g_s), stomatal aperture (SA) and reduced stomatal size (SS) and iWUE of C_3 more than C_4 grasses. Low light reduced g_s of C_4 more than C_3 grasses, WUE_i of C_3 more than C_4 grasses, and stomatal aperture and density of all species. Stomatal conductance and iWUE strongly correlated with SA. Overall, $[gCO_2]$ elicited a trade-off between SA and SS while LL reduced both SA and SD. Both treatments had little effects on maximal stomatal conductance measured using gas exchange or anatomical traits. Finally, this study revealed novel mechanistic links between stomatal and photosynthetic traits and iWUE, implicating molecular targets for breeding crops with high iWUE.

Keywords: C_3 and C_4 grasses, glacial $[CO_2]$, low light, stomatal morphology, water-use efficiency

2.1 INTRODUCTION

The grass family (Poaceae) comprises more than 10,000 species that dominate many ecological and agricultural systems (Kellogg, 2001; Vogel *et al.*, 2010). Grasses evolved 50–70 MYA. Early grass evolution is associated with enhanced drought tolerance when grass ancestors moved out of forests and into open habitats (Kellogg, 2001). Grasses are adaptable to salinity, drought, nutrient-deficient soils, and other fluctuating environments (Wood & Lenné, 2018). Grasses provide the bulk of human nutrition, are promising sources of sustainable energy (Vogel *et al.*, 2010) and the top four global agricultural commodities by quantity (sugarcane, maize, rice, wheat) (Bevan *et al.*, 2010; Wood & Lenné, 2018).

A key desirable feature of 'climate-smart' crops is high water-use efficiency (WUE) to cope with increasing events of drought and high temperature under climate change (Richards *et al.*, 1993; Ruggiero *et al.*, 2017). Crop WUE is governed by multiple factors including leaf-level instantaneous WUE (WUE_i), root architecture, biomass partitioning, etc. (Passioura, 1977; Ghannoum, 2016; Li *et al.*, 2017). iWUE reflects the exchange of [CO_2] and water vapour across the leaf surface and can be defined as CO_2 assimilation rate/stomatal conductance (A_{net}/g_s) (Farquhar & Sharkey, 1982). Photosynthesis and g_s are closely correlated under a wide range of environments (Wong *et al.*, 1979; Pinto *et al.*, 2016) such that selecting for reduced g_s, as a means of improving iWUE, often leads to reduced A_{net} and productivity (Ghannoum, 2016). It has been shown that g_s can be uncoupled from intercellular CO_2 (C_i) (von Caemmerer *et al.*, 2004), raising the prospect of improving stomatal traits with increasing CO_2 fixation, and hence higher yield (Ghannoum, 2016; Webster *et al.*, 2016). Therefore, developing the next generation of smart crops requires a greater understanding of how stomata regulate iWUE. Breeders often utilise variations within a narrow set of cultivars of the same crop species, different crops and their closely related species in the same genus to identify improved traits. The downfall of this strategy is the limited pool of genetic diversity available in a single species or a genus. Mining natural variation among diverse grasses will increase the potential of identifying beneficial stomatal traits (Anderson *et al.*, 2016; Reeves *et al.*, 2018; Cano *et al.*, 2019).

By controlling [CO_2] entry into the leaf, stomata provide the initial limitation of [CO_2] uptake. Grasses possess advanced stomata composed of two kidney-shaped guard cells flanking subsidiary cells (Kollist *et al.*, 2014b; Cai *et al.*, 2017b; Chen *et al.*, 2017). Stomatal

opening and closing govern gas exchange and are regulated by the movement of solutes and water in and out of the guard cells (Franks & Farquhar, 2007). These sophisticated structural and functional features enable fast and tight stomatal control and ensure a dynamic response to environmental fluctuations (Cai *et al.*, 2017a; Chen *et al.*, 2017; Raissig *et al.*, 2017; Rudall *et al.*, 2017). They also contribute to the success, productivity and survival of grasses in semi-arid and arid habitats (Chen *et al.*, 2016; Taylor *et al.*, 2012; Taylor *et al.*, 2018). Therefore, it is not surprising that grasses have been domesticated several times and include some of the most important cereal crops. Many grasses, including major crops (e.g., maize, sugarcane, sorghum and switchgrass) assimilate [CO_2] using the C_4 photosynthetic pathway. C_4 crops are becoming increasingly important for food and bioenergy security, with the global production and growing areas of C_4 maize and sugarcane currently surpassing that of key C_3 cereals such as wheat and rice (Varshney *et al.*, 2012; FAO, 2019).

C_4 photosynthesis operates a carbon concentrating mechanism (CCM) which elevates [CO_2] around the carbon-fixing enzyme ribulose 1,5- carboxylase/oxygenase (Rubisco) in the bundle sheath, thereby minimising photorespiration and allowing higher photosynthetic rates at relatively low stomatal conductance (Hatch, 1987; Sage, 2004). Consequently, iWUE is generally higher in C_4 relative to C_3 grasses (Taylor *et al.*, 2012). C_4 CCMs are broadly classified according to the major C_4 decarboxylase utilised, either solely or with a secondary decarboxylase (Hatch *et al.*, 1975; Wingler *et al.*, 1999; Watson-Lazowski *et al.*, 2018); nicotinamide adenine dinucleotide-malic enzyme (NAD-ME), nicotinamide adenine dinucleotide phosphate-malic enzyme (NADP-ME), and phosphoenol carboxykinase (PCK). Apart from differences in leaf anatomy and biochemistry, the three C_4 subtypes also show variations in geographic distribution according to rainfall and resource use efficiency (Hattersley, 1982; Ghannoum *et al.*, 2005, 2011). In particular, NAD-ME grasses exhibit higher iWUE at glacial (180 µl l^{-1}) [CO_2] (Pinto *et al.*, 2014) and higher plant WUE under water stress (Ghannoum *et al.*, 2002) relative to NADP-ME and PCK counterparts. Under low light, NADP-ME species have higher photosynthetic efficiency relative to NAD-ME and PCK due to more efficient CCM (Sonawane *et al.*, 2018; Sagun *et al.*, 2019). However, there is scarcity in the information regarding differences in stomatal sensitivity among the C_4 biochemical subtypes. Hence, to better understand how stomata control iWUE in grasses, it is important to compare C_3 and C_4 grasses, including the three C_4 subtypes.

Light directly and indirectly (via photosynthesis) regulate stomatal function (Aasamaa & Sõber, 2011; Lawson *et al.*, 2011; Aasamaa & Aphalo, 2016). Red light indirectly affects g_s by driving mesophyll photosynthesis and decreasing C_i (Huxman & Monson, 2003; Lawson *et al.*, 2011; Chen *et al.*, 2017). Blue light directly affects the phototropins in guard cells through photosynthesis-independent reactions leading to the activation of plasma membrane H^+-ATPase pumps (Christie, 2007; Shimazaki *et al.*, 2007; Hiyama *et al.*, 2017). The hyperpolarised plasma membrane activates inward-rectifying K^+ channels (K^+_{in}) (Kim *et al.*, 2010) allowing for K^+ uptake followed by water influx into the guard cells, and leading to stomatal opening (Schroeder *et al.*, 1987; Shimazaki *et al.*, 2007; Kim *et al.*, 2010; Marten *et al.*, 2010). Following long-term exposure to high light, stomatal density (SD) and stomatal pore lengths increase in species such as tomato (Gay & Hurd, 1975), tobacco (Thomas *et al.*, 2004), *Arabidopsis ssd-1* mutants (Schlüter *et al.*, 2003) and *Eucalyptus globulus* (James & Bell, 2000). Conversely, decreased stomatal density and stomatal index (SI), but not stomatal size (SS) were observed in tobacco leaves (Thomas *et al.*, 2004; Gerardin *et al.*, 2018) and *Coffea arabica* (Pompelli *et al.*, 2010) under shade treatments.

A period of low (glacial) atmosphere [CO_2] ([gCO_2]) during the Oligocene is thought to be the primary driver for the evolution of C_4 photosynthesis (Ehleringer *et al.*, 1997; Sage, 2004; Christin *et al.*, 2008). Adaptation to [gCO_2] includes higher stomatal density (SD) compared to current atmospheric [CO_2] (Woodward, 1987; Woodward & Kelly, 1995). Stomata generally open at low [CO_2] and close at elevated [CO_2] both in light and darkness (Assmann, 1999; Lawson *et al.*, 2011; Azoulay-Shemer *et al.*, 2015). Growth at [gCO_2] increased stomatal conductance in C_3 and C_4 leaves (Sage & Coleman, 2001; Maherali *et al.*, 2002; Pinto *et al.*, 2014). In particular, growth at 100 ppm [CO_2] increased SD by 42% in the C_3 model plant, *Arabidopsis* relative to growth at 380 ppm [CO_2] (Li *et al.*, 2014). Conversely, growth at elevated [CO_2] ([eCO_2]) reduced SD, g_s, and sensitivity to CO_2 (Woodward & Kelly, 1995; Medlyn *et al.*, 2001; Maherali *et al.*, 2002; Leakey, 2009; Lawson *et al.*, 2011; Xu *et al.*, 2016b). In summary, light and [CO_2] exert a significant influence on stomatal function; however, the interactive effects of these two photosynthetic factors on stomatal function have not yet been fully explored in C_4 grasses and among C_4 subtypes.

Here, closely related C_3 and C_4 grasses with different biochemical subtypes were grown under [gCO_2] (180 µl l^{-1}) and low light (200 µmol m^{-2} s^{-1}) as well as control conditions

(1,000 µmol m^{-2} s^{-1} of light and 400 µl l^{-1} of [CO_2]) with the aim to further explore stomatal responses to environmental stimuli. One of the hypotheses was that growth at [gCO_2] result in higher g_s and SD and that this effect is stronger in C_3 than C_4 grasses because C_3 photosynthesis is highly CO_2 sensitive. In addition, it was hypothesised that growth at low light result in lower g_s and SD, which is stronger in C_4 than C_3 grasses because C_4 photosynthesis is highly light-sensitive. Finally, it was hypothesised that light leads to a greater stomatal response than [CO_2] because grasses are continuously exposed to fluctuations of light rather than [CO_2] in their open environment, while atmospheric [CO_2] gradually changed over time. This Chapter has shed light on how stomatal morphological and physiological traits control iWUE in C_3 and C_4 grasses that are acclimated to low light and [CO_2].

2.2 MATERIALS AND METHODS

2.2.1 Plant culture and growth conditions

Eight C_3 and C_4 grasses (Poaceae) representing different photosynthetic and biochemical subtypes were grown and acclimated in walk-in growth chambers (Biochambers, Winnipeg, Canada) controlled by LI-820 CO_2 gas analysers (LI-COR Inc., Lincoln, NE, USA) similar to the growing conditions described by Watson-Lazowski *et al.*, (2019). These grass species included C_3: *Panicum bisulcatum* (Thunb.) and *Steinchisma laxa* (Zuloaga); C_4 NAD-ME: *Panicum miliaceum* (L.) and *Leptochloa fusca* [(L.) Kunth.]; C_4 NADP-ME: *Panicum antidotale* (Retz.) and *Setaria viridis* [(L.) Beauv.]; C_4 PCK: *Megathyrsus maximus* (Jacq., synonyms: *Panicum maximum, Urochloa maxima*) and *Chloris gayana* (Kunth.). Two species, *L. fusca* (NAD-ME) and *C. gayana* (PCK) belong to subfamily Chloridoideae while the remaining six species belong to Subfamily Panicoideae (Grass Phylogeny Working Group II, 2012). All species were individually planted in five biological replicates into 3 L pots containing soil (Osmocote® Professional Seed Raising Mix, Scotts, Australia) and trace elements supplement (Osmocote® Plus Trace Elements, Scotts, Australia). Initially, seeds were germinated at 400 µl l^{-1} [CO_2] chamber to obtain uniform healthy seedlings and to prevent early seedling deterioration. Then, plants were transferred to respective growth chambers with different light (high: 1000 µmol m^{-2} s^{-1}; low: 200 µmol m^{-2} s^{-1}) and [CO_2] (ambient: 400 µl l^{-1}; glacial: 180 µl l^{-1}) treatments. The four treatment combinations were high light, ambient [CO_2] (HL+[aCO_2] [control]); high light, glacial [CO_2] (HL+[gCO_2]); low light, ambient [CO_2] (LL+[aCO_2]); and low light, glacial [CO_2] (LL+[gCO_2]). The average day/night temperature was 28/22°C, relative humidity (RH) was 60%, and the photoperiod was 14 h. Plants were watered to full capacity every 1-2 days, fertilised as required and randomised twice a week to reduce the effects of within-chamber variation.

2.2.2 Leaf gas exchange

Five weeks after germination, gas exchange was measured with an LI-6400XT infrared gas analyser (LI-COR Inc., Lincoln, NE, USA) using the youngest fully expanded leaf from the main stem (Watson-Lazowski *et al.*, 2019). Cuvette conditions were maintained at 60% RH, 28°C leaf temperature, and 350 mol s^{-1} flow rate. Measurements were taken between 10:00

and 15:00 inside growth chambers. At least eight technical replicates in five biological replicates per species were measured.

Steady-state measurements of net CO_2 assimilation rate (A_{net}), stomatal conductance (g_s), intercellular CO_2 (C_i) and intrinsic water use efficiency (iWUE; A_{net}/g_s) were made for all eight grass species at the four growth conditions and at uniform conditions (light-saturated (2,000 µmol m^{-2} s^{-1}), [CO_2]-limited (180 µl l^{-1} [CO_2]) to estimate maximal g_s. Prior to measurements, the leaves were allowed to stabilise for approximately 10-15 min until steady-state CO_2 uptake was reached.

2.2.3 Stomatal morphology

Stomatal impressions were characterised based on the methods described by Weyers & Johansen, (1985), Nobuhito & Katsuya, (2008) and Parsons *et al.*, (2019) with some modifications. Images were captured from the adaxial and abaxial surfaces of all eight grass species using the same leaf where the steady-state gas exchange was measured. Dried clear nail varnish impressions were transferred to glass slides (Knittel Glass, Germany), and epidermal imprints containing stomatal patterns were taken using a CCD camera (NIS-F1 Nikon, Tokyo, Japan) attached to a Nikon microscope equipped with a DS-U3 controller (Nikon, Tokyo, Japan). Images were captured at 200× and 400× total magnification and processed using Nikon NIS Element imaging software (Nikon, Tokyo, Japan). Stomatal images from leaf epidermal imprints were captured between two major veins of the leaf lamina to ensure uniformity of stomatal location. Images were analysed using Image J software (NIH, USA). Ten stomatal parameters (**Figure S2. 1**) based from Caine *et al.*, (2018) and Gerardin *et al.,* (2018) with the addition of subsidiary cell measurements in grasses, were measured as follows: guard cell width (GCW), guard cell length (GCL), subsidiary cell width (SCW), aperture width (AW), aperture length (AL), stomatal aperture (SA), stomatal size (SS), stomatal density (SD), stomatal index (SI), and the number of open stomata per unit area (OD). Stomatal size and aperture area were calculated by assuming the area of an ellipse whereby:

$$SA = \left(\left[\frac{AW}{2}\right] * \left[\frac{AL}{2}\right] * \pi\right) \qquad \text{equation 2.1}$$

$$SS = \left([GCW + SCW] * \left[\frac{GCL}{2}\right] * \pi\right) - SA \qquad \text{equation 2.2}$$

such that AW/2 and GCW+SCW were the short axes while AL/2 and GCL/2 were the long axis of *SA* and *SS*, respectively. Stomatal density was calculated as the number of stomata per unit area (0.15 mm^2 field of view) while open stomatal density was determined by counting the frequency of open stomata per unit area (less than 0.5 µm aperture width were considered close). Stomatal index was calculated as the ratio of stomata to total cells in the epidermis (stomata plus non-stomatal cells) multiplied by 100. Three random microscopic fields (six total) from the adaxial and abaxial surfaces per biological replicate were measured totalling >300 stomata per species in each growth chamber, and the mean of the adaxial and abaxial surfaces was used (*leaf side p=0.75, df=1,7*).

Maximum stomatal aperture (a_{max}) was measured following Liu *et al.*, (2014) and Mak *et al.*, (2014) with some modifications. The mid-portion of the second fully expanded leaf was harvested and soaked immediately in stomata opening buffer (50 mM KCl, 5 mM Na-MES, pH 6.1) after which the abaxial leaf epidermis was promptly peeled. Peels were mounted in a 35-mm petri dish with 0.13 mm glass bottom (MatTek Corp, MA, USA) coated with silicone adhesive (B-521, Factor II, Lakeside, AZ 85929), and then 2 ml of opening buffer was added. Epidermal peels were incubated for 2 hr at 700 µmol m^{-2} s^{-1} light intensity to induce stomatal opening. a_{max} was calculated similarly to SA.

2.2.4. Calculation of maximum theoretical conductance (g_{s_amax}) based on stomatal traits

The theoretical maximum conductance to water vapour (g_{s_amax}) was calculated using the maximum stomatal aperture (a_{max}) determined from epidermal peels. One-sided g_{s_amax} was calculated using the equation presented by Franks & Beerling, (2009) based on the Brown & Escombe, (1900) diffusion model of gases for plants. It is written as:

$$g_{s\_amax} = \left(\frac{d}{v}\right)\left(\frac{SD.a_{max}}{l+\frac{\pi}{2}\sqrt{\frac{a_{max}}{\pi}}}\right) \qquad \text{equation 2.3}$$

where d = diffusivity of water vapor at 25°C (0.0000249 m^{-2} s^{-1}); v = molar volume of air (0.0224 m^3 mol^{-1}); SD = stomata density (m^{-2}); a_{max} = maximum stomatal aperture (m^2) and l is the stomata pore depth which is assumed to be equivalent to guard cell width (m). The total, two-sided g_{s_amax} was calculated as g_{s_amax} (abaxial) + g_{s_amax} (adaxial). The model assumes maximal stomatal aperture and that all stomata are open. The total, two-sided g_{s_amax} was calculated as g_{s_amax} (abaxial) × 2 since both leaf sides generally do not differ in SD similar to Caine *et al.*, (2018).

2.2.5 Statistical analyses

ANOVA was performed using R (V.3.4.2; R Core Team, 2017) from linear models (*lm*) specifying species (n=8) as the error component of the 2×2 full factorial experimental design. Homoscedasticities and normalities were checked by examining the quantile plots and the re-fitted when necessary. Since the comparisons consisted of hierarchal (nested) terms, the *F*-statistic was re-calculated such that the signal (numerator mean squares) to noise (denominator mean squares) ratio reflected the true inference on the effects of [CO_2], light, [CO_2]+light, type/subtype, and their respective two-way and three-way interactions.

The effect of glacial [CO_2] treatment was the average effects of chambers with [gCO_2] regardless of light conditions (HL+[gCO_2] and LL+[gCO_2]) while the effect of ambient [CO_2] was the average effects of [aCO_2] chambers (HL+[aCO_2] and LL+[aCO_2]) regardless of light treatment. The low light effect was the average effect of the chambers with LL conditions (LL+[aCO_2]and LL+[gCO_2]) while the high light effect was the mean variation within chambers with HL conditions (HL+[aCO_2] and HL+[gCO_2]). Subsequently, the equivalent *p-value* was calculated for a given degrees of freedom. When significant, means were ranked using Tukey's *post-hoc* at a stringency of α=0.05. Linear correlations between two variables were expressed in r^2, followed by significance values. Figures were plotted using the *ggplot2* package (Wickham, 2017).

2.3 RESULTS

2.3.1 Glacial [CO_2] and low light differentially affect leaf gas exchange of C_3 and C_4 grasses

When measured under control conditions, photosynthetic rates (A_{net}) decreased significantly under [gCO_2] (p=0.0053) and were greatly inhibited under LL (p<0.0000) in all species **(Figure 2. 1A, Table 2. 1**). At HL, [gCO_2] reduced A_{net} in C_3 by 45% more than 20% reduction in C_4 grasses relative to the control (HL+[aCO_2]). At [aCO_2], LL reduced A_{net} in C_4 (-63%) more than in C_3 (-44%) grasses (Light × Type: p=0.0068). Combined effects of LL+[gCO_2] exacerbated the reduction of A_{net}, especially in C_3 species (**Figure 2. 1A, Table 2. 3**). Multiple comparisons across all species and treatments showed that both PCK species (*C. gayana* and *M. maximus*) had higher A_{net} compared to all other species (**Table 2. 3).**

Low light had a stronger and opposite effect on g_s relative to [gCO_2] (**Figure 2. 1B** , **Table 2. 1** and **Table 2. 3**, [CO_2] × Light: p= 0.0150). Stomatal conductance increased at [gCO_2] (p=0.0010; **Table 2. 1**) and decreased under LL (p<0.0000; **Table 2. 1**) for all species. Relative to the control (HL+[aCO_2]), g_s increased more in NADP-ME (+100%) and C_3 (+82%) relative to NAD-ME (+54%) and PCK (+40%) under HL+[gCO_2]. LL+[aCO_2] reduced g_s more in C_4 (-62%) than in C_3 (-15%) grasses. LL+[gCO_2] decreased g_s in C_4 grasses, while C_3 g_s was similar to the control (**Figure 2. 1B, Table 2. 3**).

Leaf-level water use efficiency (iWUE) were generally higher in C_4 than C_3 grasses (Type: p=0.0001, **Table 2. 1**). Relative to the control, [gCO_2] reduced iWUE (p=0.0003) in C_3 (-70%) more than in C_4 (-50%) grasses. Conversely, LL reduced iWUE in C_3 grasses only (**Figure 2. 1C, Table 2. 1 and Table 2. 3**). Overall, C_i followed the same response pattern as iWUE (**Table 2. 1 and Table 2. 3**).

To estimate photosynthetic acclimation and maximal stomatal conductance (g_{s_sat}), all plants were measured under saturating light (2,000 µmol m^{-2} s^{-1}) and low [CO_2] (180 µl l^{-1}). Overall, light-saturated and [CO_2]-limited photosynthesis rates (A_{sat}) were higher in C_4 compared to C_3 grasses (Type: p=0.0392; **Table 2. 1 and Table 2. 3).** The two Chloridoideae species *L. fusca* and *C. gayana* had higher A_{sat} relative to the other six species. The responses of A_{sat} and g_{s_sat} to LL and gCO_2 were mostly species-specific and independent of the biochemical subtype. Relative to the control, LL downregulated A_{sat} of *S. laxa* (C_3), *P.*

miliaceum (NAD-ME), *S. italica* (NADP-ME) and *M. maximus* (PCK). Glacial [CO_2] upregulated A_{sat} of five out of the eight grasses under HL. LL+[gCO_2] reduced A_{sat} in all species except *P. bisulcatum* (C_3) and *C. gayana* (PCK) (**Table 2. 1 and Table 2. 3**). Glacial [CO_2] increased g_{s_sat} of the two C_3 species (*P. bisulcatum* and *S. laxa*) and reduced it in *C. gayana* (PCK). Low light reduced g_{s_sat} in *P. miliaceum* (NAD-ME) and *M. maximus* (PCK), while LL+gCO_2 reduced g_{s_sat} in *L. fusca* (NAD-ME) and the two NADP-ME (*P. antidotale* and *S. italica*) species (**Table 2. 3**).

2.3.2 Low light reduced stomatal aperture and density while glacial [CO_2] elicited a trade-off between SA and SS

The stomatal complex of all the eight grass species was characterized as paracytic (composed of two lateral subsidiary cells (SC), non-oblique (SC parallel to the guard cells), and amphistomatous (stomata are present on both sides of the leaf) (**Figure S2. 2**) following the morphological definition of Rudall *et al.*, (2017).

Overall, stomatal aperture (SA) was bigger at gCO_2 and smaller under LL (**Figure 2. 2A, Table 2. 1**; CO_2: p=0.0004,Light: p=0.0122). Stomatal size (SS) decreased at [gCO_2], but not affected by LL (**Figure 2. 2A, Table 2. 1;** [CO_2]: p=0.0290, Light: p=0.1646) except for PCK species ([CO_2] × Light × Type: p=0.0174; **Table 2. 1 and Table 2. 4**). Under LL, stomatal index (SI) and stomatal density (SD), marginally decreased (**Figure 2. 2E and Figure 2. 2C; Table 2. 1**; p=0.0368, p=0.0316,) while the density of open stomata (OD) was greatly reduced (**Figure 2. 2D; Table 2. 1**; p=0.0185). Glacial [CO_2] did not affect SI and SD (p=0.2515, p=0.2852, **Table 2. 1**); but marginally increased OD (p=0.0516, **Table 2. 1**). Subsequently, the effects of low light were greater than [gCO_2] in reducing the ratio of stomatal cells to non-stomatal cells (SI, [CO_2] × Light: p=0.0271, **Table 2. 1**). Irrespective of growth conditions, OD was lowest in NAD-ME and highest among C_3 (Type: p=0.0062, **Table 2. 1 and Table 2. 4**), indicating an evolutionary divergence underlying higher iWUE in C_4.

Stomatal traits varied with species independent of subtype (**Table 2. 1 and Table 2. 4; Figure 2. 2**). Across growth treatments, SA and SS were biggest in *P. bisulcatum* (C_3) and smallest in *C. gayana* (PCK) compared to the other species. SD was highest in *C. gayana*;

SI was highest in *P. antidotale* (NADP-ME), while OD was highest in *C. gayana* and smallest in *P. antidotale* (**Table 2. 1 and Table 2. 4**).

Overall, stomatal aperture increased linearly with stomatal size (r^2=0.340, p<0.01, **Table 2. 2**) and the linear response were stronger when compared at respective growth conditions (**Figure 2. 3**; control: r^2=0.77, p=0.0036; HL+[gCO_2]: r^2=0.62, p=0.02; LL+[aCO_2]: r^2=0.88, p=0.0006; LL+[gCO_2]: r^2=0.72, p=0.0081). SD linearly decreased as stomatal size increased (r^2=0.307, p<0.01; **Figure 2. 3**) and SD linearly increased with OD (r^2=0.496, p<0.01; **Table 2. 2**), while SI showed negative correlation with SS only (r^2=0.131; p<0.05; **Table 2. 2**). Leaf iWUE was strongly negatively correlated with SA at LL and/or [gCO_2] (**Figure 2. 4**).

2.3.4 Estimating maximum g_s using morphological parameters

Based on stomatal morphology parameters, g_{s_amax} increased at [gCO_2] in five out of the eight species (p=0.0326; **Table 2. 1 and Table 2. 4**). It was also positively and weakly correlated to g_s (r^2=0.174; p<0.05; **Table 2. 2**), SD (r^2=0.291; p<0.01; **Table 2. 2**), and OD (r^2=0.333; p<0.01; **Table 2. 2**). Species-wise, *S. italica* (NADP-ME) and *C. gayana* (PCK) had highest g_{s_amax} across all growth conditions (**Table 2. 4**).

2.4 DISCUSSION

The overall goal of this research was to better understand stomatal control of iWUE in order to develop future cereal crops with improved WUE as well as better heat and drought tolerance, with the specific objective to compare the stomatal responses of C_3 and C_4 grasses to short-term and long-term manipulations in [CO_2] and light. Our results reveal new insight into the comparative physiology and differential regulation of C_3 and C_4 grass stomata by [CO_2] and light.

2.4.1 Grass stomatal conductance and environmental response acclimate through changes on stomatal aperture rather than stomatal density

Stomata are microscopic structures of leaves and stems formed by two specialised guard cells that control the exchange of [CO_2] and water vapour. Stomatal size (SS) and density (SD) are the anatomical determinants of maximum stomatal conductance of CO_2 (g_{s_amax}) to sites of assimilation (Franks & Beerling, 2009). In the fossil record, atmospheric [CO_2] concentration was several times higher than current ambient [CO_2] when vascular plants first appeared, but subsequent periods of falling [CO_2] challenged plants with diminished [CO_2] availability. Selection for higher g_{s_amax} among angiosperms under lower atmospheric CO_2 during the Cretaceous is characterised by smaller SS and higher SD (Franks & Beerling, 2009). It has been shown that grass stomata acclimate to low [CO_2] and to some extent, low light by changes in stomatal opening and frequency (Maherali *et al.*, 2002). However, our data clearly showed that grass stomatal conductance correlates best with SA (r^2=0.472; p<0.01; **Table 2. 2**) while SD (p > 0.05; **Table 2. 2**) is generally not affected by [gCO_2], and could not predict g_s (**Table 2. 2, Figure 2. 5**). Only when we accounted for the frequency of open stomata, OD, a good relationship was obtained between OD and g_s (r^2=0.473; p<0.01; **Table 2. 2**). Hence, I concluded that SA, and not SD, predict g_s in C_3 and C_4 grasses alike. Although a global inverse relationship exists between SD and atmospheric [CO_2] concentration (Woodward, 1987; Woodward & Kelly, 1995; Franks & Beerling, 2009; Gerald *et al.*, 2016), it appears to be not universal (Gerald *et al.*, 2016) in grasses as demonstrated in this study and by Maherali *et al.*, (2002) who reported no correlation between SD and g_s in C_3 and C_4 grasses grown at sub-ambient or [eCO_2].

Stomatal size and density are the anatomical determinants of maximal anatomical stomatal conductance (g_{s_amax}) (Franks & Beerling, 2009). In this study, g_s strongly correlated with SA (r^2=0.472; p<0.01; **Table 2. 2**) and g_{s_amax} (r^2=0.174; p<0.05; **Table 2. 2**) but not SD (**Table 2. 2, Figure 2. 5**); and g_s was a relatively constant fraction of g_{s_amax} across species and treatments (**Table 2. 3 and Table 2. 4**). These patterns appear widespread as they are in line with work using Arabidopsis SD mutants demonstrating that operational stomatal conductance can be estimated as a function of g_{s_amax}, independently of SD (Dow *et al.*, 2014a,b). Accordingly, Dow *et al.*, (2014a), concluded that the short-term g_s response to [CO_2] is a pore-specific property and that the CO_2 sensing mechanism is driven by guard cell activities that result in stomatal aperture modulation. This study showed that the same applies across different C_3 and C_4 grass species, demonstrating the universality of these stomatal responses to [CO_2] but not light as discussed below.

This study also provides new evidence of stomatal morphological acclimation (SS and SA) of C_3 grasses and different C_4 subtypes to [gCO_2] over a shorter time frame compared to previous reports (Maherali *et al.*, 2002). Smaller SS is a well-characterized strategy to speed up solute flux in and out of guard cells by increasing the surface area to volume ratio (Chen *et al.*, 2012), and shown to occur in several species (Tanaka *et al.*, 2013; Lawson & Blatt, 2014; Papanatsiou *et al.*, 2017). The advantage of grass stomata architecture enables small changes in guard cell width to translate into larger changes in SA (Hetherington & Woodward, 2003; Franks & Farquhar, 2007). This strategy enables grass stomata to respond rapidly to [gCO_2]. In line with the effects of [gCO_2,] LL reduced g_s mainly through smaller SA rather than SD or SI (**Figure 2. 2**). In addition, there was a general negative relationship between stomatal size and density (**Figure 2. 5**). This negative linear relationship is well exemplified in the two PCK species which tended to have smaller SS and higher SD relative to the other C_4 grasses (**Figure 2. 2**). Yet this indicated no bearing on stomatal conductance as all C_4 grasses tended to have similar g_s.

2.4.2 Acclimation of steady-state stomatal conductance at uniform conditions is species-specific

In addition to g_s at growth conditions, maximal stomatal conductance at common gas exchange conditions (2,000 µmol m^{-2} s^{-1} light and 180 µl l^{-1} [CO_2]) or using stomatal

morphological traits was measured to monitor acclimation to growth conditions. Only [gCO_2] led to acclimations of g_{s_sat} and g_{s_amax}, while LL had little effect. Nevertheless, the two stomatal estimates (g_{s_sat} and g_{s_amax}) did not correlate, possibly because gas exchange conditions were not sufficient to induce maximal stomatal opening. Earlier studies by Maherali *et al.*, (2002) showed that stomatal acclimation of C_3 and C_4 grasses were grown at sub-ambient or elevated [CO_2] did not vary according to photosynthetic type. Previous studies have also demonstrated that stomatal responses are species-specific not only among grasses but also among dicotyledonous herbs (Merilo *et al.*, 2014) and temperate deciduous trees (Aasamaa & Sõber, 2011; Aasamaa & Aphalo, 2016). Within monocots, there is some diversity in stomatal morphology (Rudall *et al.*, 2017). Members of the subfamilies Araceae, Petrosaviceae, Dioscoreacea; family Liliales and Asparagales possess anomocytic stomata (no subsidiary cells) while most members of the Poales where our species belong consist of the typical paracytic stomata (Rudall *et al.*, 2017).

2.4.3 C_3 and C_4 stomata show greater sensitivity to [gCO_2] and LL, respectively while C_4 grasses maintain greater iWUE under all conditions

iWUE was compromised by both [gCO_2] and LL to a greater extent in C_3 relative to C_4 grasses. In both cases, this was related to the higher efficiency of C_4 photosynthesis as a result of the CCM even under sub-optimal conditions (Vogan & Sage, 2012; Pinto *et al.*, 2014; Taylor *et al.*, 2018; Watson-Lazowski *et al.*, 2019).

Apart from smaller and faster stomata in the PCK species, the C_4 subtypes generally had similar stomatal traits and responses, with the exception of a greater stomatal sensitivity to [gCO_2] exhibited by NADP-ME (on par with C_3) relative to other C_4 grasses (**Figure 2. 2B; Table 2. 4**). Previous studies using a broader set of species also showed that NADP-ME grasses have a greater stomatal sensitivity to low [CO_2] relative to species of the other two subtypes (Pinto *et al.*, 2014, 2016). In addition, Liu and Osborne, (2015) found that the Chloridoideae (NAD-ME and PCK subtypes) generally have smaller and denser stomata than Panicoideae (all subtypes, with NADP-ME predominance) grasses. More recently, Watson-Lazowski *et al.*, (2019) showed that *βCA1* transcript, a gene implicated to play a role in stomatal aperture control, was downregulated in NAD-ME subtype relative to NADP-ME and PCK. These differences in stomatal traits and sensitivity align with well-

known physiological and ecological differences between the highly productive NADP-ME/Pancoideae grasses and the arid-distributed NAD-ME/Chloridoideae (Hattersley, 1982; Liu & Osborne, 2015). Due to these ecological differences, it was suggested that stomata of NAD-ME and PCK species do not open as wide as NADP-ME species in response to [gCO_2] to avoid hydraulic failure or retain water against drought, which are more lethal survival factors than reduced photosynthesis under environmental stresses (Aasamaa & Sõber, 2011).

In addition to the few subtype effects, there were a number of interesting C_3 *versus* C_4 differences in stomatal traits. Firstly, C_3 grasses generally had higher g_s, SA and SS; and lower WUE_i relative to C_4 grasses, while SD, SI and g_{s_amax} showed no particular trend confirming what was previously reported in a small subset of species possessing dumbbell-shaped stomata (Maherali *et al.*, 2002; Malone *et al.*, 2016). Secondly, the results contrast with a previous study by Morison & Gifford, (1983) which found no differences between C_4 (*Z. mays* and *P. plicatum*) and C_3 (*O. sativa* and *P. aquatica)* in stomatal sensitivity to short-term changes in CO_2. This lack of difference may be due to the fact that comparisons were made only in cabinet grown grasses at ambient [CO_2] and ambient light conditions (630 µmol quanta m^{-2} s^{-1}) in contrast to the glacial [CO_2] and low light conditions used in this study. Similarly, Vogan & Sage (2012) found no differences in stomatal responses to C_i among closely related C_3, C_3-C_4, and C_4 Eudicot species (*Flaveria, Heliotropium* and *Alternanthera*) after acclimation to low [CO_2]. The discrepancy with our results may be due to the difference in stomatal morphology between Eudicot and grass species, where grasses have dumbbell-shaped stomata with subsidiary cells for fast opening and closure (Chen *et al.*, 2017; Raissig *et al.*, 2017). Acclimation studies of stomatal traits to LL, specifically among grasses, are rather scarce. Our data are in line with previous studies which showed that shade reduced g_s of C_4 grasses (Sonawane *et al.*, 2018), and reduced SD and SI but not SS among species with dumbbell-shaped stomata (Carins Murphy *et al.*, 2016; Aasamaa & Aphalo, 2016; Gerardin *et al.*, 2018).

2.5 CONCLUSION

The morphological and physiological responses of stomata among closely related C_3 and C_4 grasses to [gCO_2] and LL were examined to help elucidate current understanding and seek new morphological and physiological traits that control leaf iWUE. I have shown that higher iWUE during [gCO_2] and LL conditions among C_4 grasses relative to C_3 is largely dependent on stomatal aperture. Variations in gas exchange traits were present at the photosynthetic type and C_4 subtype level, but this did not apply to stomatal morphology. These results suggest other mechanisms could explain the variations in iWUE among subtypes (e.g. leaf hydraulic conductance). Overall, regardless of the photosynthetic type and C_4 biochemical subtype, growth at [gCO_2] conferred larger SA, smaller SS, elevated g_s, and consequently reduced iWUE. Conversely, acclimation to low light includes lower operational g_s, smaller SA, and decrease in SD and SI. Finally, Chapter 2 highlighted that iWUE is dependent on the dynamic trait, stomatal aperture, to growth at glacial [CO_2] and low light and recommend to explore traits that confer faster stomatal aperture control.

Table 2. 1 Statistical analysis summary of the main effects and interactions of [CO_2], light, species, and type/subtype for leaf gas exchange and stomatal morphology parameters among eight grass species acclimated at glacial [CO_2] and low light.

Species was used as a random effect while the functional type was utilised as the fixed effect. Bold numbers indicate significant effect at α=0.05.

Parameters	Main Effects (*p*)				Interactions (*p*)			
	$[CO_2]$	Light	Type	Species	$[CO_2]$ × Light	$[CO_2]$ × Type	Light × Type	$[CO_2]$ × Light × Type
Gas exchange								
$[CO_2]$ assimilation rate, A_{net} (µmol $[CO_2]$ m^{-2} s^{-1})	**0.0053**	**0.0000**	**0.0094**	**0.0000**	0.0737	0.9341	**0.0068**	0.9579
Stomatal conductance, g_s (mol H_2O m^{-2} s^{-1})	**0.0010**	**0.0000**	**0.0017**	**0.0021**	**0.0150**	0.3394	0.0753	0.3124
Leaf WUE (A_{net}/g_s), iWUE (µmol $[CO_2]$ $(mol\ H_2O)^{-1}$)	**0.0003**	0.7736	**0.0001**	**0.0152**	0.7377	0.1668	0.1293	0.3817
Intercellular $[CO_2]$, C_i (µmol mol^{-1})	**0.0004**	**0.0387**	**0.0050**	**0.0000**	0.0910	0.7091	0.8211	0.6508
Light-saturated assimilation rate, A_{sat} (µmol $[CO_2]$ m^{-2} s^{-1})	0.6187	0.0540	**0.0392**	**0.0000**	0.2764	0.8547	0.6741	0.5941
Light-saturated maximum conductance, g_{s_sat} (mol H_2O m^{-2} s^{-1})	0.3722	**0.0229**	0.2899	**0.0000**	0.8880	0.3504	0.0527	0.1935
Stomatal morphology								
Stomatal aperture, SA (µm^2)	**0.0004**	**0.0122**	0.1714	**0.0000**	0.0512	0.3253	0.1441	0.3183
Stomatal size, SS (µm^2)	**0.0290**	0.1646	0.3696	**0.0000**	0.4172	0.1159	0.1275	**0.0174**
Stomatal index, SI (%)	0.2515	**0.0368**	0.1166	**0.0000**	**0.0271**	0.6352	0.7032	0.0796
Stomatal density, SD (mm^{-2})	0.2852	**0.0316**	0.5337	**0.0000**	0.5648	0.4558	0.1830	0.3857
Density of open stomata, OD (µm^{-2})	0.0516	**0.0185**	**0.0062**	**0.0000**	0.7977	0.9144	0.5205	0.3672
Maximum anatomical conductance, g_{s_amax} (mol H_2O m^{-2} s^{-1})	**0.0326**	0.1596	0.8925	**0.0000**	0.1662	0.5979	0.4648	0.3769

Table 2. 2 Correlation matrices between measured stomatal traits for eight grasses acclimated to glacial [CO_2] and low light.

Linear regression direction is indicated in the parenthesis. Values represent r^2 between two parameters. Significance codes are as follows: *significant at $p<0.05$; **significant at $p<0.01$; ^{ns}not significant ($p>0.05$).

	g_s	iWUE	C_i	A_{sat}	g_{s_sat}	SA	SS	SI	SD	OD	g_{s_amax}
A_{net}	ns	0.179*	ns	0.387**	0.291**	ns	ns	ns	ns	ns	ns
g_s		(-) 0.398**	ns	ns	ns	0.472**	ns	ns	ns	0.473**	0.174*
iWUE			ns	0.321**	ns	(-) 0.472**	ns	ns	ns	(-) 0.213**	ns
C_i				(-) 0.394*	ns	ns	ns	ns	ns	ns	ns
A_{sat}					0.398**	(-) 0.175*	(-) 0.144*	ns	ns	ns	ns
g_{s_sat}						ns	ns	ns	ns	ns	ns
SA							0.340**	ns	ns	ns	ns
SS								(-) 0.131*	(-) 0.307**	ns	ns
SI									ns	ns	ns
SD										0.496**	0.291**
OD											0.333**
g_{s_amax}											

Table 2. 3 Gas exchange parameters for eight grass species acclimated to glacial [CO_2] and low light.

Values are means ± SE (n=3-5). Lower case letters in bold indicate the ranking of species within treatments. Numbers in superscript indicate the ranking of treatments within species. Tukey's HSD *post hoc* at 5% level was employed. Values with the same letter (or number) are not significantly different at α=0.05**.**

Parameter	Treatment	C_3		NAD-ME		NADP-ME		PCK	
		P. bisulcatum	*S. laxa*	*P. miliaceum*	*L. fusca*	*P. antidotale*	*S. italica*	*M. maximus*	*C. gayana*
A_{net} ($\mu mol\ m^{-2}\ s^{-1}$)	High Light Ambient [CO_2]	17.58 ± 0.55 **d**^{1}	19.79 ± 0.64 **d**^{1}	33.63 ± 0.51 **b**^{1}	32.14 ± 0.34 **bc**^{1}	31.94 ± 0.74 **bc**^{1}	30.64 ± 0.51 **c**^{1}	30.65 ± 0.59 **c**^{1}	37.64 ± 1.28 **a**^{1}
	High Light Glacial [CO_2]	9.10 ± 0.30 **d**^{2}	11.58 ± 0.80 **d**^{2}	22.91 ± 0.58 **c**^{2}	29.24 ± 0.34 **a**^{2}	20.96 ± 0.57 **c**^{2}	27.95 ± 0.37 **ab**^{2}	27.41 ± 1.11 **ab**^{2}	26.52 ± 1.09 **b**^{2}
	Low Light Ambient [CO_2]	10.63 ± 0.29 **b**^{2}	9.48 ± 0.57 **b**^{2}	10.71 ± 0.33 **b**^{3}	14.70 ± 0.61 **a**^{3}	11.75 ± 0.68 **b**^{3}	9.48 ± 0.52 **b**^{3}	11.13 ± 0.28 **b**^{3}	17.27 ± 1.07 **a**^{3}
	Low Light Glacial [CO_2]	5.84 ± 0.14 **d**^{3}	5.87 ± 0.23 **d**^{3}	10.07 ± 0.24 **bc**^{3}	8.61 ± 0.36 **c**^{4}	8.53 ± 0.11 **c**^{4}	8.95 ± 0.31 **c**^{3}	12.11 ± 0.33 **ab**^{3}	14.43 ± 0.10 **a**^{4}
g_s ($mol\ m^{-2}\ s^{-1}$)	High Light Ambient [CO_2]	0.34 ± 0.01 **a**^{2}	0.35 ± 0.02 **a**^{2}	0.31 ± 0.01 **a**^{2}	0.34 ± 0.01 **a**^{2}	0.25 ± 0.01 **b**^{2}	0.25 ± 0.01 **b**^{2}	0.25 ± 0.00 **b**^{2}	0.33 ± 0.01 **a**^{2}
	High Light Glacial [CO_2]	0.60 ± 0.03 **ab**^{1}	0.66 ± 0.02 **a**^{1}	0.45 ± 0.02 **de**^{1}	0.54 ± 0.02 **c**^{1}	0.57 ± 0.02 **bc**^{1}	0.46 ± 0.01 **d**^{1}	0.42 ± 0.02 **de**^{1}	0.40 ± 0.01 **e**^{1}
	Low Light Ambient [CO_2]	0.27 ± 0.01 **b**^{3}	0.34 ± 0.01 **a**^{2}	0.10 ± 0.02 **cd**^{4}	0.15 ± 0.01 **c**^{3}	0.11 ± 0.00 **cd**^{3}	0.08 ± 0.01 **d**^{4}	0.09 ± 0.00 **cd**^{3}	0.14 ± 0.02 **cd**^{3}
	Low Light Glacial [CO_2]	0.36 ± 0.01 **a**^{2}	0.34 ± 0.02 **a**^{2}	0.20 ± 0.01 **bc**^{3}	0.15 ± 0.01 **c**^{3}	0.15 ± 0.01 **c**^{3}	0.17 ± 0.01 **bc**^{3}	0.23 ± 0.01 **b**^{2}	0.18 ± 0.01 **bc**^{3}
iWUE [$\mu mol\ [CO_2]\ (mol\ H_2O)^{-1}$]	High Light Ambient [CO_2]	54.82 ± 1.78**d**^{1}	58.94 ± 1.33**d**^{1}	107.12 ± 1.72**bc**^{1}	94.33 ± 2.55**c**^{2}	126.08 ± 1.95**a**^{1}	119.56 ± 6.23**ab**^{1}	122.10 ± 1.50**a**^{1}	102.44 ± 3.52**c**^{1}
	High Light Glacial [CO_2]	15.20 ± 0.49**d**^{3}	18.95 ± 1.00**d**^{3}	50.86 ± 8.06**bc**^{2}	54.69 ± 1.54**b**^{3}	35.57 ± 0.72**bc**^{4}	60.27 ± 1.47**c**^{2}	65.02 ± 1.14**bc**^{2}	65.65 ± 3.27**a**^{3}
	Low Light Ambient [CO_2]	40.23 ± 2.22**d**^{2}	31.59 ± 0.94**d**^{2}	115.02 ± 8.06**bc**^{1}	120.26 ± 3.96**ab**^{1}	103.64 ± 6.75**c**^{2}	119.76 ± 11.17**ab**^{1}	133.42 ± 3.82**a**^{1}	113.96 ± 9.04**bc**^{1}
	Low Light Glacial [CO_2]	16.04 ± 0.42**d**^{3}	17.51 ± 0.77**d**^{3}	50.17 ± 1.83**bc**^{2}	63.68 ± 2.02**b**^{3}	56.40 ± 1.72**bc**^{3}	49.18 ± 0.82**c**^{2}	57.10 ± 1.82**bc**^{2}	79.81 ± 4.84**a**^{2}
C_i ($\mu mol\ mol^{-1}$)	High Light Ambient [CO_2]	266.99 ± 2.37 **a**^{2}	263.90 ± 1.25 **a**^{2}	129.26 ± 2.14 **d**^{2}	204.31 ± 4.84 **b**^{1}	140.98 ± 5.37 **d**^{2}	174.39 ± 12.85 **c**^{2}	127.58 ± 3.29 **d**^{2}	196.28 ± 6.17 **bc**^{2}
	High Light Glacial [CO_2]	136.33 ± 0.95 **a**^{3}	124.10 ± 1.38 **a**^{3}	43.67 ± 0.46 **c**^{4}	54.12 ± 2.45 **c**^{3}	85.77 ± 0.96 **b**^{3}	40.50 ± 2.56 **c**^{4}	55.56 ± 0.35 **c**^{3}	51.34 ± 5.23 **c**^{3}
	Low Light Ambient [CO_2]	304.86 ± 3.75 **a**^{1}	327.10 ± 2.35 **a**^{1}	221.23 ± 17.18 **c**^{1}	183.48 ± 5.36 **d**^{2}	201.74 ± 10.48 **cd**^{1}	247.65 ± 15.23 **b**^{1}	151.59 ± 5.93 **e**^{1}	219.45 ± 11.72 **c**^{1}
	Low Light Glacial [CO_2]	140.46 ± 0.94 **a**^{3}	140.06 ± 1.31 **a**^{3}	84.18 ± 4.67 **b**^{3}	66.53 ± 3.10 **bc**^{3}	66.23 ± 2.76 **bc**^{3}	82.91 ± 1.62 **b**^{3}	57.00 ± 3.06 **c**^{3}	47.50 ± 1.05 **c**^{3}
A_{sat} ($\mu mol\ m^{-2}\ s^{-1}$)	High Light Ambient [CO_2]	8.74 ± 0.46 **d**^{ns}	10.47 ± 0.25 **d**^{2}	25.63 ± 1.01 **c**^{1}	33.79 ± 0.22 **a**^{2}	25.97 ± 0.98 **c**^{1}	30.60 ± 0.23 **b**^{1}	24.54 ± 0.31 **c**^{2}	34.85 ± 0.76 **a**^{2}
	High Light Glacial [CO_2]	9.05 ± 0.37 **e**^{ns}	13.24 ± 0.13 **d**^{1}	25.93 ± 1.53 **c**^{1}	37.08 ± 0.77 **a**^{1}	23.03 ± 0.15 **c**^{2}	31.92 ± 0.55 **b**^{1}	31.01 ± 0.61 **b**^{1}	28.29 ± 1.52 **b**^{3}
	Low Light Ambient [CO_2]	7.71 ± 0.18 **e**^{ns}	8.39 ± 0.08 **e**^{2}	22.19 ± 0.30 **c**^{2}	34.13 ± 1.01 **b**^{2}	21.20 ± 0.09 **cd**^{2}	21.57 ± 0.35 **c**^{2}	18.31 ± 0.67 **d**^{4}	39.53 ± 0.34 **a**^{1}
	Low Light Glacial [CO_2]	8.74 ± 0.30 **c**^{ns}	8.52 ± 0.46 **c**^{2}	22.42 ± 0.44 **b**^{2}	22.05 ± 0.20 **b**^{3}	21.54 ± 0.28 **b**^{2}	20.36 ± 0.48 **b**^{2}	22.00 ± 0.66 **b**^{3}	32.94 ± 0.49 **a**^{2}
g_{s_sat} ($mol\ m^{-2}\ s^{-1}$)	High Light Ambient [CO_2]	0.49 ± 0.03 **d**^{2}	0.51 ± 0.02 **d**^{1,2}	0.76 ± 0.07 **abc**^{1}	0.92 ± 0.04 **a**^{1}	0.82 ± 0.04 **ab**^{1}	0.71 ± 0.05 **bc**^{1}	0.59 ± 0.01 **cd**^{1,2}	0.91 ± 0.03 **a**^{1}
	High Light Glacial [CO_2]	0.69 ± 0.01 **ab**^{1}	0.65 ± 0.03 **ab**^{1}	0.68 ± 0.07 **ab**^{1}	0.81 ± 0.04 **a**^{1,2}	0.76 ± 0.02 **a**^{1}	0.67 ± 0.02 **ab**^{1}	0.57 ± 0.03 **b**^{1,2}	0.54 ± 0.03 **b**^{2}
	Low Light Ambient [CO_2]	0.42 ± 0.03 **d**^{2}	0.55 ± 0.02 **bcd**^{1,2}	0.43 ± 0.03 **d**^{2}	0.73 ± 0.03 **ab**^{2}	0.71 ± 0.04 **abc**^{1}	0.62 ± 0.07 **bc**^{1}	0.53 ± 0.06 **cd**^{2}	0.87 ± 0.01 **a**^{1}
	Low Light Glacial [CO_2]	0.55 ± 0.04 **bc**^{1,2}	0.49 ± 0.03 **cd**^{2}	0.71 ± 0.05 **b**^{1}	0.48 ± 0.06 **cd**^{3}	0.33 ± 0.01 **d**^{2}	0.40 ± 0.01 **cd**^{2}	0.71 ± 0.03 **b**^{1}	0.90 ± 0.09 **a**^{1}

Table 2. 4 Summary of stomatal traits for eight grass species acclimated to glacial [CO_2] and low light.

Values are means ± SE (n=3-5). Lower case letters in bold indicate the ranking of species within treatments. Numbers in superscript indicate the ranking of treatments within species. Tukey's HSD *post hoc* at 5% level was employed. Values with the same letter (or number) are not significantly different at α=0.05.

Parameter	Treatment	C_3		NAD-ME		NADP-ME		PCK	
		P. bisulcatum	*S. laxa*	*P. miliaceum*	*L. fusca*	*P. antidotale*	*S. italica*	*M. maximus*	*C. gayana*
SA (μm^2)	High Light Ambient [CO_2]	51.96 ± 1.28 **a**^{2}	28.97 ± 1.13 **c**^{3}	42.89 ± 0.86 **b**^{2}	30.20 ± 2.46 **c**^{2}	32.30 ± 1.62 **c**^{2}	25.95 ± 1.73 **c**^{2,3}	15.77 ± 0.92 **d**^{2}	12.21 ± 0.18 **d**^{2}
	High Light Glacial [CO_2]	84.31 ± 1.69 **a**^{1}	45.89 ± 1.58 **cd**^{1}	57.83 ± 4.38 **b**^{1}	49.56 ± 2.44 **bcd**^{1}	54.34 ± 2.14 **bc**^{1}	42.46 ± 2.76 **d**^{1}	28.06 ± 0.25 **e**^{1}	19.21 ± 0.73 **f**^{1,2}
	Low Light Ambient [CO_2]	42.15 ± 1.66 **a**^{3}	28.17 ± 0.69 **b**^{3}	24.80 ± 0.98 **bc**^{3}	17.42 ± 0.83 **cd**^{3}	27.61 ± 0.24 **b**^{2}	20.47 ± 0.72 **bc**^{2}	10.43 ± 0.11 **d**^{1}	17.15 ± 0.68 **cd**^{2}
	Low Light Glacial [CO_2]	57.63 ± 3.44 **a**^{2}	38.13 ± 1.77 **b**^{2}	40.34 ± 0.52 **b**^{2}	21.16 ± 0.98 **d**^{3}	33.42 ± 0.84 **bc**^{2}	29.36 ± 1.53 **cd**^{2}	26.11 ± 1.01 **cd**^{2}	25.66 ± 0.31 **cd**^{1}
SS (μm^2)	High Light Ambient [CO_2]	834.56 ± 11.55 **b**^{2}	520.46 ± 42.21 **e**^{1}	1026.06 ± 12.8 **a**^{1}	609.25 ± 15.83 **d**^{1}	713.10 ± 16.07 **c**^{1}	565.88 ± 4.99 **de**^{1}	344.75 ± 12.85 **f**^{1}	254.43 ± 9.56 **g**^{3}
	High Light Glacial [CO_2]	655.92 ± 20.57 **b**^{3}	469.76 ± 16.46 **cd**^{1}	811.39 ± 28.25 **a**^{2}	407.20 ± 6.67 **d**^{2}	497.81 ± 5.69 **c**^{3}	503.92 ± 17.35 **c**^{1}	309.82 ± 5.20 **e**^{1}	308.50 ± 2.50 **e**^{2,3}
	Low Light Ambient [CO_2]	927.47 ± 24.66 **a**^{1}	527.36 ± 13.50 **b**^{1}	603.15 ± 12.83 **b**^{3}	367.44 ± 8.04 **c**^{2}	614.29 ± 25.3 **b**^{2}	387.80 ± 6.77 **c**^{2}	328.99 ± 5.59 **c**^{1}	358.75 ± 2.81 **c**^{1,2}
	Low Light Glacial [CO_2]	693.43 ± 43.42 **a**^{3}	395.08 ± 10.41 **bc**^{2}	635.25 ± 14.98 **a**^{3}	375.92 ± 4.54 **bc**^{2}	636.14 ± 2.83 **a**^{1,2}	415.89 ± 9.02 **b**^{2}	328.08 ± 3.65 **c**^{1}	386.36 ± 2.06 **bc**^{1}
SD (mm^{-2})	High Light Ambient [CO_2]	121.91 ± 3.01 **b**^{2}	133.09 ± 10.91 **b**^{1}	69.26 ± 1.97 **c**^{1}	123.90 ± 1.94 **b**^{2}	67.49 ± 2.13 **c**^{1}	140.08 ± 3.79 **b**^{1}	133.77 ± 8.41 **b**^{2}	211.45 ± 22.15 **a**^{1}
	High Light Glacial [CO_2]	153.11 ± 5.33 **b**^{1}	133.56 ± 3.81 **b**^{1}	83.52 ± 4.41 **c**^{1}	154.26 ± 6.41 **b**^{1}	75.14 ± 1.44 **c**^{1}	141.82 ± 5.37 **b**^{1}	163.23 ± 3.24 **ab**^{1}	185.81 ± 7.40 **a**^{1,2}
	Low Light Ambient [CO_2]	105.69 ± 2.47 **b**^{2}	110.26 ± 2.71 **b**^{1}	84.41 ± 1.98 **bc**^{1}	96.63 ± 1.04 **bc**^{3}	64.46 ± 0.73 **c**^{1}	149.00 ± 2.67 **a**^{1}	105.79 ± 4.82 **b**^{3}	166.54 ± 7.89 **a**^{2,3}
	Low Light Glacial [CO_2]	130.23 ± 9.23 **ab**^{1,2}	124.07 ± 2.85 **abc**^{1}	80.09 ± 3.34 **d**^{1}	100.57 ± 0.48 **bcd**^{2,3}	84.75 ± 0.59 **d**^{1}	150.18 ± 11.37 **a**^{1}	98.26 ± 3.36 **cd**^{3}	146.01 ± 6.77 **a**^{3}
SI (%)	High Light Ambient [CO_2]	18.91 ± 0.61 **d**^{2}	24.59 ± 0.58 **bc**^{1}	19.88 ± 0.81 **d**^{1}	21.81 ± 0.60 **cd**^{1}	29.38 ± 0.57 **a**^{1}	25.92 ± 0.36 **b**^{1}	20.81 ± 1.16 **d**^{1,2}	18.77 ± 0.94 **d**^{1}
	High Light Glacial [CO_2]	23.32 ± 0.34 **bc**^{1}	25.62 ± 0.61 **b**^{1}	20.10 ± 0.80 **c**^{1}	22.80 ± 0.69 **bc**^{1}	29.58 ± 1.39 **a**^{1}	24.99 ± 0.66 **b**^{1,2}	23.04 ± 0.55 **bc**^{1}	20.89 ± 0.64 **bc**^{1}
	Low Light Ambient [CO_2]	18.29 ± 0.29 **c**^{2}	22.84 ± 0.38 **b**^{1,2}	19.85 ± 0.20 **bc**^{1}	16.62 ± 0.57 **c**^{2}	28.56 ± 1.51 **a**^{1}	23.16 ± 0.58 **b**^{1,2}	18.30 ± 0.94 **c**^{2}	20.00 ± 0.49 **cd**^{1}
	Low Light Glacial [CO_2]	18.92 ± 0.85 **cd**^{2}	21.51 ± 0.56 **bc**^{2}	17.55 ± 0.94 **d**^{1}	16.99 ± 0.60 **d**^{2}	30.68 ± 0.56 **a**^{1}	22.58 ± 1.04 **b**^{2}	19.37 ± 0.49 **bcd**^{2}	19.78 ± 0.30 **bcd**^{1}
OD (mm^{-2})	High Light Ambient [CO_2]	98.94 ± 3.38 **a**^{2}	114.21 ± 9.87 **a**^{1,2}	63.73 ± 1.91 **b**^{1,2}	62.58 ± 3.61 **b**^{2}	50.31 ± 5.85 **b**^{1,2}	101.83 ± 7.89 **a**^{1}	95.76 ± 8.36 **a**^{2}	99.08 ± 7.47 **a**^{2}
	High Light Glacial [CO_2]	133.01 ± 4.25 **ab**^{1}	119.24 ± 3.53 **bc**^{1}	77.88 ± 4.87 **d**^{1}	119.34 ± 5.31 **bc**^{1}	70.72 ± 0.96 **d**^{1}	109.82 ± 3.81 **c**^{1}	153.82 ± 3.40 **a**^{1}	126.16 ± 6.06 **bc**^{1}
	Low Light Ambient [CO_2]	49.92 ± 3.21 **b**^{3}	85.72 ± 4.82 **a**^{3}	33.18 ± 2.94 **b**^{3}	40.39 ± 3.78 **b**^{3}	40.45 ± 0.91 **b**^{2}	49.77 ± 1.75 **b**^{2}	32.38 ± 1.43 **b**^{4}	84.20 ± 2.97 **a**^{2}
	Low Light Glacial [CO_2]	107.99 ± 7.88 **a**^{2}	98.81 ± 3.36 **ab**^{2,3}	54.44 ± 3.18 **c**^{2}	57.99 ± 2.09 **c**^{2,3}	57.99 ± 2.09 **c**^{2}	97.47 ± 6.46 **ab**^{1}	52.14 ± 4.56 **c**^{3}	82.83 ± 4.48 **b**^{2}
g_{s_amax} (mol m^{-2} s^{-1})	High Light Ambient [CO_2]	1.60 ± 0.05 **bc**^{2}	1.22 ± 0.07 **cd**^{3}	1.36 ± 0.11 **bcd**^{2}	1.64 ± 0.04 **bc**^{2}	1.26 ± 0.01 **cd**^{1}	2.13 ± 0.06 **a**^{1}	1.10 ± 0.02 **d**^{1}	1.76 ± 0.20 **ab**^{2}
	High Light Glacial [CO_2]	1.98 ± 0.04 **abc**^{1}	1.87 ± 0.08 **cd**^{1,2}	2.05 ± 0.10 **abc**^{1}	2.33 ± 0.11 **ab**^{1}	1.39 ± 0.03 **e**^{1}	2.37 ± 0.12 **a**^{1}	1.43 ± 0.01 **de**^{1}	1.91 ± 0.08 **bc**^{2}
	Low Light Ambient [CO_2]	1.24 ± 0.03 **bc**^{3}	1.68 ± 0.09 **b**^{2}	1.23 ± 0.07 **bc**^{2}	0.72 ± 0.04 **de**^{3}	1.19 ± 0.01 **cd**^{1}	1.60 ± 0.06 **bc**^{2}	0.66 ± 0.04 **e**^{2}	2.57 ± 0.12 **a**^{1}
	Low Light Glacial [CO_2]	1.31 ± 0.07 **c**^{2,3}	2.22 ± 0.24 **a**^{1}	1.38 ± 0.08 **bc**^{2}	0.78 ± 0.04 **d**^{3}	1.25 ± 0.07 **c**^{1}	2.30 ± 0.11 **a**^{1}	1.06 ± 0.08 **cd**^{1}	1.77 ± 0.15 **b**^{2}

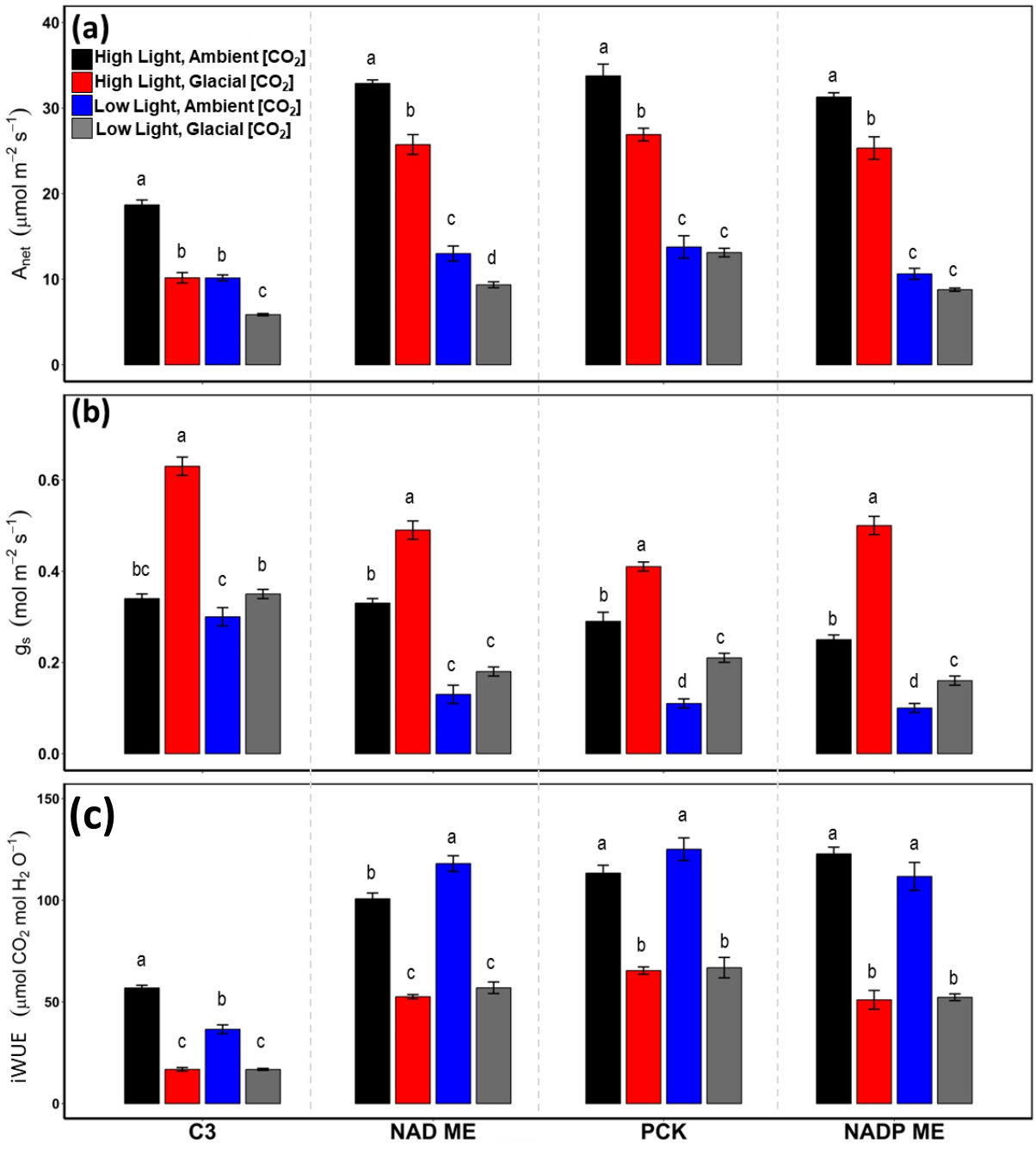

Figure 2. 1 Effects of glacial [CO_2] and low light on gas exchange parameters of two C_3 and six C_4 grasses (two of each subtype):

(**A**) Net CO_2 assimilation rate (A_{net}), (**B**) stomatal conductance (g_s), and (**C**) Leaf intrinsic water-use efficiency (iWUE = A_{net}/g_s) measured at growth conditions. Data represent means ± SE with species as replicate within each type/subtype. Means with the same letter are not significantly different at α=0.05 using Tukey's HSD *post hoc*.

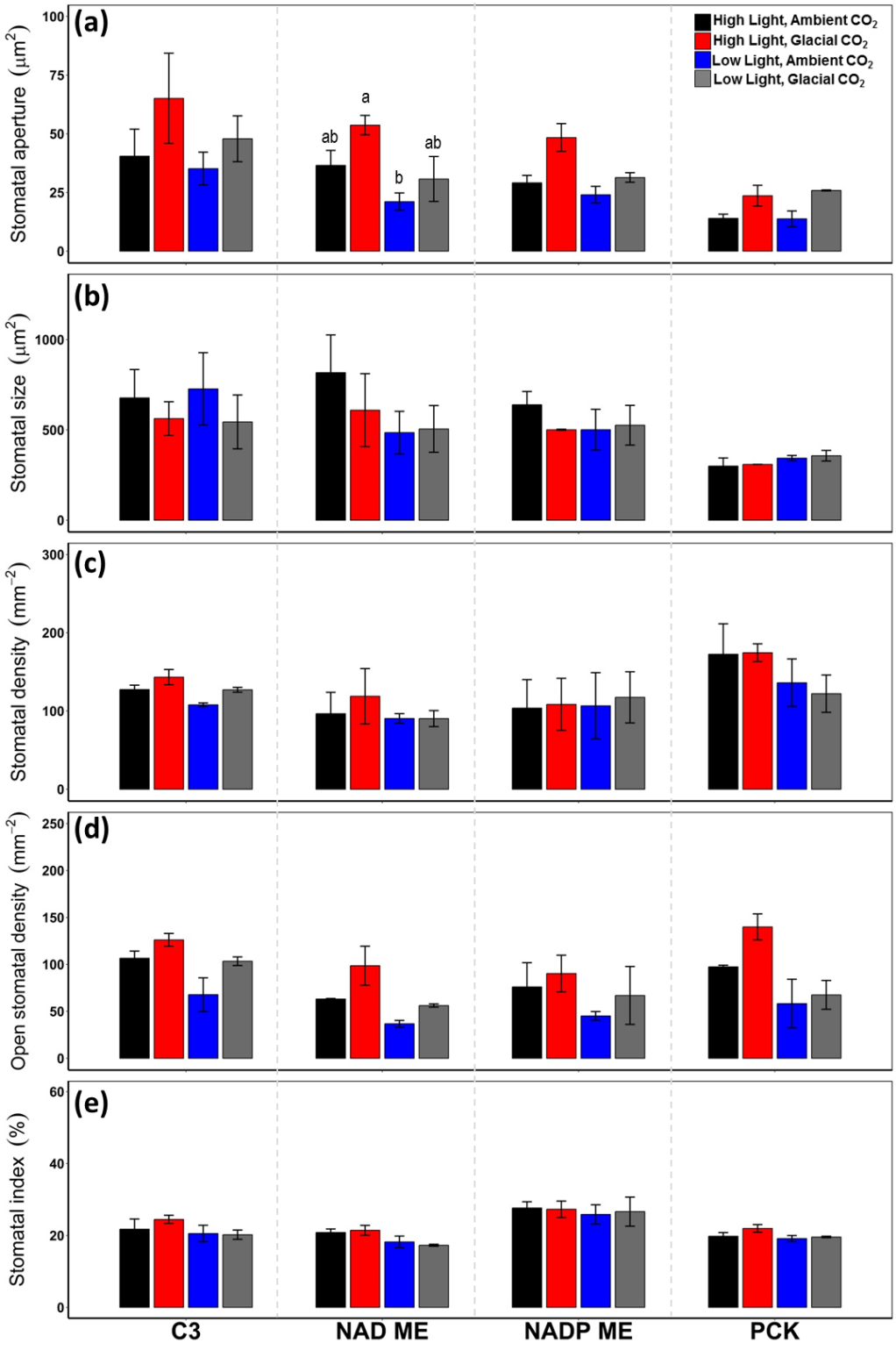

Figure 2. 2 Acclimation of stomata traits to glacial [CO_2] and low light in two C_3 and six C_4 grasses (two of each subtype)

(**A**) stomatal aperture, (**B**) stomatal size, (**C**) stomatal density, (**D**) density of open stomata, (**E**) stomatal index. Data represent means ± SE of the species within each type/subtype consisting of 3-5 biological replicates with >300 stomata measured per species. Means with the same letter are not significantly different at α=0.05 using Tukey's HSD *post hoc*.

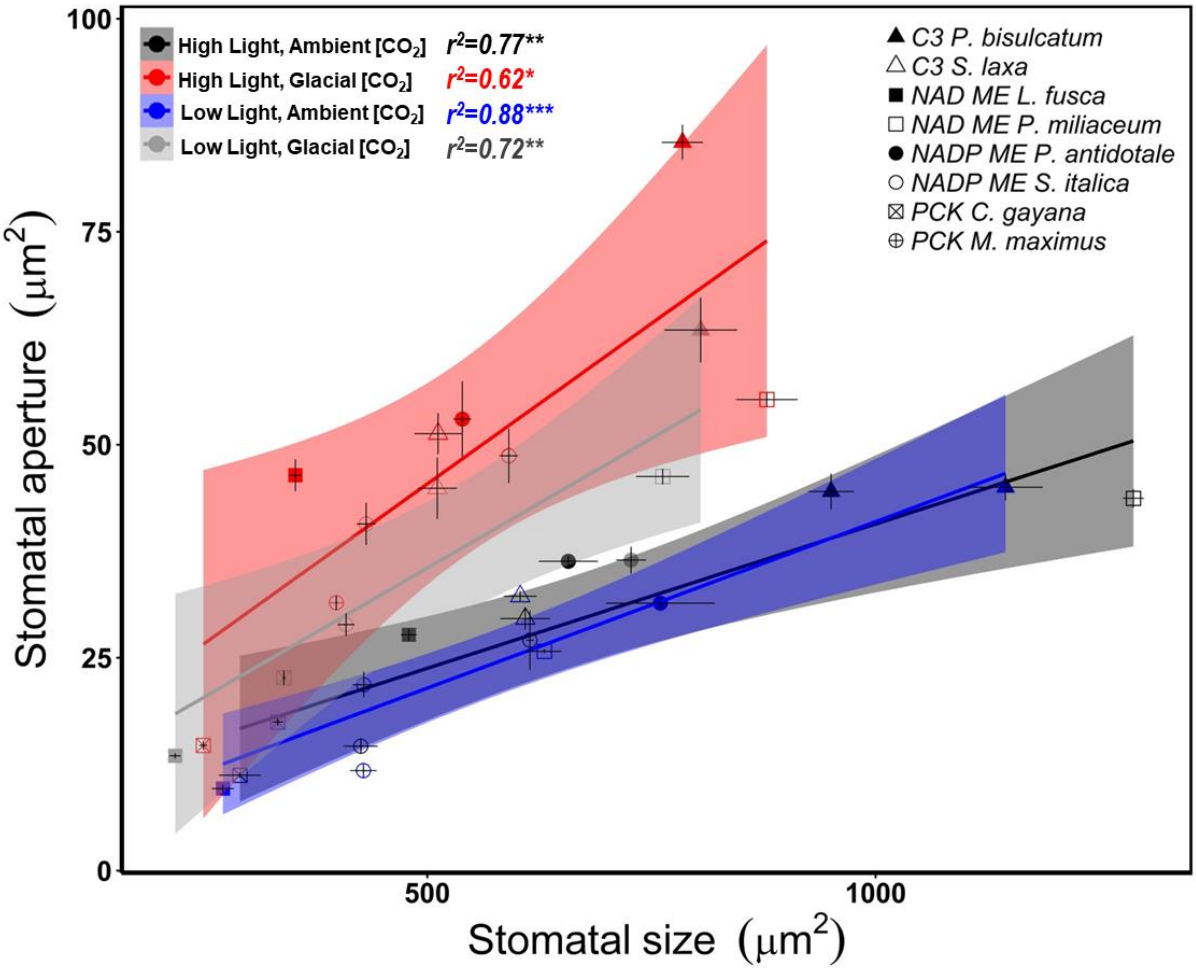

Figure 2. 3 Acclimation responses of stomatal size and stomatal aperture to glacial [CO_2] and low light among two C_3 and six C_4 grasses (two of each subtype).

Dots represent the mean ± SE of 3-5 biological replicates consisting of >300 stomata in each species. Shaded regions represent the 95% confidence interval of the linear model in each growth conditions. Fitted linear model equations are: High Light-Ambient [CO_2]: $SA = 0.0474 \times SS + 1.1798$; High Light-Glacial [$CO_2$]: $SA = 0.088 \times SS + 4.1179$; Low Light-Ambient [$CO_2$]: $SA = 0.0456 \times SS + 0.0887$; Low Light-Glacial [$CO_2$]: $SA = 0.0622 \times SS + 3.9239$. $^{ns}p>0.05$; *$p<0.05$; **$p<0.01$; ***$p<0.001$.

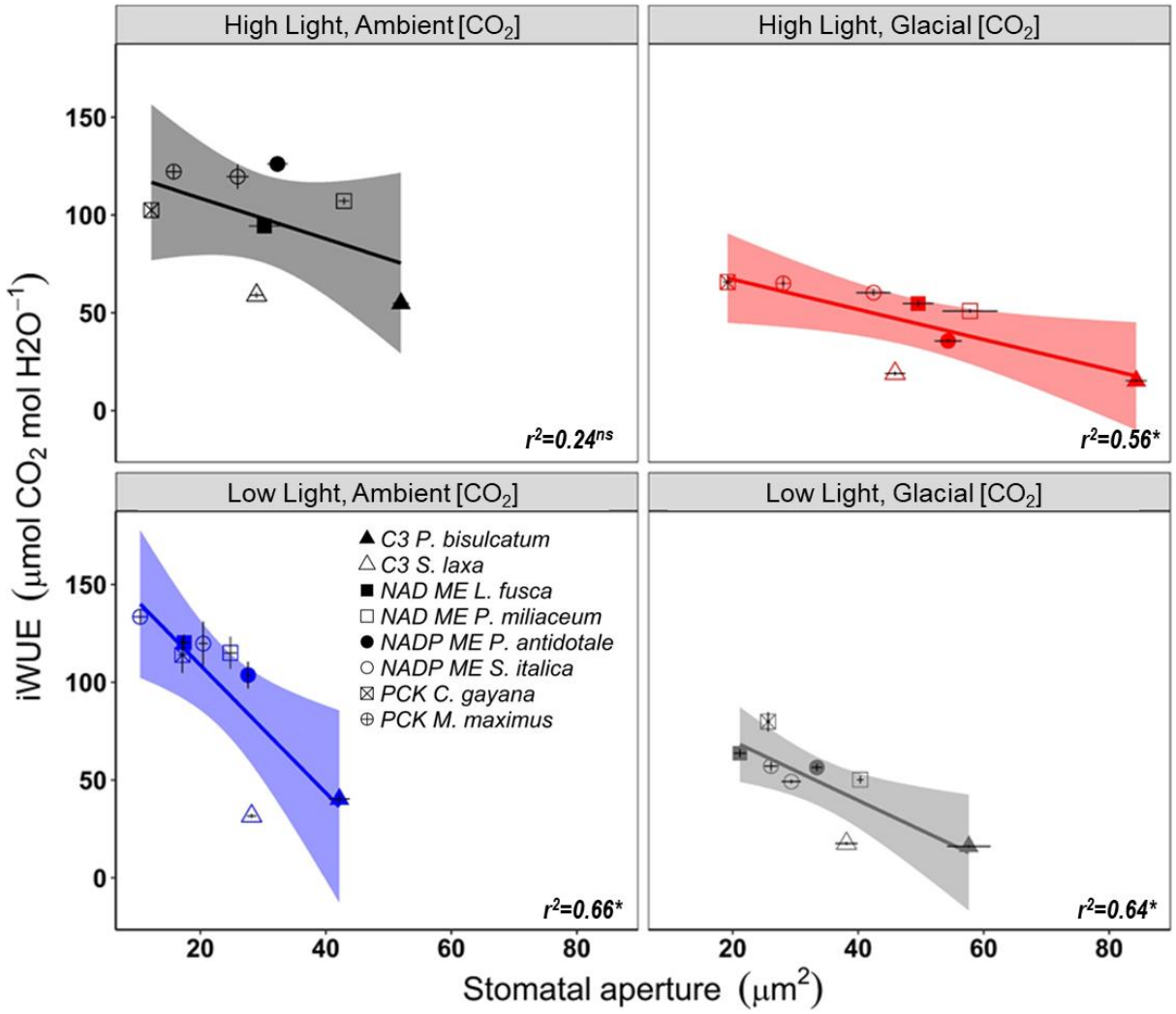

Figure 2. 4 The relationship between iWUE and SA for eight grasses acclimated to glacial [CO_2] and low light.

Data are means ± SE of 3-5 biological replicates consisting of >150 stomata in each species. Shaded regions represent the 95% confidence interval of the linear model in each growth conditions. Fitted linear model equations are: High Light-Ambient [CO_2]: $iWUE = 129.36 - 1.0384 \times SA$; High Light-Glacial [$CO_2$]: $iWUE = 82.464 - 0.769 \times SA$; Low Light-Ambient [$CO_2$]: $iWUE = 174.05 - 3.2651 \times SA$; Low Light-Glacial [$CO_2$]: $iWUE = 100.24 - 1.5158 \times SA$. $^{ns}p>0.05$; $*p<0.05$; $**p<0.01$; $***p<0.001$.

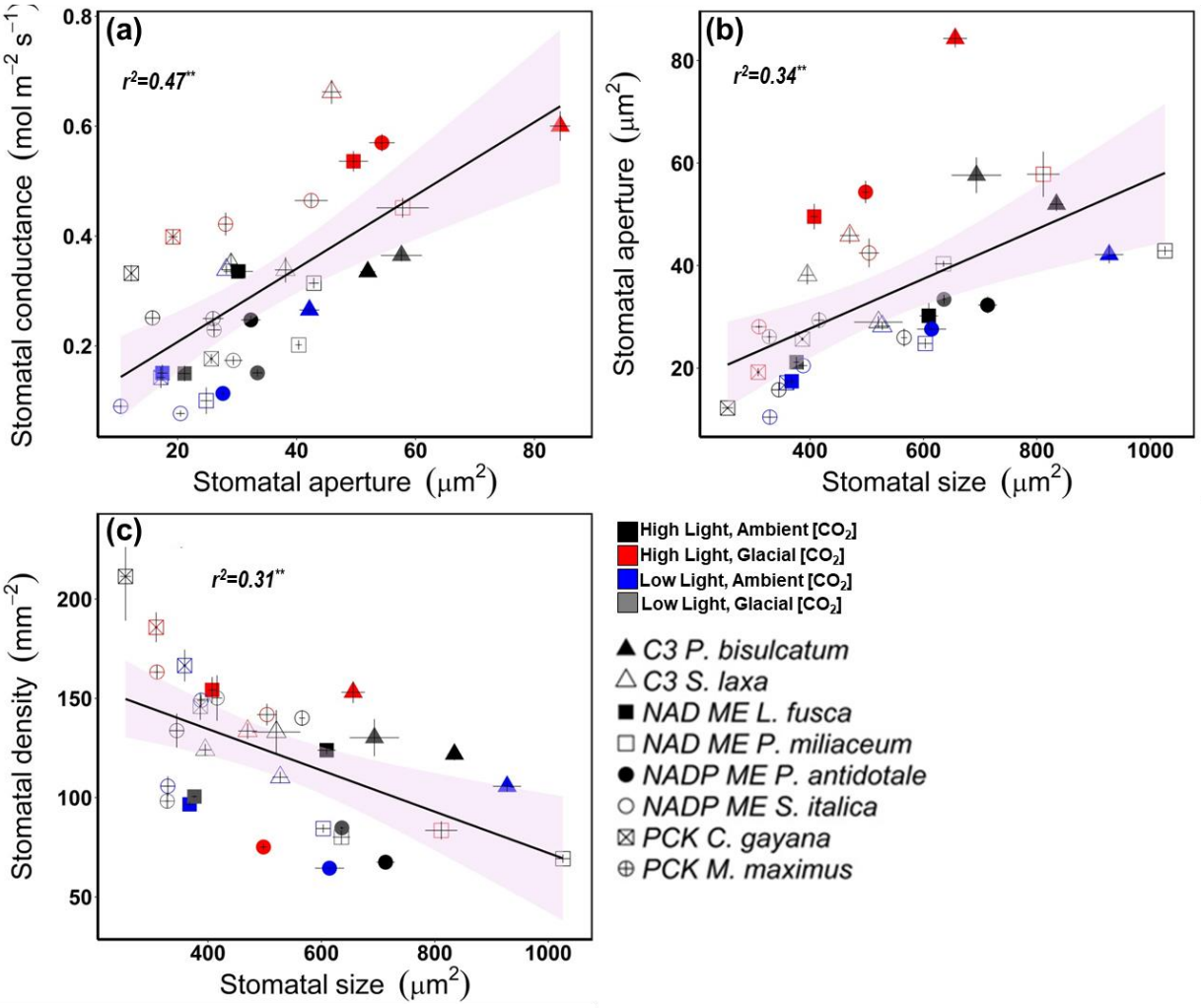

Figure 2. 5 Acclimation responses of stomatal and gas exchange traits to glacial [CO_2] and low light among two C_3 and six C_4 grasses (two of each subtype).

Dots represent the mean ± SE of 3-5 biological replicates consisting of >300 stomata in each species whilst colours denote growth conditions. Shaded regions represent the 95% confidence interval of the linear model in each growth conditions. Fitted linear models are as follows: (**a**) $g_s = 0.0067 \times SA + 0.0742$; (**b**) $SA = 0.0485 \times SS + 8.3318$; (**c**) $SD = 176.19 - 0.1041 \times SS$ **p<0.05; **p<0.01; ***p<0.001*.

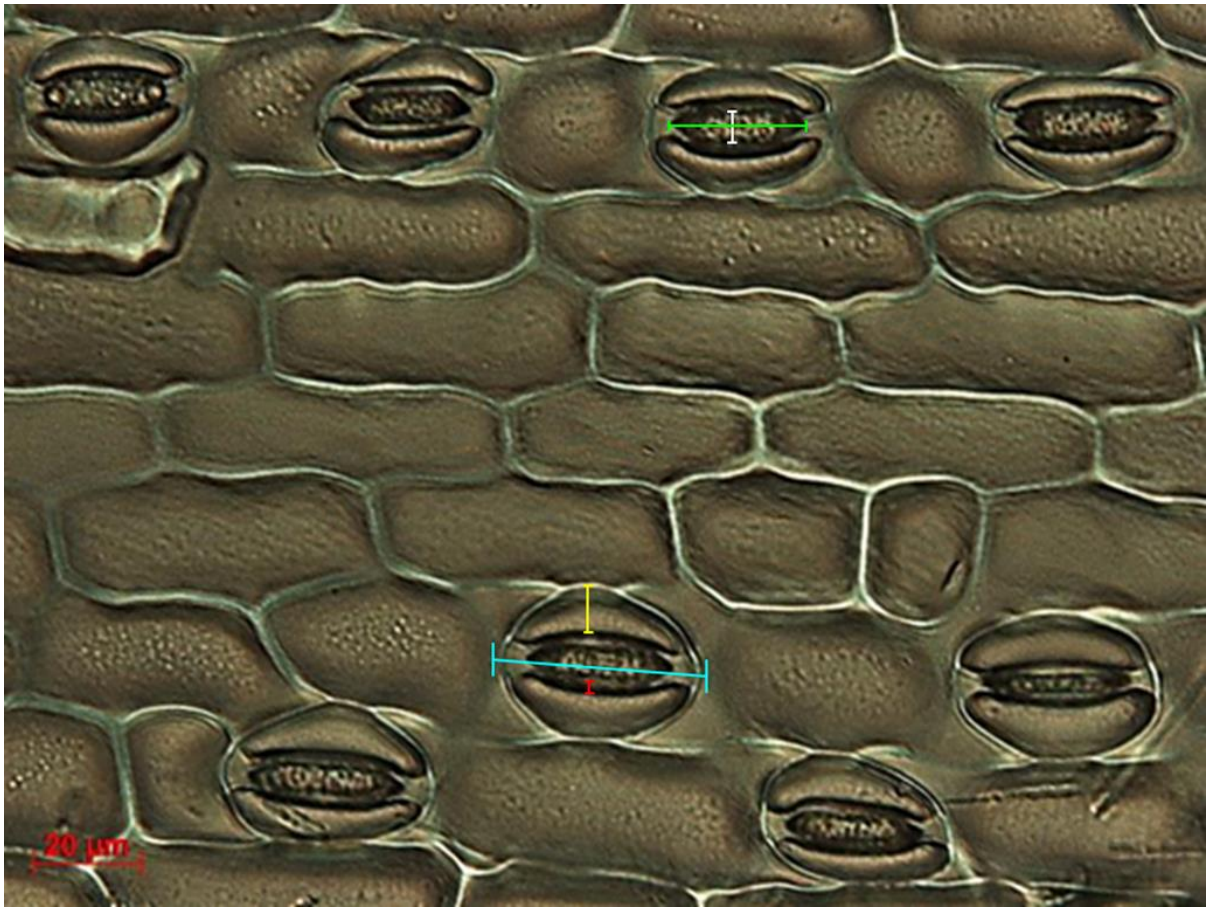

Figure S2. 1 Measurements of stomatal morphology at 400× total magnification.

The green line represents aperture length (AL) while the white line signifies aperture width (AW), which were the parameters used in estimating stomatal aperture (SA). Stomatal size (SS) was estimated using guard cell length (GCL) as the long axis of the ellipse (blue line) and the sum of guard cell width (GCW, red line) and subsidiary cell width (SCW, yellow) as the short axis.

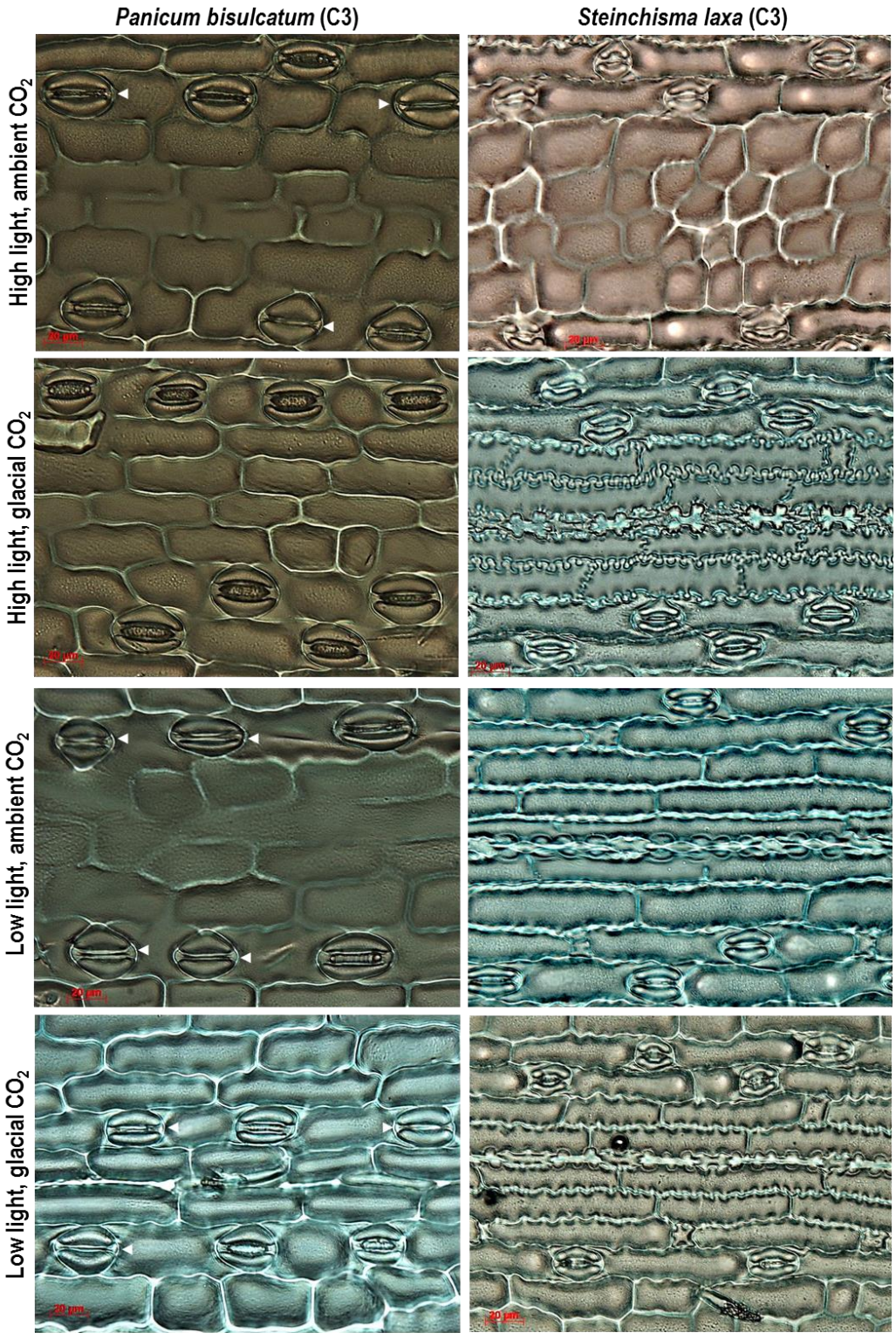

Figure S2. 2 Representative leaf epidermal and stomatal structures for eight grass species grown under four treatment combinations.

Control or HL+[aCO_2]; HL+[gCO_2]; LL+[aCO_2]; and LL+[gCO_2]. The species are *P. bisulcatum and S. laxa* (C_3); *P. antidotale* and *S. italica* (C_4-NADP-ME); *P. miliaceum and L. fusca* (C_4-NAD-ME); and *M. maximus* and *C. gayana* (C_4-PCK). White triangles indicate closed stomata.

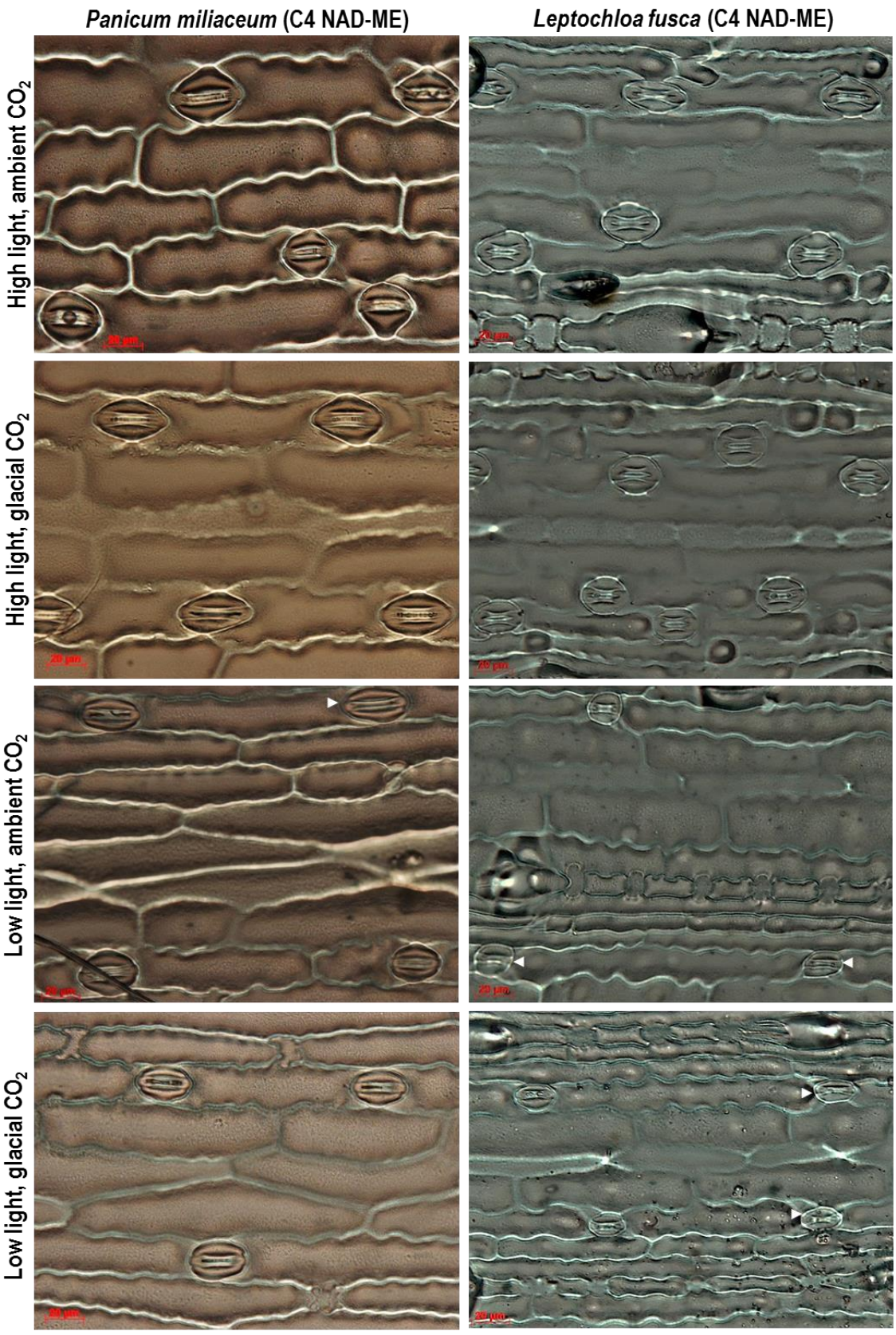

Figure S2.2 *cont'd…*

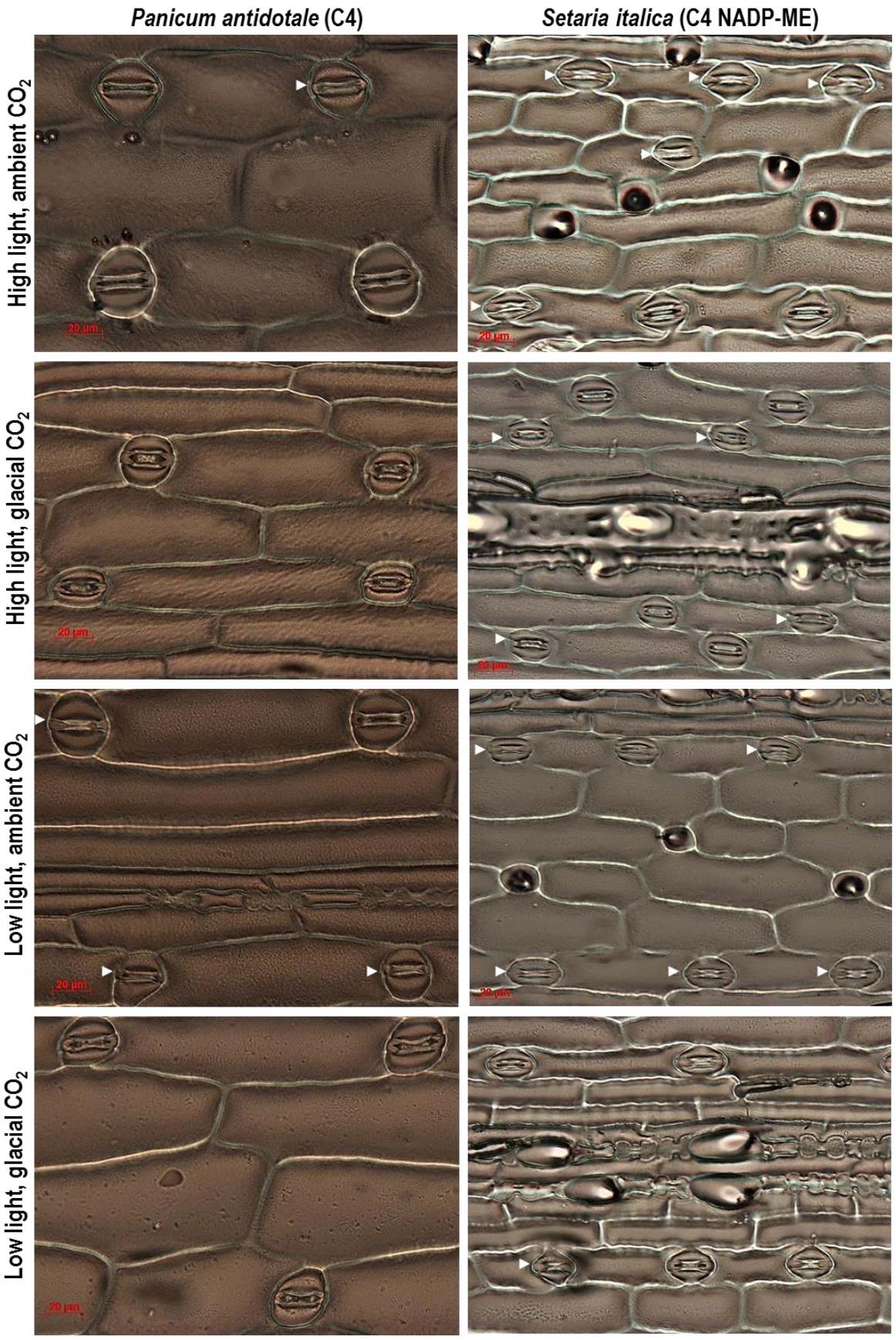

Figure S2.2 *cont'd…*

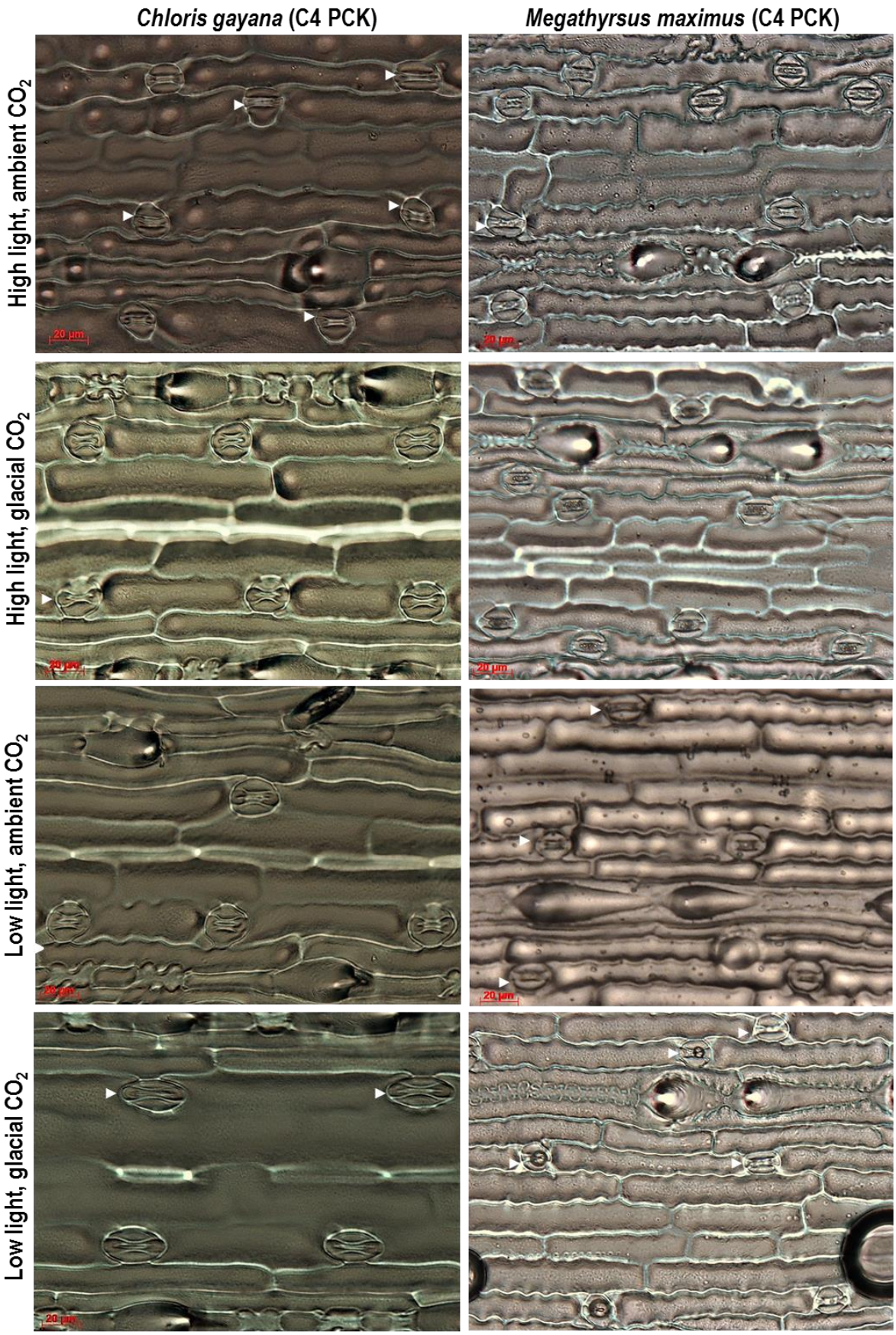

Figure S2.2 *cont'd…*

CHAPTER 3

FASTER STOMATAL OPENING HALF-TIMES IN GRASSES LINK TO SMALLER STOMATAL APERTURE AND LOWER GUARD CELL K^+ INFLUX PROVIDING TARGETS FOR IMPROVING LEAF-LEVEL iWUE

ABSTRACT

The rapidity of stomatal closure and opening in grasses is a result of the sophisticated stomatal geometry underpinning the superior functional response of grass stomata to fluctuating environmental conditions. However, it remains unclear whether the speed of stomatal responses of C_3 and C_4 grasses is influenced by two photosynthetic factors, [CO_2] and light. This study builds on Chapter 2 and is geared towards examining the response of stomatal speed and K^+ fluxes in guard cells of grasses acclimated to glacial [CO_2] ([gCO_2] = 180 µl l^{-1}) and low light (LL = 200 µmol m^{-2} s^{-1}). I grew four species from the Panicoideae subfamily representing the C_3 photosynthetic type and the three C_4 biochemical subtypes. The rate of stomatal closure and opening was measured to estimate the effects of stomatal speed on the forgone photosynthesis and excess transpiration during light transitions. I also utilised Microelectrode Ion Flux Estimation (MIFE) to measure guard cell K^+ fluxes. I found a species-specific response in opening and closing $t_{1/2}$ among the closely related Panicoideae grasses with interesting trends. Stomata with faster opening $t_{1/2}$ showed slower closing $t_{1/2}$ under control conditions. This relationship is reversed when the stomata were acclimated to [gCO_2] or LL treatment. I also report, for the first time, that in dumbbell-shaped stomata, faster opening $t_{1/2}$ forgo less photosynthesis and faster closing $t_{1/2}$ results in lower water loss during light transitions. This study also reports that [gCO_2] elicited higher guard cell K^+ influx for stomatal opening in grass guard cells regardless of photosynthetic types while LL stimulated K^+ influx only in guard cells of the C_3 species. In summary, combined analyses of stomatal and gas exchange traits in this study reveal novel mechanistic links between SA, g_s, iWUE, opening $t_{1/2}$ and K^+ influx, providing new knowledge for breeding crops with high iWUE.

Keywords: closing and opening half-times, forgone photosynthesis, guard cell K^+ flux, light transitions, water-use efficiency

3.1 INTRODUCTION

The unique morphological geometry of grass stomata allows for faster shuttling of osmotica between the two stomatal cell types (guard cells [GC] and subsidiary cells [SC]), translating to faster closing and opening compared to other stomatal types (Franks & Farquhar, 2007; McAusland *et al.*, 2016; Cai *et al.*, 2017b; Chen *et al.*, 2017). The uneven sizes of the two cell types (with GC being smaller than SC) and dumbbell-shaped GCs, results in lower water and solute exchange required for full stomatal opening and closure compared to kidney-shaped stomata (Chen *et al.*, 2017). When SCs become fully turgid, movement of GCs is fully impeded resulting in tighter stomatal closure (Franks & Farquhar, 2007) and eventually less water loss (Cai *et al.*, 2017a; Chen *et al.*, 2017).

Recently, there is a surge of studies investigating the speed of stomatal opening and closure in response to light/shade transitions as a surrogate measure for stomatal efficiency. It was popularly termed as stomatal kinetics or stomatal dynamics (Lawson & Blatt, 2014; Elliott-Kingston *et al.*, 2016; Martins *et al.*, 2016; Xiong *et al.*, 2016, 2018; Papanatsiou *et al.*, 2017; Vialet-Chabrand *et al.*, 2017a; Deans *et al.*, 2018; Taylor *et al.*, 2018). Measurements of stomatal kinetics involve monitoring how rates of stomatal conductance (g_s) increase or decrease by adjusting light intensity within the measuring chamber of an infrared gas analyser. The dynamic response of stomatal conductance during light transitions is best described by a sigmoidal model (Vico *et al.*, 2011). During stomatal opening, after illumination from transient or long-term low light (LL), g_s response is divided into three steps: (1) an initial lag time; (2) an exponential increase in g_s and; (3) a new steady-state plateau (Tausz *et al.*, 2005; Vialet-Chabrand *et al.*, 2013; McAusland *et al.*, 2016). The rapidity of stomatal closure also follows a similar but inverse pattern. This was demonstrated by Elliott-Kingston *et al.*, (2016) where they compared stomatal closing in species with different functional types across diverse taxa using the exponential decay function, which yielded a model fit of $r^2 > 0.91$. The exponential growth and decay models generated a time constant (k) and were used to compare the rapidity of stomatal response. The time constant was utilised to allow for the comparison of species with different initial and final steady-states that is independent of their g_s amplitude, providing a more accurate interpretation of response times (McAusland *et al.*, 2016; Deans *et al.*, 2018; Gerardin *et al.*, 2018).

Similar to most of the plant lineages, grasses experience short and long-term light perturbations (Qu *et al.*, 2017; Taylor & Long, 2017). During periods of low light,

photosynthesis (A_{net}) and transpiration rates (E) decline, however, under different rates (McAusland *et al.*, 2016; Lawson & Vialet-Chabrand, 2018), with E being slower as a result of photosynthetic activity down-regulation and stomatal closure (Deans *et al.*, 2018). Under stressful conditions, while leaves are not likely to gain more photosynthesis (A_{net}), slower stomatal closure tends to lose more water via transpiration, resulting in a lower instantaneous water-use efficiency (Knapp & Smith, 1987; Lawson *et al.*, 2012; Deans *et al.*, 2018). Conversely, stomata with faster responses during opening will forgo less [CO_2] losses than slower opening stomata, reaching the new steady-state A_{net} uptake (McAusland *et al.*, 2016; Vialet-Chabrand *et al.*, 2017a; Deans *et al.*, 2018; Lawson & Vialet-Chabrand, 2018). Hence, during conditions such as soil water deficit, high evaporative demand, and long periods of low light, faster stomatal movement is advantageous in optimising water-use efficiency, thus conserving soil water and decreasing hydraulic stress (Osborne & Sack, 2012; Lawson & Blatt, 2014; McAusland *et al.*, 2016; Deans *et al.*, 2018; Taylor *et al.*, 2018). Therefore, the rates of stomatal closure or opening are valuable traits for optimised iWUE (Knapp & Smith, 1987; Lawson *et al.*, 2012; Deans *et al.*, 2018).

Under natural conditions, Deans *et al.*, (2018) showed that shade-adapted leaves among fifteen species of ferns, gymnosperms, and angiosperms possessed faster stomatal opening but slower stomatal closure. Comparing the three plant groups, Xiong *et al.*, (2018) demonstrated that stomatal opening was faster in ferns and gymnosperms compared to angiosperms in dark-adapted leaves upon exposure to light, while the opposite was observed for the closing time in light-adapted leaves. In addition, Gerardin *et al.* (2018) showed that stomatal closure and opening were attenuated in shade-grown tobacco. Using the exponential model of Elliott-Kingston *et al.*, (2016), the speed of stomatal closure and opening can be estimated. The exponential growth model has been derived to estimate the forgone photosynthesis (potential CO_2 assimilation forgone due to non-photosynthetic induction during increase irradiance) and excessive transpiration (potential water loss due to slow closing stomata during periods of low irradiance) during light transitions. Deans *et al.*, (2018) utilised a model that estimated the potential of water loss via excess transpiration during transient stomatal closure after a decrease in irradiance and the potential forgone CO_2 assimilation during stomatal opening after an increase in light intensity. The models were described as the time-integrated differences between two steady states of A_{net} and E, which showed that species with faster stomatal opening showed less forgone photosynthesis. They

also showed shade-adapted species which utilise these faster opening times had slower stomatal closure times (Deans *et al.*, 2018).

Acclimations of stomatal speed to growth at glacial [CO_2] ([gCO_2]) could provide important insights on the adaptations of C_4 grass stomata to low [CO_2] to increase the efficiency of photosynthesis for their evolution and diversification (Ehleringer *et al.*, 1997; Sage, 2004; Christin *et al.*, 2008). Most studies involving stomatal acclimation to glacial [CO_2] had focused mostly on stomatal morphology and leaf biochemistry (Maherali *et al.*, 2002; Vogan & Sage, 2012; Pinto *et al.*, 2014). Studies by Merilo *et al.*, (2014) and Morison & Gifford, (1983) focused on the effects of low [CO_2] concentrations on stomatal responses but did not involve acclimations but rather short-term exposure to low-cuvette [CO_2] concentrations. Only a few studies have focused on the effects of growth to glacial [CO_2] on stomatal kinetics. Recently, Taylor *et al.*, (2018) compared four C_3 and four C_4 grass species acclimated to glacial [200 µmol mol^{-1}], ambient [400 µmol mol^{-1}], and elevated [640 µmol mol^{-1}] [CO_2], and showed that C_3 leaves decrease g_s faster than C_4 leaves. However, the comparisons included the amplitude of steady-state g_s between the two photosynthetic types during the estimation of the rates of g_s change from light to shade. The limitation of this comparison is that plant functional types tend to vary in steady-state g_s; hence, plants with higher steady-state g_s will likely to have higher response rates. Thus, the best way to compare the rapidity of the temporal response of g_s to a step-change in light among species is by comparing their time constants (Vialet-Chabrand *et al.*, 2013; McAusland *et al.*, 2016; Deans *et al.*, 2018).

Aside from the dynamic movement of stomatal aperture, the involvement of potassium ions, the major cation that drives water uptake in guard cells of grasses acclimated to [gCO_2] and low light, were also investigated. Cell-specific ion flux assays in guard cells were initially achieved by performing voltage-clamp assays in protoplast isolated cells (Chen *et al.*, 2012a). However, this method involves laborious steps such as cell wall digestion and the problems of protoplast stability under osmotic pressure (Chen *et al.*, 2012a), as well as the unwanted selective K^+ channel endocytosis in the plasma membrane of plants under the presence of abscisic acid (Sutter *et al.*, 2007). The microelectrode ion flux estimation (MIFE) assay made it possible to measure fluxes of different ions in different tissues and cell types such as barley roots subjected to salt stress (Chen *et al.*, 2005), soybean leaf mesophyll in drought stress (Mak *et al.*, 2014) and stomatal guard cells in *Arabidopsis* (Chen *et al.*, 2012; Pornsiriwong *et al.*, 2017) and other plant species (Zhao *et al.*, 2019).

In Chapter 2, it was shown that acclimation to a single generation of glacial [CO_2] and low light elicited morphological responses on stomatal morphology and photosynthetic traits. The dynamic role of stomatal aperture in controlling leaf iWUE was particularly highlighted. In this chapter, the aims of this Chapter were 1.) to investigate the dynamics of stomatal control by examining the rates of stomatal opening and closure and the K^+ fluxes in guard cells of intact leaves of four Panicoid species, representing the C_3 photosynthetic type and three C_4 biochemical subtypes and 2.) to study whether faster stomatal opening in grasses forgoes less photosynthesis and slower closing stomata losses more water vapour during transient light transitions. I hypothesised that each grass species follows the species-specific response of stomatal kinetics traits to [gCO_2] and LL as was observed in Chapter 2 for stomatal traits. I likewise hypothesised that more significant net K^+ influxes would be found during growth to [gCO_2] due to the bigger opening of stomatal aperture (SA). Consequently, acclimations to LL will induce lower K^+ influxes due to smaller SA.

3.2 MATERIALS AND METHODS

3.2.1 Plant culture and growth conditions

Four grasses representing the C_3 photosynthetic type and three C_4 biochemical subtypes from the Panicoideae subfamily were grown under the same conditions (growth chambers, photoperiod, relative humidity, watering cycle, nutrient supplement) as described in Chapter 2.2.1). The four species were: *Panicum bisulcatum* (C_3), *Panicum miliaceum* (C_4-NAD-ME), *Panicum antidotale* (C_4-NADP-ME) and *Megathyrsus maximus* (C_4-PCK) (Grass Phylogeny Working Group II, 2012). Each species was planted in three biological replicates and grown in four chambers with different [CO_2] concentration (ambient: 400 µl l^{-1}; glacial: 180 µl l^{-1}) and light intensity (high: 1,000 µmol m^{-2} s^{-1}; low: 200 µmol m^{-2} s^{-1}). The control chamber condition includes high light (HL) and ambient [CO_2] (HL+[aCO_2]). The other growth chambers include a single [CO_2]-limited chamber (HL+[gCO_2]), light-limited (LL+[aCO_2]) and dual limitations of [CO_2] and light (LL+[gCO_2]).

3.2.2 Stomatal responses to light transitions

The rates of stomatal closure in response to low light (100 µmol m^{-2} s^{-1}) followed by rate of stomatal opening in response to high light (1,000 µmol m^{-2} s^{-1}) were measured under similar conditions as steady-state measurements for four Panicoidea species: *P. bisulcatum* (C_3), *P. miliaceum* (C_4-NAD-ME), *P. antidotale* (C_4-NADP-ME) and *M. maximus* (C_4-PCK). Initially, leaves were pre-adapted at 400 µl [CO_2] l^{-1} and 1,000 µmol m^{-2} s^{-1} for 20-30 min until reaching steady-state CO_2 uptake. Subsequently, steady-state g_s was auto-logged every 10 s for 15 min after which light intensity was reduced to 100 µmol m^{-2} s^{-1}. The exponential decay of g_s was monitored every 10 s until a new steady-state was achieved (~20 min). Light intensity was then increased to 1,000 µmol m^{-2} s^{-1} to monitor the rate of stomatal opening (**Figure 3. 1**).

The rate of stomatal closure was fitted using an exponential decay model as described by Elliott-Kingston *et al.,* (2016):

$$g_s(t) = g_s(\infty_c) + (g_s[\mathrm{i}] - g_s[\infty_c]) \cdot e^{-kt} \qquad \text{equation 3.1}$$

where $g_s(t)$ is the stomatal conductance at the time point (t), g_s (∞_c) is the stomatal conductance at the new steady-state after irradiance was switched to 100 µmol m^{-2} s^{-1}, g_s[i] is the initial steady-state conductance at $t = 0$, k is the exponential decay constant, and closing half-time ($t_{1/2}$) is the time required for the initial g_s to decrease by 50%.

The rate of g_s opening was fitted using an exponential growth model:

$$g_s(t) = g_s(\infty_r) + (g_s[\mathrm{i}] - g_s[\infty_r]) \cdot (1 - e^{-kt}) \qquad \text{equation 3.2}$$

where $g_s(t)$ is the stomatal conductance at the time point (t), g_s (∞_r) is the stomatal conductance at the new steady-state after irradiance was switched back to 1000 µmol m^{-2} s^{-1}, g_s[i] is the initial steady-state conductance at 100 µmol m^{-2} s^{-1}, k is the exponential growth constant, and opening half-time ($t_{1/2}$) is the time required for the steady-state g_s at 100 µmol m^{-2} s^{-1} to double exponentially. Closing and opening half-times were calculated using the respective exponential decay or rise constants (k) as $t_{1/2} = \mathrm{Log}_e(2)/k$. Lower opening and closing $t_{1/2}$ means faster response time.

3.2.3 Estimation of excess transpiration and forgone photosynthesis during light transitions

Excess transpiration (ΔW, **Figure 3. 2A**) due to slow stomatal closure during transitions from HL (1,000 µmol m^{-2} s^{-1}) to LL (100 µmol m^{-2} s^{-1}) was estimated according to Deans *et al.*, (2018). It was defined as the time-integrated difference between the initial and final steady-state transpiration rates (E):

$$Excess\ transpiration\ (\Delta W) = \int_0^{t\infty} \left(E_{[i]} - E_{[\infty]}\right) \mathrm{d}t \qquad \text{equation 3.3}$$

where E[i] was the initial steady-state E at 1,000 µmol m^{-2} $s^{-1,}$ and $E[\infty]$ was the transpiration rate at time point 90% (t_{90}) wherein 90% of the residual E is no longer changing under the new steady-state (100 µmol m^{-2} s^{-1}).

Forgone potential photosynthesis (ΔC, **Figure 3. 2B**) due to slow stomatal opening during transitions from LL to HL was defined as the time-integrated difference between the final and initial A_{net} rates according to (Deans *et al.*, 2018):

$$Forgone\ photosynthesis\ (\Delta C) = \int_0^{t\infty} \left(A_{net[\infty]} - A_{net[i]}\right) \mathrm{d}t \qquad \text{equation 3.4}$$

where $A_{net}[\infty]$ was the final steady-state assimilation rate at HL (1,000 µmol m^{-2} s^{-1}) and $A_{net}[i]$ was the residual steady-state assimilation rate at LL (100 µmol m^{-2} s^{-1}).

3.2.4 Microelectrode ion flux estimation

The fluxes of K^+, a major ion responsible for controlling the volume of guard cells to achieve the opening and closure of stomata, were measured for four Panicoidea species: *P. bisulcatum* (C_3), *P. miliaceum* (C_4-NAD-ME), *P. antidotale* (C_4-NADP-ME) and *M. maximus* (C_4-PCK). Measurements were performed using microelectrode ion flux estimation on guard cells of leaf epidermal peels (Chen *et al.*, 2005, 2012a; Pornsiriwong *et al.*, 2017) with some modifications. Prior to measurements, ion-selective microelectrodes were prepared as described by Chen *et al.*, (2005) and subsequently backfilled with backfilling solution (200 mM KCl). The tip was broken to achieve a small (2-3 µm) diameter and was front-filled with potassium ionophore I (Sigma, Switzerland), a liquid ion exchanger to achieve high microelectrode resistance (4–6 GΩ). The microelectrodes were then mounted into the micromanipulator holder with AgCl wire together with a reference microelectrode backfilled with 1 M KCl in 2% agar. The microelectrodes were calibrated using 2, 5, and 10 mM KCl achieving a calibration slope of 55 mV and a correlation coefficient ≥ 0.999.

Leaf epidermal layers from the abaxial leaf surface were peeled and were soaked in an opening buffer (50 mM KCl, 5 mM Na-MES, pH 6.1) after prompt-peeling to ensure stomatal integrity and reduce mechanical damage to the cells. The peels were mounted on a glass cover slide using a silicon prosthetic adhesive (Dow-Corning, USA) and immersed in a chamber filled with the stomatal measuring solution (10 mM KCl, 0.5 mM $CaCl_2$, 5 mM MES-KOH, pH 6.1) in a 45-degree position. The peels equilibrated in the stomata measuring solution were focused on the same plane together with the microelectrodes that were focused on top of the guard cells and moving in two positions, near the cells (10 µm) and away from the cell surface (40 µm) in 5-sec cycle, 80 µm amplitude for 10 min. The first and last-minute measurements were disregarded from the calculation. The steady-state ion flux was calculated using the basic planar diffusion geometry described by (Newman, 2001) via the

MIFEFLUX software. The same leaf and species used for g_s kinetics measurements were assayed. Leaves from LL+[gCO_2] conditions were not assayed as the integrity of the epidermal peels were not fit for analysis.

3.2.5 Statistical analyses

Analysis of variance (ANOVA) was performed using R (V.3.4.2; R Core Team, 2017). Linear models (*lm*) were used to calculate the effects of [CO_2], light, [CO_2]+ light, species and respective two-way and three-way interactions. Similar to Chapter 2, I calculated the effects of [CO_2], light and [CO_2]+ light using the species as the error component (n=4, *df*=3) rather than the residual error of the linear model.

Likewise, [gCO_2] effect was the average effects of chambers with glacial [CO_2] treatment while [aCO_2] effect was the mean variation based from chambers with ambient [CO_2] treatment regardless of light conditions. Meanwhile, HL effects were the average effects containing high light treatment (HL+[aCO_2] and HL+[gCO_2]) while LL effects were the mean variation for chambers with LL treatment (LL+[aCO_2] and LL+[gCO_2]) regardless of [CO_2] conditions. Tukey's HSD *post hoc* test was employed to infer multiple comparisons at α=0.05, and figures were plotted using the *ggplot2* package (Wickham, 2017).

Model fitting for the g_s kinetics was carried out using SigmaPlot 12 (Systat Software Inc., USA) and means were also compared using Tukey's *post-hoc* test at α=0.05. Stomatal traits and gas exchange parameters were correlated from the stomatal dynamics and ion flux traits from the four species used in this study.

3.3 RESULTS

3.3.1 Speed of grass stomatal closure and opening to light transitions

Closing and opening $t_{1/2}$ varied between species and exhibited significant Species × [CO_2] (p<0.0000, **Table 3. 1**) and Species × Light interactions (p<0.0000, **Table 3. 1**). In two C_4 subtypes, single and dual effects of glacial CO_2 and low light decreased closing $t_{1/2}$ in *M. maximus* (PCK) and opening $t_{1/2}$ in *P. antidotale* (NADP-ME) relative to control conditions (Species × [CO_2]: p<0.0000; **Table 3. 3; Figure 3. 3**). In *P. bisulcatum* (C_3), acclimation to [aCO_2]+LL stimulated faster closing $t_{1/2}$ while acclimation to [gCO_2]+HL elicited slower opening $t_{1/2}$ relative to the other three growth conditions (Species × [CO_2]; Species × Light; p<0.0000, **Table 3. 3; Figure 3. 3**). LL imparted slower closing $t_{1/2}$ in *P. antidotale* while faster opening $t_{1/2}$ in *P. miliaceum.* On the other hand, closing $t_{1/2}$ in *P. miliaceum* and opening $t_{1/2}$ in *M. maximus* were unchanged (**Table 3. 3; Figure 3. 3**).

Comparing the closing $t_{1/2}$ between species, *P. antidotale* had the fastest closing $t_{1/2}$ under control conditions ([aCO_2]+HL) (**Figure 3. 3A**). In contrast, growth at [gCO_2]+HL resulted in slowest closing $t_{1/2}$ in *P. bisulcatum* compared to the other three C_4 Panicoids (**Table 3. 3**). Growth at [aCO_2]+LL resulted to faster closing $t_{1/2}$ in *M. maximus* while acclimation [gCO_2]+LL attenuated closing $t_{1/2}$ in *P. bisulcatum* and *P. miliaceum* relative to the other two C_4 subtype representative.

M. maximus had consistently faster opening $t_{1/2}$ when grown at the control and single limitations of [CO_2] and light conditions (**Table 3. 3, Figure 3. 3**). At conditions where both light intensity and [CO_2] concentrations were limited, there were no discernible variations in opening $t_{1/2}$ between the four closely-related grass species (**Table 3. 3**). Opening $t_{1/2}$ was negatively correlated to closing $t_{1/2}$ under control conditions (r^2=0.42, p=0.023, **Figure 3. 4A**). Under single effects of [gCO_2] and LL, closing $t_{1/2}$ and opening $t_{1/2}$ had a positive linear correlation (r^2=0.58, p=0.004; r^2=0.45, p=0.018, **Figure 3. 4**). In contrast, no correlation was found between closing $t_{1/2}$ and opening $t_{1/2}$ to growth at [gCO_2]+LL (r^2=0.08, p=0.38, **Figure 3. 4D**).

3.3.2 Excess transpiration and forgone photosynthesis are most affected by low light

Growth at low light decreased excess transpiration in *P. bisulcatum* during transitions from high light (HL) to low light (LL). Lower excess transpiration (ΔW) during stomatal closure was elicited only at [aCO_2]+LL in *P. miliaceum* while acclimation to gCO_2+LL in *M. maximus*. On the other hand, no differences in water loss were detected between growth conditions in *P. antidotale* (**Figure 3. 3A**). During low light transitions, ΔW was consistently highest in *P. bisulcatum* (C_3) relative to the other three C_4 Panicoids in all growth conditions (**Table 3. 3**).

Forgone photosynthesis (ΔC) during transitions from LL to HL decreased in *P. miliaceum* and *P. antidotale* under acclimation to low light (**Figure 3. 5B**). In contrast, there were no differences in forgone photosynthesis during stomatal opening in *P. bisulcatum* and *M. maximus* across all the four growth conditions (**Figure 3. 5B**). HL stimulated the highest forgone photosynthesis in *P. antidotale* followed by *P. miliaceum* then *P. bisulcatum* and *M. maximus* regardless of [CO_2] conditions (**Table 3. 3**). LL, however, did not elicit differences in forgone photosynthesis among the grass species (**Table 3. 3**).

Excess transpiration during HL to LL transitions was positively correlated to closing $t_{1/2}$ (r^2=0.41, p=0.02**, Figure 3. 6A**, **Table 3. 3**). Similarly, forgone photosynthesis during transitions from LL to HL was positively correlated to opening $t_{1/2}$ (r^2=0.47, p=0.0035, **Figure 3. 6A**, **Table 3. 3**).

3.3.3 High guard cell K^+ influx is negatively correlated to iWUE

[CO_2] and light intensity significantly affected the guard cell K^+ homeostasis ([CO_2]: *p<0.0000,* Light: *p<0.0000*, **Table 3. 1)**. Relative to the control, net K^+ influx into guard cells increased at [gCO_2] for all four species, but only significantly decreased at LL in *P. bisulcatum*. (**Figure 3. 7A, Table 3. 1 and Table 3. 3**). C_3 grass *P. bisulcatum* maintained a higher net K^+ influx rate compared to the C_4 grasses under most conditions (**Figure 3. 7A, Table 3. 3**). Under LL conditions, *P. bisulcatum* and *P. miliaceum* had higher guard cell K^+ influx compared to *P. antidotale* and *M. maximus* (Light × Species: p=0.0032, **Figure 3. 7A, Table 3. 3**). Net K^+ influx in grass guard cells was positively correlated to SA (r^2=0.588,

p<0.01, **Table 3. 2**), g_{s_amax} (r^2=0.664, p<0.01, **Table 3. 2**), ΔW during transient stomatal closure (r^2=0.588, p<0.01, **Table 3. 2**), g_s (r^2=*0.563*, p<0.01, **Table 3. 2**) and OD (r^2=*0.365*, p<0.05, **Table 3. 2**).

3.3.4 Correlation between gas exchange and stomatal traits

The traits measured for the four grass species from Chapter 2 was analysed for correlations between the stomatal dynamics and guard cell ion fluxes from this chapter. There were no correlations for closing $t_{1/2}$ to any gas exchange, stomatal morphology, and guard cell ion flux traits (**Table 3. 2**) but moderately strong linear correlation with excess transpiration during HL to LL transitions (ΔW; r^2=0.410, p=0.01; **Table 3. 2**). Weak linear correlations were found between opening $t_{1/2}$ and stomatal conductance (g_s; r^2=0.283, p=0.034; (**Table 3. 2**); stomatal aperture (SA; r^2=0.397, p=0.009, **Table 3. 2**); stomatal size (SS; r^2=0.284, p=0.050, **Table 3. 2**); and maximum theoretical conductance (g_{s_amax}; r^2=0.283, p=0.044; **Table 3. 2**). ΔW loss was negatively correlated to CO_2 assimilation rate at saturated light and [CO_2]-limited conditions (A_{sat}; r^2=0.567, p=0.001; **Table 3. 2**), and positively correlated to SA (r^2=0.457, p=0.004; **Figure 3. 6C, Table 3. 2)**; closing $t_{1/2}$ (r^2=0.410, p=0.01; **Table 3. 2**); net K^+ influx (r^2=0.588, p=0.004; **Table 3. 2**) and SS (r^2=0.26, p=0.045; **Figure 3. 6D, Table 3. 2**). Forgone photosynthesis (ΔC) was moderately correlated to net photosynthetic rates at growth conditions (A_{net}; r^2=0.365, p=0.013; **Table 3. 2**); g_s at saturated light and [CO_2]-limited conditions (g_{s_sat}; r^2=0.567, p=0.003; **Table 3. 2**); and opening $t_{1/2}$ (r^2=0.468, p<0.05; **Table 3. 2**). Forgone photosynthesis was also negatively correlated to stomatal density (SD; r^2= 0.292, p=0.031; **Table 3. 2**). Lastly, I found that net K^+ influx was strongly correlated to SA (r^2=0.830, p<0.0000; **Figure 3. 6C, Table 3. 2**) and g_{s_amax} (r^2=0.664, p=0.001; **Table 3. 2**); moderately strong positive correlation to g_s (r^2=0.563, p=0.005; **Figure 3. 7B, Table 3. 2**); negatively correlation to intrinsic water use efficiency (iWUE; r^2= 0.587, p=0.004; **Table 3. 2**); and weakly correlated with the density of open stomata (OD; r^2= 0.365, p=0.037; **Table 3. 2**).

3.4 DISCUSSION

In this study, I subjected one C_3 and three C_4 grasses belonging to three biochemical subtypes of the Panicoidea lineage to different growth conditions in order to decipher vital stomatal kinetic and ion flux traits that correlate to iWUE in grasses. I found key species-specific differences in the responses of these grasses to [gCO_2] and LL.

3.4.1 C_4 grasses show more efficient stomatal dynamics in response to high light transition

Stomata constantly respond to changing light intensity on a scale of seconds through to seasons (Lawson & Blatt, 2014; McAusland *et al.*, 2016; Lawson & Vialet-Chabrand, 2018). Stomatal opening and closing usually occur at a slower rate than photosynthetic activation (Henry *et al.*, 2020), creating asynchrony between CO_2 uptake and H_2O loss which compromises iWUE (Deans *et al.*, 2018; Lawson & Vialet-Chabrand, 2018). Hence, dynamic stomatal responses are critical for the optimisation of iWUE, in addition to advanced stomatal morphology and patterning (Cai *et al.*, 2017b; Vialet-Chabrand *et al.*, 2017b; Lawson & Vialet-Chabrand, 2018; Slattery *et al.*, 2018). Stomatal kinetics in response to short-term sun and shade flecks have been examined from various angles, including the effects of phylogeny (Xiong *et al.*, 2018), the period of taxa diversification (Elliott-Kingston *et al.*, 2016), photosynthetic type (Taylor *et al.*, 2018), the effect of stomatal clustering (Papanatsiou *et al.*, 2017) and guard cell shape (McAusland *et al.*, 2016; Xiong *et al.*, 2018).

In this study, stomatal opening (measured as SA), had profound impacts on stomatal efficiency such that more open stomata (higher SA) tended to have lower iWUE (r^2= 0.397, p<0.01; **Table 3. 2**), slower opening (i.e., greater opening half-time), greater excessive transpiration and forgone photosynthesis on the transition to HL (**Table 3. 2**). Overall, stomatal opening (**Figure 3. 3B**). was in magnitude faster than stomatal closure (**Figure 3. 3A**). This variation could be due to differences in the utilisation of ion transport mechanisms (*e.g.* channels *versus* transporters), metabolism of starch and sucrose relating stomatal movement, and differential response to environmental cues (Chen *et al.*, 2017; Lawson & Matthews, 2020).

Stomatal opening was significantly faster (i.e., smaller opening half-time) in C_4 grasses relative to the C_3 grass, especially under [gCO_2] and LL (**Figure 3. 3B**). Hence, natural selection pressures have led to characteristic adaptation in grasses, whereby stomata of [CO_2]-saturated C_4 leaves open fast on transition to HL, achieving high productivity. In contrast, [CO_2]-limited C_3 leaves show slower stomatal opening at [gCO_2], possibly due to hydraulic constraints. The results suggest that the complexity of C_4 photosynthesis with its two C_3 and C_4 metabolic cycles operating across two photosynthetic tissues and requiring substantial transfer metabolite gradients does not compromise the ability of C_4 plants to utilise high light transients (Slattery *et al.*, 2018). These results are also in line with the greater photosynthetic efficiency of C_4 grasses in response to sun flecks highlighting their heightened photosynthetic efficiency and productivity in response to increased light (McAusland *et al.*, 2016). Amongst the three subtypes of C_4 grasses, the PCK species showed a faster stomatal opening in response to HL. The PCK subtype is characterised by high photosynthetic efficiency at LL (Sonawane *et al.*, 2018; Sagun *et al.*, 2019) and more efficient Rubisco (Sharwood, 2017).

In contrast, stomatal closing half-time neither differed systematically between C_3 and C_4 grasses nor showed a consistent response to [gCO_2] or LL. Rather, C_3 and NAD-ME grasses showed more excessive transpiration due to their slower stomatal closure rate on the transition to LL. This may highlight the [CO_2] limitation of C_3 *versus* C_4 pathway and of NAD-ME *versus* NADP-ME and PCK subtypes (Pinto *et al.*, 2016; Sonawane *et al.*, 2018). Slower stomatal closing time may also be related to hydraulic conductivity. Although stomatal closing half-time did not directly correlate with any parameter (other than opening half-time), there were interesting observations. Firstly, excessive water loss, derived from closing half-time and transpiration rates at initial and final steady states, correlated strongly with K^+ influx. Secondly, grass leaves with higher stomatal density (r^2= 0.292, p<0.05; **Table 3. 2**) showed less forgone photosynthesis on opening to HL. These aspects are worth investigating further using a larger set of C_3 and C_4 species as Deans *et al.*, (2018) showed that excessive transpiration and stomatal closing have no relationship among C_3 kidney-shaped stomata.

3.4.2 C_3 and C_4 grass guard cell K^+ flux responds similarly to [gCO_2] but differently to LL

Stomata respond distinctively to [CO_2] and light, and grass stomata have evolved specialised molecular, physiological, and morphological features for long-term geological [CO_2] variation and short-term light fluctuation (Shimazaki *et al.*, 2007; Kim *et al.*, 2010; Chen *et al.*, 2017). During stomatal opening and closure, K^+ fluxes across the guard cell membranes are one of the key determinants of the complex signalling pathways in response to variations of [CO_2], light and other stimuli (Kim *et al.*, 2010). In this study, both SA (r^2= 0.830, p<0.01; **Table 3. 2**) and g_s (r^2= 0.563, p<0.01; **Table 3. 2**) measured under growth conditions strongly and positively correlated with guard cell K^+ influx (**Table 3. 2 and Figure 3. 7**). These results indicated that stomatal are tightly regulated by K^+, which can accumulate up to a few hundred mill moles of concentration in guard cells (Hills *et al.*, 2012). These relationships are based on well-understood guard cell function, whereby K^+, anion and solute influx are followed by H_2O uptake, leading to stomatal opening (Chen *et al.*, 2012b, 2017). What is significant in this study is that g_s measured *in planta* using leaf gas exchange correlated well with K^+ influx measured on epidermal peels under standard conditions (r^2= 0.563, p<0.01; **Table 3. 2**), indicating K^+ homeostasis of guard cells of isolated epidermal peels may generally reflect *in vivo* leaf gas exchange. This was true for the C_3 grass under all conditions, and for the C_4 grasses under control and [gCO_2], but not in the LL conditions. Therefore, the increase in guard cell K^+ influx at [gCO_2] was proportional to g_s, indicating a common [CO_2] acclimation and signalling response in grasses. Moreover, there was different stomatal acclimation and possibly signalling responses to light between C_3 and C_4 grasses because K^+ influx was not affected by growth at LL in C_4 grasses while it was decreased in proportion with g_s in the C_3 grass (**Figure 3. 7A**). It has been proposed that chloride ions were not sufficient to compensate for the high K^+ influx, and thus, malate ions were postulated and were observed to be correlated to stomatal opening in guard cells (Pearson, 1973; Vavasseur & Raghavendra, 2005). In the C_4 cycle, malate production is highly dependent on the activity of phosphoenol carboxylase (PEPC) (Sage, 2004; Vavasseur & Raghavendra, 2005) which suggests that C_4 photosynthesis may profoundly affect the K^+ fluxes between the two photosynthetic types. On the other hand, Aubry *et al.*, (2016) compared the transcriptome profile of guard cells between C_3 and C_4 stomata and showed that the core C_4 cycle genes were upregulated in C_4 guard cells, but no variations were detected in ion signalling and CO_2 sensing pathways. These two important conclusions

may have profound implications for the way stomata operate and acclimate in C_3 and C_4 grasses (Vavasseur & Raghavendra, 2005; Aubry *et al.*, 2016). Understanding the different acclimation and signalling pathways of stomata in C_3 and C_4 grasses will be the subject of another future research.

3.4.3 Linking stomatal dynamics with g_s and iWUE

The other objective of this study was to determine whether C_3 and C_4 grasses have different stomatal and guard cell dynamics that could be linked to variations in g_s or iWUE. The speed of opening and closing in response to short-term light transitions was considered as criteria for assessing stomatal sensitivity and efficiency. Rapid stomatal opening and closure during fluctuating environmental conditions underpin the superior functional responses of grass stomata which are thought to impact the temporal response of iWUE (Chen *et al.*, 2016; Lawson & Blatt, 2014; Vialet-Chabrand *et al.*, 2017). In our study, larger SA was correlated with slower stomatal opening response time and greater guard cell K^+ influx across species and treatments. In particular, my results showed that the impact of [gCO_2] and LL on the closing ([CO_2], Light: $p<0.0000$; **Table 3. 1**) and opening half-times ([CO_2]: $p=0.0023$, Light: $p=0.0062$; **Table 3. 1**) of one C_3 and three C_4 grasses were small and species-specific (**Figure 3. 3; Table 3. 1 and Table 3. 3**). However, species with bigger SA, g_s and g_{s_amax} showed a slower response to light transitions, i.e., had greater opening $t_{1/2}$. In contrast, closing $t_{1/2}$ showed no correlation to any of the important stomatal and gas exchange traits, suggesting that these grasses could possess a different mechanism for opening and closing. C_3 stomata wasted more H_2O on the transition to LL and fixed less [CO_2] on transition to HL relative to C_4 grasses, under all conditions. Hence, C_3 grasses had a lower [CO_2]/[H_2O] balance under both steady-state and dynamic conditions. Taken together, my data indicate that larger SA and g_s impart slower stomatal opening rates which are associated with higher guard cell K^+ influx and ultimately, lower iWUE. Therefore, the negative relationship of iWUE with SA, K^+ influx and stomatal opening among C_3 and C_4 grasses offer a mechanistic explanation for the link between iWUE and g_s that can be exploited for identifying molecular targets for breeding crops with high iWUE.

3.5 CONCLUSION

The stomatal kinetics and net K^+ fluxes in guard cells of four Panicoid grasses representing C_3 photosynthetic type and C_4 biochemical subtype acclimated to [gCO_2] and LL were investigated to probe for physiological traits controlling leaf iWUE in grasses. The findings show that the responses of stomatal closure and opening were highly species-specific with interesting trends. Under control conditions, slow-closing stomata tended to have faster opening times. However, when grown under [gCO_2] or LL, the pattern faster closing stomata also correlated positively with faster opening half-time. It was also found that faster closing stomata indeed forgo less water vapour and faster stomatal opening forgo less photosynthesis during light/dark transitions. Likewise, it was shown that K^+ influx in guard cells of C_3 and C_4 stomata increase as a result of bigger stomata aperture during growth at [gCO_2]. LL induced lower guard cell K^+ influx only in C_3 species relative to control conditions. Taken together with the morphological and gas exchange traits from Chapter 2, it is summarised that iWUE is dependent on stomatal aperture driven by turgor control through K^+ flux in guard cells. In the future, breeding for high iWUE in C_3 and C_4 cereal crop genotypes may also need to consider those with highly efficient K^+ uptake for speedy stomatal regulation.

Table 3. 1 Summary of statistical analyses for stomatal kinetics and ion flux parameters in four grass species representing C_3, C_4 NAD-ME, C_4 NADP-ME, and C_4 PCK Panicoidea acclimated to glacial [CO_2] and low light.

Bold values indicate significant main and interactive effects at 95% confidence interval using species as the error component in [CO_2], Light, and [CO_2] × Light effects.

Parameters	Main Effects (*p*)			Interactions (*p*)			
	[CO_2]	Light	Species	[CO_2] × Light	[CO_2] × Species	Light × Species	[CO_2] × Light × Species
Closing half-time Closing $t_{1/2}$ (min)	0.4239	0.6658	**0.0000**	0.6811	**0.0000**	**0.0000**	**0.0001**
Opening half-time Opening $t_{1/2}$ (min)	0.8976	0.0609	**0.0000**	0.7284	**0.0023**	**0.0062**	**0.0018**
Excessive transpiration, ΔW (mol m^{-2})	0.3888	0.1440	**0.0000**	0.2505	**0.0473**	**0.0000**	0.4580
Forgone photosynthesis, ΔC (mmol m^{-2})	0.2408	0.2077	**0.0000**	0.6223	**0.0274**	**0.0000**	0.6005
Net K^+ influx K^+ flux (nmol m^{-2} s^{-1})	**0.0000**	**0.0000**	**0.0000**	-	**0.0000**	**0.0032**	-

Table 3. 2 Correlation matrix between stomatal dynamics, ion fluxes, stomatal morphology, and gas exchange traits.

Values represent r^2 between two parameters. Linear regression direction is indicated in the parenthesis. Significance codes are as follows: *significant at $p<0.05$; **significant at $p<0.01$; [ns]not significant ($p>0.05$). [a]Low light glacial [CO_2] treatment was not included.

	Closing $t_{1/2}$	**Opening $t_{1/2}$**	**ΔW**	**ΔC**	**K^+ flux[a]**
A_{net}	ns	ns	ns	0.365*	ns
g_s	ns	0.283*	ns	ns	0.563**
iWUE	ns	ns	ns	ns	(-) 0.587**
C_i	ns	ns	0.25*	ns	ns
A_{sat}	ns	ns	(-) 0.567**	ns	ns
g_{s_sat}	ns	ns	ns	0.403**	ns
SA	ns	0.397**	0.457**	ns	0.830**
SS	ns	0.284*	0.256*	ns	ns
SI	ns	ns	ns	ns	ns
SD	ns	ns	ns	(-) 0.292*	ns
OD	ns	ns	ns	ns	0.365*
g_{s_amax}	ns	0.260*	0.292*	ns	0.664**
Closing $t_{1/2}$		ns	0.410*	ns	ns
Opening $t_{1/2}$			ns	0.468*	ns
ΔW				ns	0.588**
ΔC					ns

Table 3. 3 Summary of stomatal kinetics and ion flux parameters for four grass species acclimated to glacial [CO_2] and low light.

Values are means ± SE (n=3). Lower case letters in bold indicate the ranking of species within treatments. Numbers in superscript indicate the ranking of treatments within species. Tukey's HSD *post hoc* at 5% level was employed. Values with the same letter (or number) are not significantly different at α=0.05.

Parameter	Treatment	C_3	NAD-ME	NADP-ME	PCK
		P. bisulcatum	*P. miliaceum*	*P. antidotale*	*M. maximus*
Closing $t_{1/2}$ (min)	High Light Ambient [CO_2]	6.78 ± 0.87 **a**^{1}	4.94 ± 0.68 **a**^{1}	2.00 ± 0.74 **b**^{2}	7.58 ± 1.41 **a**^{1}
	High Light Glacial [CO_2]	7.33 ± 1.30 **a**^{1}	4.44 ± 0.62 **b**^{1}	2.00 ± 0.17 **b**^{2}	2.00 ± 0.17 **b**^{2}
	Low Light Ambient [CO_2]	4.00 ± 0.73 **b**^{2}	4.50 ± 0.19 **ab**^{1}	6.94 ± 0.75 **a**^{1}	1.28 ± 0.11 **c**^{2}
	Low Light Glacial [CO_2]	5.44 ± 0.94 **a**^{1,2}	6.06 ± 0.45 **a**^{1}	2.17 ± 0.38 **b**^{2}	1.50 ± 0.19 **b**^{2}
Opening $t_{1/2}$ (min)	High Light Ambient [CO_2]	0.94 ± 0.28 **bc**^{2}	1.50 ± 0.10 **b**^{1}	2.50 ± 0.51 **a**^{1}	0.58 ± 0.05 **c**^{1}
	High Light Glacial [CO_2]	2.28 ± 0.28 **a**^{1}	1.44 ± 0.06 **b**^{1}	1.67 ± 0.10 **ab**^{2}	0.61 ± 0.06 **c**^{1}
	Low Light Ambient [CO_2]	1.28 ± 0.06 **a**^{2}	0.61 ± 0.06 **ab**^{2}	1.17 ± 0.10 **a**^{2}	0.44 ± 0.06 **b**^{1}
	Low Light Glacial [CO_2]	1.17 ± 0.20 **a**^{2}	0.56 ± 0.15 **a**^{2}	1.06 ± 0.06 **a**^{2}	0.50 ± 0.10 **a**^{1}
Excess transpiration (mol^{-2} s^{-1})	High Light Ambient [CO_2]	2.66 ± 0.10 **a**^{1}	1.19 ± 0.18 **b**^{1}	1.00 ± 0.12 **b**^{1}	1.21 ± 0.07 **b**^{1}
	High Light Glacial [CO_2]	2.27 ± 0.15 **a**^{1}	1.28 ± 0.17 **b**^{1}	0.83 ± 0.20 **b**^{1}	0.81± 0.10 **b**^{1,2}
	Low Light Ambient [CO_2]	1.26 ± 0.17 **a**^{2}	0.63 ± 0.02 **b**^{2}	0.91 ± 0.23 **ab**^{1}	0.87 ± 0.08 **ab**^{1,2}
	Low Light Glacial [CO_2]	1.36 ± 0.14 **a**^{2}	0.76 ± 0.16 **bc**^{1,2}	1.07 ± 0.14 **ab**^{1}	0.38 ± 0.07 **c**^{2}
Forgone photosynthesis (mmol m^{-2} s^{-1})	High Light Ambient [CO_2]	3.25 ± 0.58 **c**^{1}	6.61 ± 0.44 **b**^{1}	9.97 ± 0.96 **a**^{1}	2.25 ± 0.14 **c**^{1}
	High Light Glacial [CO_2]	2.67 ± 0.36 **c**^{1}	5.71 ± 0.48 **b**^{1}	8.36 ± 1.03 **a**^{1}	2.10 ± 0.38 **c**^{1}
	Low Light Ambient [CO_2]	2.67 ± 0.47 **a**^{1}	3.51 ± 0.15 **a**^{2}	3.24 ± 0.51 **a**^{2}	1.86 ± 0.47 **a**^{1}
	Low Light Glacial [CO_2]	2.40 ± 0.28 **a**^{1}	2.02 ± 0.25 **a**^{2}	1.49 ± 0.25 **a**^{2}	3.04 ± 0.52 **a**^{1}
K^+ flux ($nmol^{-2}$ s^{-1})	High Light Ambient [CO_2]	813.21 ± 37.10 **a**^{2}	428.72 ± 23.96 **b**^{2}	340.59 ± 10.76 **b**^{2}	266.96 ± 22.89 **b**^{2}
	High Light Glacial [CO_2]	1584.48 ± 83.49 **a**^{1}	754.97 ± 56.63 **b**^{1}	540.40 ± 28.11 **c**^{1}	477.43 ± 22.79 **c**^{1}
	Low Light Ambient [CO_2]	443.07 ± 40.65 **a**^{3}	347.74 ± 9.44 **ab**^{2}	267.06 ± 11.15 **bc**^{2}	175.36 ± 8.40 **c**^{2}

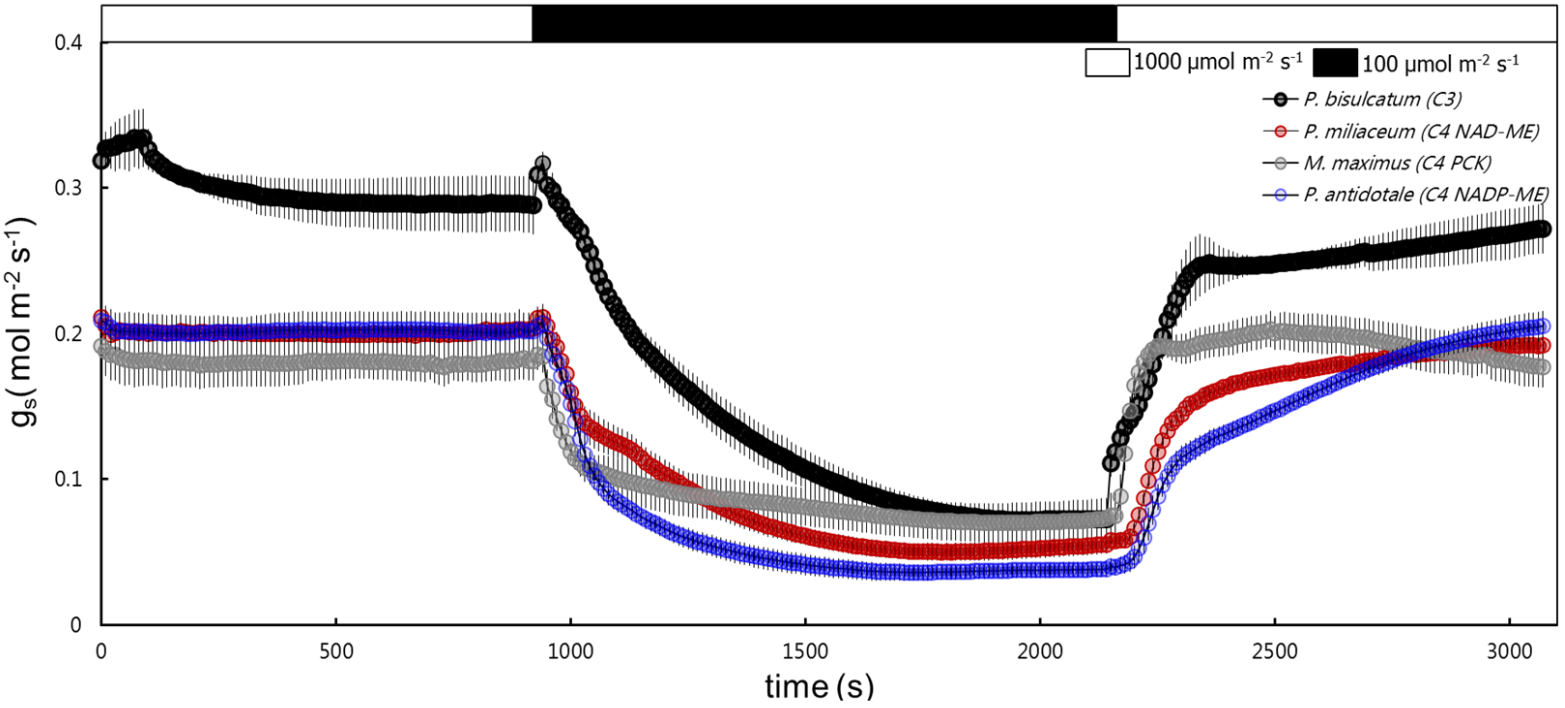

Figure 3. 1 Representation of time-resolved stomatal dynamics during short-term light transitions (1000 to 100 to 1000 µmol quanta m^{-2} s^{-1}) in *P. bisulcatum* (C_3), *P. miliaceum* (C_4-NAD-ME), *P. antidotale* (C_4-NADP-ME) and *M. maximus* (C_4-PCK).

A young fully expanded leaf was initially acclimatized at 1000 quanta µmol m^{-2} s^{-1}, 400 µmol [CO_2] l^{-1} and 28°C until steady-state g_s was achieved. Subsequently, light intensity was switched down to 100 µmol m^{-2} $s^{-1,}$ and g_s was monitored every 10 s for 20 min to examine the rate of g_s decay. After a new steady state was reached, light intensity was switched back to 1000 µmol m^{-2} s^{-1} to monitor stomatal opening. Each dot represents the mean ± SE of three biological replicates.

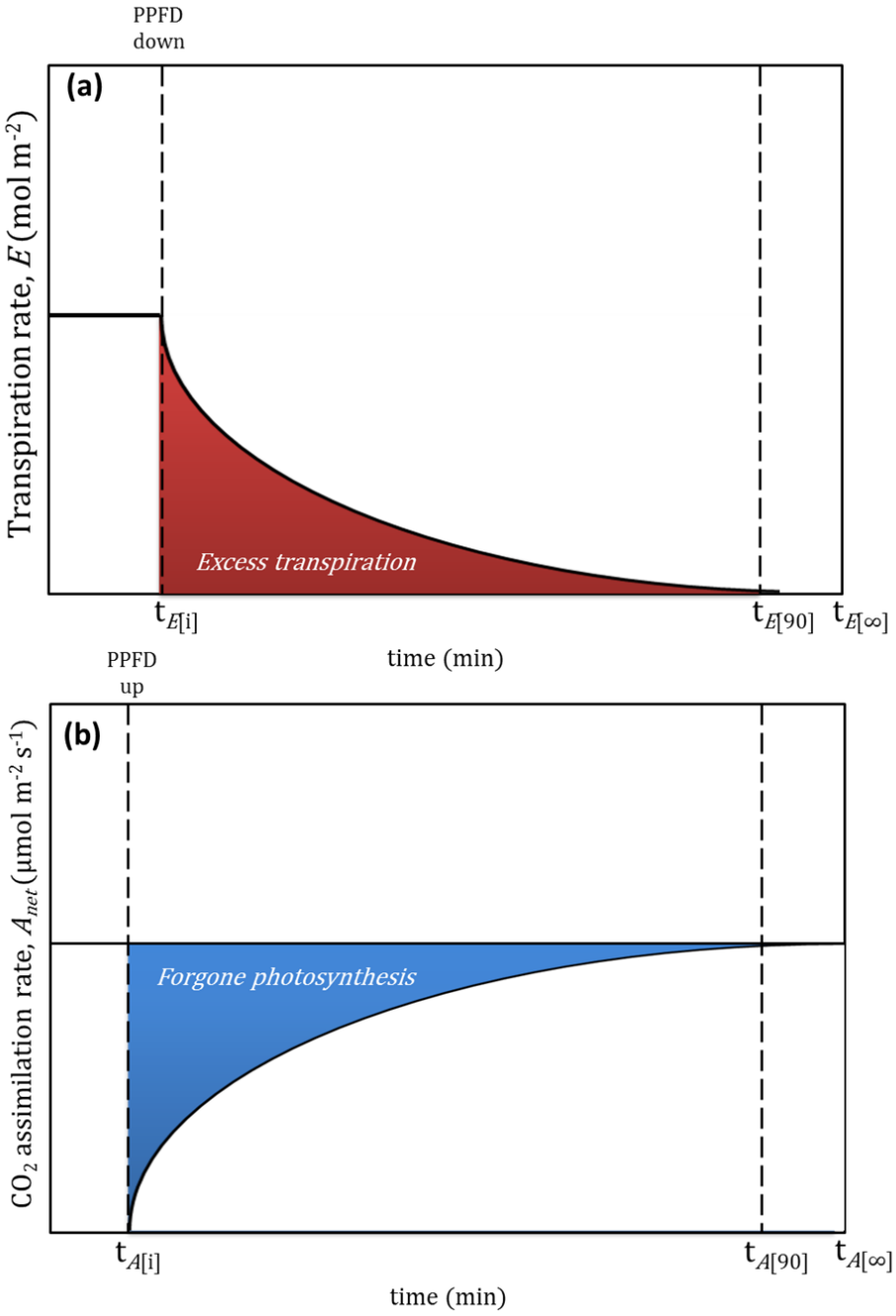

Figure 3. 2 Estimating excess transpiration and forgone photosynthesis.

Illustration of the time-integrated difference between initial and final transpiration rates (**A**); and CO_2 assimilation rates (**B**) used in estimating the potential water loss during transient stomatal closure due to decrease in light intensity (red area) and forgone photosynthesis (blue area) during transient stomatal opening due to increase in irradiance. Time points $t_{E[i]}$ and $t_{A[i]}$ represents the initial time where light intensity was modified while $t_{E[90]}$ and $t_{A[90]}$ signifies the time point where each parameter is 90% steady-state. Likewise, time points $t_{E[\infty]}$ and $t_{A[\infty]}$ illustrates the time where both parameters are incomplete stead-state.

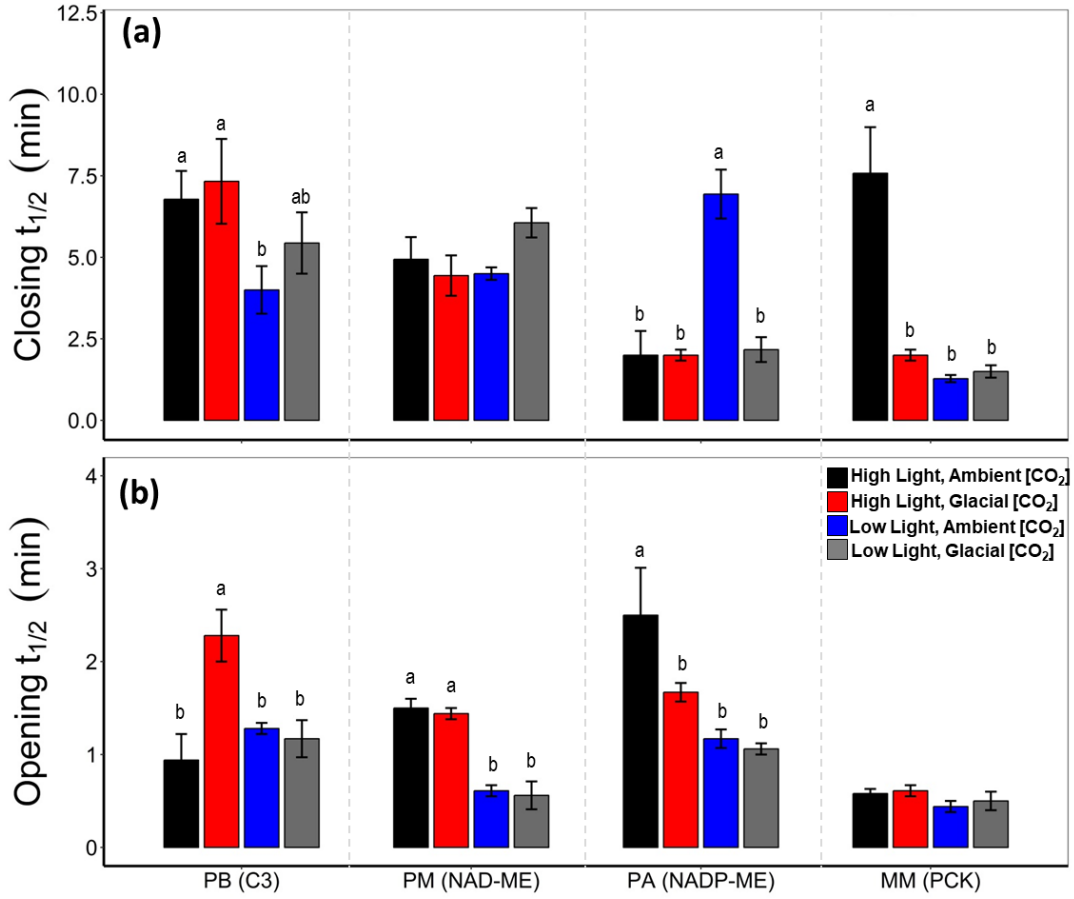

Figure 3. 3 Stomatal responses to light transitions in four grass species acclimated to glacial [CO_2] and low light:

(**A**) closing half-time and (**B**) opening half-time of *P. bisulcatum* (PB, C_3), *P. miliaceum* (PM, C_4-NAD-ME), *P. antidotale* (PA, C_4-NADP-ME) and *M. maximus* (MM, C_4-PCK). Values are means ± SE (n=3 plants). Means with the same letter are not significantly different at α=0.05 using Tukey's HSD *post hoc*.

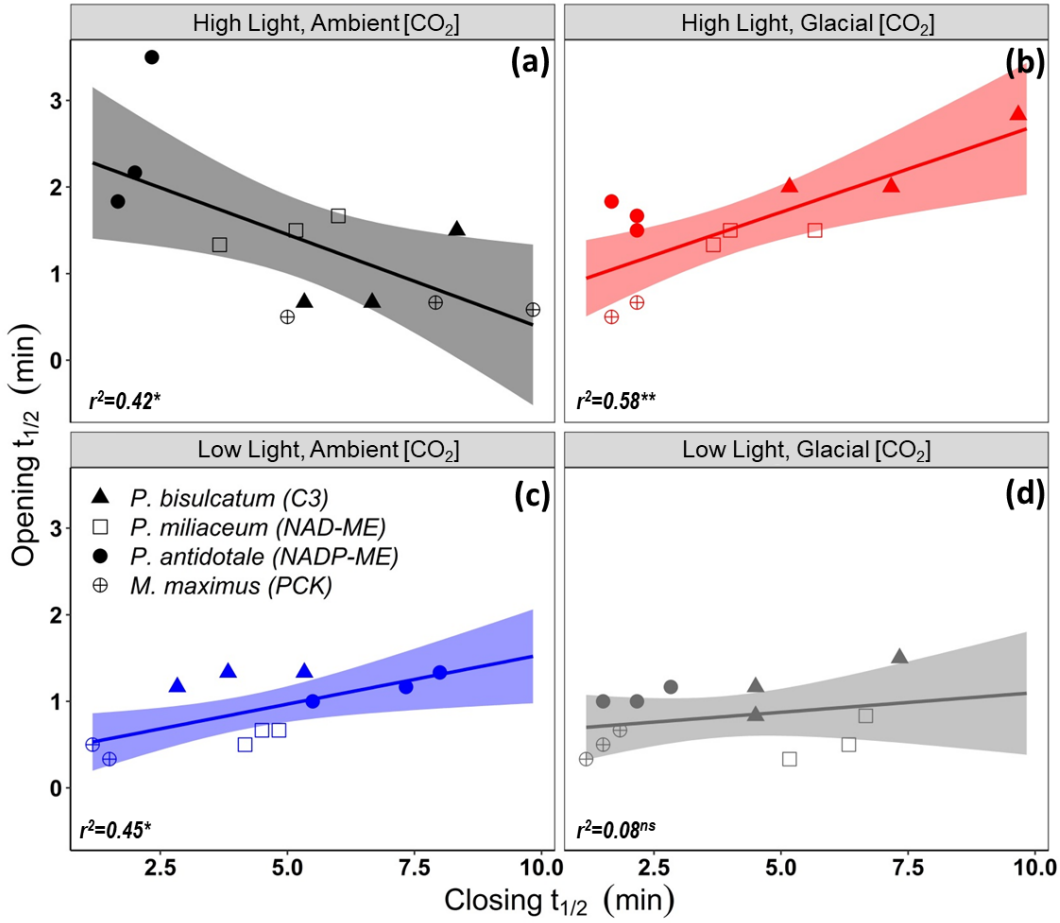

Figure 3. 4 Stomatal opening and closing correlation among four grasses acclimated to glacial [CO_2] and low light.

Dots represent the biological replicates (n=3) of each species. Shaded regions represent the 95% confidence interval of the linear model in each growth conditions. Fitted linear model equations are: High Light-Ambient [CO_2]: *opening* $t_{1/2}$ = 2.5327 - 0.216 × *closing* $t_{1/2}$; High Light-Glacial [CO_2]: *opening* $t_{1/2}$ = 0.1992 × *closing* $t_{1/2}$ + 0.7141; Low Light-Ambient [CO_2]: *opening* $t_{1/2}$ = 0.1142 × *closing* $t_{1/2}$ + 0.3977; Low Light-Glacial [CO_2]: *opening* $t_{1/2}$ = 0.0454 × *closing* $t_{1/2}$ + 0.6474. . $^{ns}p>0.05$; *$p<0.05$; **$p<0.01$; ***$p<0.001$.

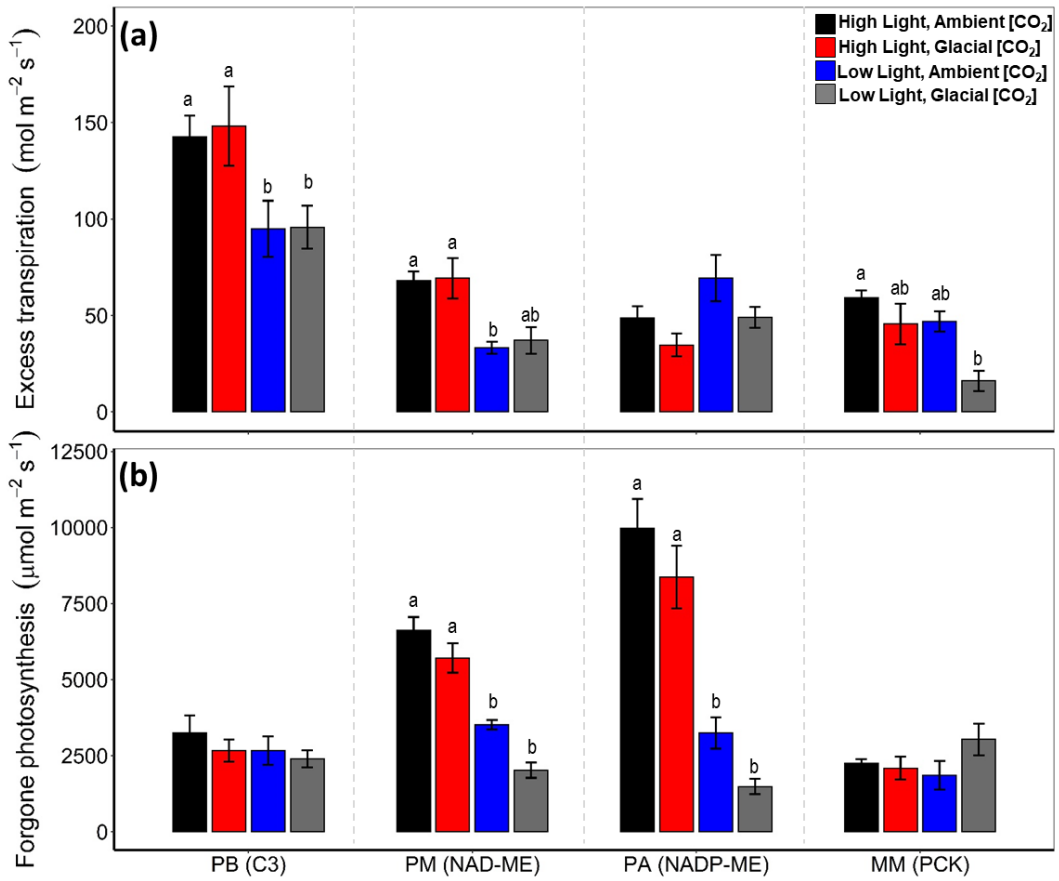

Figure 3. 5 Effects of glacial [CO_2] and low light to water loss (A) due to excess transpiration during transient stomatal closure from high light to low light transition; and forgone photosynthesis (B) during transient stomatal opening from low light to high light transitions.

Values are means ± SE (n=3). The effects of growth treatments among each species were ranked using Tukey's HSD *post hoc* at α=0.05. Species label: *P. bisulcatum* (PB, C_3), *P. miliaceum* (PM, C_4-NAD-ME), *P. antidotale* (PA, C_4-NADP-ME) and *M. maximus* (MM, C_4-PCK).

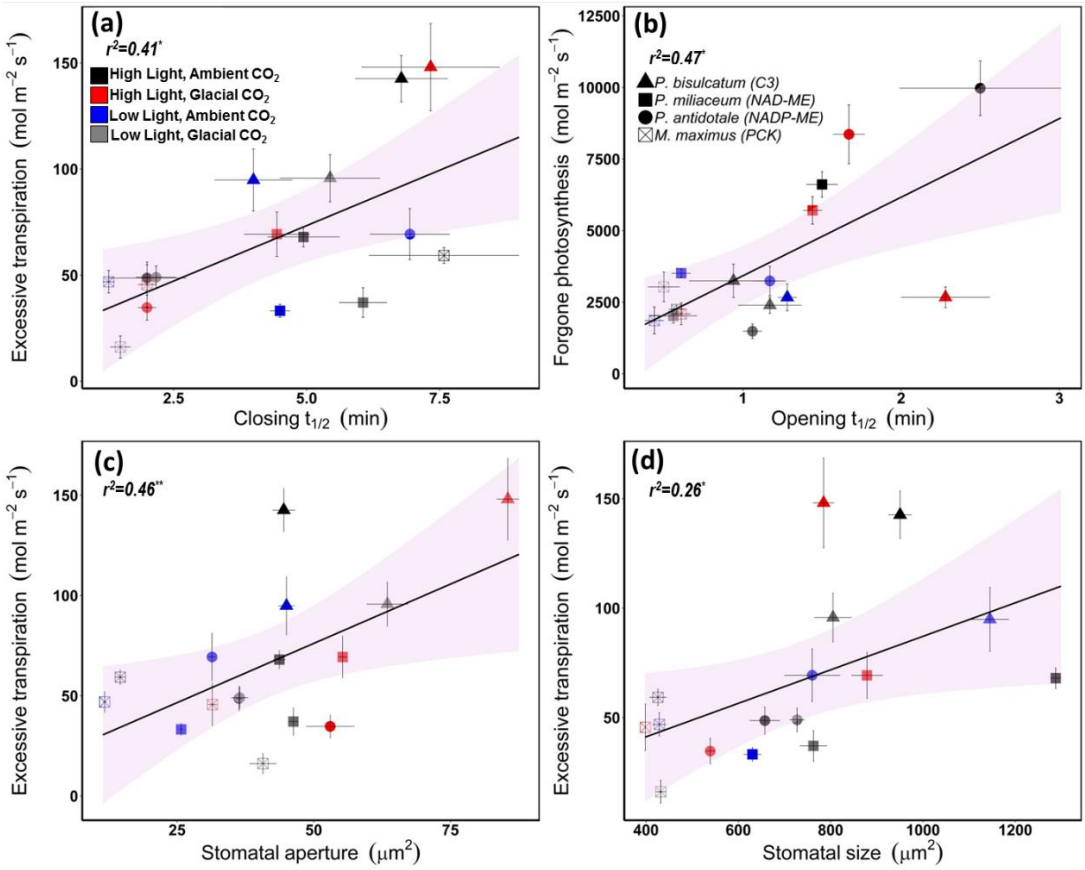

Figure 3. 6 Correlations between stomatal morphology and stomatal kinetics traits.

Linear correlations between stomatal closing half-time (closing $t_{1/2}$) and water loss (H_2O loss) due to excessive transpiration (**A**); and stomatal opening half-time (opening $t_{1/2}$), forgone photosynthesis (ΔC, **B**), relationships between water loss (H_2O loss) due to excessive transpiration to stomatal morphology traits: (**C**) stomatal aperture and (**D**) stomatal size; among four Panicoid grasses acclimated to glacial [CO_2] and/or low light. Dots represent mean ± SE (n=3) while colours represent growing conditions. Shaded regions represent the 95% confidence interval of the linear model. Fitted linear model equations are: (a) $\Delta W = 0.1719 \times t_{1/2(close)} + 0.4828$; (b) $\Delta C = 2.7417 \times t_{1/2(open)} + 0.684$; (c) $\Delta W = 1.3594 \times SA + 12.634$; (d) $\Delta W = 0.087 \times SS + 11.993$. $^{ns}p>0.05$; $*p<0.05$; $**p<0.01$; $***p<0.001$.

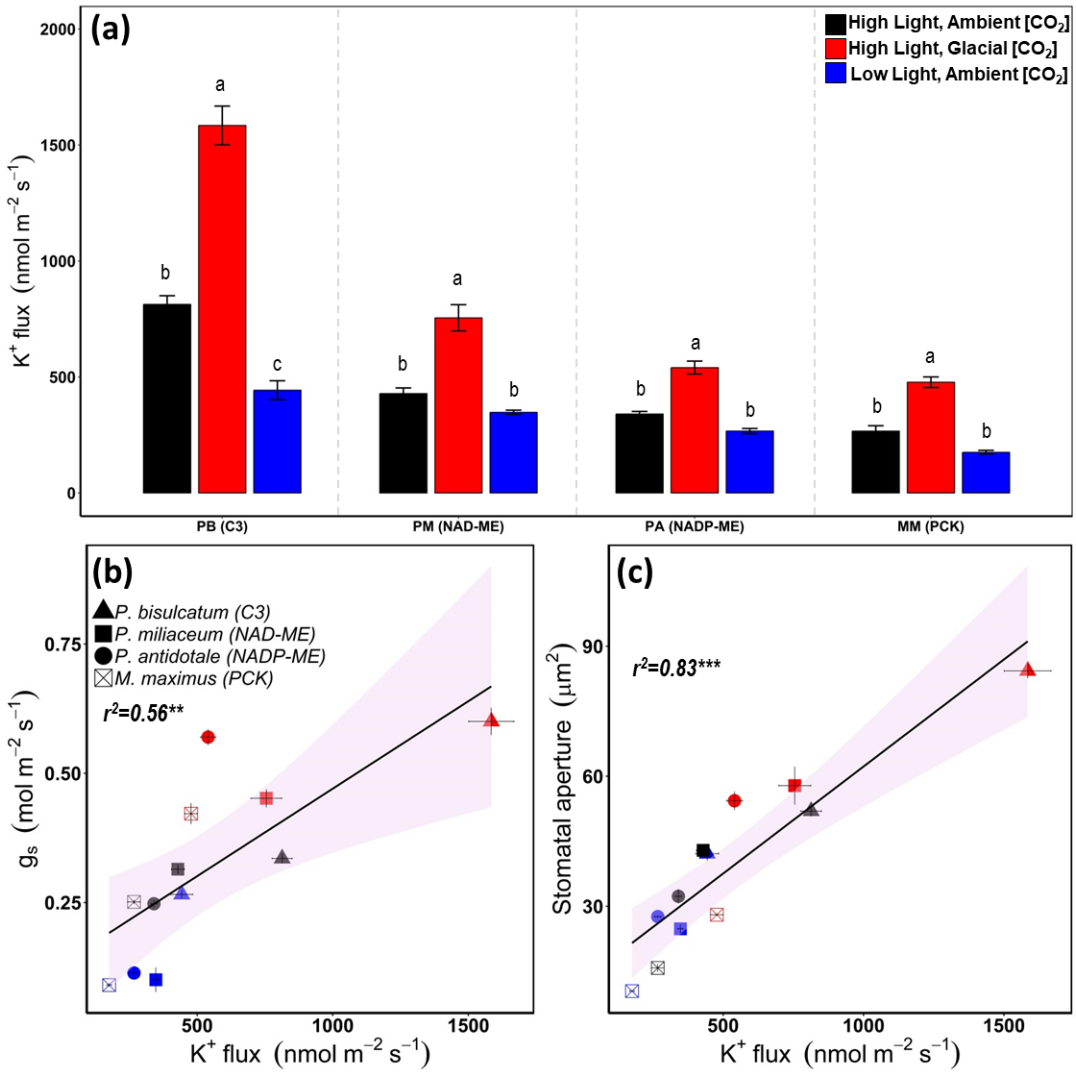

Figure 3. 7 Potassium ion influx profiles and correlations to gas exchange and stomatal traits.

Net K^+ influx of guard cells (**A**) and its relationship with g_s (**B**) and stomatal aperture (**C**) in four grass species acclimated to glacial [CO_2] or low light. Values are means ± SE of n=7-9 stomata and ranked using Tukey's HSD *post hoc* test at α=0.05. Fitted linear models are as follows: (b) $g_s = 0.0003 \times K^+flux + 0.1319$, and (c) $SA = 0.0494 \times K^+flux + 14.729$. $^{ns}p>0.05$; $*p<0.05$; $**p<0.01$; $***p<0.001$. See Figure 3.3 for species abbreviations.

CHAPTER 4

WET CHEMICAL OXIDATION SYSTEM: A TOOL FOR ANALYSING CARBON ISOTOPE COMPOSITION OF SUGARS EXTRACTED FROM LEAVES OF C_3 AND C_4 GRASSES

ABSTRACT

In C_3 plants, the composition of stable carbon isotopes ($\delta^{13}C$) has been used to screen for improved water-use efficiency (WUE). Carbon isotope discrimination is more complex in C_4 plants, weakening the links between $\delta^{13}C$ and WUE. Therefore, there is a need to better understand photosynthetic and post-photosynthetic discrimination in C_4 leaves in order to improve our interpretation of $\delta^{13}C$ variations. Post-photosynthetic fractionations include those occurring during carbohydrate metabolism. This chapter focuses on developing a method to analyse the $\delta^{13}C$ of leaf sugars extracted from C_3 and C_4 grasses. The classical analysis of CO_2 isotopologues (^{12}C and ^{13}C) includes pyrolysis of whole leaf materials in elemental analysers coupled to isotope ratio mass spectrometry (EA-IRMS). Recent advances in high-performance liquid chromatography (HPLC) interfaced to a wet chemical oxidiser (WCO) permit compound-specific isotope analysis of suitable compounds in aqueous solutions. Here, I utilised the Liquiface® WCO system coupled to Agilent 1260 Infinity HPLC and Isoprime 1000 IRMS to examine the reproducibility and accuracy of the equipment in measuring the $\delta^{13}C$ of international standards and soluble sugars extracted from leaves of *Oryza sativa* (C_3) and *Zea mays* (C_4). Results showed that the WCO interface produced reproducible and accurate measurements (<0.5‰ SD) of two sucrose standards and is comparable to the classical EA-IRMS method. The data also showed that rice sucrose was ^{13}C enriched compared to fructose and glucose, while maize had ^{13}C-enriched sucrose, glucose and fructose relative to the whole leaf. In conclusion, this method can resolve $\delta^{13}C$ of sucrose, glucose, and fructose in leaves, paving the way for screening more species under different conditions to improve our understanding of post-photosynthetic fractionation.

Keywords: carbon isotope composition, CSIA, EA-IRMS, HPLC-IRMS, wet chemical oxidation, $\delta^{13}C$.

4.1 INTRODUCTION

There are three naturally occurring isotopes of carbon: 12, 13 and 14, with ^{12}C and ^{13}C being stable, occurring in a natural proportion of approximately 99:1 (Smith, 1972). In the troposphere, the photosynthetic substrate, CO_2, contains the two naturally occurring stable carbon isotopes, ^{12}C and ^{13}C, with the heavier isotope being scarcer (1.1%) (O'Leary, 1981; Farquhar *et al.*, 1989; von Caemmerer *et al.*, 2014). The lighter isotopologue is often preferentially selected and has a higher enzymatic rate during leaf biochemical reactions when compared to the heavier isotopologue, and thus creates products with more negative carbon isotope composition (signature) compared to the atmosphere (O'Leary, 1981; Fry, 2006; Tcherkez *et al.*, 2011; Cernusak *et al.*, 2013). The stable carbon isotope composition in leaves, commonly expressed in delta notation ($\delta^{13}C$, ‰), is the deviation of the heavier/lighter ratio ($^{13}C/^{12}C$) of the sample carbon isotopes (R_{sample}) relative to the $^{13}C/^{12}C$ ratio of the international carbonate standard, the Vienna Pee-Dee Belemnite (R_{PDB}= 0.0112372).

$$\delta^{13}\mathrm{C} = (R_{sample}/R_{PDB}) - 1 \qquad \text{equation 4.1}$$

Fractionations occur during the physical-chemical reactions of carbon fixation in leaves, passing on their reduced signatures. Hence, biogenic materials have more depleted $\delta^{13}C$ compared to the atmosphere (Craig, 1953, 1957; Tcherkez *et al.*, 2011; Cernusak *et al.*, 2013). Another isotopic term, $\Delta^{13}C$, has been introduced by Farquhar *et al.*, (1982) to refer to the photosynthetic carbon isotope discrimination in leaves relative to the atmospheric CO_2 ($^{13}C/^{12}C_{air}$). It was defined as:

$$\Delta^{13}C_{product} = ([R_{air}/R_{product}] - 1) \times 1000 \qquad \text{equation 4.2}$$

where R_{air} and $R_{product}$ are the $^{13}C/^{12}C$ ratios of the atmosphere and the photosynthetic product, respectively (Farquhar *et al.*, 1982; von Caemmerer *et al.*, 2014) and are obtained from δ notation expressed per mil:

$$\Delta^{13}C_{product}\ (‰) = \frac{\delta_{air}(‰) - \delta_{product}(‰)}{\delta_{product}(‰) + 1000} \times 1000 \qquad \text{equation 4.3}$$

Farquhar and colleagues also developed an expression of $\Delta^{13}C$ derived from leaf gas exchange parameters and which explicitly includes C_i/C_a (the ratio of intercellular to ambient CO_2 partial pressure) for both C_3 and C_4 plants. During C_3 photosynthesis, carbon isotope discrimination can be expressed as:

$$\Delta^{13}C = a + (b - a)\frac{C_i}{C_a} \qquad \text{equation 4.4}$$

where a = discrimination due to diffusion through stomata (4.4‰) and b = discrimination due to Rubisco carboxylation (27-30‰) (Farquhar *et al.*, 1989). At the leaf-level, water-use efficiency (iWUE) can be expressed as:

$$iWUE = \frac{A}{g_s} = 1 - \frac{C_i}{C_a} \qquad \text{equation 4.5}$$

where A is photosynthetic rates and g_s is stomatal conductance. Hence, equations 4.4 and 4.5 demonstrate a direct link between $\Delta^{13}C$ and C_i/C_a, or iWUE in C_3 leaves. Measurements employing stable carbon isotope signatures have been popularly used as proxy selection tool ever since Farquhar & Richards (1984) pioneered the work on selecting wheat genotypes with improved WUE using $\Delta^{13}C$. Breeding crops with improved iWUE has been successful for C_3 plants as $\Delta^{13}C$ is primarily controlled by C_i/C_a, and the mechanism is relatively straightforward and well understood (Farquhar *et al.*, 1989).

During C_4 photosynthesis, carbon isotope discrimination ($\Delta^{13}C$) can be related to the ratio of intercellular to ambient CO_2 partial pressure (C_i/C_a) and leakiness (ϕ), defined as the ratio of bundle sheath leak rate to PEP carboxylase (PEPC) rate:

$$\Delta^{13}C = a + (b_4 + (b_3 - s)\phi - a)\frac{C_i}{C_a} \qquad \text{equation 4.6}$$

where a is the fractionation during diffusion of CO_2 in air (4.4 ‰), b_4 is the fractionation associated with PEP carboxylation and the preceding isotopic equilibrium during dissolution and conversion to bicarbonate (fractionations defined below), s is the fractionation during the leakage of CO_2 out of the bundle sheath cells (1.8 ‰), and b_3 is the fractionation during Rubisco carboxylation (Farquhar, 1983). This equation has recently been updated to include the ternary formulation to take into account the influence of transpiration on CO_2 diffusion

between the atmosphere and the intercellular air spaces (Farquhar & Cernusak, 2012). Importantly, equation 4.6 shows that the dependence of Δ on C_i/C_a varies with ϕ, which complicates the interpretation of $\Delta^{13}C$ and even more $\delta^{13}C$ in C_4 leaves (Henderson *et al.*, 1992a,b). Nevertheless, there have been attempts to correlate $\Delta^{13}C$ with iWUE, which yielded limited success (Henderson *et al.*, 1992a; Cousins *et al.*, 2008; von Caemmerer *et al.*, 2014; Ellsworth & Cousins, 2016).

Leaf dry matter $\delta^{13}C$ provides an integrated measure of leaf carbon isotope exchange as opposed to $\Delta^{13}C$, which can only provide a spot measure of carbon isotope discrimination. In addition, measuring $\delta^{13}C$ is quicker and more straightforward than measuring $\Delta^{13}C$, and hence makes an attractive tool for estimating WUE for a large number of lines such as in a breeding program. Recently, Cousins and colleagues (Feldman *et al.*, 2018; Ellsworth *et al.*, 2019) have reported a relationship between whole plant WUE and $\delta^{13}C$ measured within a recombinant inbred population of the model C_4 grass *Setaria viridis* grown under highly controlled environments. However, the effectiveness of $\delta^{13}C$ as a tool for measuring WUE across multiple C_4 grass species (Ghannoum *et al.*, 2001b) or multiple genotypes was grown under less controlled environments Henderson *et al.*, (1998) remains limited. Therefore, there is a need to better understand the causes of variations in $\delta^{13}C$, in order to improve our ability to interpret it and improve its usefulness as a proxy for iWUE in C_4 plants (von Caemmerer *et al.*, 2014; Ellsworth & Cousins, 2016). In particular, we need to better understand the impact of post-photosynthetic carbon isotope fraction on $\delta^{13}C$.

Significant gaps still exist in our knowledge about post-photosynthetic leaf level and downstream metabolic processes and isotopic fractionations. The role of post-photosynthetic fractionation has received little attention with respect to variations in $\delta^{13}C$ among C_4 plants (Ghannoum *et al.*, 2001b; von Caemmerer *et al.*, 2014). For example, isotopic discrimination during respiration may impact the carbon isotope composition of leaf dry matter (Henderson *et al.*, 1992a; Hobbie & Werner, 2004). Leaf dry matter carbon is in part derived from photosynthesis from older leaves rather than current photosynthates. In addition, the isotopic composition of organic compounds within a leaf vary due to the isotope effects of the biochemical pathways used for their synthesis, and it is well-known that different carbon pools have different ^{13}C signatures (Hobbie & Werner, 2004; Bowling *et al.*, 2008; Cernusak *et al.*, 2009; Tcherkez *et al.*, 2011). For example, lipid, lignin, protein and organic acids are typically depleted in ^{13}C compared to the bulk leaf isotopic signature, while sucrose, starch and cellulose are typically isotopically enriched. Hence, differences in

$\delta^{13}C$ can arise if the different plants partition their carbon in varying proportions to the different pools. The role of C isotope fractionation during metabolism is pursued in this thesis by comparing the ^{13}C signature of leaf dry matter with that of sugars (short term C storage) and cellulose (long term C storage). Therefore, Chapter 4 focusses on developing the analytical tools, while Chapter 5 explores metabolic fractionation between C_4 grasses with different biochemical subtypes.

The traditional technique for measuring carbon isotope signature is through the combustion of bulk plant material by an elemental analyser (EA) coupled to isotope ratio mass spectrometry (IRMS) (Godin & McCullagh, 2011). The disadvantage of this method is that it cannot assay the isotope composition of a particular compound from the bulk sample directly. Hence, a key challenge of my PhD project was to find a technique that would assay the isotopic signatures of these metabolites as they are in aqueous solution in the leaf. Compound-specific isotope analysis (CSIA) is still a developing field in stable isotope analysis and has been designed to examine the $\delta^{13}C$ of various metabolites that must generally be isolated from bulk sample materials. Nevertheless, state of the art of the technique is limited to gas chromatography (GC)-based assays, and non-volatile organic compounds must be derivatized by silylation, alkylation, acylation, esterification or other methods in order to volatilise the compounds and improve chromatographic separation (Meier-Augenstein, 2004; Morrison *et al.*, 2010; Elsner *et al.*, 2012). For example, CSIA of monosaccharides was previously achieved by derivatising the sugars through the addition of trimethylsilyl groups [$-Si(CH_3)_3$], alditol acetate [$-OCH_3COOH$], or methylboronic acid [$-CH_3B(OH)_2$] (Merkle & Poppe, 1994; MacKo *et al.*, 1998; Gross & Glaser, 2004; Faraco *et al.*, 2016). This technique involves the addition of carbon atoms from the derivatising agents that dilute the ^{13}C signal and pose challenges when comparing isotopic signatures with lesser differences (Gross & Glaser, 2004; Krummen *et al.*, 2004). For instance, derivatising through trimethylsilyl ether adds all the three methyl constituents to the compound, thus adding to the whole ^{13}C signature of the analyte (Godin & McCullagh, 2011).

An LC-based (liquid chromatography) system, interfaced to a wet chemical oxidiser (WCO), converts metabolites from an aqueous solution to CO_2 which is then carried by helium gas through an open split into an IRMS (Krummen *et al.*, 2004). This makes it possible for an LC-based CSIA without derivatisation of the compounds to conduct assays (Krummen *et al.*, 2004; Boschker *et al.*, 2008; Abaye *et al.*, 2011; Federherr *et al.*, 2016). Of the two

market-available WCO system (LC-isolink and Liquiface), the latter is less utilised due to its later introduction in the market and hence scantier studies (Morrison *et al.*, 2010; Godin & McCullagh, 2011).

The aim of this chapter was to develop a method for measuring carbon isotope signatures of sugars using the WCO interface (Liquiface, Isoprime Ltd) in order to better understand variations in leaf $\delta^{13}C$ due to post-photosynthetic fractionation, and ultimately develop a high throughput screening tool for leaf-level water-use efficiency. In particular, this chapter will assess the accuracy and reproducibility of the HPLC-WCO-IRMS for examining the $\delta^{13}C$ of sugar standards and sugars extracted from leaf materials of common C_3 and C_4 crop species. The specific objectives of the study were to (i) assess the suitability of Hi-Plex H column (Agilent Technologies Inc.) in resolving sugar standards and sugar mixtures in leaf materials; (ii) test the limits of detection, accuracy, and memory effects of the HPLC-WCO-IRMS interface; and (iii) to measure the $\delta^{13}C$ of major leaf sugar metabolites in C_3 (*Oryza sativa)* and C_4 (*Zea mays)* crops. These methods can then be used in a subsequent experiment described in **Chapter 5**.

4.2 MATERIALS AND METHODS

4.2.1 Plant culture

Two grass crops, *Oryza sativa* L. and *Zea mays* L., representing C_3 and C_4 photosynthetic pathways were grown in a naturally-lit glasshouse at the Hawkesbury Institute for the Environment (33º36'49" S, 150º44'54" E) from December 2017, to February 2018. A total of six biological replicates were transplanted into 6 L pots containing soil (Osmocote® Professional Seed Raising Mix, Scotts, Australia) and trace elements supplement (Osmocote® Plus Trace Elements, Scotts, Australia). The glasshouse conditions were maintained at a day/night temperature of 28°C/22°C, relative humidity (RH) of 60-65%, and a photoperiod of 16 h. Plants were watered throughout the experiment. Species were randomised twice a week to minimise within-chamber variations. Non-senescing fully expanded leaves were harvested and immediately immersed in liquid nitrogen. Snap-frozen leaves were freeze-dried at -55°C for 48 hr using Martin Christ Alpha 1-2 LD plus freeze dryer (John Morris Scientific Pty Ltd., Australia). Subsequently, the leaf samples were finely ground at 30 hertz for two minutes using Retsch Mixer Mill MM 200 (The McCrone Group, Illinois, USA). The ground leaf tissues were stored in 20 ml glass vials and kept in the dark at 4°C until further use.

4.2.2 Sugar standards

Two sucrose standards with C_3 and C_4 carbon isotope signatures were used to optimise run efficiency and compare fractionation between the two chromatographic methods described below. The sucrose international standard IAEA-CH-6 (a.k.a ANU sucrose) is a C_4-derived sugar (sugarcane) with a $\delta^{13}C$ signature of -10.45‰ relative to Vienna Pee Dee Belemnite (VPDB) standard while Beet89 sucrose is a laboratory standard from a Beet (C_3) sugar bought in 1989 and repeatedly analysed against international standards. It has a $\delta^{13}C$ signature of -24.62‰ relative to VPDB.

4.2.3 Preparation of standards and purification of soluble sugars

The ground leaf samples collected from the glasshouse-grown species were weighed to 120 ± 1.0 mg and transferred to 2 ml tubes. The soluble carbohydrates from the ground leaves were twice-extracted using 1.5 ml of cold Milli-Q grade water, mixed for 20 sec using a vortex until homogenous, and centrifuged at 13000 rpm for 3 min. The pooled aqueous fraction (2.5 ml) was filtered using a Millex™GP filter unit with a 0.22 µm membrane pore size (Merck Millipore Ltd, MA, USA). Consequently, the aqueous fractions were deionised using CentriPure® P10 columns (EMP BIOTECH, Berlin, Germany). The column matrix (Zetadex 25) is constituted of a mixed bed ion exchange resin with size exclusion capacity for rapid desalting and removal of ionic (mostly organic acids and salts) and heavy protein contaminants. The column pore size had a molecular weight cut-off of 5 kD. The purified fraction was stored at -5^{o}C until further analysis. For HPLC analysis, 1.5 ml of the purified fraction was divided into aliquots of 2 ml in screw cap autosampler vials made of borosilicate glass (Agilent Technologies). Similarly, sugar standards were weighed and dissolved to degassed Milli-Q grade water and transferred to tinted autosampler vials for HPLC analysis. D-(+)-glucose (G8270; Sigma Aldrich) and D-(-)-fructose (F2543; Sigma Aldrich) were used as HPLC standards along with IAEA-CH-6 and Beet89 sucrose to compare the elution time with the sugars from the leaf samples (**Figure 4. 3A**).

4.2.4 HPLC-Liquiface-IRMS instrumentation and analytical set-up

The separation of three major post-photosynthetic sugar metabolites and sugar standards (sucrose, glucose, and fructose) were eluted isocratically using an Agilent 1260 Infinity II high-performance liquid chromatography (HPLC) system (Agilent Technologies, Inc., Santa Clara, CA, USA). The mobile phase consisted of 0.0085 M sulfuric acid degassed in ultrapure helium (1260 degasser; G1322A) and stored in a 2 L bottle. The elution conditions were: flow rate of 0.5 ml min^{-1}; sample injection volume of 20 µl, refractive index detector (RID) temperature of 35^{o}C, and HPLC column temperature of 25^{o}C based on the manufacturer's recommendation (Ball *et al.*, 2011). The sugars were separated using an Agilent Hi-Plex H column (p/n PL1170-6830) consisting of 8% cross-linked H^{+} resin (8 µm resin size) with column dimension of 7.7 mm diameter and 300 mm length (Ball *et al.*, 2011). The Agilent Hi-Plex H column was fitted with a Pursuit XRs guard column for Hi-Plex H (PL 1170-1830, Agilent Inc., Santa Clara, CA, USA) with a pore size of 5 microns to

preserve the column efficiency. Real-time detection of eluted sugars was monitored using the Agilent G1362A refractive index detector (RID) and the column oven temperature was maintained using the thermostat column compartment (Agilent TCC, G1316A). The sugars were identified based form the elution times of a mixture containing IAEA sucrose, glucose, and fructose described in Section 4.2.2 and from the Hi-Plex H compendium library (**Appendix 4. 1**). As citric acid co-elutes with glucose (**Appendix 4. 1**), previous removal of organic acids using CentriPure® P10 columns allowed for the single peak resolution of glucose (**Figure 4. 3A**).

The HPLC was interfaced with Liquiface (Isoprime Ltd, Cheadle Hulme, UK; **Figure 4. 1**), a wet chemical oxidation system that oxidises organic compounds in aqueous solution to CO_2 which is then carried by a helium gas carrier towards the IRMS interface to measure the carbon isotope signature (Isoprime, 2011). Sugar eluates from the HPLC interface mix with a degassed 20% sodium persulfate (Sigma Aldrich, St. Louis, MO, USA; CAS: 7775-27-1) oxidiser; and a degassed dilute acid catalyst, 1% orthophosphoric acid (Univar, Ajax Finechem Pty. Ltd.; UN No. 1805 PG III) inside the mixing cross (**Figure 4. 1**). The eluates, together with the oxidiser and the catalyst undergo oxidation accelerated by a heated chamber (90^{o}C), converting the eluates to CO_2 and water. The converted CO_2 and water are then cooled to ambient room temperature in the cooling loop consisting of a coiled capillary stainless steel spiral tube with a fan (Isoprime, 2011). Cooled CO_2 and water pass through the gas exchanger where CO_2 is separated from water. The water is exhausted to a waste bottle while the stream of CO_2 is dried using a Nafion™ membrane (Permapure) in counter-flowing dry helium. The WCO flow rate is controlled using a peristaltic pump and was maintained at 0.3 ml min^{-1}. Prior to measurement, the instrument CO_2 background was checked to ensure that it was $<1.5\times10^{-9}$A with a 600µA trap current. The Liquiface WCO interface also allows for a direct injection of pre-purified solutions using a 20 µL loop rheodyne valve. The resulting purified CO_2 gas stream from the WCO system flows through an open split and then to the IRMS (**Figure 4. 1**; Isoprime, 2011). The Liquiface WCO system was coupled to an Isoprime100 IRMS system (Isoprime Ltd, Cheadle, UK) where the isotope signatures of $^{12}C^{16}O_2$ (*m/z 44*), $^{13}C^{16}O_2$ (*m/z 45*), and $^{12}C^{18}O^{16}O$ (*m/z 46*) were measured. Four pulses of reference gas were acquired at the beginning (three pulses) and at the end (one pulse) to calibrate the sample $\delta^{13}C$ (**Figure 4. 9 and Figure 4. 10**).

Chromatogram analyses in the HPLC system were performed using Chemstation for LC Systems software (Rev. B.04.03 [16], Agilent Technology, 2001-2010) while IRMS

analyses were performed using the IonVantage for Isoprime software (Build1610, with 1601 Patch1, 2014). The entire EA-IRMS and WCO-IRMS analyses were performed at the Stable Isotopes Laboratory/Farquhar Laboratory, Research School of Biology, The Australian National University, Canberra, Australia.

4.2.5 EA-IRMS carbon isotope analysis

Whole bulk leaf $\delta^{13}C$ was analysed using an Elemental Analyser (EA) coupled to IRMS. Prior to measurements, finely ground lyophilised leaf tissues were transferred to tin capsules (Sercon Ltd, Crewe UK) and weighed to 2 ± 0.1 mg using a Mettler Toledo AT21 balance. Folded tin capsules containing the samples were loaded in a sample carousel and combusted by the Dumas oxidation process using a CE1100 Elemental Analyser at 1000°C with oxygen and chromium oxide, and subsequently reduced over copper at 650°C. Gaseous water and nitrogen from combustion was scrubbed out using magnesium perchlorate and Porapak column while the resulting CO_2 was processed utilising a helium gas carrier. Carbon isotope signatures were analysed using Isoprime100 IRMS system described in Section 4.2.4.

4.2.6 Data Analysis and $\delta^{13}C$ Normalisation

Measured carbon isotope signatures ($\delta^{13}C$) were expressed per mil (‰). For both the HPLC-WCO-IRMS interface and the EA-IRMS system, the $\delta^{13}C$ were referenced to an international carbonate standard, converting them to the VPDB scale using the equation:

$$\delta^{13}C_{sample}(‰) = \left(\frac{R_{sample}}{R_{VPDP}} - 1\right) \times 1000 \qquad \text{equation 4.7}$$

where R_{sample} and R_{VPDP} were the $^{13}C/^{12}C$ of the samples and the international standard, Vienna Pee Dee Belemnite (0.0111802) (Craig, 1957; Farquhar *et al.*, 1989; Werner & Brand, 2001). The $\delta^{13}C$ sample offsets for both HPLC-WCO-IRMS and EA-IRMS were corrected using two-point normalisation utilising the two sucrose standards described in Section 4.2.1. The normalisation equation was a linear regression equation plotting ANU sucrose and Beet89 sucrose together with the unknown sample:

$$\delta^{13}C_{sample} = \frac{\delta^{13}C_{A,C4\ suc} - \delta^{13}C_{A,C3\ suc}}{\delta^{13}C_{M,C4\ suc} - \delta^{13}C_{M,C3\ suc}} \times \left(\delta^{13}C_{M,sample} - \delta^{13}C_{M,C3\ suc}\right) + \delta^{13}C_{A,C4\ suc}$$

equation 4.8

where $\delta^{13}C_{sample}$ is the normalised value of the sample; $\delta^{13}C_{A,C4\ suc}$ describes the accepted value of ANU sucrose (-10.45‰); while $\delta^{13}C_{A,C3\ suc}$ is the accepted value for Beet89 sucrose (-24.62‰); $\delta^{13}C_{M,C4\ suc}$, $\delta^{13}C_{M,C3\ suc}$ and $\delta^{13}C_{M,sample}$ represents the analytical values of both standards and the sample of interest, measured either by HPLC-WCO-IRMS or EA-IRMS.

Analyses were performed using R (V.3.4.2; R Core Team, 2017) Values were expressed as mean ± SE or ± SD (to facilitate comparisons to other literatures) and ranked using Fisher's LSD *post hoc* at α=0.05.

4.3 RESULTS

4.3.1 HPLC column resolution of sugars, limits of detection, and reproducibility

The elution of IAEA-CH-6, the C_4 sucrose standard, using the Hi-Plex column showed baseline isocratic resolution for a range of concentrations (**Table 4. 1 and Figure 4. 2**). Across different sucrose concentrations, retention time did not vary significantly (**Table 4. 1**). IRMS *m/z* signal intensity linearly decreased as the sucrose concentration decreased (**Table 4. 1**). Similarly, CO_2 peak intensity measured from the IRMS decreased as sucrose concentration decreased (**Table 4. 1 and Figure 4. 2**). Between 0.1 to 2.5 mg ml^{-1} sugar concentrations, the $\delta^{13}C$ signatures were within the acceptable $\delta^{13}C$ of IAEA-CH-6. Diluting it further showed large discrepancies and inconsistent $\delta^{13}C$ values relative to the true value of IAEA-CH-6 (**Table 4. 1**).

A mixture of three neutral sugars: sucrose (peak 1, 12.5 min), glucose (peak 2, 14 min), and fructose (peak 3, 15.5 min) showed isocratic and baseline separation using the Agilent Hi-Plex H column under the parameters outlined in section 4.2.4 (**Figure 4. 3A**). However, a peculiar negative peak was observed during HPLC runs whether with standards (**Figure 4. 3A and Figure 4. 4B**), blanks, (**Figure 4. 3B and Figure 4. 4A**) or leaf materials (**Figure 4. 5**). At 11 minutes after the run commenced, a negative peak protrudes before resolving the three major sugars (**Figure 4. 2**). Injection of blank solutions (**Figure 4. 3B and Figure 4. 4A**) showed the presence of a similar negative peak. Investigation of the chromatogram RID signals showed stable RID real-time readings and absence of other negative peaks other than the ones observed. Close examination of the column properties from the Hi-Plex H column compendium (Ball *et al.*, 2011) showed that the negative peak was intrinsic to the column (**Appendix 4. 1 and Appendix 4. 2**) during sample injection and resolution of sugars, sugar derivatives, alcohols, and organic acids. Fortunately, the presence of the negative peak did not result in discrepancies in resolving sugar peaks and carbon isotope signatures of either the standards (**Figure 4. 2 and Figure 4. 3A**) or leaf samples (**Figure 4. 5 and Figure 4. 8**). A higher concentration of mobile phase (0.05 M phosphoric acid) also showed noisy RID signals in blank solutions (**Figure 4. 4A**) and demonstrated weak hydrolysis of IEAE sucrose into its monosaccharide components (**Figure 4. 4B**).

The extent of fractionation was also measured for both EA-IRMS and HPLC-WCO-IRMS interfaces. Results showed that both interfaces did not have significant fractionation when

compared to the accepted $\delta^{13}C$ of both IAEA-CH-6 and Beet89 sucrose standards (**Figure 4. 6**). Using the EA-IRMS, the average deviation from the accepted values of both sugar standards was 0.08 ± 0.02 ‰ (**Figure 4. 6A**) while the HPLC-WCO-IRMS interface had an average deviation of 0.17 ± 0.08 ‰ (**Figure 4. 6B**). Overall, the linear regression slopes were ~1 for both interfaces and similarly had an r^2 of ≥ 0.999 (**Figure 4. 6A and Figure 4. 6B**). Plotting, both EA-IRMS and WCO-IRMS interfaces showed a strong 1:1 relationship (**Figure 4. 6C**; r^2=0.9991, $p<0.0000$).

4.3.2 Memory effects

The memory effect is the carryover $\delta^{13}C$ signature from the previous sample (Skrzypek & Ford, 2018). It is most apparent when consecutive samples of dissimilar carbon isotope signatures are measured (Skrzypek & Ford, 2018). This phenomenon occurs when traces of the previous samples are not eliminated from the system and contaminates the succeeding analytes, and thus altering the carbon isotope composition leading to inaccurate measurements.

In this study, the two sucrose standards with contrasting $\delta^{13}C$ signatures were analysed to examine the memory effects of the HPLC-WCO-IRMS interface (Agilent-Isoprime tandem). IAEA-CH-6 having a $\delta^{13}C$ of -10.45‰ was analysed in four consecutive runs followed by Beet89 with a $\delta^{13}C$ signature of -24.62‰, also with four analytical runs. This was performed twice in one batch run for a total of 16 analyses. The results showed that the WCO interface did not have memory effects at the flow rate of 0.5 ml min^{-1} and 20 µl injection volume of samples (**Figure 4. 7**) as the normalised values for both IAEA-CH-6 and Beet89 sucrose remained near the true values despite the consecutive runs and contrasting carbon isotope signatures.

4.3.3 Measuring $\delta^{13}C$ of neutral carbohydrates in leaf samples

The Agilent Hi-Plex H column run with the parameters described in section 4.2.4 successfully resolved sucrose (peak 1), glucose (peak 2) and fructose (peak 3) extracted from whole leaves of the C_3 crop, *O. sativa* (**Figure 4. 5A**) and the C_4 crop, *Z. mays* (**Figure 4. 5B**). The retention times of sucrose, glucose, and fructose in both leaves were 10.5 min, 11.5

min, and 12.5 min, respectively (**Figure 4. 5**). In both species, sucrose had the lowest peak height, and glucose had slightly higher peaks relative to fructose (**Figure 4. 5**).

On the other hand, the carbon isotope composition of these three sugars showed precise values as evident in the small standard errors (0.32‰ average SE; Figure 4.8). In both species, whole-leaf $\delta^{13}C$ measured using EA-IRMS had an error value of <0.18‰ (SE, n=6 biological replicates). For the two monosaccharides and a disaccharide, the standard error range was between 0.16‰ to 0.33‰ for both *O. sativa* and *Z. mays*. In *O. sativa*, sucrose was ^{13}C-enriched and fructose ^{13}C-depleted relative to whole leaf, which had ^{13}C signature similar to glucose. In *Z. mays,* sucrose, glucose and fructose were ^{13}C-enriched relative to the whole leaf, with sucrose being more ^{13}C-enriched relative to glucose and fructose (**Figure 4. 8**).

4.4 DISCUSSION

In this study, I analysed the HPLC-WCO-IRMS analytical set-up from Agilent Technologies Inc. and Isoprime Ltd to elucidate the compound-specific carbon isotope composition of sugar standards with C_3 and C_4 signatures and sugar metabolites extracted from representative C_3 and C_4 grass crops. The interface was able to resolve neutral sugars in aqueous solutions and precisely measured the $\delta^{13}C$ of these compounds in leaf samples of common cereal crops.

4.4.1 HPLC resolution of neutral sugars using Agilent Hi-Plex H

The first objective of this experiment was to determine whether the Hi-Plex H column is suitable for resolving mono and di-saccharides isotopic standards in solutions. The isocratic elution of a single sugar (IAEA-CH-6 or Beet89 sucrose, **Figure 4. 2**) and baseline separations of multiple sugars (**Figure 4. 3A and Figure 4. 5A-B**) is one of the critical requirements for a successful HPLC-based compound-specific carbon isotope assay in aqueous solutions (Chen *et al.*, 2010b; Sevcik *et al.*, 2011; Rinne *et al.*, 2012; Zhang, 2013). In this study, it was possible to successfully resolve IAEA-CH-6 (**Figure 4. 2**) and solutions containing a mixture of sucrose, glucose and fructose isocratically (**Figure 4. 3A**) using the Hi-Plex H column and the recommended HPLC conditions outlined by Ball *et al.,* (2011). However, a peculiar negative peak consistently emerged after chromatography runs (**Figure 4. 3A and Figure 4. 5A-B**). Careful examination of bubbles within the LC system and refractive index detectors was prompted, but the negative peak persisted even when running a blank (**Figure 4. 3B**). Scrutiny of the column properties showed that this negative peak observed at 9 minutes after LC run commenced, was intrinsic to the column when using dilute acids as mobile phase (Ball *et al.,* 2011). The intensity of the negative peak also corresponds to what was described in the Hi-Plex column compendium (Ball *et al.,* 2011). The negative peak was seemingly more pronounced in this study compared to the compendium. However, an examination of the compendium data showed similar intensity. This might be due to the lower amounts of soluble sugars injected, thus having lower peaks and exacerbating the positive peaks when compared to the negative peak. Based on the manufacturer's analysis, they injected 10 mg ml^{-1} while I injected between 0.1 to 0.3 mg ml^{-1}. Nonetheless, the carbon isotope signatures were not affected as the metabolites of interest

were resolved after the negative peak. Similar peak resolution including the negative peak was also observed from identifying and quantifying sugars, carboxylates, alcohols, and aldehydes of microbial fermentation products utilising the same column and HPLC system (Lai *et al.*, 2016). In the same way, the mixture of sugars, alcohols, and organic acids was resolved after the negative peak using the refractive index detector. This was not observed when the UV detector was utilised instead of RID (Lai *et al.*, 2016). Nonetheless, they were able to quantify 21 compounds from microbial products of *E.coli* and *S. cerevisiae* (Lai *et al.*, 2016), including the sugars of interest.

This study, therefore, pioneers the analysis of sugar standards and whole leaf soluble sugars analysis using the Agilent Hi-Plex H column coupled to the Isoprime Liquiface wet chemical oxidation system.

4.4.2 Detection limits, linearity and memory effects

The second objective of the study was to examine the reproducibility and accuracy of the Liquiface WCO analytical system. The $\delta^{13}C$ of the international sucrose standard IEAE-CH-6 had an acceptable reproducibility (SE <0.50‰) from a concentration range between 0.1 mg ml^{-1} to 2.5 mg ml^{-1}. Further dilution reduced the accuracy and precision of the $\delta^{13}C$ assessments (**Table 4. 1**). To date between the two WCO interfaces, IsoLink (Thermo Electron) and Liquiface (Isoprime Ltd), the latter had been used less popularly; hence, little literature was available on its application (Morrison *et al.*, 2010; Abaye *et al.*, 2011; Godin & McCullagh, 2011). Using direct injection to the Liquiface WCO system, Morrison *et al.*, (2010) demonstrated that a high level of analytical precision when glucose (SD = 0.06‰) and sucrose (SD = 0.03‰) were assayed using an ICS-3000 ion chromatography system coupled to Liquiface WCO interface. On the other hand, Abaye *et al.*, (2011) reported a precise measurement of IEAE-CH-6 sucrose (SD = 0.41‰) using the Isoprime WCO and IRMS analytical set up coupled to the same HPLC used by Morrison *et al.*, (2010) when they examined the $\delta^{13}C$ of amino acids employing strong anion exchange chromatography. Employing the LC-Isolink WCO system, Boschker *et al.*, (2008) reported an accuracy of ± 0.50‰ (SD) when $\delta^{13}C$ signatures of neutral soluble sugars were analysed in typical coastal marine materials. Similarly, Rinne *et al.*, (2012) also showed ± 0.16‰ to ± 0.50‰ accuracy in $\delta^{13}C$ of fructose, glucose, and sucrose. Moreover, Basler & Dyckmans, (2013) reported

an accuracy of <0.6‰ for $\delta^{13}C$ of sugars with greater than 2.5nM extracted from soils samples utilising a Carbo Pac 20 HPLC column (3 × 150 mm) and the LC-Isolink WCO system coupled to Delta-V IRMS. My results have demonstrated that the measurements fall within the acceptable range (<0.50‰ SD; <0.40‰ SE) and therefore accurate values were demonstrated using the Agilent 1260 Infinity II HPLC system coupled to Liquiface WCO and Isoprime IRMS interface.

The results also highlight a miniscule to negligible fractionation against the acceptable values of IEAE-CH-6 sucrose and Beet89 sucrose standards (**Figure 4. 6**). The 'gold standard' for measuring $\delta^{13}C$ signatures, the EA-IRMS and the new HPLC-WCO-IRMS analytical system showed similar offset against the two internal sucrose standards (**Figure 4. 6A and Figure 4. 6B**). The study also showed that the two-point calibration between EA-IRMS and HPLC-WCO-IRMS had a slope of 1 (r^2 = 0.999, **Figure 4. 6C**) signifying a similar accuracy between the two analytical systems. Comparable results were also reported by Morrison *et al.*, (2010) utilising the Liquiface as a choice of WCO system. Utilising the LC-Isolink system, similar regression slopes were also reported using the same sugar standards (Boschker *et al.*, 2008; Basler & Dyckmans, 2013; Skrzypek & Ford, 2018).

The memory effect was also measured as a criterion for reproducibility. The results demonstrated that successive runs of metabolites with contrasting $\delta^{13}C$ did not produce sample-to-sample carry-over signals. Skrzypek & Ford (2018) recently showed that the LC-Isolink system did not display memory effects by employing drastic spread in $\delta^{13}C$ (ANCA61 [-28.76‰] *versus* USGS41 [+37.63‰]). I, therefore, report that the Liquiface (Isoprime Ltd) WCO system did not show memory effects and thus produce accurate and reproducible measurements.

4.4.3 Analysis of $\delta^{13}C$ of three major soluble sugars in leaves of major C_3 and C_4 crops

It has been established that photosynthetic types have varied carbon isotope signatures due to the significant differences in leaf photosynthetic biochemistry (Cernusak *et al.*, 2013). This has been exploited to ascertain the photosynthetic pathways of unknown species (Bender, 1968). The variations in $\delta^{13}C$ between photosynthetic types are highly attributed to the affinity of initial enzymes in fractionating against the heavier isotopologue, $^{13}CO_2$

(Tcherkez *et al.*, 2011). In C_3 species, CO_2 ($^{12}CO_2$ and $^{13}CO_2$) from the atmosphere diffuses inside the leaf, and Rubisco (the first enzyme that integrates CO_2 into organic metabolite pools) greatly discriminates against $^{13}CO_2$ by 29‰ (Farquhar & von Caemmerer, 1981; Farquhar *et al.*, 1982, 1989). On the other hand, the C_4 pathway enables the initial hydration of CO_2 to bicarbonate (through carbonic anhydrase) favouring ^{13}C enrichment coupled by carboxylation of PEPC which exerts a lower fractionation (3‰) relative to Rubisco (Farquhar, 1983; Farquhar *et al.*, 1989; Tcherkez *et al.*, 2011; Cernusak *et al.*, 2013). PEPC fixes CO_2 transiently into C_4 acids which are decarboxylated in the bundle sheath where CO_2 is subsequently released for ultimate fixation by Rubisco. This CO_2 concentrating mechanism elevates CO_2 partial pressure inside the bundle sheath leaving little opportunity for Rubisco to further fractionate CO_2, except for a small window during the leakage of CO_2 out of the bundle sheath ($s \approx 1.8$‰; equation 4.5) (Henderson *et al.*, 1992a; von Caemmerer *et al.*, 2014). Consequently, bulk C_4 leaves have an average $\delta^{13}C$ of -12.5‰ (Cerling *et al.*, 1997; Cernusak *et al.*, 2013) compared to a depleted $\delta^{13}C$ signature (-28‰) in C_3 leaves (Kohn, 2010; Cernusak *et al.*, 2013). To further elucidate how post-photosynthetic fractionations affect leaf $\delta^{13}C$, this chapter aimed at developing methods for accurately analysing the $\delta^{13}C$ signatures of the major fast-turnover and transport sugars in grass leaves.

Data presented here showed that sucrose had the lowest chromatogram peaks relative to glucose and fructose, which were present in a roughly similar amount for both *O. sativa* and *Z. mays*. Similarly, sucrose concentration was lower than fructose and glucose in leaves of eucalypt (C_3) trees (Merchant *et al.*, 2010). Sucrose synthesis and accumulation in leaves depends on the concerted action of three enzymes: sucrose synthase (SS), invertase (INV) and sucrose phosphate synthase (SPS). INV irreversibly cleaves sucrose into glucose and fructose and is localised into the cell wall, vacuole and cytoplasm. SS catalyses the reversible cleavage/synthesis of sucrose into/from UDP-glucose (UDPG) and fructose. SPS is the main sucrose synthesising enzyme. It uses UDPG and Fructose-6-P to synthesise sucrose-6-P that is then dephosphorylated into sucrose by sucrose phosphate phosphatase (SPP) (Turgeon, 1989; Paul & Foyer, 2001; Ruan, 2014). When plants are growing fast and have a high demand for sugars, sucrose-cleaving enzymes are very active, especially in developing leaves, and sucrose is generally the least abundant sugar. In mature leaves, sucrose-cleaving enzymes usually maintain lower activities compared to sucrose-synthesising enzymes (Zhu *et al.*, 2018). Hence, low sucrose concentration in this study likely reflects the active growth of the two grass species.

In addition, the carbon isotope signatures of the three major sugar metabolites in the C_3 and C_4 species displayed varied patterns compared to their whole leaf $\delta^{13}C$ signatures (**Figure 4. 8**). In this study, sucrose was heaviest in both species compared to the leaf as a whole for both C_3 and C_4 representative crops. In control leaves of eucalypts, $\delta^{13}C$ of sucrose was intermediate between more enriched glucose and more depleted fructose (Smith *et al.*, 2016). In several *Quercus* species, fructose exhibited the most ^{13}C enrichment compared with glucose and sucrose, and there were no marked differences in isotopic signature between the light and the dark period (Werner *et al.*, 2009a). Other studies reported diurnal variations in sucrose $\delta^{13}C$, with day-sucrose being typically ^{13}C depleted as most ^{13}C is carried through by triose phosphates towards starch biosynthesis, while night sucrose is ^{13}C enriched due to starch breakdown during respiration (Tcherkez *et al.*, 2004, 2011). Hence, various factors can affect the carbon isotope signature of the three interconnected metabolites measured in this study, including water supply, time of day, the contribution from the phloem, and respiration (Werner *et al.*, 2009a; Merchant *et al.*, 2010; Smith *et al.*, 2016; Dethloff *et al.*, 2017). In this study, leaves were harvested during the day; however, the origin of the sucrose measured could not be ascertained as diurnal carbon isotope composition of leaf starch were not measured, which could partly explain why sucrose was ^{13}C enriched in the two species. Also, the phenomenon of sugar mixing during metabolite exchange through phloem transport between the heterotrophic and autotrophic tissues (Brüggemann *et al.*, 2011) adds to this complexity. Glucose $\delta^{13}C$ was intermediate to sucrose and fructose signatures, but the origins of the free glucose (e.g. fructose isomerisation, starch breakdown, cellulose degradation, etc.) was not assayed. In addition, photosynthetic pathway (C_3 or C_4) can affect the $\delta^{13}C$ of sugar metabolites. For example, sucrose and starch synthesis occur in the mesophyll of C_3 leaves. In C_4 leaves, starch synthesis almost exclusively occurs in the bundle sheath, while sucrose synthesis predominantly occurs in the mesophyll with a variable contribution from the bundle sheath (Lunn & Furbank, 1999a). Hence, metabolite trafficking between the two cell types and specific localisation of carbohydrate biosynthesis will likely involve variable fractionations in the C_4 leaf. Tracing the fate of carbon incorporated into the leaves after photosynthesis could identify the origins of these carbons atoms and could better unravel the carbon fluxomics in leaves.

Several applications of WCO have previously endeavoured. In the food industry, this method has been employed to discriminate pure honey with adulterated honey. Results from Cabañero *et al.*, (2006) showed that unadulterated honey had $\delta^{13}C$ for sucrose, glucose, and

fructose fall within -26.3 ± 1.0‰, -25.0 ± 1.0‰, and -25.2 ± 1.0‰ (mean ± SD) respectively; while adulterated honey contained had $\delta^{13}C$ signatures which were more ^{13}C-enriched and were probably due to C_4-photosynthesis-derived fructose contamination- for example, high fructose corn syrup. On the other hand, C_3 needles from tree species (*Picea abies* and *Larix decidua*) subjected to HPLC-WCO-IRMS assay showed heavier fructose $\delta^{13}C$ than glucose and sucrose (Rinne *et al.*, 2012). In *Nicotiana sylvestris* leaves assayed for compound-specific-isotope analysis of different leaf metabolites, well-watered plants showed heavier glucose $\delta^{13}C$ compared to sucrose and fructose (Ghashghaie *et al.*, 2001). The technique, however, did not employ a WCO system but rather a more laborious HPLC-IRMS method whereby metabolite fractions were individually collected after peak resolution from HPLC and then subsequently freeze-dried and subjected to IRMS. Nonetheless, it provided insights on carbon fluxes during drought in this species. Earlier studies by Brugnoli *et al.*, (1988) in several C_3 species demonstrated the strong correlation of soluble sugar $\delta^{13}C$ with instantaneous water-use efficiency. The method, however, involved laborious steps, including acid digestions and overnight incubations.

In summary, there is a considerable variation in patterns of $\delta^{13}C$ of polar sugars within species of the same photosynthetic type. The results have demonstrated the potential of HPLC-WCO-IRMS interface for high throughput screening of sugars from C_3 and C_4 crops and could measure $\delta^{13}C$ of different sugar metabolites in leaves using a reproducible and less laborious WCO system.

4.5 CONCLUSION

The wet-chemical oxidation system, coupled to HPLC and IRMS was investigated for its capacity to analyse compound-specific carbon isotope analysis of sugar standards and sugar metabolites representing C_3 and C_4 photosynthetic type. My results have demonstrated the accuracy and reproducibility of the Agilent Infinity System (HPLC) coupled to Liquiface WCO interface as a means to measure $\delta^{13}C$ of sucrose, glucose, and fructose. Only a few studies have reported on the utilisation of Liquiface as a choice of WCO assay (Morrison *et al.*, 2010; Abaye *et al.*, 2011; Basler & Dyckmans, 2013) compared to the more popular Isolink interface (Krummen *et al.*, 2004; Godin & McCullagh, 2011). Therefore, my data can be added to the scanty literature examining Liquiface as WCO system for analysing leaf sugars and sugar standards. In the future, I recommend the analysis of a larger number of species at different times of the days and different growth conditions to analyse general trends in sugar 'fluxomics' (Ratcliffe & Shachar-Hill, 2006; Kruger & Ratcliffe, 2009; Tcherkez *et al.*, 2011). Between photosynthetic types and C_4 biochemical subtypes as a tool to examine post-photosynthetic turn-over of ^{13}C in leaves and better understand how leaf $\delta^{13}C$ can be used as a screening tool for leaf-level water-use efficiency.

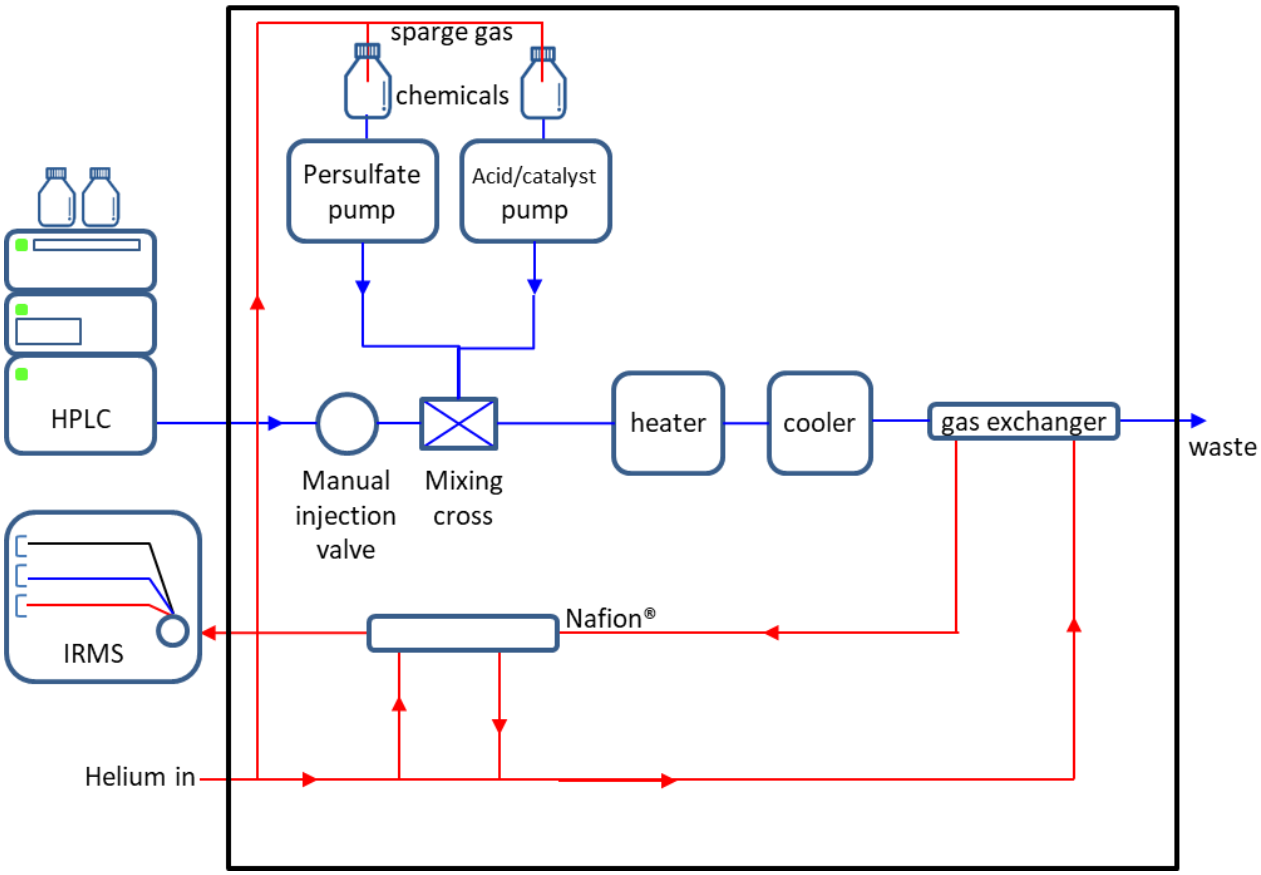

Figure 4. 1 The schematic diagram of the wet chemical oxidation system interfaced with the HPLC system and IRMS used to assay compound-specific carbon isotope signature of sugars.

Metabolites are separated using HPLC. Sequential peaks are oxidised in the WCO system, and each metabolite is subjected to IRMS analyses for $\delta^{13}C$ measurements. The diagram was redrawn from Isoprime (2011) compendium.

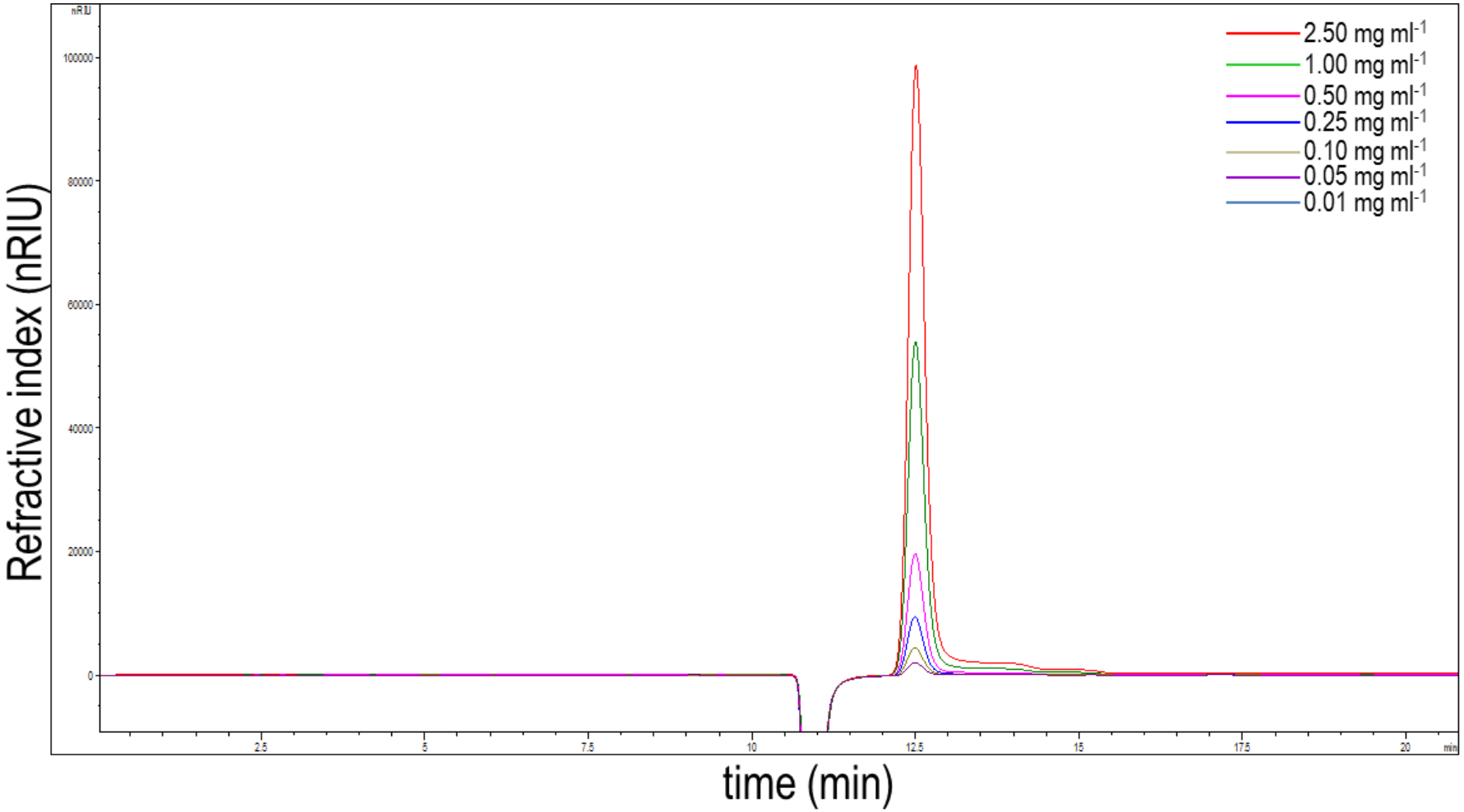

Figure 4. 2 HPLC elution profile of the international sucrose standard, IAEA-CH-6 (peak 12.5 min), over time in different concentrations to estimate the limits of detection.

Table 4. 1 Testing the limits of detection and reproducibility of the Hi-Plex H HPLC column interfaced to the Liquiface (Isoprime) wet chemical oxidation system.

Values for retention time and *m/z* peak height are mean ± SE (n=5) while $\delta^{13}C$ represents mean $\pm$ SE, SD (n=5) of unnormalised values of IAEA-CH-6 sucrose ($\delta^{13}C$ signature of -10.45‰) at several concentrations. Means with the same letters are not significantly different at α=0.05 using Fisher's LSD *post hoc*. n.d denotes not detected in the IRMS.

Concentration (mg ml^{-1})	Retention time (sec)	Carbon isotope composition, $\delta^{13}C$ (‰)	*m/z* peak height (nA)
2.50	832.76 $\pm$ 2.11 **a**	-9.63 $\pm$ 0.16, 0.36 **a**	1.69 $\pm$ 0.14 **a**
1.00	827.32 $\pm$ 0.73 **a**	-9.53 $\pm$ 0.14, 0.32 **a**	0.86 $\pm$ 0.09 **b**
0.50	831.86 $\pm$ 2.79 **a**	-9.36 $\pm$ 0.14, 0.31 **a**	0.50 $\pm$ 0.08 **c**
0.25	827.33 $\pm$ 1.01 **a**	-9.17 $\pm$ 0.28, 0.57 **a**	0.22 $\pm$ 0.04 **d**
0.10	826.15 $\pm$ 0.93 **a**	-9.61 $\pm$ 0.40, 0.80 **a**	0.15 $\pm$ 0.04 **d**
0.05	831.74 $\pm$ 4.26 **a**	-12.96 $\pm$ 10.10, 22.59 **a**	0.05 $\pm$ 0.01 **d**
0.01	n.d.	n.d.	n.d.

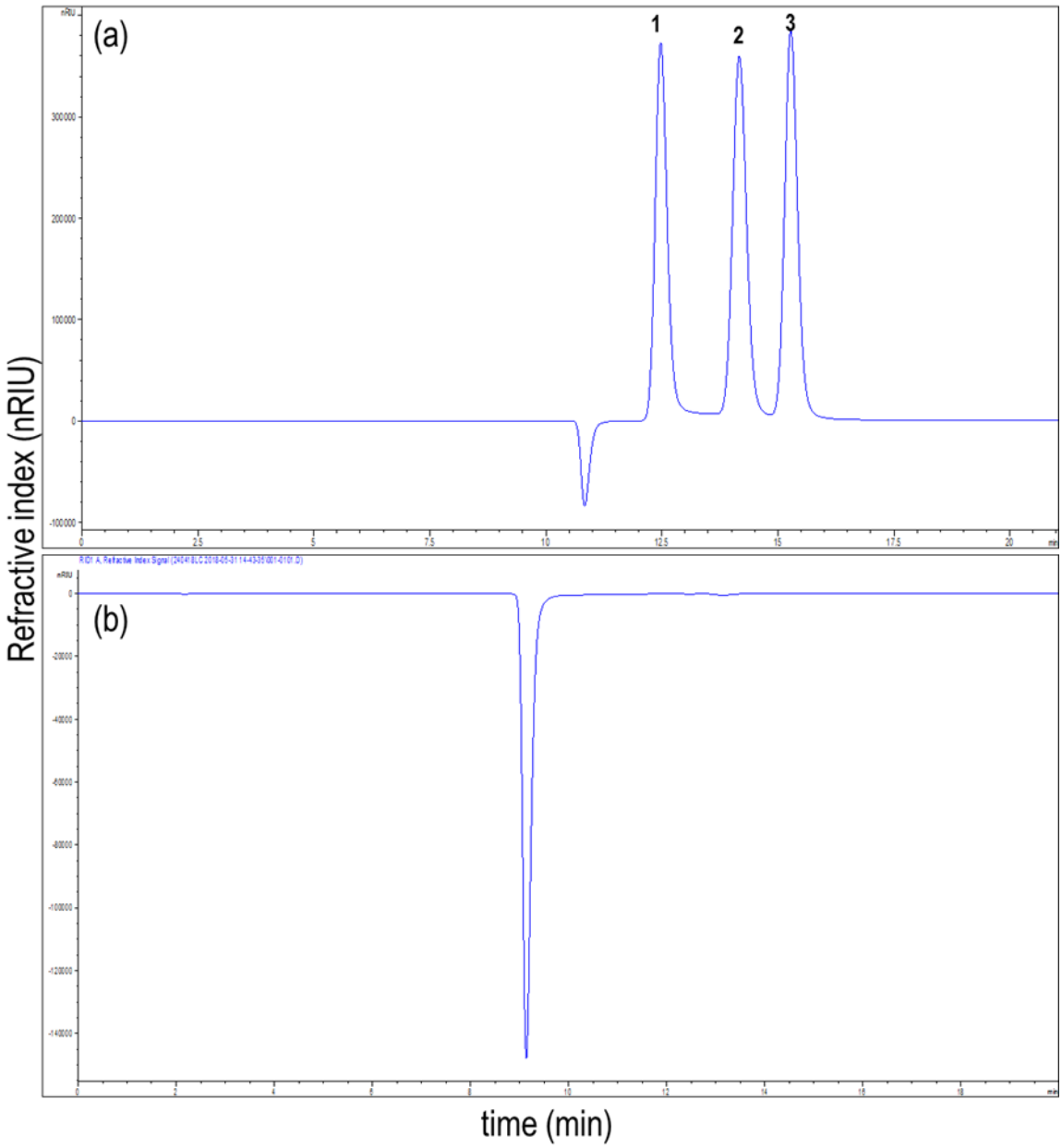

Figure 4. 3 The isocratic elution (A) of a sugar mixture constituting 2 mg ml^{-1} sucrose (1), glucose (2), and fructose (3) along with the peculiar negative peak in both sample (a) and blank solutions (B), before the elution of three sugars.

The negative peak is typical to the column as outlined in the HPLC column compendium (Ball *et al.*, 2011), which did not affect the analysis of $\delta^{13}C$ in the three sugars. The flow rate was adjusted to 0.6 ml min^{-1} in b to facilitate faster resolution.

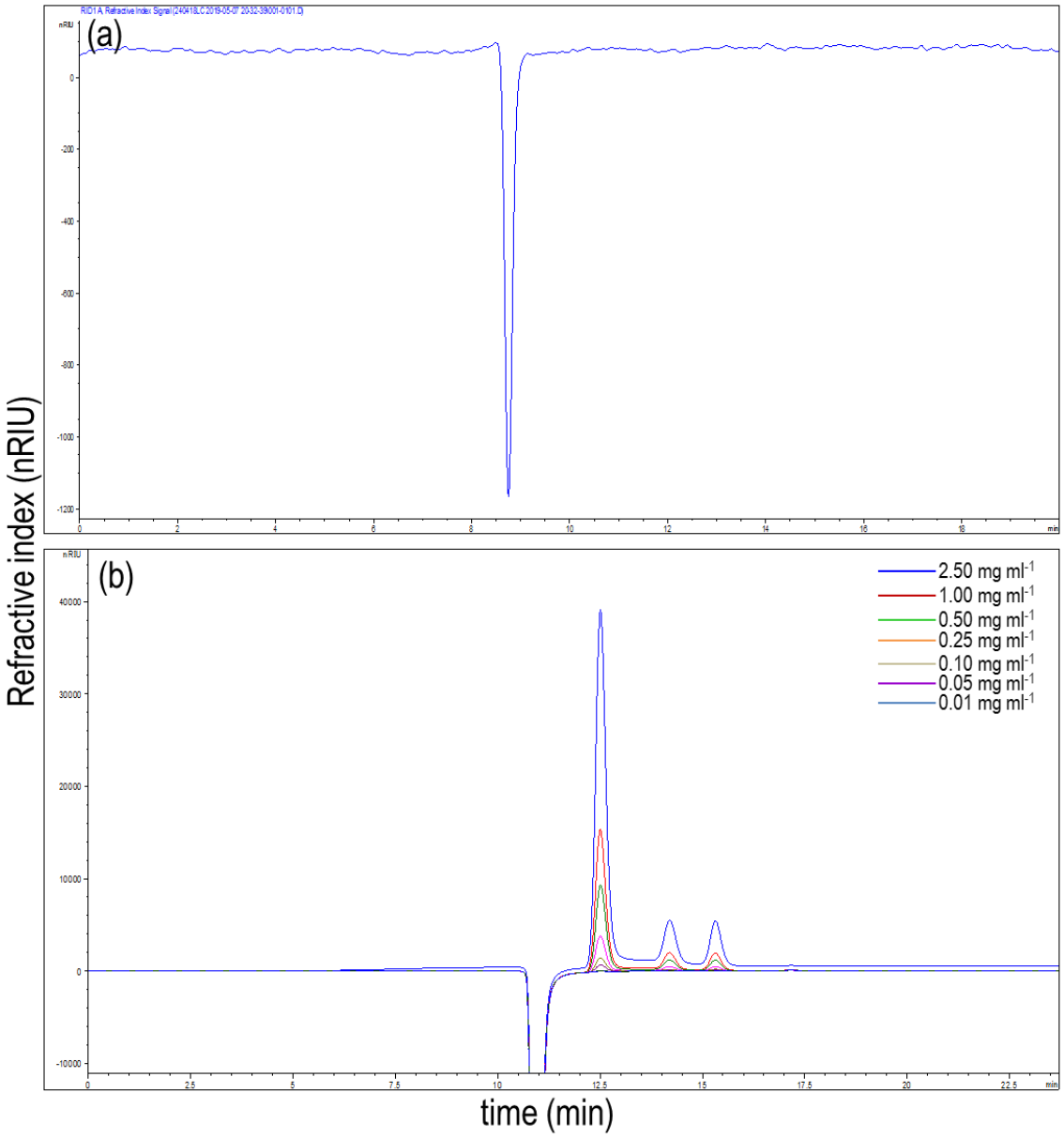

Figure 4. 4 Effects of mobile phase in the resolving IEAE sucrose using HPLC-RID.

Mobile phase assay using dilute phosphoric acid (0.05 M) showed noisy background refractive index signal (A) and weak hydrolysis of IEAE sucrose to its component monosaccharides, glucose and fructose (B) across different concentrations.

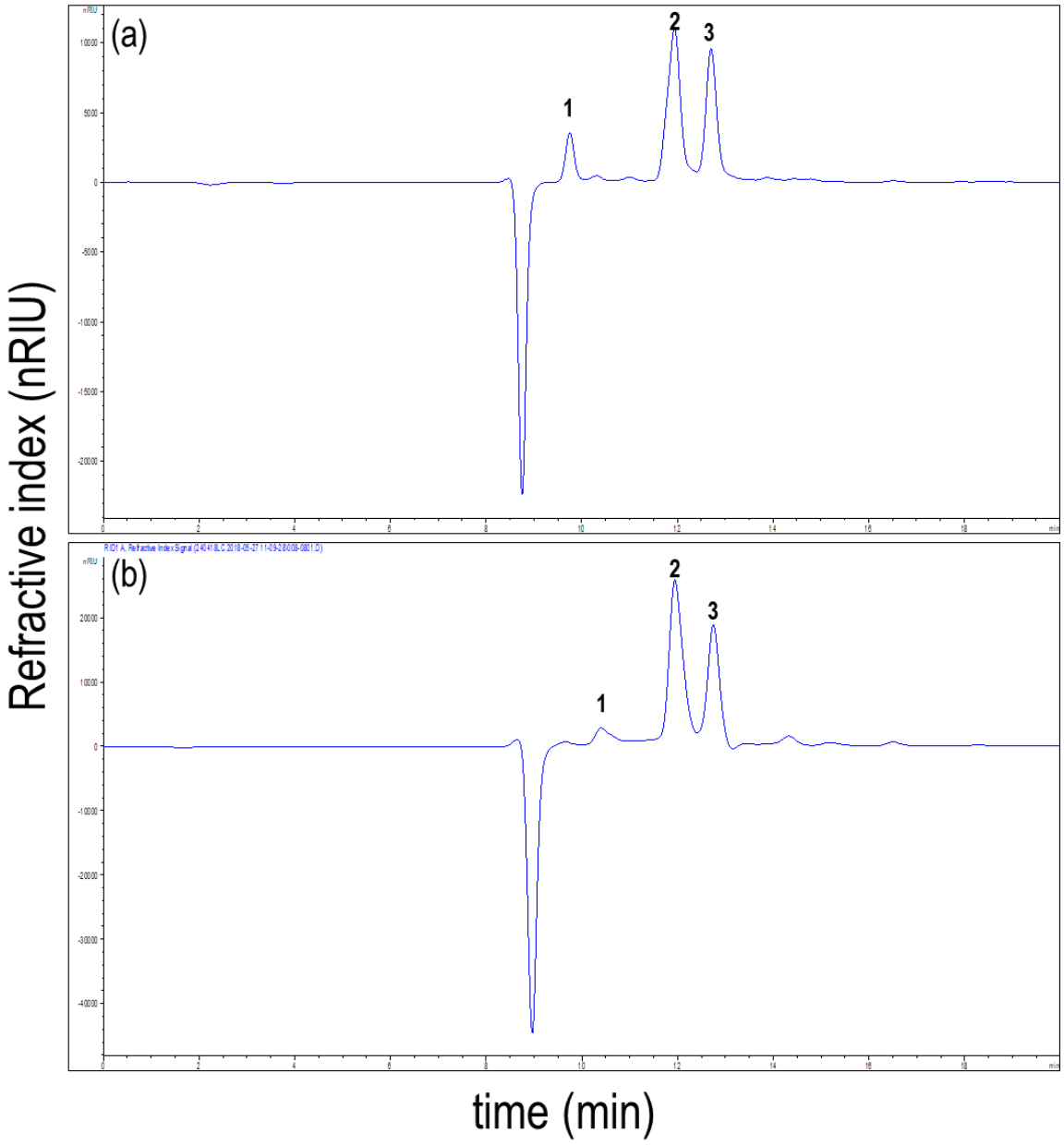

Figure 4. 5 Representative chromatographic resolution of sucrose (1), glucose (2), and fructose (3) in leaves of C_3 crop *Oryza sativa* (A) and in leaves of C_4 crop *Zea mays* (B) and using the Agilent Hi-Plex H column.

HPLC run parameters were: 0.0085 M H_2SO_4 as mobile phase; 0.6 ml min^{-1} flow rate; 25ºC column temperature; 35ºC RID temperature and 20 µL injection volume. The flow rate was adjusted to 0.6 ml min^{-1} to facilitate faster elution of sugars while not affecting the $\delta^{13}C$.

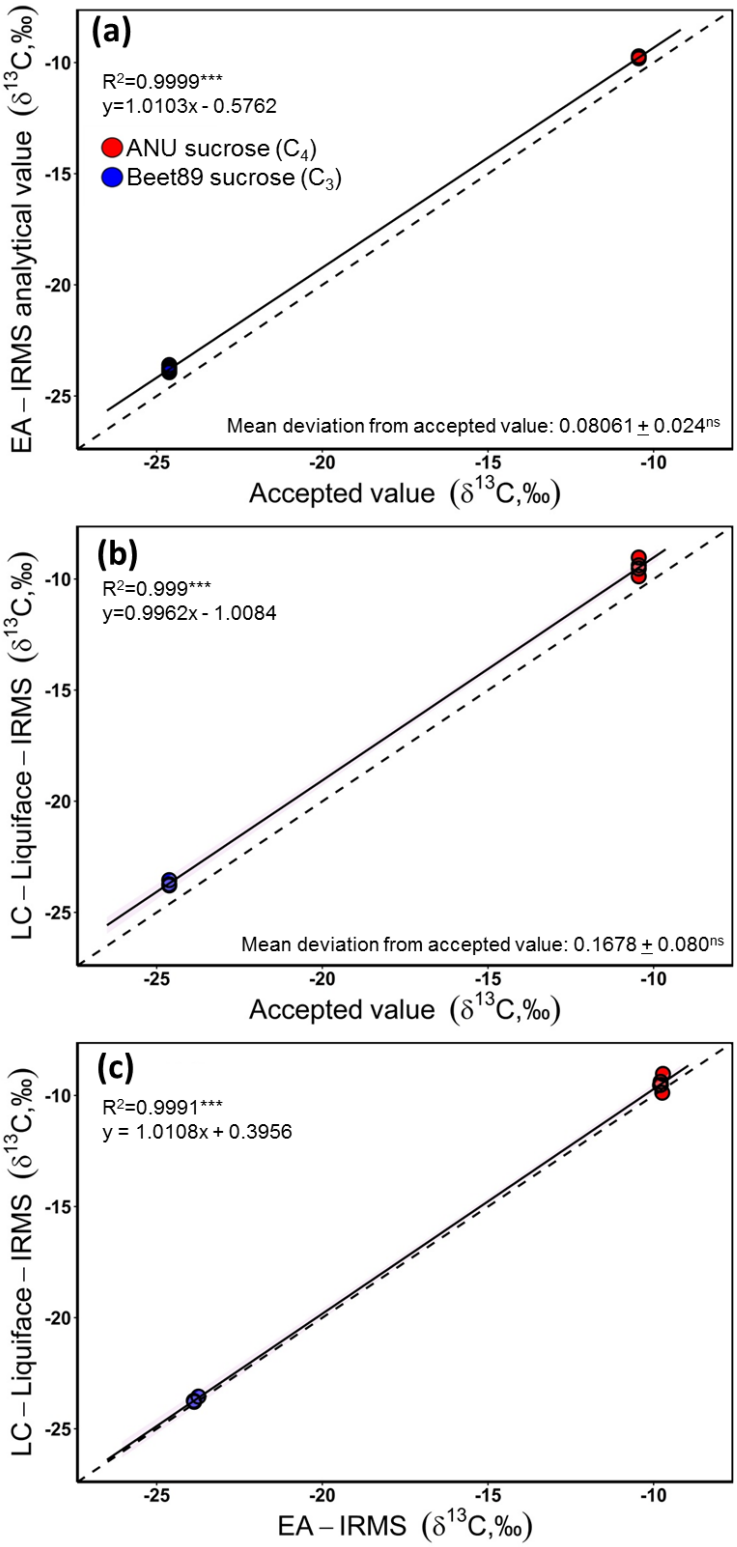

Figure 4. 6 Estimating the fractionation of EA-IRMS system (A) and HPLC-WCO-IRMS (B) against the accepted carbon isotope signature of ANU sucrose (n=4) and Beet89 sucrose (n=4).

Comparison between the $\delta^{13}C$ obtained from EA-IRMS and HPLC-WCO-IRMS (**C**) systems. Dotted lines represent the 1:1 values. Significance codes: **p<0.05; **p<0.01; ***p<0.001; ^{ns}p>0.05.*

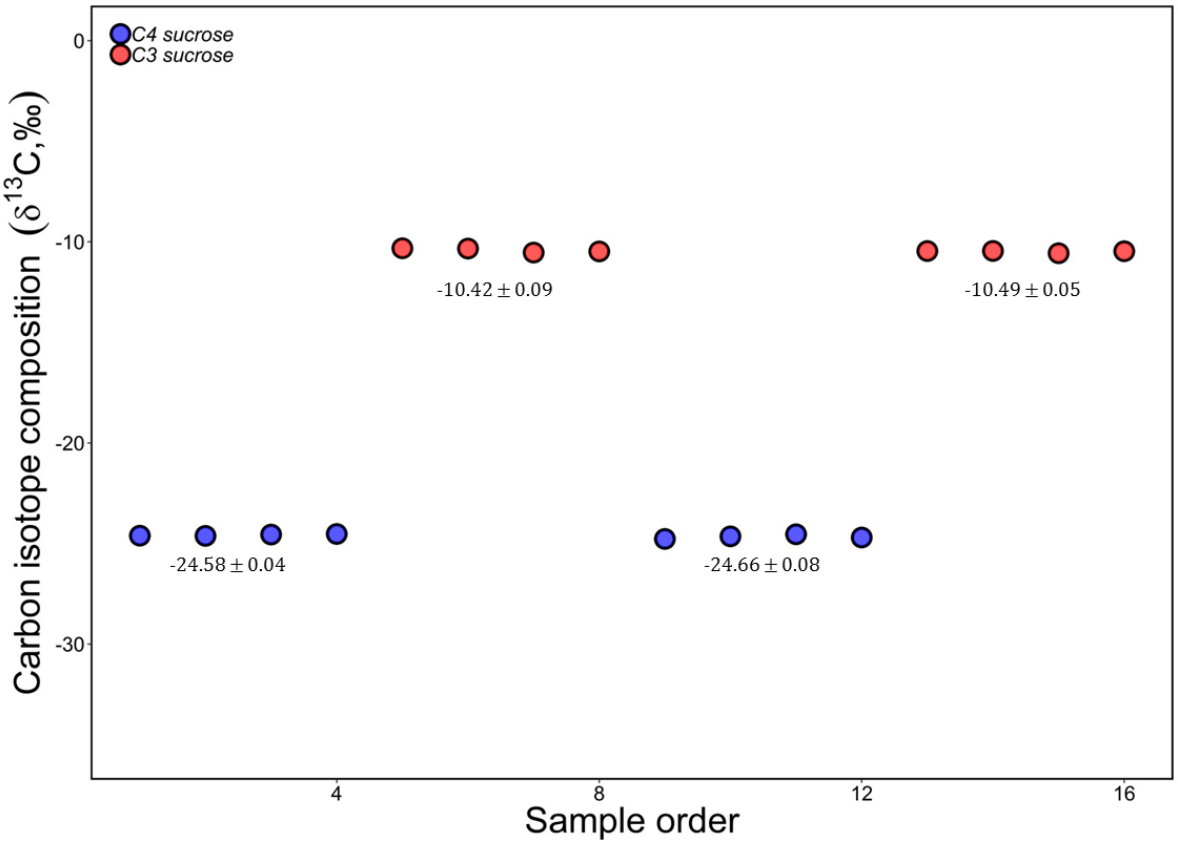

Figure 4. 7 Examination of the memory effect in HPLC-WCO-IRMS assay utilising two contrasting sucrose $\delta^{13}C$.

Dots represent the values of normalised $\delta^{13}C$ in successive runs. Blue dots represent a C_4 sucrose signature (IAEA-CH-6 sucrose) while red dots represent C_3 sucrose (Beet 89).

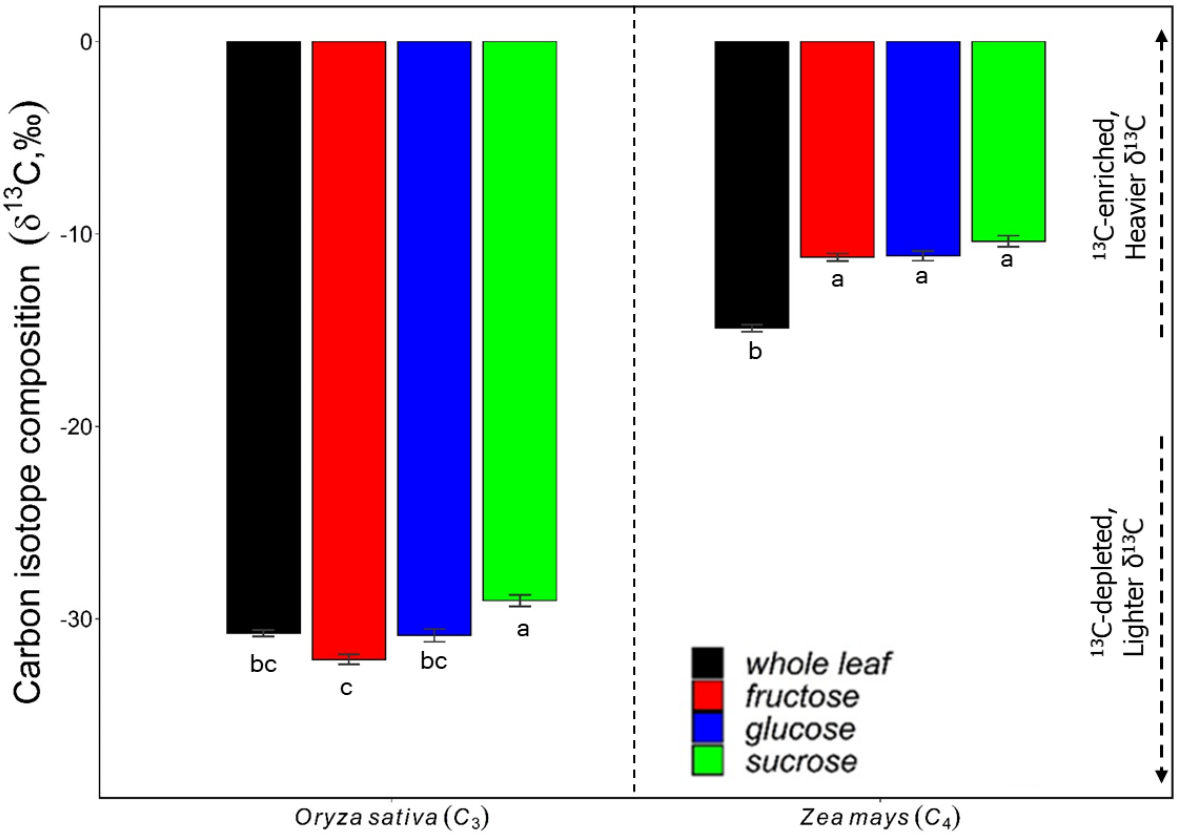

Figure 4. 8 The carbon isotope composition of the whole leaf (black) analysed using EA-IRMS and fructose (red), glucose (blue), and sucrose (green) measured using the HPLC-WCO-IRMS interface of *O. sativa* (C_3, n=6) and *Z. mays* (C_4, n=6).

Values are mean ± SE and ranked within species using Fisher's LSD *post-hoc* at α=0.05. Similar letters indicate non-significant difference within species.

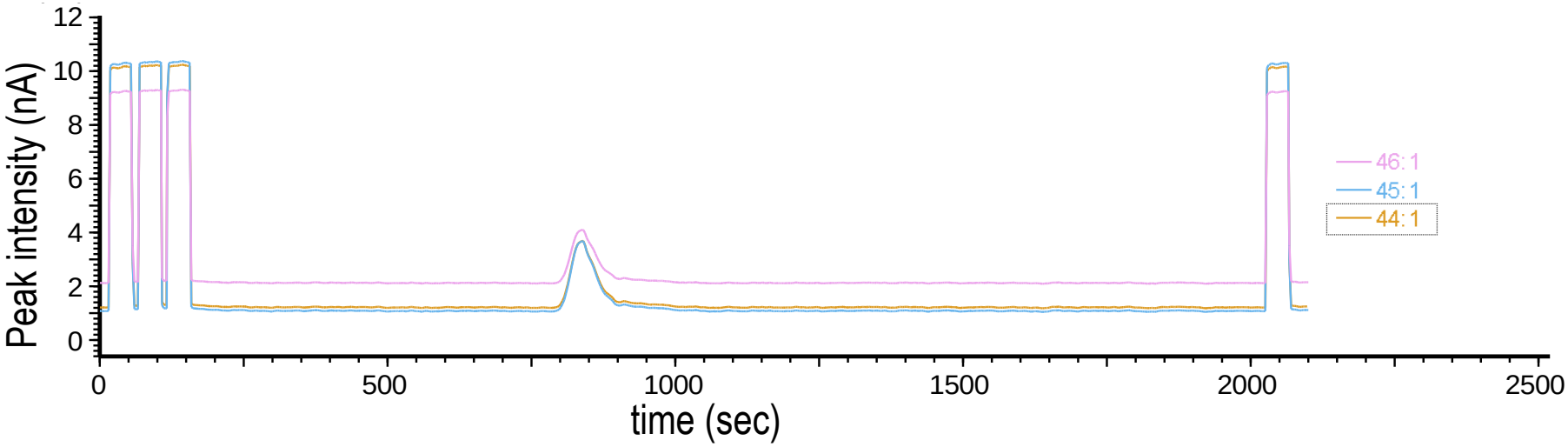

Figure 4. 9 The IRMS chromatogram of IAEA-CH-6 (2.5 mg ml^{-1}) after wet chemical oxidation using Liquiface-IRMS (Isoprime) system.

The three lines represent the signals of $^{12}C^{16}O_2$ (*m/z 44*, orange), $^{13}C^{16}O_2$ (*m/z 45*, blue), and $^{12}C^{18}O^{16}O$ (*m/z 46*, purple). Three pulses of references gases from the beginning of the run and one pulse before the end were used to calibrate and monitor the carbon isotope signature.

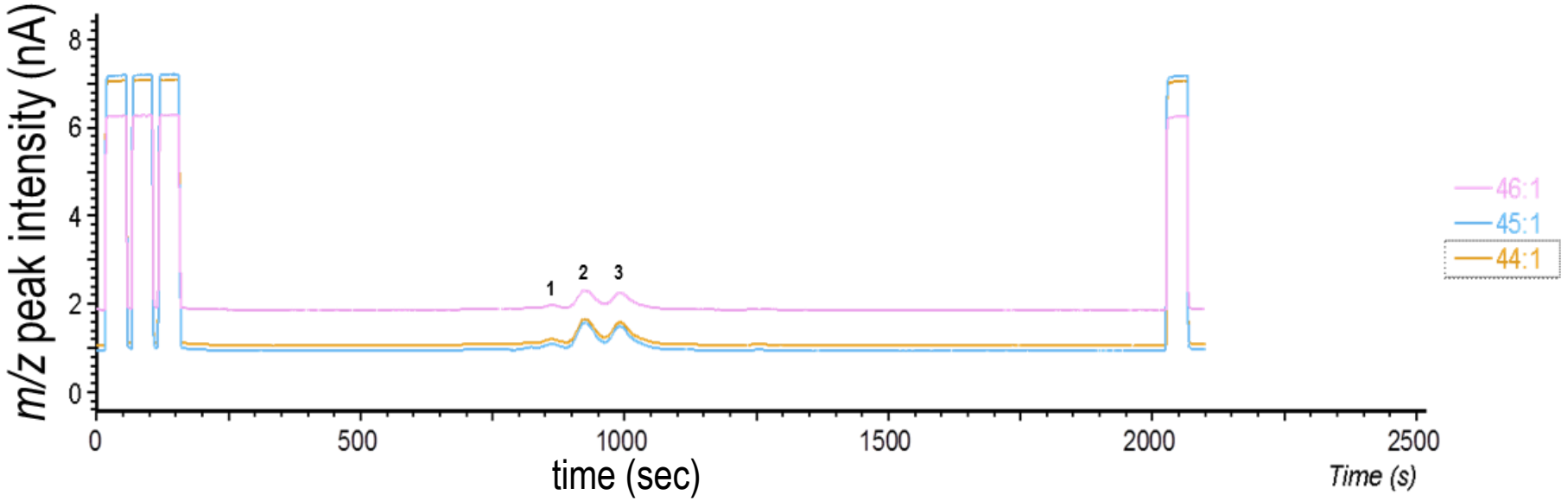

Figure 4. 10 The *m/z* chromatogram of sucrose (peak 1), glucose (peak 2), and fructose (peak 3) in *Z. mays* leaves after wet chemical oxidation using HPLC-Liquiface-IRMS (Agilent-Isoprime) system.

The three lines represent the signals of $^{12}C^{16}O_2$ (*m/z 44*, orange), $^{13}C^{16}O_2$ (*m/z 45*, blue), and $^{12}C^{18}O^{16}O$ (*m/z 46*, purple). Three pulses of references gases from the beginning of the run and one pulse before the end were used to calibrate and monitor the carbon isotope signature.

Conditions

Column	Agilent Hi-Plex H, 7.7 × 300 mm, 8 µm (p/n PL1170-6830)
Sample	Sugars + acid mixture
Sample size	10 mg/mL each
Mobile phase	0.05 M H_2SO_4
Flow rate	0.5 mL/min
Injection volume	20 µL
Temperature	Ambient
Detector	RI

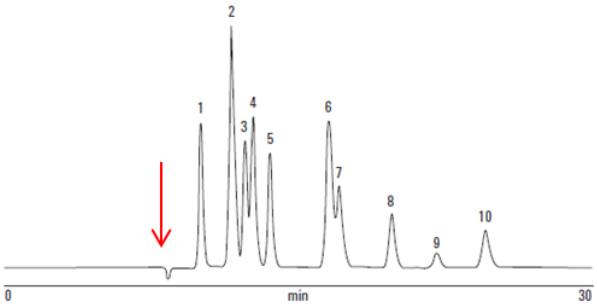

Figure 1. Separation of a sugars and acids mixture using an Agilent Hi-Plex H 8 µm column. See Table 1 for peak identification.

Table 1. Peak Identification for Figure 1

Peak	Name	Time (min)	Height (µV)	Area (%)	Width 50% (min)	As. USP	10% Asymmetry	Res. HW	Plate counts	Plates/m
1	Sucrose	10.04	193813.4	9.998	0.23	1.20	1.15	0.00	10870	36233
2	Citric acid, glucose	11.60	323837.5	21.448	0.30	1.24	1.18	3.48	8312	27708
3	Tartaric acid	12.28	170815.1	9.038	0.26	0.87	0.91	1.46	12812	42705
4	Fructose	12.70	203381.4	12.313	0.28	1.29	1.15	0.91	11430	38099
5	Malic acid	13.55	154736.4	9.548	0.27	1.14	1.12	1.85	14375	47918
6	Lactic acid, glycerol	16.53	196730.6	16.474	0.41	0.98	1.05	5.22	9104	30346
7	Succinic acid	17.07	110886.3	8.846	0.40	1.66	1.47	0.78	10298	34325
8	Acetic acid	19.72	73828.0	5.480	0.33	1.17	1.16	4.28	19217	64056
9	Methanol	22.00	19729.7	1.724	0.36	1.25	1.14	3.88	20778	69259
10	Ethanol	24.47	50557.3	5.131	0.42	1.25	1.20	3.75	19042	63475
Total			**1498315.5**	**100.000**						

Appendix 4. 1 Resolution of sugars, alcohols, and organic acids using the Hi-Plex H column based from the Compendium of Hi-Plex columns for Agilent HPLC system.

The figure was obtained from Compendium of Hi-Plex columns, page 47 in support of the negative peak observed in this study. The red arrow indicates the negative peak before the elution of target compounds, as also observed in this study (Ball *et al.*, 2011).

Instrumentation

Column	Agilent Hi-Plex H, 7.7 × 300 mm, 8 µm (p/n PL1170-6830)
Detector	RI

Materials and Reagents

Mobile phase	0.005 M H_2SO_4 (sugars), 0.0005 M H_2SO_4 (compounds of physiological significance)

Conditions

Flow rate	0.6 mL/min
Temperatures	60 °C (sugars), 55 °C (compounds of physiological significance)

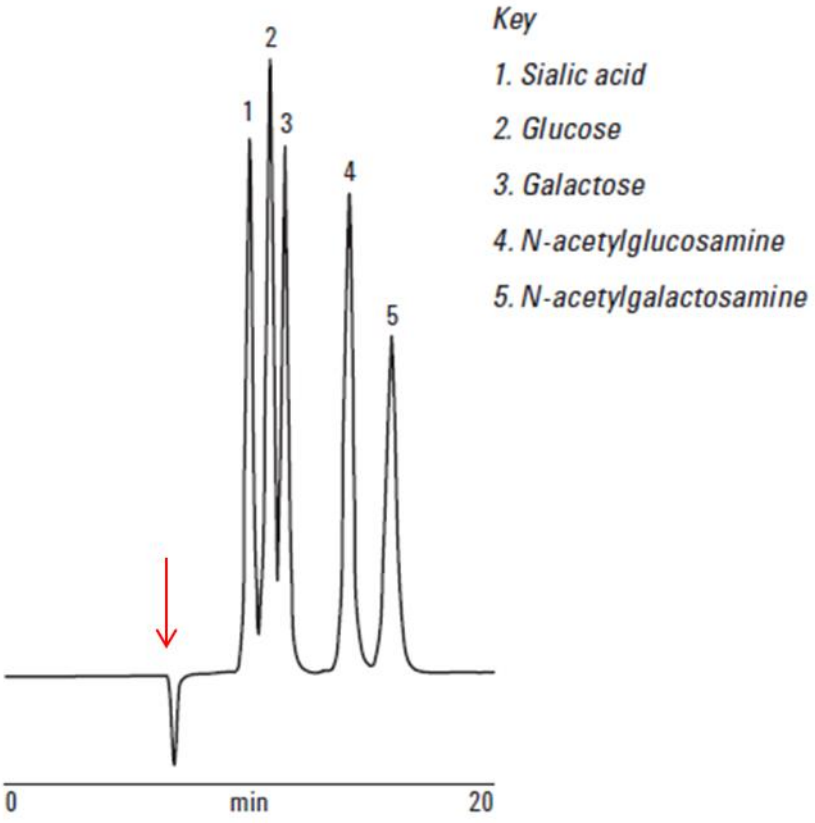

Figure 1. Good separation of glucose and galactose from their derivatives achieved by HPLC with Agilent Hi-Plex H columns.

Appendix 4. 2 Resolution of sugars, sugar-derivatives and organic acids using the Hi-Plex H column based from the Compendium of Hi-Plex columns for Agilent HPLC system.

The figure was obtained from Compendium of Hi-Plex columns, page 64, in support of the negative peak observed in this study. The red arrow indicates the negative peak before the elution of target compounds similarly observed in this experiment (Ball *et al.*, 2011).

CHAPTER 5

CARBON ISOTOPE COMPOSITION OF SOLUBLE SUGARS IN LEAVES OF C_3 AND C_4 GRASSES WITH DIFFERENT BIOCHEMICAL SUBTYPES

ABSTRACT

Post-photosynthetic carbon isotope fractionation may partly explain why leaf carbon isotope composition ($\delta^{13}C$) and intrinsic water use efficiency (iWUE) do not correlate well in C_4 pants, as well as the difference in leaf $\delta^{13}C$ between the two main subtypes (NADP-ME and NAD-ME) of C_4 photosynthesis. Four C_3, five NAD-ME, and four NADP-ME grass species were grown in a glasshouse under common conditions. Fully expanded and non-senescing leaves were lyophilised and analysed. Leaf dry matter and cellulose $\delta^{13}C$ were measured using EA-IRMS, while $\delta^{13}C$ of three main soluble sugars (sucrose, glucose and fructose) were analysed using HPLC-WCO-IRMS. Overall, sucrose $\delta^{13}C$ deviated the most and cellulose $\delta^{13}C$ deviated the least relative to the bulk leaf. Among C_3 grasses, the $\delta^{13}C$ of soluble sugars did not differ but were positively correlated with each other, reflecting the simpler carbon metabolism in C_3 leaves. Among NADP-ME and NAD-ME species, the previously observed differences in leaf and cellulose $\delta^{13}C$ were not significant due to *Z. mays* having $\delta^{13}C$ untypical of NADP-ME subtype. However, fructose $\delta^{13}C$ was 1.6 ‰ more ^{13}C-enriched in NADP-ME relative to NAD-ME species. In addition, leaf and cellulose $\delta^{13}C$ correlated well with stomatal conductance (but not with iWUE) in C_4 (but in C_3) grasses, highlighting the dominant role played by stomata in determining leaf $\delta^{13}C$ and iWUE of C_4 species. It is proposed that examining position-specific isotope analysis (PSIA) of fructose, glucose and sucrose in species of the two C_4 subtypes as well as fractionation studies on leaf carbohydrate enzymes such as the invertases may shed light on the contribution of soluble sugars and post-photosynthetic carboxylation on variations in leaf $\delta^{13}C$, and better understand the link between leaf $\delta^{13}C$ and iWUE amongst C_4 species.

Keywords: C_4 subtypes, HPLC, IRMS, post-photosynthetic fractionation, wet chemical oxidation.

5.1 INTRODUCTION

The CO_2 concentrating mechanism (CCM) leads to the saturation of C_4 photosynthesis at lower intercellular CO_2 partial pressure (C_i) and stomatal conductance (g_s) relative to C_3 photosynthesis. Consequently, C_4 plants generally have better leaf-level intrinsic water-use efficiency (iWUE) as well as whole plant WUE than their C_3 counterparts (Taylor *et al.*, 2012). In C_3 plants, leaf carbon isotope composition ($\delta^{13}C$) has been used with relative success as a proxy tool for screening WUE (Farquhar & Richards, 1984; Condon *et al.*, 2004). The application of this technique for C_4 plants has been hampered by a number of factors, even though a theoretical framework has been developed linking C_4 photosynthesis with carbon isotope discrimination ($\Delta^{13}C$) as follows (Farquhar, 1983; Henderson *et al.*, 1992b):

$$\Delta^{13}C = a + (b_4 + (b_3 - s)\phi - a)\frac{C_i}{C_a} \qquad \text{equation 5.1}$$

where C_i/C_a is the ratio of intercellular to ambient CO_2 partial pressure, ϕ is leakiness defined as the ratio of the CO_2 leak rate out of the bundle sheath to the rate of PEP carboxylase (PEPC), a is the fractionation during diffusion of CO_2 in air (4.4 ‰), b_4 is the fractionation associated with PEPC and the preceding isotopic equilibrium during dissolution and conversion to bicarbonate, s is the fractionation during the leakage of CO_2 out of the bundle sheath (1.8 ‰), and b_3 is the fractionation during Rubisco carboxylation. This equation has recently been updated to include the ternary formulation to take into account the influence of transpiration on CO_2 diffusion between the atmosphere and the intercellular air spaces (Farquhar & Cernusak, 2012). Additionally, C_i/C_a is linked to $iWUE_i$ and ϕ is linked to $\delta^{13}C$ as follows:

$$iWUE = \frac{A_{net}}{g_s} = 1 - \frac{C_i}{C_a} \qquad \text{equation 5.2}$$

$$\Delta^{13}C_{drymatter}\ (‰) = \frac{\delta_{air}(‰) - \delta_{drymatter}(‰)}{\delta_{drymatter}(‰) + 1000} \times 1000 \qquad \text{equation 5.3}$$

where $\delta^{13}C_{air}$ and $\delta^{13}C_{drymatter}$ are the stable carbon isotope composition of air and leaf dry matter, respectively. $\delta^{13}C$ (‰) is the deviation of the heavier/lighter ratio ($^{13}C/^{12}C$) of the sample carbon isotopes (R_{sample}) relative to the $^{13}C/^{12}C$ ratio of the international carbonate standard, the Vienna Pee-Dee Belemnite (R_{PDB} = 0.0112372):

$$\delta^{13}C = (R_{sample}/R_{PDB}) - 1 \qquad \text{equation 5.4}$$

Equation 5.1 is primarily derived from photosynthetic parameters and indicates that the dependence of $\Delta^{13}C$ on C_i/C_a (and hence, iWUE) varies with bundle sheath leakiness (Henderson *et al.*, 1992b). The advent of tuneable diode laser absorption spectroscopy (TDL) allowed for instantaneous measurements (on-line) of leaf-level $\Delta^{13}C$ during leaf gas exchange measurements and thus sparked a renewed interest in understanding the basis of leaf-level carbon isotope discrimination in C_4 species. Therefore, a number of studies have attempted to measure ϕ in C_4 leaves in order to both understand its variations and its effect on $\Delta^{13}C$ (Henderson *et al.*, 1992a; Cousins *et al.*, 2008; von Caemmerer *et al.*, 2014; Sonawane *et al.*, 2017, 2018). However, variations in ϕ are still poorly understood (von Caemmerer *et al.*, 2014). While $\Delta^{13}C$ is useful for understanding C_4 photosynthesis, it is laborious to measure, and $\delta^{13}C$ is a more convenient parameter for screening large populations for variations in iWUE (Ellsworth & Cousins, 2016). In addition, our improved ability to measure $\Delta^{13}C$ and estimate ϕ has shed little light on the relationship between leaf dry matter $\delta^{13}C$ and WUE. Early attempts using C_4 crops and grasses have not been conclusive (Meinzer *et al.*, 1994; Henderson *et al.*, 1998; Ghannoum *et al.*, 2001a, 2002). Recently, Feldman *et al.*, (2018) and Ellsworth *et al.*, (2019) have reported a relationship between whole plant WUE and dry matter $\delta^{13}C$ measured within a recombinant inbred population of the model C_4 grass *Setaria viridis* grown under highly controlled environments. These recent studies renew hopes in the effectiveness of $\delta^{13}C$ as a tool for measuring iWUE. Nevertheless, the overall evidence, so far, suggests that we need to better understand the causes of variation in leaf dry matter $\delta^{13}C$ before it can widely be applied for screening $iWUE_i$ in C_4 plants.

The C_4 photosynthetic pathway exists in different subtypes (NADP-ME, NAD-ME, and PCK) with different leaf biochemistry and anatomy (Hatch, 1987). Amongst C_4 grasses, species with the NAD-ME C_4 subtype tend to have higher WUE than NADP-ME grasses under water stress (Ghannoum *et al.*, 2002). Additionally, the C_4 subtypes have long been known to have variations in their carbon isotope composition (Hattersley, 1982; von Caemmerer *et al.*, 2014). Early work by Hattersley (1982) demonstrated a 1.35‰ difference in the whole leaf $\delta^{13}C$ between NADP-ME and NAD-ME subtypes of C_4 grasses, with NADP-ME having higher $\delta^{13}C$. These differences have fuelled hypotheses that the two C_4 subtypes vary in bundle sheath leakiness and hence the efficiency of their C_4-CCM; however, this has not been supported by subsequent work. Using a number of monocots and dicots, Henderson *et al.*, (1992a) showed that bundle sheath leakiness did not differ between subtypes possessing suberised lamella (NADP-ME) and those without suberised lamellae (NAD-ME). In addition, Cousins *et al.*,

(2008) validated these results and showed that photosynthetic carbon isotope discrimination, measured instantaneously using TDL, was not different among C_4 grasses with different biochemical subtypes while maintaining their difference in whole leaf carbon isotope signature. Subsequently, Sonawane *et al.*, (2017, 2018) showed that $\Delta^{13}C$ is similar between C_4 grasses with different subtypes exposed to various leaf temperatures and that photosynthetic $\Delta^{13}C$ and leaf dry matter $\delta^{13}C$ differed between NAD-ME and NADP-ME subtypes under low light. Moreover, studies using a large number of species showed that leaf dry matter $\delta^{13}C$ was consistently different between 18 species of NAD-ME and NADP-ME grown under drought and well-watered conditions (Ghannoum *et al.*, 2002). These differences were carried up to the leaf cellulose $\delta^{13}C$ signature under different growth conditions (Ghannoum *et al.*, 2001a, 2011; von Caemmerer *et al.*, 2014). Taken together, these findings suggest that variations in leaf $\delta^{13}C$ amongst the C_4 subtypes could occur after photosynthesis (post-photosynthetic).

Variations in $\delta^{13}C$ are due to factors which affect $\Delta^{13}C$ (e.g., C_i/C_a, ϕ) as well as post-photosynthetic factors such as fractionations (von Caemmerer *et al.*, 2014). Several studies have postulated the involvement of post-photosynthetic fractionation as a major contributor to variations in leaf carbon isotope composition (Tcherkez *et al.*, 2011; Cernusak *et al.*, 2013; von Caemmerer *et al.*, 2014; Ellsworth & Cousins, 2016). However, there is still a scarcity of information regarding the contribution of post-photosynthetic metabolites in these $\delta^{13}C$ differences. Post-photosynthetic fractionation encompasses the redistribution ^{13}C after Rubisco carboxylation, including post-carboxylation (metabolic) fractionation, respiratory fractionation, and fractionation during transport (Gessler *et al.*, 2008; Brüggemann *et al.*, 2011). These processes are of particular importance as they alter the isotopic signatures imprinted on the newly assimilated metabolite during the downstream metabolic processes (Werner *et al.*, 2011). For example, different leaf metabolic pools differ in carbon isotope signatures. Cellulose, sucrose, and starch are usually ^{13}C enriched relative to the whole leaf while lipids, organic acids, amino acids are typically ^{13}C depleted (Park & Epstein, 1961; O'Leary, 1981; Hobbie & Werner, 2004; von Caemmerer *et al.*, 2014). Between major plant organs, the autotrophic tissues (*e.g.* leaves) are isotopically lighter than the heterotrophic tissues (stem and roots) (Badeck *et al.*, 2005; Cernusak *et al.*, 2009). This chapter focuses on the post-carboxylation fractionation specifically the major short-term, soluble sugar pools (sucrose, glucose, and fructose) as the other two fractionation processes (respiration and transport) occur further downstream in terms of isotopic redistribution. I also consider cellulose as a long-term carbon store. Therefore, I hypothesise that differences in leaf $\delta^{13}C$ between

NADP-ME and NAD-ME subtypes (and between C_3 and C_4 photosynthetic types) are partly due to post-photosynthetic metabolic fractions. Consequently, variations in leaf $\delta^{13}C$ will be partly explained by variations in $\delta^{13}C$ of soluble sugars and will be carried through to the cellulose $\delta^{13}C$. The specific aim of this study was to compare the carbon isotope signatures of primary leaf non-structural carbohydrates (sucrose, glucose, and fructose) using HPLC-WCO-IRMS previously optimised from Chapter 4 among C_3 and C_4 grasses, and between NAD-ME and NADP-ME C_4 subtypes.

5.2 MATERIALS AND METHODS

5.2.1 Plant culture

Grasses representing C_3 and two subtypes (NAD-ME and NADP-ME) of C_4 photosynthesis were grown in a naturally-lit glasshouse under similar conditions as outlined in Chapter 4 from February 23, 2018 to April 26, 2018. Plants were randomised twice a week to reduce within chamber variations and well-watered as required. The species included C_3: *Oryza sativa* (L.), *Panicum bisulcatum* (Thunb.), *Triticum turgidum* (L.), *Steinchisma laxa* (Zuloaga); C_4 NAD-ME: *Panicum coloratum* (L.), *Eragrostis curvula* (Schrad.), *Panicum miliaceum* (L.), *Cynodon dactylon* (L.), and *Leptochloa fusca* [(L.) Kunth.]; C_4 NADP-ME: *Z. mays* (L.), *Panicum antidotale* (Retz.), *Cenchrus cilirais* (L.), and *Setaria viridis* [(L.) Beauv.] (Grass Phylogeny Working Group II, 2012). Fully expanded and non-senescing leaves were harvested from 15:00 to 17:00 and snap-frozen in liquid nitrogen. Leaves were then lyophilised using Martin Christ Alpha 1-2 LD plus freeze dryer (John Morris Scientific Pty Ltd., Australia) at -55°C for 48 hr. Subsequently, freeze-dried leaves were finely ground at 30 hertz for two minutes using Retsch Mixer Mill MM 200 (The McCrone Group, Illinois, USA) and stored in glass vials until analysis.

5.2.2 Leaf gas exchange

Gas exchange measurements were made using LI-6400XT infrared gas analyser (LI-COR Inc., Lincoln, NE, USA) on the first fully expanded leaves of six-week-old plants. For grasses with very narrow leaves (e.g. *E. curvula, C. dactylon, C. ciliaris*), three to four leaves were placed in the 3 × 2 cm cuvette, and the leaf area was corrected. Measurement conditions were: 1000 µmol m^{-2} s^{-1} PPFD, 28°C leaf temperature, 350 mol s^{-1} flow rate, and 60-65% relative humidity. Steady-state measurements of CO_2 assimilation rate (A_{net}), stomatal conductance (g_s), intercellular CO_2 partial pressure (C_i), the ratio of intercellular CO_2 to ambient CO_2 (C_i/C_a), and intrinsic water-use efficiency ($iWUE_i$) were obtained from four to six biological replicates between 10:00 to 16:00.

5.2.3 Standards

Similar to Chapter 4, the two sucrose standards, IAEA-CH-6 ($\delta^{13}C$ = -10.45‰) and Beet89 sucrose ($\delta^{13}C$ = -24.62‰) were also utilised in both EA-IRMS and HPLC-WCO-IRMS assays to calculate carbon isotope signature offsets.

5.2.4 Soluble sugars and cellulose extraction/purification

Ground freeze-dried leaf samples were weighed to 120 ± 1.0 mg and transferred to 2 ml screw-cap tubes. In the same way, soluble carbohydrates were twice extracted using 1.5 ml Milli-Q grade water, vortexed, and centrifuged at 13,000 rpm for 2 min. The aqueous fraction was filtered using a Millex™GP membrane filter (Merck Millipore Ltd, MA, USA), and deionised/deproteinised using CentriPure P10 columns (EMP BIOTECH, Berlin, Germany). The purified aqueous fractions were aliquoted to crim-top autosampler vials for HPLC-WCO-IRMS assay.

Cellulose extraction and purification from leaves were assayed using a modified Zhou *et al.*, (2010) method. The pellet from the above step was added with 1000 µl chloroform: methanol (1:1), vortexed, and incubated at 40ºC for 20 min. The mixture was centrifuged at 13,000 rpm for 5 min, and the organic phase was discarded. The chloroform: methanol (1:1) step was repeated for four to five times until pigments were removed. Excess chloroform was removed by washing with 1000 µl methanol incubated at 40ºC for 20 min and pelleted at 13,000 rpm for 5 min. After which, the pellet was subsequently washed with 1000 µl acetone and digested with 1000 µl 8:2:1 acetic acid: nitric acid: water solution at 90ºC for 1 hr. The mixture was cooled down to ambient room temperature and spun at 13,000 rpm for 10 min and subsequently washed twice with 95% ethanol. The resulting pellet was air-dried to evaporate excess ethanol and oven-dried at 50ºC for 12 hrs. The resulting cellulose pellet was transferred to new 2 ml Eppendorf tubes.

5.2.5 Carbon isotope assays using HPLC-WCO-IRMS and EA-IRMS

The desalted and deproteinised aqueous fraction from the above step (Section 5.2.4) was subjected to HPLC-WCO-IRMS using Agilent 1260 Infinity II high-performance liquid

chromatography (HPLC) system (Agilent Technologies, Inc., Santa Clara, CA, USA) interfaced to a wet chemical oxidiser, Liquiface (Isoprime Ltd, Cheadle Hulme, UK), and unto an isotope ratio mass spectrometer (Isoprime, 2011). Similar HPLC-WCO-IRMS parameters, reagents, and HPLC column were utilised as outlined in Chapter 4.2.4.

EA-IRMS was employed to assay for cellulose and whole leaf $\delta^{13}C$. Finely ground whole leaf materials from section 5.2.1 and air-dried cellulose from section 5.2.4 was weighed to 2 ± 0.1 mg using a Mettler Toledo AT21 balance. Consequently, the samples were transferred in tin capsules (Sercon Ltd, Crewe UK), folded and subjected to pyrolysis and mass spectrometry assay as described in Chapter 4.2.5.

Photosynthetic carbon isotope discrimination ($\Delta^{13}C$) was calculated using equation 5.3 assuming $\delta_{air}(‰)$ is -8‰ (Sonawane *et al.*, 2018).

5.2.6 Data analysis

The carbon isotope composition and data normalisation were expressed relative to the VPDB scale, similar to Chapter 4.2.6. Statistical analyses were performed using R (V.3.4.2; R Core Team, 2017). Values represent mean $\pm$ SE of biological replicates when compared between species. Among functional types comparison, values represent mean $\pm$ SE with species as replicate. When significant, means were ranked using Fisher's LSD *post hoc* at α=0.05. Correlations were expressed as $r^{2,}$ followed by significance values.

5.3 RESULTS

5.3.1 Leaf gas exchange

Relative to C_3 grasses, C_4 grasses had higher net CO_2 assimilation rates (A_{net}) and intrinsic water-use efficiency ($iWUE_i$); and lower stomatal conductance (g_s) and intercellular CO_2 (C_i) (**Figure 5. 1, Table 5. 1 and Table 5. 2**). C_i/C_a ratio was highest in C_3 species followed by NADP-ME then NAD-ME (**Figure 5. 1C, Table 5. 2**). Photosynthetic type (C_4 > C_3) and C_4 subtype (NAD-ME > NADP-ME) differences were also evident in $iWUE_i$ (**Figure 5. 1D, Table 5. 1 and Table 5. 2**).

Species-wise, *O. sativa* had the lowest A_{net}, g_s, and WUE_i amongst the glasshouse-grown C_3 grasses (**Table 5. 2**). Among C_4 subtypes, two NAD-ME species, *L. fusca* and *P. coloratum* had the highest A_{net} while two NADP-ME species, *P. antidotale* and *S. viridis* had the lowest A_{net} (**Table 5. 2**). Two species with morphologically narrow leaf width, *E. curvula* (NAD-ME) and *C. ciliaris* (NADP-ME) had the lowest g_s, C_i, C_i/C_a, and highest iWUE (**Table 5. 2**).

iWUE was inversely correlated with C_i and C_i/C_a in C_3 and C_4 species. Within C_4 species, iWUE was inversely correlated g_s. In addition, g_s, C_i and C_i/C_a were positively correlated among the C_4 grasses (**Table 5. 4 and Table 5. 5**).

5.3.2 Carbon isotope composition

As expected, C_3 leaves were more ^{13}C-depleted (i.e., more negative $\delta^{13}C$), followed by NAD-ME than NADP-ME, although the difference between the two C_4 subtypes was marginally significant possibly due to small number of species (**Figure 5. 2, Table 5. 3**). C_3 species also had lighter cellulose and sugar signatures relative to C_4 leaves (**Figure 5. 2, Table 5. 3**). The carbon isotope signatures of leaf cellulose, glucose and sucrose did not differ between the two C_4 subtypes; however, fructose $\delta^{13}C$ was 1.69‰ heavier in NADP-ME than NAD-ME grasses (**Figure 5. 2, Table 5. 3**).

For each species, sucrose was the most ^{13}C-enriched metabolite amongst the three measured sugars (**Table 5. 5**). On average, $\delta^{13}C$ of sucrose increased by 2.28 ‰ (92.5 %) and 3.76-4.11 ‰ (71.4-72.7 %) relative to the leaf in C_3 and C_4 species, respectively (**Figure 5. 6**). In the C_3 species, cellulose, sucrose and glucose were more enriched in ^{13}C while fructose was less

enriched relative to the leaf (**Figure 5. 2 and Figure 5. 6, Table 5. 3**). In the C_4 species, cellulose, sucrose, glucose and fructose were more ^{13}C-enriched relative to the leaf. The largest discrimination step occurred at the level of sucrose (from glucose and fructose) and cellulose synthesis, with very little difference between leaf and cellulose $\delta^{13}C$ (**Figure 5. 2 and Figure 5. 6, Table 5. 3**). Interestingly, the carbon isotope signatures of glucose and fructose were opposite between the two C_4 subtypes; with fructose being lighter than glucose in NAD-ME species and *vice versa* for NADP-ME species (**Figure 5. 6**).

5.3.3 Correlations with leaf and metabolite $\delta^{13}C$ among C_3 and C_4 grasses

Due to large differences in carbon isotopic signatures between photosynthetic types, C_3 and C_4 species were grouped separately for correlation analysis (**Table 5. 4 and Table 5. 5**). Among C_3 grasses, there were no correlations between leaf gas exchange parameters and any of the leaf or metabolite carbon isotope compositions (**Table 5. 4**). Leaf $\delta^{13}C$ linearly correlated with $\delta^{13}C$ of glucose (r^2=0.927, p<0.05), sucrose (r^2=0.992, p<0.01; **Table 5. 4**) and cellulose (r^2=0.916, p<0.05; **Table 5. 4**). Likewise, $\delta^{13}C$ of cellulose and glucose were correlated (r^2=0.964, p<0.05; **Table 5. 4**) in C_3 species (**Figure 5. 4, Table 5. 4**).

Among NAD-ME and NADP-ME C_4 grasses, leaf and cellulose $\delta^{13}C$ were positively correlated (r^2=0.619, p<0.05). In addition, stomatal conductance (g_s) was negatively correlated with leaf $\delta^{13}C$ (r^2=0.466, p<0.05) and cellulose $\delta^{13}C$ (r^2=0.596, p<0.05) in C_4 species (**Figure 5. 5, Table 5. 5**). The key parameter iWUE was not correlated with leaf or metabolite $\delta^{13}C$ in either C_3 or C_4 species (**Table 5. 4 and Table 5. 5**).

5.4 DISCUSSION

In this study, four C_3, five C_4/NAD-ME and four C_4/NADP-ME grass species were grown under common conditions to compare the carbon isotope signatures of major soluble and structural carbohydrates in leaves (**Figure 5. 7A**) using a coupled HPLC-WCO-IRMS system to better understand the metabolic aspects of post-photosynthetic fractionation. Leaf gas exchange was also measured to reveal how iWUE and its components correlate with leaf and metabolite $\delta^{13}C$. The study revealed novel insights about both aspects, and the key points are discussed below.

5.4.1 Compound specific carbon isotope analysis reveals differences in C_3 and C_4 carbohydrate metabolism

As expected, leaf dry matter and carbohydrates were more ^{13}C depleted in C_3 relative to C_4 grasses (Bender, 1971; Brugnoli *et al.*, 1988; Cerling *et al.*, 1997). Enrichment of whole leaf and cellulose $\delta^{13}C$ may be due to the enrichment of non-structural carbohydrates (**Figure 5. 4**), the immediate product of photosynthesis (Tcherkez *et al.*, 2011; Cernusak *et al.*, 2013). The results of this study are in line with what is typically observed for C_3 plants where the carbon isotope signatures of sugars largely reflect the average fractionation of the initial carboxylation reaction by Rubisco (around 29‰) (Farquhar *et al.*, 1982, 1989; Evans *et al.*, 1986; Cernusak *et al.*, 2013).

Very few studies have analysed the carbon isotopic signatures of leaf metabolites in C_3 or C_4 plants (Brugnoli *et al.*, 1988; Ghashghaie *et al.*, 2001). This study revealed a number of interesting differences in the $\delta^{13}C$ of soluble carbohydrates behaviour between the two photosynthetic types (**Figure 5. 2 and Figure 5. 6**). In the C_3 species, fructose was more ^{13}C depleted (i.e., greater ^{13}C discrimination) while the other three compounds (cellulose, sucrose and glucose) were less ^{13}C depleted relative to the leaf (**Figure 5. 2, Figure 5. 3, and Figure 5.** 6). Analysis of intramolecular patterns in C_3 hexoses showed that invertase (EC 3.2.1.26), the enzyme that hydrolyses sucrose into glucose and fructose moieties (**Figure 5. 7A**), fractionates against ^{13}C producing a depleted C-2 position (carbon atom position) in fructose (Gilbert *et al.*, 2012).

In the C_4 species, all metabolites were less ^{13}C depleted relative to the leaf. Moreover, sucrose was the most ^{13}C depleted metabolite relative to the leaf, and this difference was greater in C_4 relative to C_3 leaves (**Figure 5. 2, Figure 5. 3, and Figure 5.** 6). These results point to the differences in carbohydrate, particularly sucrose, metabolism between C_3 and C_4 plants. In C_3 leaves, sucrose metabolism occurs in one cell type, while sucrose metabolism occurs predominantly, but not exclusively, in the mesophyll cells of C_4 leaves (Lunn & Furbank, 1999b). In addition, the precursors for sugar metabolism arising from the Calvin cycle (e.g., phosphoglycerate and glyceraldehyde 3-phosphate) are shuttled back and forth between the two cell types of C_4 leaves (Hatch, 1987). Moreover, sucrose must be transported to the bundle sheath on its way to the phloem for export out of the source leaf (**Figure 5. 7B**). Therefore, it is likely that sucrose, glucose, and fructose are more frequently interconverted by SPS/SPP, SS, and INV in C_4 relative to C_3 leaves (**Figure 5. 7B**), which would markedly change the ^{13}C signatures between the two photosynthetic types. Hence, the strong correlations observed among the $\delta^{13}C$ of the leaf, cellulose, sucrose, glucose, and fructose in C_3 (but not in C_4 species) reflect the linearity of metabolism in the former species (**Figure 5. 2 and Figure 5.** 4).

5.4.2 Differences in $\delta^{13}C$ of leaf dry matter and carbohydrates between NAD-ME and NADP-ME C_4 grasses

The difference in leaf carbon isotope composition between NAD-ME and NADP-ME species was not significant in this study (**Figure 5. 2 and Table 5. 2**) contrary to what was reported previously (Hattersley, 1982; Ghannoum *et al.*, 2001a; Cousins *et al.*, 2008; von Caemmerer *et al.*, 2014). This could be due to the small number of species (4 NADP-ME and 5 NAD-ME species) used herein comparison with previous studies. For example, Ghannoum *et al.*, (2001) compared 15 NADP-ME and 9 NAD-ME species, while Hattersley, (1982) utilised 11 NADP-ME and 9 NAD-ME species. Cousins *et al.* (2008) used a similar number of species (5 NAD-ME and 7 NADP-ME). In this study, *Z. mays* belonging to the Andropogonea tribe in the grass family (Grass Phylogeny Working Group II, 2012), had the most ^{13}C depleted leaf dry matter among all the C_4 species (**Table 5. 3**) which is unusual for an NADP-ME species, whichThis in turn, caused the statistically insignificant difference between the two C_4 subtypes (**Table 5. 1**). The atypical differences could be due to the $\delta^{13}C$ varietal differences that exist within the *Z. mays* species (Monneveux *et al.*, 2007; Kolbe *et al.*, 2018; Twohey *et al.*, 2019) and as also

observed for *S. bicolor* (Henderson *et al.,* 1998) which could be a consequence of selection and domestication.

There were a number of significant differences in the carbon isotope signatures of carbohydrates between the two C_4 subtypes. Relative to the leaf, the discrimination profile of fructose and glucose seems to be reversed between the two C_4 subtypes, culminating into a similar deviation of sucrose $\delta^{13}C$ relative to the leaf (**Figure 5. 6B-C**). These differences may partly reflect differences in sugar metabolism between the C_4 subtypes. For example, the compartmentation of sucrose and starch synthesis differs between NAD-ME and NADP-ME species (Lunn & Furbank, 1999b). As argued above, this will affect the pathway of sucrose metabolism and transport along the mesophyll-bundle sheath-phloem continuum, and hence impact the ^{13}C signatures of the three soluble sugars in the various C_4 species.

Moreover, fructose $\delta^{13}C$ was 1.6 ‰ ^{13}C more enriched in NADP-ME relative to NAD-ME species (**Figure 5. 2 and Figure 5.** 3**, Table 5. 3**). To my knowledge, there has not been an attempt to assay the $\delta^{13}C$ of immediate post-photosynthetic metabolites (major soluble sugars) for the purpose of elucidating the variations in $\delta^{13}C$ in C_4 grasses. In leaves of *Quercus* species (oaks, C_3 trees), it was shown that fructose was ^{13}C-enriched relative to sucrose and glucose (Werner *et al.,* 2009b). Here, it is also shown that fructose might be one of the candidate metabolites that could contribute to the differences in whole leaf and cellulose $\delta^{13}C$ between the two subtypes, although metabolites other than sugars should also be considered. This raises the prospect of probing of the fractionation and enzyme activities of invertases in leaves of these two subtypes. Earlier work by Mauve *et al.,* (2010) showed that fructose has a minimal fractionation of 1 ‰ when assayed *in vitro*. Another prospect is to investigate intramolecular $\delta^{13}C$ patterns within the fructose molecule in these two C_4 subtypes to better understand fluxomics and sugar allocations in leaves of C_4 species (Kruger & Ratcliffe, 2009; Tcherkez *et al.*, 2011).

5.4.3 Leaf and cellulose $\delta^{13}C$ correlate with stomatal conductance in C_4 grasses

One of the objectives of this study was to better understand variations in leaf $\delta^{13}C$ because it is being considered as a selection tool for WUE_i among C_4 plants (von Caemmerer *et al.,* 2014; Ellsworth & Cousins, 2016). There have been various attempts to relate leaf $\delta^{13}C$ and WUE among C_4 species with contradictory results. Across diverse C_4 grasses, leaf $\delta^{13}C$ did not

correlate with the leaf or plant WUE (Ghannoum *et al.*, 2001a, 2002). Across sorghum genotypes, leaf $\delta^{13}C$ showed a good relationship with plant WUE (Henderson *et al.*, 1998). The same was also found within a population of recombinant inbred lines of the C_4 grass *Setaria viridis* under highly controlled environments (Feldman *et al.*, 2018; Ellsworth *et al.*, 2019). Hence, it seems leaf $\delta^{13}C$ can predict iWUE within the same species and under well-controlled conditions. However, the theoretical framework primarily links $\Delta^{13}C$ with C_i/C_a, i.e., leaf $iWUE_i$ rather than plant WUE (Farquhar, 1983). Therefore, it was suspected for sometimes that the poor relationship between $\Delta^{13}C$ and $iWUE_i$ is due to leakiness (equation 5.1).

It was hypothesised that the presence of suberized lamella in NADP-ME species could reduce of bundle sheath leakiness (Hattersley, 1982; Henderson *et al.*, 1992b; von Caemmerer *et al.*, 2014). However, measurements bundle sheath CO_2 leakiness by Henderson *et al.*, (1992a), Cousins *et al.*, (2008), and Sonawane *et al.*, (2017, 2018) showed that there were no differences in leakiness nor C_i/C_a between the C_4 subtypes under high light and well-watered conditions. Consequently, measurements of leakiness in a number of studies showed (1) limited and unpredictable variations in ϕ, and (2) could not reconcile leaf $\delta^{13}C$ with iWUE (Sonawane *et al.*, 2017, 2018). It must be noted that leaf and gas exchange operate on different time scales. While leaf gas exchange measurements describe instantaneous events, leaf $\delta^{13}C$ is a long-term parameter that integrates isotopic fractionation over the leaf lifespan. Taken together, these factors postulate for the role of post-photosynthetic fractionation in determining leaf $\delta^{13}C$ (Cousins *et al.*, 2008; von Caemmerer *et al.*, 2014; Ellsworth & Cousins, 2016).

Therefore, leaf gas exchange was measured together with leaf and carbohydrate $\delta^{13}C$. Among C_3 grasses, leaf gas exchange parameters showed no relationships with any of the $\delta^{13}C$ parameters measured. In contrast, leaf and cellulose $\delta^{13}C$ negatively correlated with stomatal conductance, but not with iWUE, among the C_4 grasses. It has been repeatedly demonstrated that g_s is the primary driver of iWUE in C_4 grasses (Li *et al.*, 2017; Cano *et al.*, 2019), unlike in C_3 plants where both photosynthesis and stomatal conductance profoundly influence iWUE, and consequently carbon isotope discrimination (Farquhar *et al.*, 1989; Sun *et al.*, 1996). Moreover, CCM in C_4 photosynthesis operates with a saturating C_i. Hence changes in g_s, do not affect C_i appreciably, and hence assimilation rates remain constant over a large range of g_s. The greater dependence of iWUE on g_s in C_4 plants is well understood and is due to the operation of the CCM in C_4 leaves which leads to the saturation of C_4 photosynthesis at low C_i (von Caemmerer & Furbank, 1999; von Caemmerer *et al.*, 2014). Hence, in ambient air, and under conditions where g_s is not too low, and C_i is not limiting, C_4 photosynthesis is often

saturated and does not change much (Cano *et al.*, 2019). Hence, most of the variations in iWUE under these conditions are brought about by low g_s (Ghannoum, 2016). This is well documented about C_4 photosynthesis and warrants caution in interpreting the relationship between leaf $\delta^{13}C$ and iWUE in C_4 plants. It is likely that most gas exchange-related variations in leaf $\delta^{13}C$ are related to variations in g_s in C_4 plants. This conclusion is well-supported by a recent study where it has been shown that a genomic segment on maize chromosome 7 influenced both carbon isotope composition and water use efficiency, possibly by affecting stomatal properties (Avramova *et al.*, 2019). A genomic link between leaf carbon isotope composition and plant water use efficiency has also been established for a recombinant inbred population of *Setaria viridis* under well-watered and water-stressed conditions (Feldman *et al.*, 2018). In conclusion, my results show the dominance of g_s in influencing iWUE and $\delta^{13}C$ in C_4 grasses (**Table 5. 5, Figure 5. 5**) and demonstrated that leaf width might be a better predictor of iWUE among C_4 grasses (Cano *et al.*, 2019).

5.5 CONCLUSION

The HPLC-WCO-IRMS system optimised in Chapter 4 was utilised to examine the carbon-isotope signatures of three major soluble sugars (sucrose, glucose, and fructose) among C_3, C_4/NADP-ME and C_4/NAD-ME grasses grown under common conditions in order to understand post-photosynthetic fractionation. Bulk leaf dry matter and cellulose $\delta^{13}C$ were also assayed using EA-IRMS. Among C_3 grasses, there were no differences in the carbon isotope discrimination of all fractions but $\delta^{13}C$ of sugar metabolites linearly correlated with leaf $\delta^{13}C$. Using the wet chemical oxidation system, I show for the first time here that fructose $\delta^{13}C$ varied between NADP-ME and NAD-ME subtypes by 1.6 ‰, but no variation was detected in $\delta^{13}C$ of glucose and sucrose. Further assays on fructose and the invertase enzyme are recommended to elucidate the sugar turnover in the leaves of C_4 grasses in order to develop a proxy method for screening iWUE.

Table 5. 1 Statistical summary using one-factor ANOVA on the gas exchange and carbon isotope traits of glasshouse-grown C_3 (n=4), C_4 NADP-ME (n=4), and C_4 NAD-ME (n=5) grasses.

Species was considered as replicate, and each species consist of n=4-6 biological replicates.

Parameter	**Species**	**Type** *C_3 vs C_4*	**Subtype** *NADP-ME vs NAD-ME*
Gas exchange			
A_{net} (µmol m^{-2} s^{-1})	**<0.0001**	**<0.0001**	0.0940
g_s (mol m^{-2} s^{-1})	**<0.0001**	**0.0114**	0.5062
C_i	**<0.0001**	**<0.0001**	0.3087
C_i/C_a	**<0.0001**	**<0.0001**	0.2990
iWUE (µmol [CO_2] mol H_2O $^{-1}$)	**<0.0001**	**0.0001**	0.3083
Isotope traits			
whole leaf $\delta^{13}C$	**<0.0001**	**<0.0001**	0.3201
cellulose $\delta^{13}C$	**<0.0001**	**<0.0001**	0.7107
sucrose $\delta^{13}C$	**<0.0001**	**<0.0001**	0.7320
glucose $\delta^{13}C$	**<0.0001**	**<0.0001**	0.6213
fructose $\delta^{13}C$	**<0.0001**	**<0.0001**	0.0772

Table 5. 2 Summary of gas exchange traits of four C_3, five NAD-ME, and four NADP-ME grasses grown at glasshouse conditions for isotopic assay of leaf metabolites.

Values are mean ± SE of 4-6 biological replicates. Letters in bold black represent the ranking of between species at a particular gas exchange trait while red letters represent the ranking of means between types/subtypes where species were considered as replicate. Means were ranked using Fisher's LSD *post hoc* at α=0.05.

Type	Species	A_{net}		g_s		C_i		C_i/C_a		iWUE	
C_3	*O. sativa*	17.01 ± 0.16	**h**	0.218 ± 0.006	**efg**	244.50 ± 2.23	**b**	0.636 ± 0.006	**b**	78.06 ± 1.42	**f**
	P. bisulcatum	23.12 ± 0.40	**f**	0.373 ± 0.025	**a**	259.79 ± 4.40	**ab**	0.691 ± 0.013	**a**	62.65 ± 3.1	**g**
	S. laxa	24.36 ± 0.25	**f**	0.345 ± 0.010	**a**	247.84 ± 1.84	**b**	0.657 ± 0.005	**ab**	70.77 ± 1.29	**fg**
	T. turgidum	20.60 ± 0.26	**g**	0.343 ± 0.016	**a**	266.58 ± 2.94	**a**	0.704 ± 0.008	**a**	60.38 ± 2.03	**g**
NAD-ME	*C. dactylon*	33.25 ± 0.38	**b**	0.224 ± 0.003	**def**	100.34 ± 1.35	**f**	0.281 ± 0.004	**g**	148.66 ± 0.83	**b**
	E. curvula	32.89 ± 0.28	**bc**	0.187 ± 0.004	**g**	61.45 ± 2.57	**g**	0.170 ± 0.007	**h**	176.28 ± 1.8	**a**
	L. fusca	35.89 ± 0.62	**a**	0.250 ± 0.005	**bcde**	108.03 ± 0.87	**ef**	0.302 ± 0.003	**fg**	143.62 ± 0.73	**bc**
	P. coloratum	34.80 ± 0.04	**a**	0.255 ± 0.001	**bcd**	111.98 ± 0.51	**ef**	0.320 ± 0.002	**efg**	136.59 ± 0.39	**c**
	P. miliaceum	31.69 ± 0.33	**c**	0.238 ± 0.003	**cde**	117.66 ± 3.64	**ef**	0.336 ± 0.011	**ef**	133.16 ± 2.33	**c**
NADP-ME	*C. ciliaris*	33.16 ± 0.88	**b**	0.191 ± 0.005	**fg**	64.60 ± 3.20	**g**	0.179 ± 0.009	**h**	174.27 ± 2.41	**a**
	P. antidotale	29.67 ± 1.74	**d**	0.251 ± 0.011	**bcde**	140.44 ± 3.99	**d**	0.401 ± 0.010	**d**	118.70 ± 2.16	**d**
	S. viridis	28.08 ± 1.60	**e**	0.264 ± 0.004	**bc**	168.25 ± 8.83	**c**	0.471 ± 0.020	**c**	106.42 ± 2.85	**e**
	Z .mays	33.10 ± 0.90	**b**	0.279 ± 0.021	**b**	124.34 ± 14.16	**de**	0.365 ± 0.041	**de**	121.87 ± 8.79	**d**
C_3		21.27 ± 1.62	**c**	0.320 ± 0.035	**a**	254.68 ± 5.15	**a**	0.672 ± 0.016	**a**	67.97 ± 4.04	**c**
NAD-ME		33.70 ± 0.74	**a**	0.231 ± 0.012	**b**	99.89 ± 10.02	**c**	0.282 ± 0.029	**c**	147.66 ± 7.65	**a**
NADP-ME		31.00 ± 1.27	**b**	0.246 ± 0.019	**b**	124.41 ± 21.9	**b**	0.354 ± 0.062	**b**	130.31 ± 15.0	**b**

Table 5. 3 Summary of gas exchange traits of four C_3, five NAD-ME, and four NADP-ME grasses grown at glasshouse conditions for isotopic assay of leaf metabolites.

Values are mean ± SE of 4-6 biological replicates. Letters in bold black represent the ranking of means between species at particular $\delta^{13}C$ trait while red letters represent the ranking of means between types where species were considered as replicate. Letters in italic superscripts represent comparisons between $\delta^{13}C$ of individual metabolic pools within species while red italic superscripts were comparisons within type/subtype. Means were ranked using Fisher's LSD *post hoc* at α=0.05.

Type	Species	Leaf $\delta^{13}C$				Fructose $\delta^{13}C$				Glucose $\delta^{13}C$				Sucrose $\delta^{13}C$				Cellulose $\delta^{13}C$			
C_3	*O. sativa*	-31.09	± 0.21	**f**	***bc***	-32.15	± 0.42	**d**	***c***	-31.03	± 0.54	**h**	***bc***	-28.61	± 0.19	**f**	***a***	-30.40	± 0.10	**f**	***b***
	P. bisulcatum	-27.30	± 0.11	**e**	***b***	-30.73	± 1.07	**d**	***c***	-26.33	± 0.24	**f**	***b***	-24.1	± 0.2	**e**	***a***	-26.78	± 0.21	**d**	***b***
	S. laxa	-31.22	± 0.21	**f**	***b***	-31.15	± 1.49	**d**	***b***	-29.57	± 0.71	**g**	***a***	-29.28	± 0.25	**f**	***a***	-29.29	± 0.33	**e**	***a***
	T. turgidum	-32.52	± 0.18	**g**	***b***	-31.77	± 0.93	**d**	***ab***	-31.65	± 0.36	**h**	***ab***	-31.01	± 0.21	**g**	***a***	-31.85	± 0.18	**g**	***ab***
NAD-ME	*C. dactylon*	-14.69	± 0.13	**cd**	***c***	-13.13	± 0.33	**ab**	***b***	-10.95	± 0.09	**a**	***a***	-10.68	± 0.27	**cd**	***a***	-14.40	± 0.38	**c**	***c***
	E. curvula	-13.13	± 0.06	**b**	***c***	-14.51	± 0.62	**bcd**	***d***	-10.52	± 0.44	**a**	***b***	-8.92	± 0.83	**a**	***a***	-13.07	± 0.10	**b**	***c***
	L. fusca	-14.61	± 0.07	**cd**	***c***	-15.91	± 0.93	**c**	***d***	-13.19	± 0.34	**b**	***b***	-11.44	± 0.19	**d**	***a***	-14.42	± 0.17	**c**	***c***
	P. coloratum	-14.50	± 0.29	**cd**	***bc***	-13.52	± 0.16	**b**	***b***	-15.44	± 0.12	**e**	***c***	-9.36	± 0.12	**ab**	***a***	-14.76	± 0.20	**c**	***c***
	P. miliaceum	-14.71	± 0.12	**cd**	***c***	-13.02	± 0.25	**ab**	***b***	-13.6	± 0.19	**bc**	***b***	-10.5	± 0.25	**bcd**	***a***	-13.29	± 0.11	**b**	***b***
NADP-ME	*C. ciliaris*	-12.48	± 0.06	**a**	***b***	-12.84	± 0.18	**ab**	***b***	-14.31	± 0.17	**cd**	***c***	-9.80	± 0.74	**abc**	***a***	-12.37	± 0.03	**a**	***b***
	P. antidotale	-13.03	± 0.14	**b**	***b***	-13.83	± 0.43	**b**	***b***	-15.28	± 0.52	**de**	***c***	-9.81	± 0.8	**abc**	***a***	-13.50	± 0.14	**b**	***b***
	S. viridis	-14.31	± 0.20	**c**	***cd***	-11.31	± 0.38	**a**	***b***	-13.28	± 0.51	**bc**	***c***	-9.97	± 0.4	**abc**	***a***	-14.73	± 0.35	**c**	***d***
	Z .mays	-14.92	± 0.18	**d**	***b***	-11.3	± 0.25	**a**	***a***	-10.83	± 0.04	**a**	***a***	-10.38	± 0.29	**bcd**	***a***	-14.42	± 0.21	**c**	***b***
C_3		-30.53	± 0.51	**b**	***a***	-31.45	± 0.49	**c**	***a***	-29.65	± 0.58	**b**	***a***	-28.25	± 0.67	**b**	***a***	-29.58	± 0.49	**b**	***a***
NAD-ME		-14.39	± 0.13	**a**	***b***	-13.98	± 0.32	**b**	***b***	-12.76	± 0.37	**a**	***b***	-10.28	± 0.24	**a**	***a***	-13.96	± 0.16	**a**	***b***
NADP-ME		-13.78	± 0.24	**a**	***b***	-12.29	± 0.30	**a**	***b***	-13.25	± 0.45	**a**	***b***	-10.02	± 0.27	**a**	***a***	-13.81	± 0.23	**a**	***b***

Table 5. 4 Correlation between measured gas exchange and carbon isotope traits in four C_3 grasses.

Linear regression direction is indicated in the parenthesis. Values represent r^2 between two parameters. Significance codes are as follows: *significant at $p<0.05$; **significant at $p<0.01$; ^{ns}not significant ($p>0.05$).

	g_s	C_i	C_i/C_a	iWUE	Whole leaf $\delta^{13}C$	Fructose $\delta^{13}C$	Glucose $\delta^{13}C$	Sucrose $\delta^{13}C$	Cellulose $\delta^{13}C$
A_{net}	ns	ns	ns	ns	ns	ns	ns	ns	ns
g_s		ns	ns	ns	ns	ns	ns	ns	ns
C_i			0.972*	(-) 0.921*	ns	ns	ns	ns	ns
C_i/C_a				(-) 0.986**	ns	ns	ns	ns	ns
iWUE					ns	ns	ns	ns	ns
Whole leaf $\delta^{13}C$						ns	0.927*	0.992**	0.916*
Fructose $\delta^{13}C$							ns	ns	ns
Glucose $\delta^{13}C$								ns	0.964*
Sucrose $\delta^{13}C$									ns

Table 5. 5 Correlation between measured gas exchange and carbon isotope traits in nine C_4 grasses (four NADP-ME and five NAD-ME species).

Linear regression direction is indicated in the parenthesis. Values represent r^2 between two parameters. Significance codes are as follows: *significant at $p<0.05$; **significant at $p<0.01$; ^{ns}not significant ($p>0.05$).

	g_s	C_i	C_i/C_a	iWUE	Whole leaf $\delta^{13}C$	Fructose $\delta^{13}C$	Glucose $\delta^{13}C$	Sucrose $\delta^{13}C$	Cellulose $\delta^{13}C$
A_{net}	ns	ns	ns	ns	ns	ns	ns	ns	ns
g_s		0.726*	0.762**	(-) 0.832**	(-) 0.466*	ns	ns	ns	(-) 0.596*
C_i			0.996**	(-) 0.968*	ns	ns	ns	ns	ns
C_i/C_a				(-) 0.986**	ns	ns	ns	ns	ns
iWUE					ns	ns	ns	ns	ns
Whole leaf $\delta^{13}C$						ns	ns	ns	0.619*
Fructose $\delta^{13}C$							ns	ns	ns
Glucose $\delta^{13}C$								ns	ns
Sucrose $\delta^{13}C$									ns

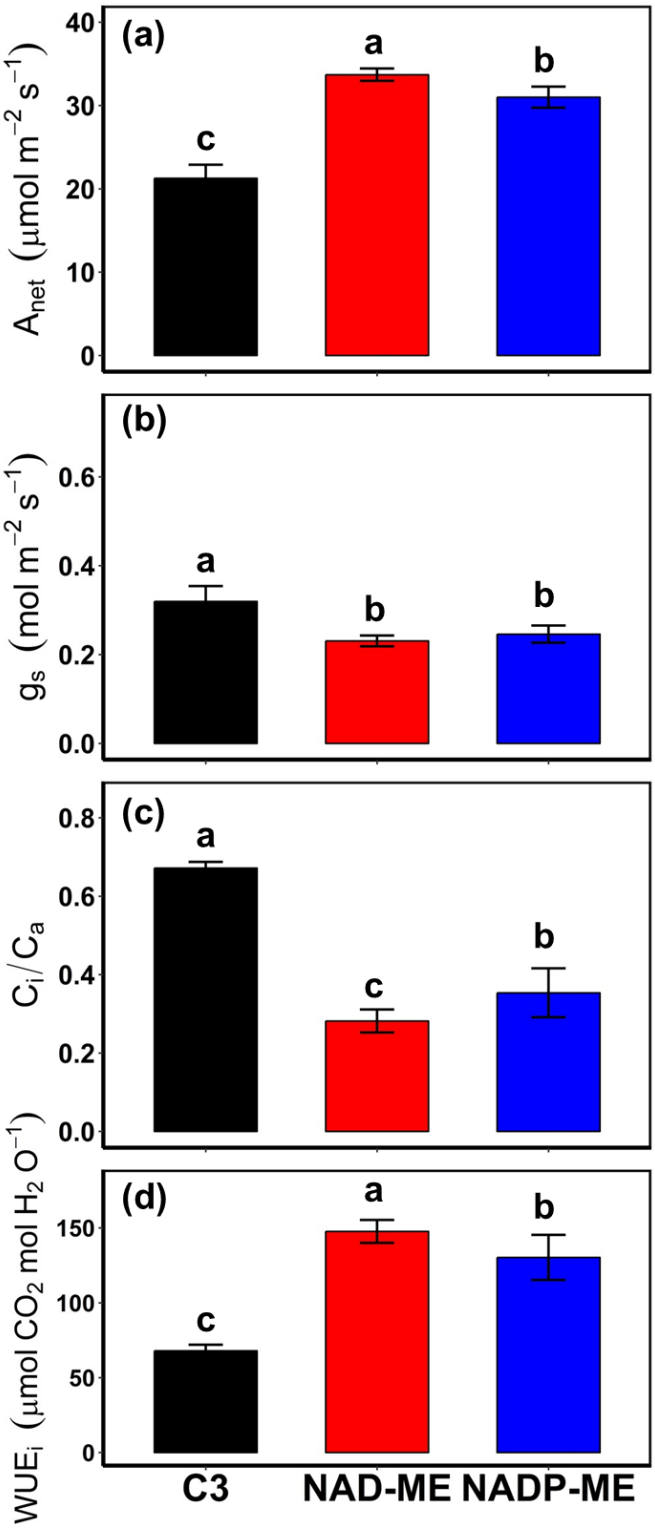

Figure 5. 1 Gas exchange traits of glasshouse-grown C_3 (n=4 species), NAD-ME (n=5 species), and NADP-ME (n=4 species) grasses.

Net CO_2 assimilation rate (**A**, A_{net}); stomatal conductance (**B**, g_s); Intercellular CO_2 (**C,** C_i); the ratio of intercellular CO_2 to the atmospheric CO_2 (**D**, C_i/C_a); and intrinsic water-use efficiency (**E, i**WUE). Data represent mean $\pm$ SE with species as replicate. Means with the same letters are not significantly different at α=0.05 using Fisher's LSD *post hoc*.

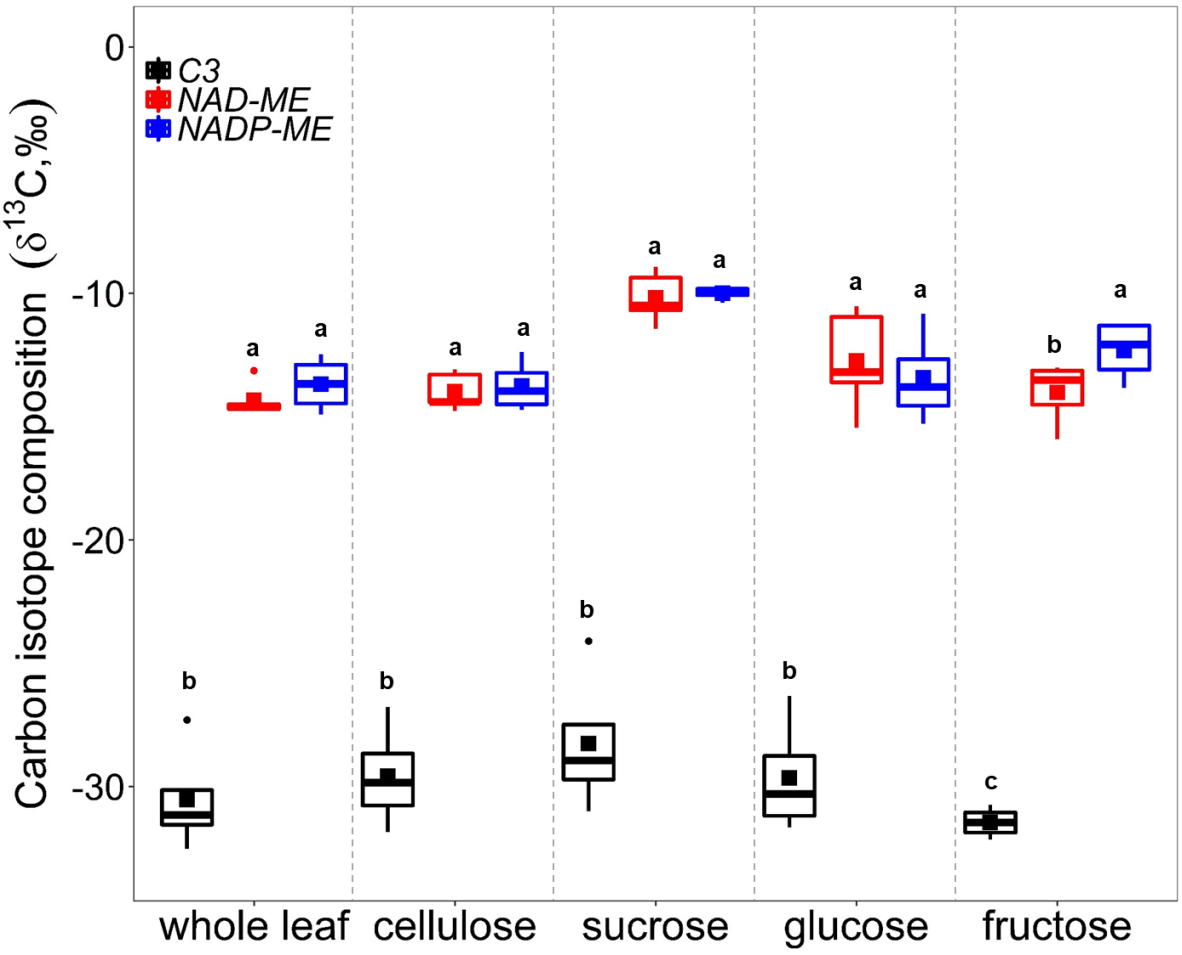

Figure 5. 2 Carbon isotope signatures of different metabolite pools among C_3, NAD-ME and NADP-ME.

Filled squares inside the boxplot represent means and means with the same letters between types among metabolite pools are not significantly different at α=0.05 using Fisher's LSD *post hoc.*

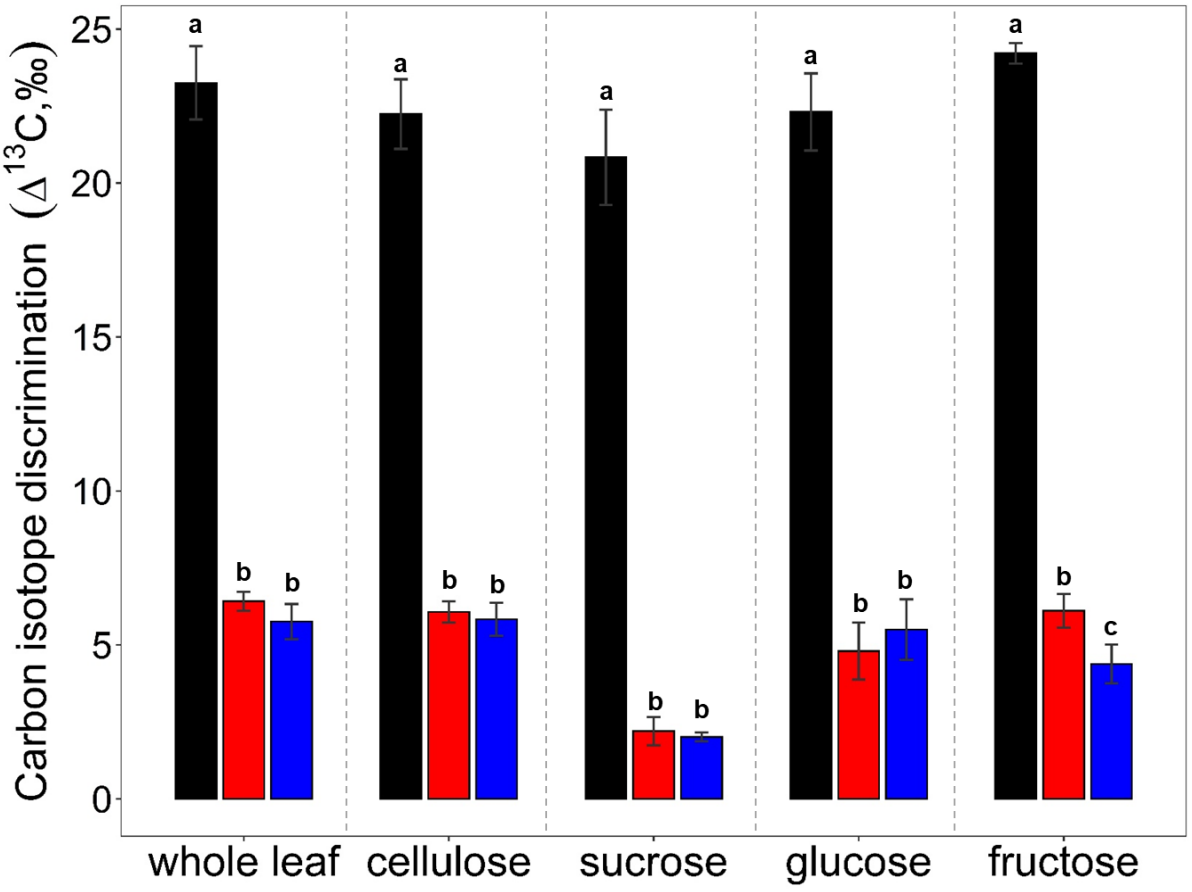

Figure 5. 3 Carbon isotope discrimination of C_3 (black), NAD-ME (red), and NADP-ME (blue) using the parameters in equation 5.3.

Filled coloured bars represent mean ± SE of C_3 (black), NAD-ME (red), and NADP-ME (blue) among bulk and sugar metabolites Means with the same letter are not significantly different at α=0.05 using Fisher's LSD *post hoc*.

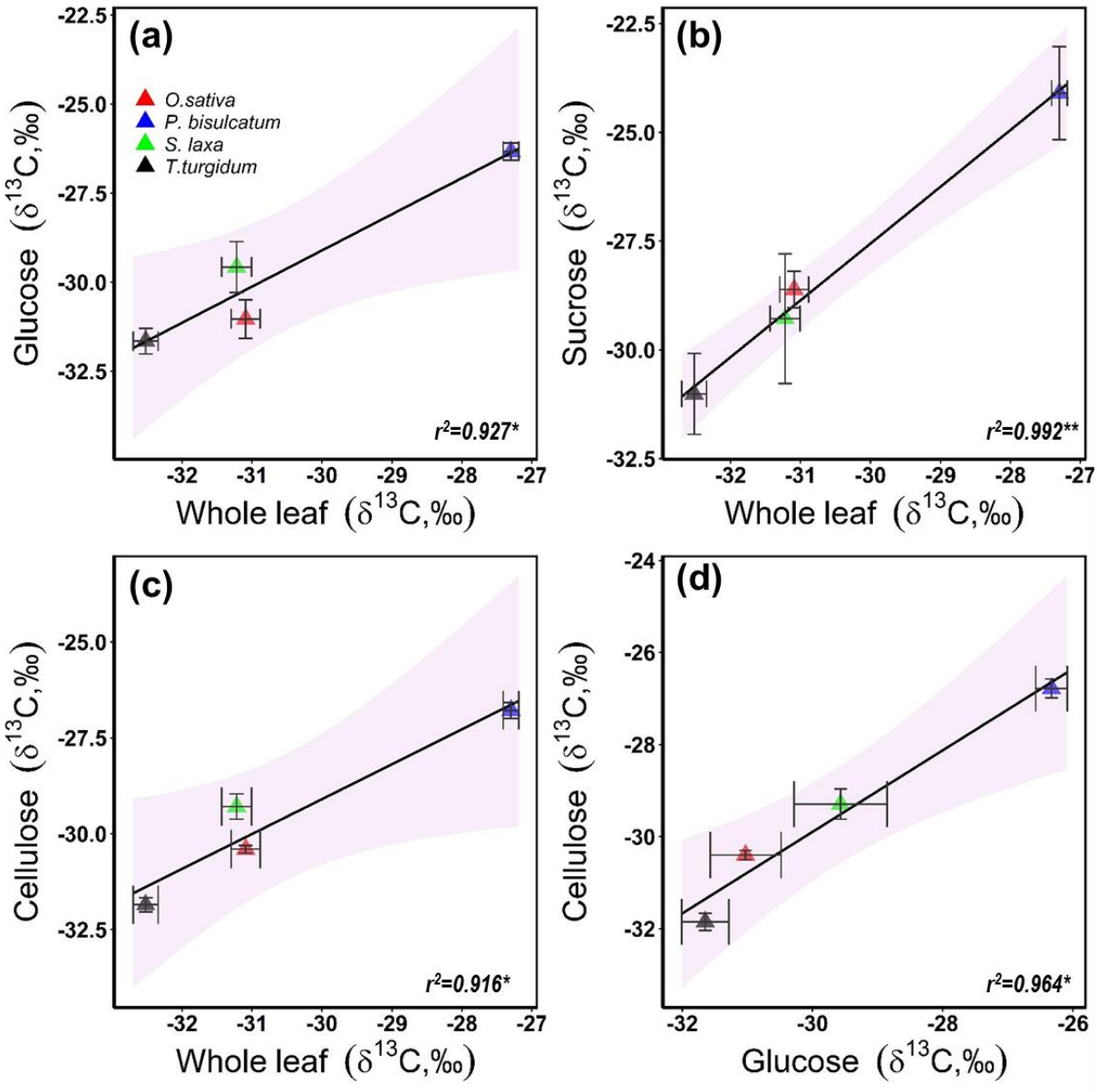

Figure 5. 4 Linear relationships between carbon isotope composition of metabolite pools in four C_3 grasses.

Dots represent the mean ± SE of four C_3 species as replicates Shaded regions represent the 95% confidence interval of the linear model. Regression equations were: (**A**) *glucose* $\delta^{13}C=1.0157 \times$ *whole leaf* $\delta^{13}C + 1.3673$; (**B**) *sucrose* $\delta^{13}C=1.3047 \times$ *whole leaf* $\delta^{13}C + 11.586$; (**C**) *cellulose* $\delta^{13}C=0.9103 \times$ *whole leaf* $\delta^{13}C - 1.787$; and (**D**) *cellulose* $\delta^{13}C=0.8853 \times$ *glucose* $\delta^{13}C - 3.3354$. Significance codes: $*p<0.05$; $**p<0.01$.

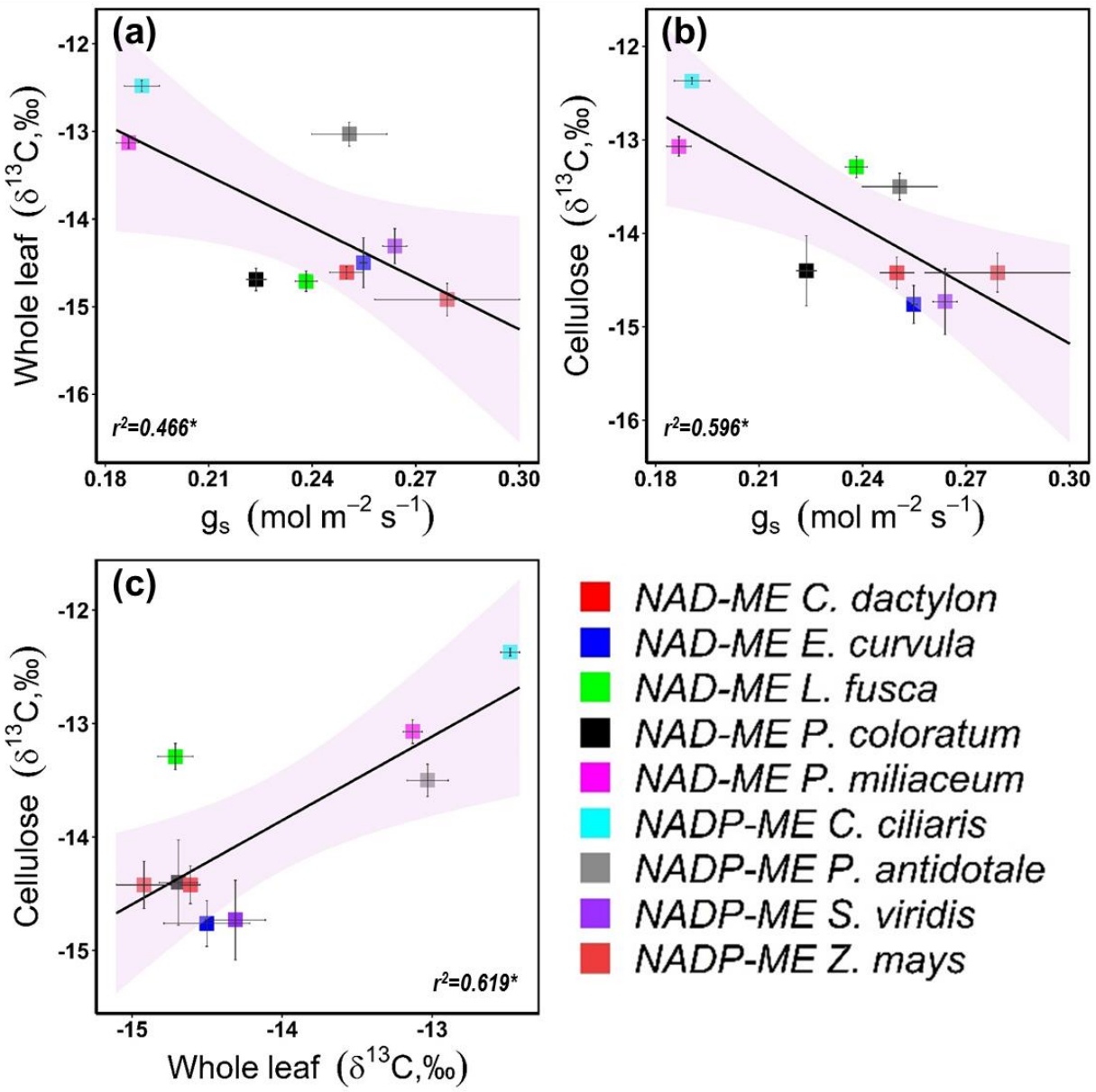

Figure 5. 5 Correlations between $\delta^{13}C$ of metabolite pools in nine C_4 grasses (five NAD-ME and four NADP-ME).

Squares represent the mean ± SE of nine C_4 species as replicates Shaded regions represent the 95% confidence interval of the linear model. Regression equations were: (**A**) *whole leaf* $\delta^{13}C = -19.474 \times g_s - 9.4173$; (**B**) *cellulose* $\delta^{13}C = -20.701 \times g_s - 8.9681$; and (**C**) *cellulose* $\delta^{13}C = 0.7339 \times$ *whole leaf* $- 3.4952$. Significance code: $*p<0.05$.

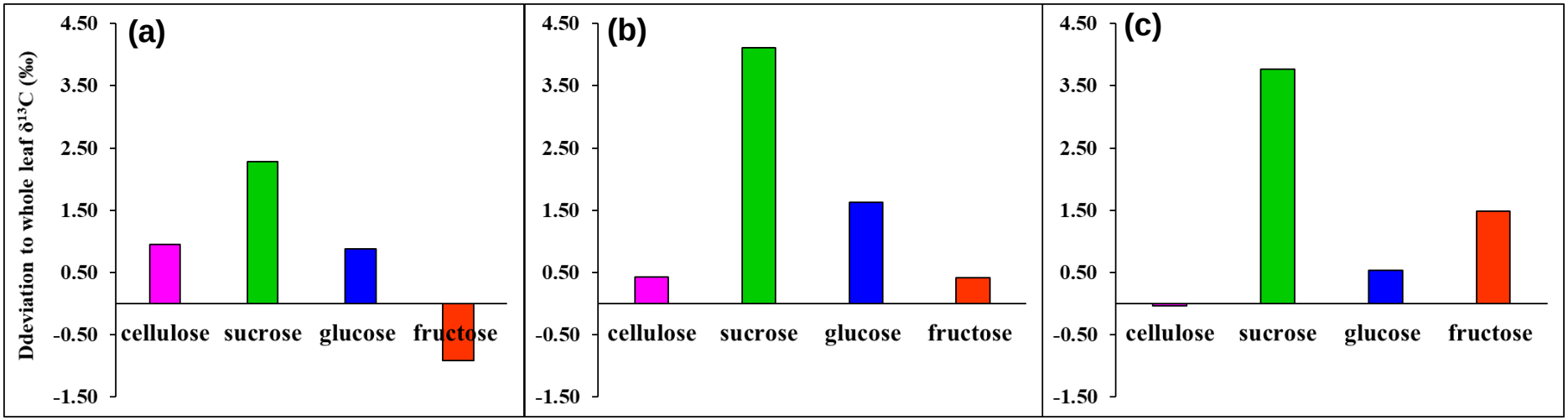

Figure 5. 6 Deviation of metabolite $\delta^{13}C$ expressed relative to the whole leaf $\delta^{13}C$

The figures illustrate deviation of cellulose (purple), sucrose (green), glucose (blue), and fructose (red) to the whole leaf among C_3 (**A**), NAD-ME (**B**), and NADP-ME (**C**).

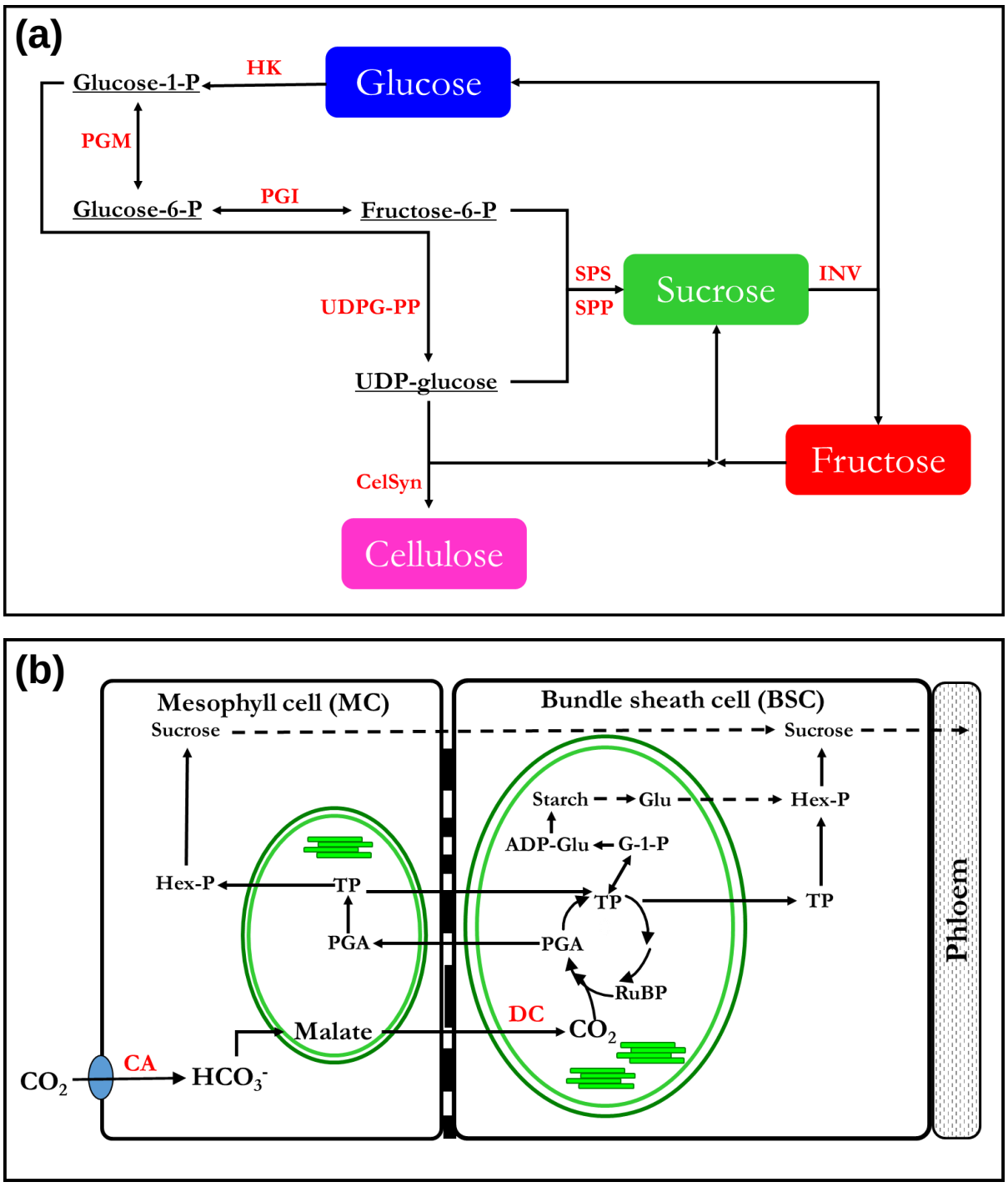

Figure 5. 7 Schematic flow of sugar metabolism in leaves (A) and the two-celled biosynthesis of sucrose among C_4 leaves (B).

Red acronyms indicate enzymes: hexokinase (HK), phosphoglucomutase (PGM), phosphoglucoisomerase (PGI), sucrose phosphate synthase (SPS), UDPG-pyrophosphorylase (UDPGG-PP), sucrose phosphate phosphatase (SPP), invertase (INV), cellulose synthase (CelSyn), carbonic anhydrase (CA), and specific decarboxylases (DC) while black acronyms represent metabolites in the sugar pathway: triosphosphate (TP), phosphoglyceraldehyde (PGA), ribulose-1,5-bisphosphate (RuBP), ADP-glucose (ADP-Glu), glucose-1-phosphate (G-1-P), hexose phosphate (Hex-P). The figure was adapted from Lunn & Furbank, (1999); Babb & Haigler, (2001); and Baroja-Fernández *et al.*, (2004).

CHAPTER 6

GENERAL DISCUSSION

6.1 OVERALL THESIS SUMMARY

6.1.1 The ecological and economical importance of C_4 grasses

Only around 3% of the Earth's more than 352,000 angiosperm species (Joppa *et al.*, 2011) fix atmospheric [CO_2] via the C_4 photosynthetic pathway, yet account for approximately 25% of terrestrial photosynthesis (Lloyd & Farquhar, 1994). C_4 grasses include some of the world's most important crops such as maize (*Zea mays*), sugarcane (*Saccharum officinarum*) and sorghum (*Sorghum bicolor*) (Sage *et al.*, 2012; Ghannoum, 2016). Other C_4 crops are utilised as fodder or biofuel sources such as Miscanthus (*Miscanthus* × *giganteus*), pearl millet (*Pennisetum glaucum*) and switchgrass (*Panicum virgatum*). Some of the world's noxious weeds are also C_4 species such as *Amaranthus* and *Setaria* spp (Fernando *et al.*, 2016; Doust *et al.*, 2017).

The high productivity of C_4 plants is a virtue of their CO_2 concentrating mechanism (CCM) (Sage, 2004). The CCM confers direct physiological advantages to C_4 photosynthesis (Björkman, 1971; Osmond *et al.*, 1982; Pearcy & Ehleringer, 1984; Long, 1999; Sage & Pearcy, 2000; Ghannoum *et al.*, 2011). In particular, C_4 plants have higher CO_2 assimilation rates, especially at high temperatures (Berry & Bjorkman, 1980; Sage & Kubien, 2007; Sonawane *et al.*, 2017). In addition, the saturation of C_4 photosynthesis at low [CO_2] allows C_4 leaves to operate with lower stomatal conductance (Taylor *et al.*, 2010b, 2012; Pinto *et al.*, 2014). This leads to higher leaf- and plant-level water use efficiency (WUE_i, WUE_{plant}) in C_4 relative to C_3 plants (Long, 1999; Sage & Pearcy, 2000; Ghannoum *et al.*, 2011). These physiological properties, as well as others, are reflected in the geographic distribution and climatic zones of the plant species with different C_4 pathways, which is positively correlated with growing season temperature. Accordingly, C_4 grasses dominate many warm and high-light environments such as tropical and sub-tropical rangelands and grasslands (Hattersley, 1983; Ehleringer *et al.*, 1997; Pau *et al.*, 2013). The high productivity achieved by C_4 plants under warm climate may have led to an ecological significance and agricultural importance (Lloyd & Farquhar, 1994; Harold Brown, 1999; Edwards *et al.*, 2010). In particular, C_4 crops are becoming increasingly important for food and bioenergy security, with the global production of C_4 maize currently surpassing that of key C_3 cereals such as wheat and rice (Varshney *et al.*, 2012; FAO, 2019).

C_4 photosynthesis has evolved in 62 lineages, such that C_4 plants are biochemically and phylogenetically diverse (Sage *et al.*, 2011). In grasses, three C_4 biochemical subtypes have been identified based on the primary C_4 acid decarboxylase enzyme operating in the bundle

sheath cells. These enzymes are nicotinamide adenine dinucleotide phosphate malic enzyme (NADP–ME), nicotinamide adenine dinucleotide malic enzyme (NAD–ME) and phosphoenolpyruvate carboxykinase (PEP-CK) (Kanai & Edwards, 1999; Bräutigam *et al.*, 2014). In many C_4 species, especially those using NADP-ME as a primary decarboxylase, PEP-CK operates as a secondary decarboxylase (Chapman & Hatch, 1981; Wingler *et al.*, 1999; Sharwood *et al.*, 2014). C_4 grasses with high PEP-CK activity frequently operate significant NADP-ME or NAD-ME activity (Burnell & Hatch, 1988; Pinto *et al.*, 2014; Lazowski *et al.*, 2018; Sonawane *et al.*, 2018). Nevertheless, the primary decarboxylase is generally associated with a suite of anatomical, biochemical and physiological features (Hattersley, 1992; Ghannoum *et al.*, 2011).

6.1.2 What controls iWUE in C_4 leaves?

A key desirable feature of climate-smart crops is improved water-use efficiency (WUE) to cope with increased temperature and water stress under climate change (Richards *et al.*, 1993; Ruggiero *et al.*, 2017). Crop WUE is governed by multiple factors, including leaf-level instantaneous WUE (Passioura, 1977). iWUE reflects the exchange of CO_2 and water vapour across the leaf surface and can be defined as CO_2 assimilation rate/stomatal conductance (A_{net}/g_s) (Farquhar & Sharkey, 1982). Photosynthesis and stomatal conductance are closely correlated under a wide range of environments (Wong *et al.*, 1979) such that adaptive selection for reduced stomatal conductance, as a mean of improving iWUE, often leads to reduced photosynthesis and productivity (Ghannoum, 2016). ***Therefore, developing the next generation of smart crops requires a greater understanding of how stomata regulate iWUE, which represent the first key objective of this thesis.***

Breeders often utilise variations within a narrow set of crop genotypes or wild relatives of crops to identify improved traits. The downfall of this strategy is the limited pool of genetic diversity available in a single species or closely related species. Mining natural variation among diverse grasses will increase the potential of identifying beneficial stomatal traits (Anderson *et al.*, 2016; Reeves *et al.*, 2018; Cano *et al.*, 2019). This goal was addressed in Chapter 2 and Chapter 3 where I grew two C_3 and six C_4 grasses (two of each subtype) at ambient or glacial [CO_2] ([aCO_2] = 400, [gCO_2] = 180 µl l^{-1}) and high or low light intensity (HL = 1,000, LL = 200 µmol m^{-2} s^{-1}). I measured steady-state and dynamic leaf gas exchange in response to light transitions (1,000 ⇆ 100 µmol m^{-2} s^{-1}), stomatal morphology and electrophysiology.

Across treatments, stomatal conductance (g_s) and iWUE correlated with guard cell K^+ influx and stomatal aperture (SA), but not with stomatal density (SD). Further, C_4 grasses had consistently lower SA, faster stomatal opening on the transition to HL, and greater steady-state and dynamic iWUE. Glacial [CO_2] increased g_s, SA and K^+ influx, and reduced iWUE of C_3 to a greater extent than C_4 grasses. LL reduced g_s of C_4 to a greater extent than C_3 grasses, as well as iWUE and K^+ influx of C_3 grasses (**Figure 6. 1**). ***The first two experimental chapters revealed novel mechanistic links between SA, g_s, iWUE and K^+ influx amongst grasses and differential dynamics and responses of C_4 stomata to light, uncovering molecular targets for breeding crops with high iWUE. These findings are further discussed in sections 6.2.1 and 6.2.2.***

6.1.3 The role of post-photosynthetic fraction in explaining the link between and leaf $\delta^{13}C$ and iWUE among C_4 grasses

In C_3 plants, iWUE is directly correlated with the carbon isotope composition of the leaf dry matter ($\delta^{13}C$) through their separate relationships with a common parameter, the ratio of intercellular to ambient CO_2 (C_i/C_a). However, leaf $\delta^{13}C$ and iWUE in C_4 plants are not consistently correlated because of CCM and factors including post-photosynthetic carbon isotope fractionation. ***The second key objective of this thesis was to elucidate the impact of post-photosynthetic fractionation, particularly carbohydrate metabolism, on leaf $\delta^{13}C$. This goal was addressed in Chapter 4 and Chapter 5.***

Before addressing this objective, it was crucial to develop a method for measuring $\delta^{13}C$ of the three key soluble sugars (glucose, fructose and sucrose), which represent the major immediate sugar pools following Rubisco fixation of CO_2. In Chapter 4, I described an emerging method using wet chemical oxidation system (WCO) coupled with high-performance liquid chromatography (HPLC) and isotope ratio mass spectrometry (IRMS). The new system satisfactorily resolved sugar metabolites in an aqueous solution and was optimised using sugars extracted from leaves of rice (C_3) and maize (C_4).

The HPLC-WCO-IRMS method was then used in Chapter 5 to analyse $\delta^{13}C$ of sugars (sucrose, fructose and glucose) of four C_3, five C_4/NAD-ME, and four C_4/NADP-ME grasses grown under common conditions. Whole leaf and cellulose $\delta^{13}C$ were also measured together with leaf gas exchange. ***Overall, results identified differences in sugar $\delta^{13}C$ between C_4 subtypes, and***

a relationship between leaf $\delta^{13}C$ and g_s among C_4 grasses. These findings are further discussed in sections 6.2.3-6.2.6.

6.2 OVERALL THESIS CONCLUSIONS

To help develop climate-smart crops, this project sought to determine how stomatal traits control iWUE in grasses and whether this depends on photosynthetic pathway or growth environment. In addition, this study elucidated the impact of post-carboxylation fractionation on leaf $\delta^{13}C$ in C_4 plants. Such improved understanding will help develop a high throughput tool for screening iWUE among C_4 crops. Based on the results reported in this thesis, I have selected to highlight six novel findings for discussion in Chapter 6.

6.2.1 Grass stomatal conductance correlates with stomatal pore size and guard cell K^+ influx, but not with stomatal density

The sophisticated morphology and molecular regulation of grass stomata provide an advantage that has allowed grasses to dominate and diversify in the open environment. On the other hand, the operation of a CO_2 concentrating mechanism amongst C_4 grasses endows them with higher iWUE than their C_3 counterparts. However, it is unclear how this relates to underlying stomatal function or varies among the three C_4 biochemical subtypes with growth conditions, especially the two major photosynthetic factors: [CO_2] and light. Hence, two C_3 and six C_4 (two of each subtype: NADP-ME, NAD-ME, and PCK) grasses were grown at ambient or glacial [CO_2] ([CO_2] = 400, [gCO_2] = 180 µl l^{-1}) and high or low light (HL = 1,000, LL = 200 µmol m^{-2} s^{-1}).

To better understand short-term stomatal responses and long-term stomatal acclimation behaviour, it was necessary to partition the stomatal response into morphological (stomatal density and index) and physiological (stomatal conductance and guard cell K^+ influx). For example, growth at glacial [CO_2] increases g_s in C_3 and C_4 leaves (Sage & Coleman, 2001; Maherali *et al.*, 2002; Pinto *et al.*, 2014) and increases SD by 42% in *Arabidopsis* relative to ambient [CO_2] (Li *et al.*, 2014). In addition, adaptation to glacial [CO_2] includes higher stomatal density compared to current atmospheric [CO_2] (Woodward, 1987; Woodward & Kelly, 1995). Results obtained in this project demonstrated that both growth light and growth [CO_2] affected stomatal conductance by changing stomatal opening rather than stomatal frequency (Figure 6.1). Neither low light nor glacial [CO_2] had significant effects on stomatal density (SD), stomatal index (SI), or maximal stomatal conductance measured using gas exchange or anatomical traits (**Figure 6. 1**). In contrast, growth at glacial [CO_2] increased stomatal conductance (g_s), stomatal aperture (SA), and to a lesser extent, stomatal size (SS), while low light reduced g_s of all grasses (**Figure 6. 1**). Consequently, g_s and iWUE strongly correlated

with SA. The advantage of grass stomata architecture enables small changes in guard cell width to translate into larger changes in SA (Hetherington & Woodward, 2003; Franks & Farquhar, 2007). The changes in stomatal conductance were mirrored by changes in guard cell K^+ influx. In response to certain stimuli (e.g., low [CO_2]), guard cell K^+, anion and solute influx are followed by H_2O uptake, leading to stomatal opening (Chen *et al.*, 2012a, 2017). Significantly, g_s measured *in planta* using leaf gas exchange generally correlated well with K^+ influx measured on epidermal peels under standard conditions.

6.2.2 Stomatal conductance and guard cell K^+ influx respond differently between C_3 and C_4 grasses

The speed and high sensitivity of stomatal closure and opening in grasses result from the sophisticated stomatal geometry underpinning the superior functional response of grass stomata to fluctuating environmental conditions. However, it remains unclear whether stomatal responses, particularly to [CO_2] and light, differ between C_3 and C_4 grasses. Results in this project demonstrated a number of significant differences between C_3 and C_4 grass stomata.

In addition to lower SA, C_4 stomata exhibited faster stomatal opening on the transition to high light, especially under glacial [CO_2] and low light (**Figure 6. 1**). Hence, stomata of [CO_2]-saturated C_4 leaves open fast during transition to high light, achieving high biomass productivity. This is in line with the greater photosynthetic efficiency of C_4 grasses in response to sun flecks, highlighting their enhanced photosynthetic efficiency and productivity in response to increased light (McAusland *et al.*, 2016). In contrast, stomatal closing half-time was not systematically different between C_3 and C_4 grasses or between these tested growth conditions. Hence, there may not be any clear adaptive advantage for having faster or slower stomatal closing rate.

Moreover, glacial [CO_2] increased g_s and K^+ influx of C_3 to a greater extent than C_4 grasses. In contrast, low light reduced g_s of C_4 to a greater extent than C_3 grasses, while K^+ influx decreased in C_3 grasses only. The heightened sensitivity of C_3 and C_4 stomata to [CO_2] and light, respectively can be explained by the larger [CO_2] limitation of C_3 photosynthesis and greater light limitation of C_4 photosynthesis under most physiological conditions (von Caemmerer, 2000). During stomatal opening and closure, K^+ fluxes across the guard cell membranes represent the key determinants of the complex signalling pathways in response to variations of [CO_2], light and other stimuli (Kim *et al.*, 2010). Therefore, my results suggest that acclimations

of K^+ influx (and hence, possibly guard cell signalling) in C_3 and C_4 grasses are similar in response to glacial [CO_2], but differ in response to low light.

6.2.3 A HPLC-WCO-IRMS method was developed to analyse sugar carbon isotope composition without derivatisation

In C_3 plants, the composition of stable carbon isotopes ($\delta^{13}C$) has been used to screen for improved WUE. Carbon isotope discrimination is more complex in C_4 plants, weakening the links between $\delta^{13}C$ and iWUE. Therefore, there is a need to better understand photosynthetic and post-photosynthetic carbon isotope discrimination in C_4 leaves in order to improve our interpretation of $\delta^{13}C$ variations. Significant gaps still exist in our knowledge about the effects of post-photosynthetic and downstream metabolic processes on isotopic fractionations. Post-photosynthetic fractionations include those occurring during post-carboxylation (i.e., after CO_2 fixation by Rubisco) and carbohydrate metabolism. Differences in leaf dry matter $\delta^{13}C$ can arise if plants partition their carbon in different proportions to the various pools, such as sugars, lipids, lignin, proteins etc.

Compound-specific isotope analysis (CSIA) is a developing field in stable isotope analysis which is designed to examine the $\delta^{13}C$ of various metabolites isolated from bulk sample materials. Most of the current techniques are limited to gas chromatography (GC)-based assays, and non-volatile organic compounds must be derivatized by silylation, alkylation, acylation, esterification or other methods in order to volatilise the compounds and improve chromatographic separation (Meier-Augenstein, 2004; Morrison *et al.*, 2010; Elsner *et al.*, 2012). A liquid chromatography-based system makes it possible to conduct CSIA assays without derivatisation of the compounds.

Consequently, I worked on developing a method to analyse the $\delta^{13}C$ of key soluble sugars (sucrose, fructose and glucose). The method utilised the Liquiface® WCO system coupled to Agilent 1260 Infinity HPLC and Isoprime 1000 IRMS. The newly developed HPLC-WCO-IRMS system produced reproducible and accurate measurements of sugar $\delta^{13}C$ and which were comparable to the classical method previously employed **(Figure 6. 2**). I was then able to use this method to analyse sugar $\delta^{13}C$ in C_3 and C_4 grasses as discussed below.

6.2.4 Fructose was more ^{13}C-enriched in NADP-ME relative to NAD-ME C_4 grasses

Grasses belonging to different C_4 subtypes have long been known to vary in their carbon isotope composition ($\delta^{13}C$) (von Caemmerer *et al.*, 2014). Early work by Hattersley, (1982) demonstrated a 1.35‰ difference in the whole leaf $\delta^{13}C$ between NADP-ME and NAD-ME subtypes of C_4 grasses, with NADP-ME having more enriched $\delta^{13}C$. These differences have been supported by later studies (Ghannoum *et al.*, 2001a, 2002). Subsequent work has demonstrated that differences in leaf dry matter $\delta^{13}C$ and photosynthetic carbon isotope discrimination ($\Delta^{13}C$) among the C_4 subtypes cannot be attributed to variations in bundle sheath leakiness, and hence the efficiency of the C_4-CCM (Henderson *et al.*, 1992b; Cousins *et al.*, 2008; Sonawane *et al.*, 2017, 2018).

This thesis raised the question of whether post-photosynthetic carbon isotope fractionation may partly explain why leaf dry matter $\delta^{13}C$ differ between C_4 grasses belonging to the two main subtypes (NADP-ME and NAD-ME). Addressing this question can also shed light on the generally poor relationship between leaf $\delta^{13}C$ and iWUE in C_4 plants (Ghannoum *et al.*, 2001a, 2002; von Caemmerer *et al.*, 2014). Using the newly optimised HPLC-WCO-IRMS method during Chapter 4 for measuring $\delta^{13}C$ of soluble sugars (sucrose, glucose and fructose), four C_3, five NAD-ME, and four NADP-ME grass species were compared. Leaf dry matter and cellulose $\delta^{13}C$ were measured using EA-IRMS.

To the best of my knowledge, this is the first study that analyses $\delta^{13}C$ of immediate post-photosynthetic metabolites (major soluble sugars) for the purpose of elucidating the variations in $\delta^{13}C$ between the C_4 subtypes. Among C_4 grasses, fructose $\delta^{13}C$ was 1.6 ‰ more ^{13}C-enriched in NADP-ME relative to NAD-ME species (**Figure 6. 3**). Hence, fructose might be one of the candidate metabolites that could contribute to the differences in whole leaf and cellulose $\delta^{13}C$ between the two C_4 subtypes, although metabolites other than sugars should also be considered in the future.

Relative to the leaf, the discrimination profile of fructose and glucose were reversed between the two C_4 subtypes, culminating into a similar deviation of sucrose $\delta^{13}C$ relative to the leaf (**Figure 6. 3**). These results may partly reflect differences in sugar metabolism between the C_4 subtypes, including the different compartmentation of sucrose and starch synthesis between NAD-ME and NADP-ME species (Lunn & Furbank, 1999a). In particular, the two subtypes have different levels of PSII activity in the bundle sheath (Hatch, 1987). Bundle sheath chloroplasts in leaves of NADP-ME grasses generally have low PSII activity (Ghannoum *et al.*, 2005), requiring a greater fraction of phosphoglycerate to be reduced into glyceraldehyde 3-

phosphate in the mesophyll cells. Hence, the extent to which precursors for sugar metabolism are shuttled back and forth between the two cell types differ according to the C_4 subtype (Hatch, 1987). Ultimately, sucrose must be transported to the bundle sheath on its way to the phloem for export out of the source leaves. This suggests that sugar metabolism is more complex in the NADP-ME pathway. Taken together, these factors may cause some differences in the ^{13}C signatures between the two C_4 NADP-ME and NAD-ME subtype.

6.2.5 C_3 and C_4 grasses have different post-carboxylation carbon isotope fractionation

Among C_3 grasses, the $\delta^{13}C$ of soluble sugars were positively correlated with each other reflecting the more straightforward carbon metabolism in C_3 leaves. These results are in line with what is typically observed for C_3 plants where the carbon isotope signatures of sugars largely reflect the fractionation of the initial carboxylation reaction by Rubisco (29‰) (Farquhar *et al.*, 1982, 1989; Evans *et al.*, 1986; Cernusak *et al.*, 2013). In addition, C_3 fructose was more ^{13}C depleted (i.e., greater ^{13}C discrimination) while the other three compounds (cellulose, sucrose and glucose) were more ^{13}C enriched relative to the leaf. Analysis of intramolecular patterns in C_3 hexoses showed that invertase, the enzyme that hydrolyses sucrose into glucose and fructose moieties fractionates against ^{13}C, producing a depleted C-2 position (carbon atom position) in fructose (Gilbert *et al.*, 2012).

Overall, sucrose $\delta^{13}C$ deviated the most and cellulose $\delta^{13}C$ deviated the least relative to the bulk leaf. In particular, sucrose was the most ^{13}C depleted metabolite relative to the leaf and this difference was greater in C_4 relative to C_3 leaves. These results point to the differences in carbohydrate, particularly sucrose, metabolism between C_3 and C_4 plants. In C_3 leaves, sucrose metabolism occurs in one cell type, while sucrose metabolism occurs predominantly, but not exclusively, in the mesophyll cells of C_4 leaves (Lunn & Furbank, 1999a). As argued above, it is likely that sucrose, glucose and fructose are more frequently interconverted and transported in C_4 relative to C_3 leaves, which would markedly change the ^{13}C signatures between the two photosynthetic types.

6.2.6 Leaf and cellulose $\delta^{13}C$ correlated with stomatal conductance among C_4 grasses

One of the main long-term objectives of this research is to better understand the link between leaf dry matter carbon isotope composition ($\delta^{13}C$) and intrinsic water-use efficiency (iWUE).

This will enable us to use leaf $\delta^{13}C$ as a proxy when screening for improved iWUE among C_4 plants (von Caemmerer *et al.*, 2014; Ellsworth & Cousins, 2016).). Hence, leaf dry matter and cellulose $\delta^{13}C$ were measured together with leaf gas exchange in five NAD-ME and four NADP-ME C_4 grasses grown under common conditions. The results showed that leaf and cellulose $\delta^{13}C$ correlated well with stomatal conductance, but not with iWUE among the C_4 grasses, highlighting the dominant role played by stomata in determining leaf $\delta^{13}C$ and iWUE of C_4 species (Ghannoum *et al.*, 2001b, 2002; Pinto *et al.*, 2016; Cano *et al.*, 2019). C_4 photosynthesis is often saturated in ambient air under non-stressful conditions (Long, 1999). This implies that most of the variations in iWUE are generally more related to stomatal conductance than photosynthesis (Ghannoum, 2016). These results call for caution in interpreting the relationship between leaf $\delta^{13}C$ and iWUE in C_4 plants and suggest that most gas exchange-related variations in leaf $\delta^{13}C$ are related to variations in g_s in C_4 plants. This conclusion may have a bearing on recent studies showing a genomic link between leaf carbon isotope composition and plant water use efficiency in the C_4 crop maize (Avramova *et al.*, 2019) and the C_4 grass *Setaria viridis* (Feldman *et al.*, 2018).

6.3 FUTURE OUTLOOK

Finally, several experiments are still needed in the future in order to further elucidate my findings here. Based on these findings, I suggest the following future research:

I. Determine the environmental response of stomatal opening and closing using a larger set of C_3 and C_4 species as well as comparisons between the diverse stomatal morphologies (paracytic, anomocytic, and tetracytic) within monocots.

II. Elucidate the different acclimation and signalling pathways of stomata in C_3 and C_4 grasses, especially as they relate to guard cell K^+ fluxes.

III. Use the newly optimised HPLC-WCO-IRMS system to screen the carbon isotope composition of sugars from a diverse set of C_3 and C_4 grasses and crops.

IV. Probe the isotopic fractionation of invertases as well as investigate intramolecular carbon isotope patterns within the fructose molecule in leaves of C_4 grasses with different biochemical subtypes. This may shed light on the contribution of soluble sugars towards the differences in post-photosynthetic fraction and on leaf $\delta^{13}C$, as well as better understand the link between leaf $\delta^{13}C$ and iWUE amongst C_4 species.

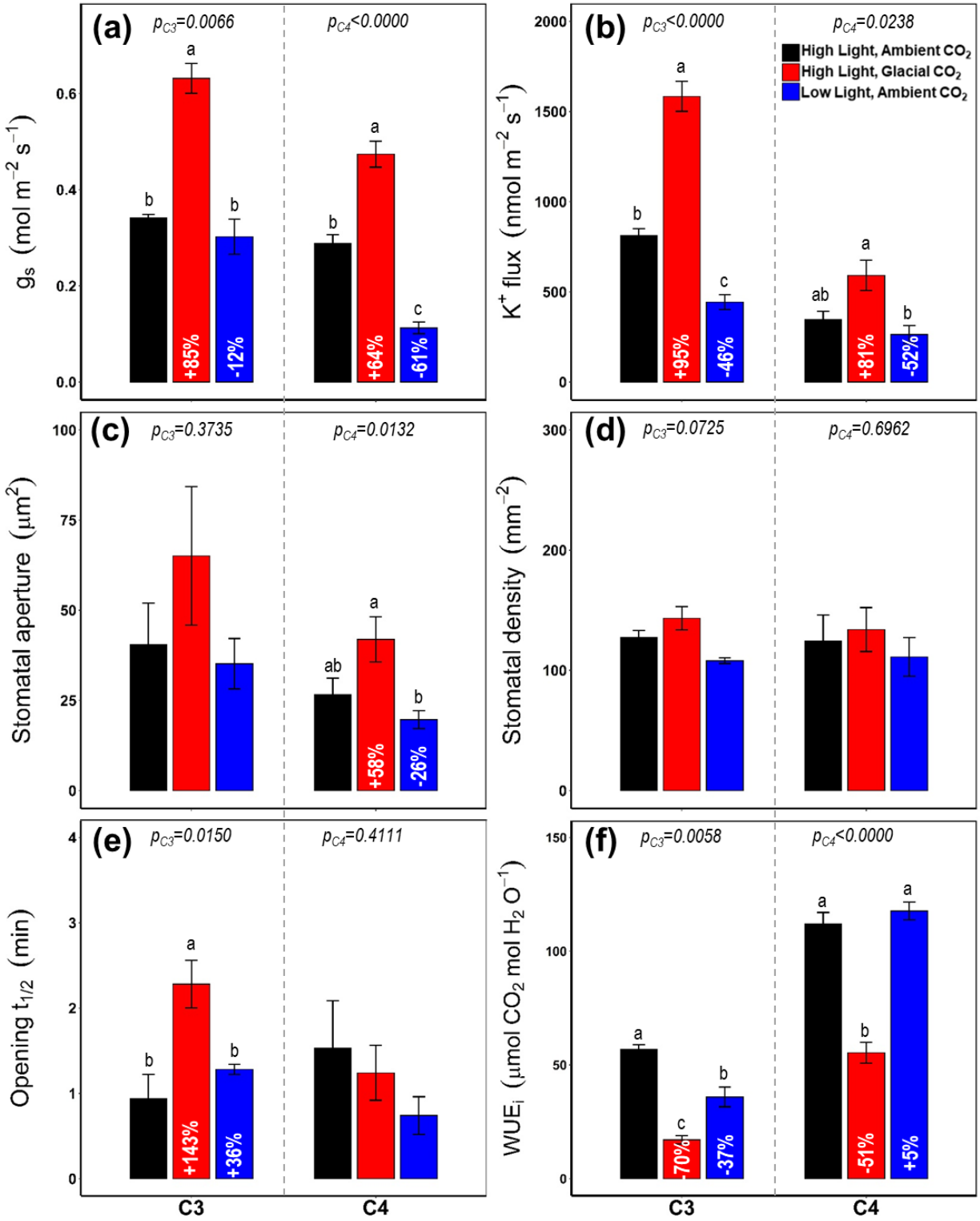

Figure 6. 1 Acclimation responses of gas exchange, stomatal morphology, and ion flux traits among two C_3 (n=2 species) and C_4 (n=6 species) grasses to glacial [CO_2] and low light.

Significant differences were compared between growth conditions in each photosynthetic type in the following traits: **(A)** stomatal conductance, **(B)** K^+ influx profile, **(C)** stomatal aperture, **(D)** stomatal density, **(E)** opening half-time, and **(F)** intrinsic water-use efficiency. When significant, values in white texts inside the bars represent relative per cent change to control conditions (high light ambient [CO_2]).

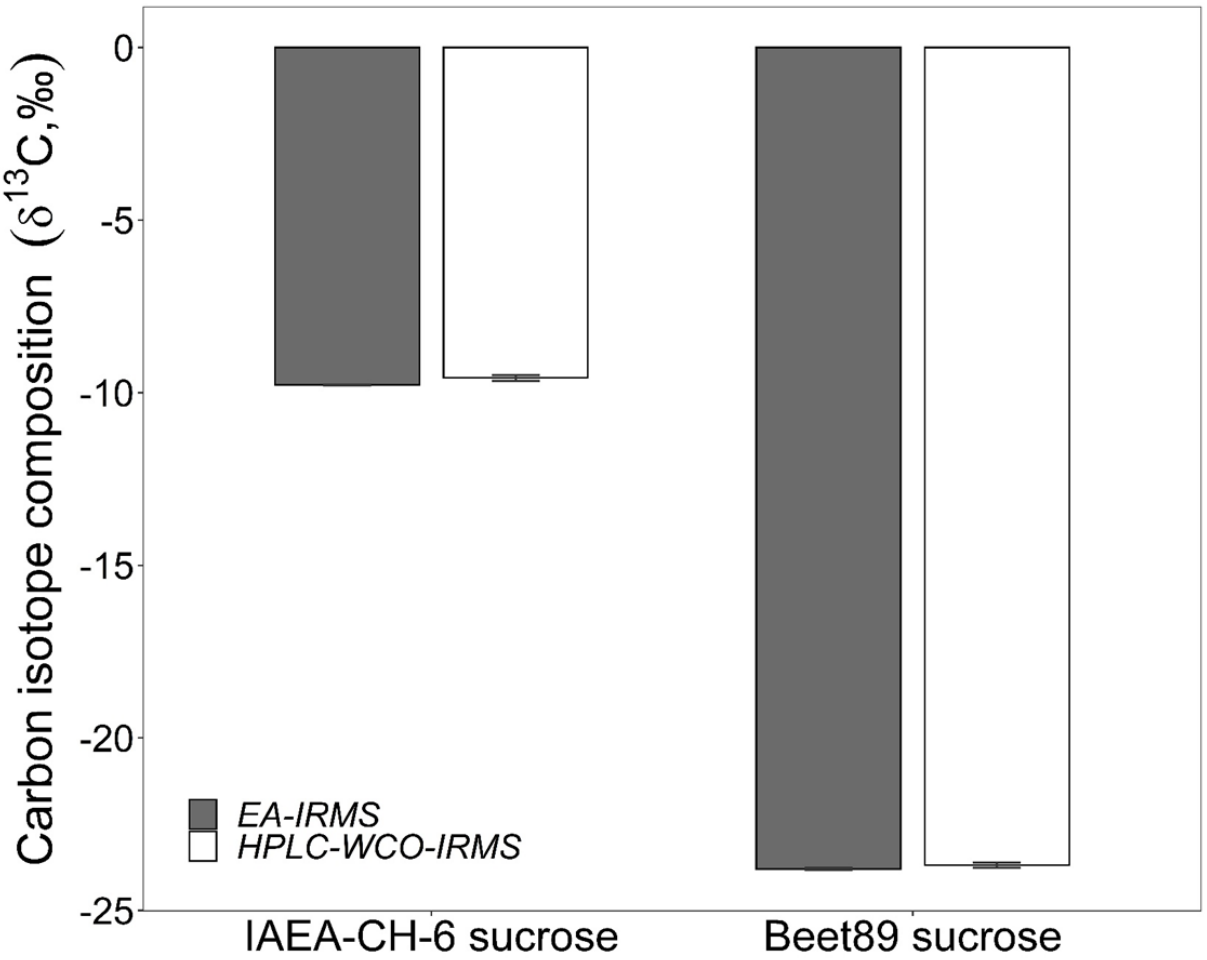

Figure 6. 2 Comparison of two IRMS methods used in this study.

Grey bars represent the classical EA-IRMS assay while white bars represent HPLC-WCO-IRMS interface optimised in this study, comparing IAEA-CH-6 sucrose (C_4 signature) and Beet89 sucrose (C_3 signature). No statistical difference was found between the two assays.

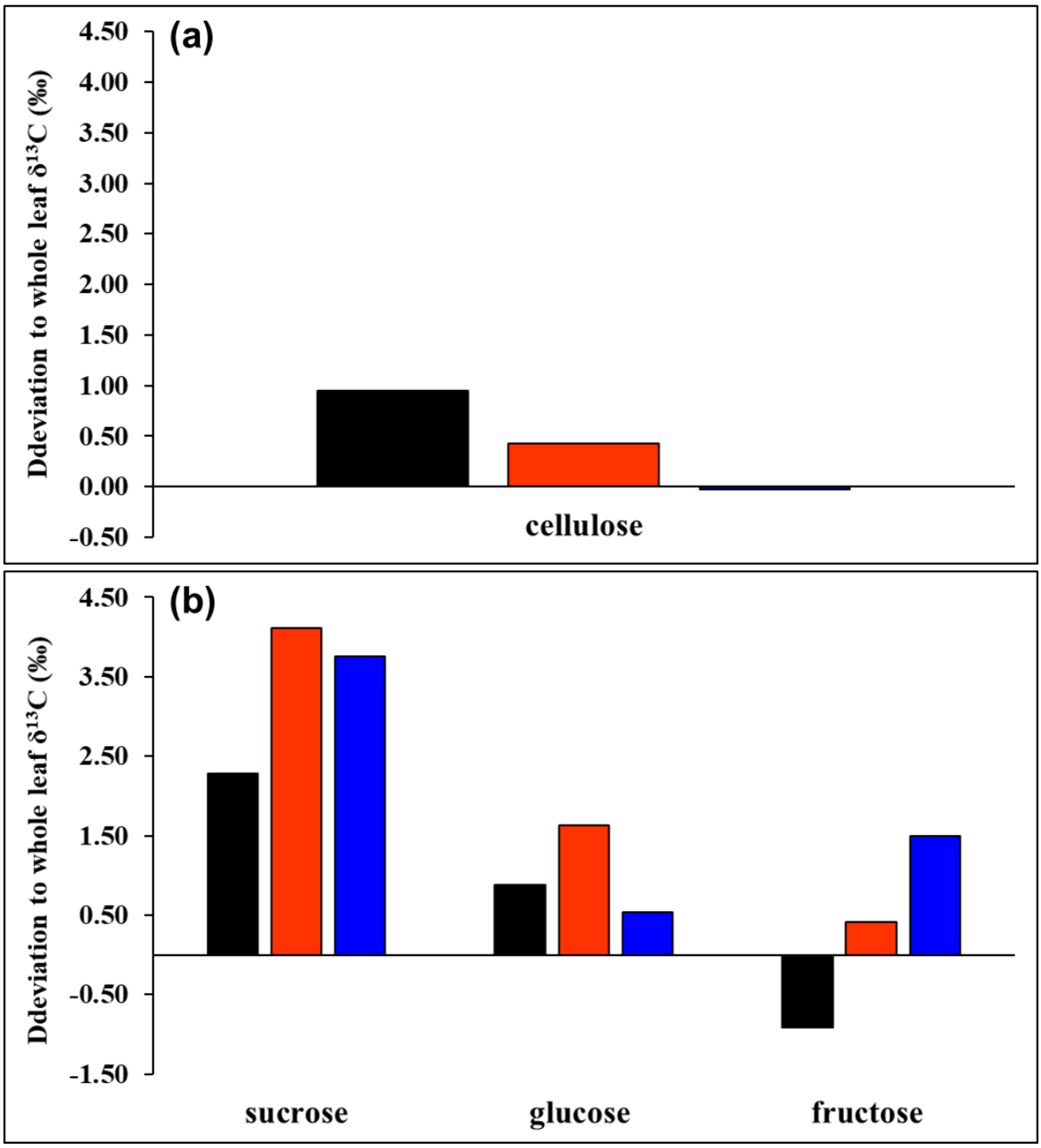

Figure 6. 3 $\delta^{13}C$ deviation of metabolite pools expressed relative to whole leaf $\delta^{13}C$.

Figures show cellulose **(A)** and soluble sugars, sucrose, glucose, and fructose **(B)** in C_3 (black), NAD-ME (red), and NADP-ME (blue) grasses.

REFERENCES

Aasamaa K, Aphalo PJ. **2016**. The acclimation of *Tilia cordata* stomatal opening in response to light, and stomatal anatomy to vegetational shade and its components (J Pereira, Ed.). *Tree Physiology* **37**: 209–219.

Aasamaa K, Sõber A. **2011**. Responses of stomatal conductance to simultaneous changes in two environmental factors. *Tree Physiology* **31**: 855–864.

Abaye DA, Morrison DJ, Preston T. **2011**. Strong anion exchange liquid chromatographic separation of protein amino acids for natural ^{13}C-abundance determination by isotope ratio mass spectrometry. *Rapid Communications in Mass Spectrometry* **25**: 429–435.

Anderson JE, Kono TJY, Stupar RM, Kantar MB, Morrell PL. **2016**. Environmental Association Analyses Identify Candidates for Abiotic Stress Tolerance in *Glycine soja*, the Wild Progenitor of Cultivated Soybeans. *G3: Genes|Genomes|Genetics* **6**: 835–843.

Assmann SM. **1999**. The cellular basis of guard cell sensing of rising CO_2. *Plant, Cell and Environment* **22**: 629–637.

Assmann SM, Jegla T. **2016**. Guard cell sensory systems: recent insights on stomatal responses to light, abscisic acid, and CO_2. *Current Opinion in Plant Biology* **33**: 157–167.

Aubry S, Aresheva O, Reyna-Llorens I, Smith-Unna RD, Hibberd J., Genty B. **2016**. A Specific Transcriptome Signature for Guard Cells from the C_4 Plant *Gynandropsis gynandra*. *Plant Physiology* **170**: 1345–1357.

Avramova V, Meziane A, Bauer E, Blankenagel S, Eggels S, Gresset S, Grill E, Niculaes C, Ouzunova M, Poppenberger B, *et al.* 2019. Carbon isotope composition, water use efficiency, and drought sensitivity are controlled by a common genomic segment in maize. *Theoretical and Applied Genetics* **132**: 53–63.

Azoulay-Shemer T, Palomares A, Bagheri A, Israelsson-Nordstrom M, Engineer CB, Bargmann BOR, Stephan AB, Schroeder JI. **2015**. Guard cell photosynthesis is critical for stomatal turgor production, yet does not directly mediate CO_2 and ABA-induced stomatal closing. *Plant Journal* **83**: 567–581.

Babb VM, Haigler CH. **2001**. Sucrose phosphate synthase activity rises in correlation with high-rate cellulose synthesis in three heterotrophic systems. *Plant Physiology* **127**: 1234–1242.

Babla M, Cai S, Chen G, Tissue DT, Cazzonelli CI, Chen ZH. **2019**. Molecular Evolution and Interaction of Membrane Transport and Photoreception in Plants. *Frontiers in Genetics* **10**: 1–17.

Badeck FW, Tcherkez G, Nogués S, Piel C, Ghashghaie J. **2005**. Post-photosynthetic

fractionation of stable carbon isotopes between plant organs - A widespread phenomenon. *Rapid Communications in Mass Spectrometry* **19**: 1381–1391.

Ball S, Bullock S, Lloyd L, Mapp K, Ewen A. **2011**. Analysis of carbohydrates , alcohols, and organic acids temperature effects on invert Sugar. *Agilent Hi Plex Columns Applications Compedium*: 96.

Baroja-Fernández E, Muñoz FJ, Zandueta-Criado A, Morán-Zorzano MT, Viale AM, Alonso-Casajús N, Pozueta-Romero J. **2004**. Most of ADP-glucose linked to starch biosynthesis occurs outside the chloroplast in source leaves. *Proceedings of the National Academy of Sciences of the United States of America* **101**: 13080–13085.

Basler A, Dyckmans J. **2013**. Compound-specific $\delta^{13}C$ analysis of monosaccharides from soil extracts by high-performance liquid chromatography/isotope ratio mass spectrometry. *Rapid Communications in Mass Spectrometry* **27**: 2546–2550.

Bellasio C, Griffiths H. **2014**. The operation of two decarboxylases, transamination, and partitioning of C_4 metabolic processes between mesophyll and bundle sheath cells allows light capture to be balanced for the maize C_4 pathway. *Plant Physiology* **164**: 466–480.

Bender MM. **1968**. Mass Spectrometric Studies of Carbon 13 Variations in Corn and Other Grasses. *Radiocarbon* **10**: 468–472.

Bender MM. **1971**. Variations in the $^{13}C/^{12}C$ ratios of plants in relation to the pathway of photosynthetic carbon dioxide fixation. *Phytochemistry* **10**: 1239–1244.

Berry J, Bjorkman O. **1980**. Photosynthetic Response and Adaptation to Temperature in Higher Plants. *Annual Review of Plant Physiology* **31**: 491–543.

Bevan MW, Garvin DF, Vogel JP. **2010**. *Brachypodium distachyon* genomics for sustainable food and fuel production. *Current Opinion in Biotechnology* **21**: 211–217.

Björkman O. **1971**. Comparative photosynthetic CO2 exchange in higher plants. In: Hatch MD, Osmond C, Slatyer R, eds. Photosynthesis and Photorespiration. New York: Wiley-Interscience, 18–32.

Boschker HT., Moerdijk-Poortvliet TC., van Breugel P, Houtekamer M, Middelburg J. 2008. A versatile method for stable carbon isotope analysis of carbohydrates by high-performance liquid chromatography/isotope ratio mass spectrometry. *Rapid communications in mass spectrometry : RCM* **22**: 3902–3908.

Bowling DR, Pataki DE, Randerson JT. **2008**. Carbon isotopes in terrestrial ecosystem pools and CO_2 fluxes. *New Phytologist* **178**: 24–40.

Bräutigam A, Schliesky S, Külahoglu C, Osborne CP, Weber APM. **2014**. Towards an integrative model of C_4 photosynthetic subtypes: Insights from comparative transcriptome

analysis of NAD-ME, NADP-ME, and PEP-CK C_4 species. *Journal of Experimental Botany* **65**: 3579–3593.

Brearley J, Venis MA, Blatt MR. **1997**. The effect of elevated CO_2 concentrations on K^+ and anion channels of Vicia faba L. guard cells. *Planta* **203**: 145–154.

Brown HT, Escombe F. **1900**. Static diffusion of gases and liquids in relation to the assimilation of carbon and translocation in plants. *Annals of Botany*.

Brüggemann N, Gessler A, Kayler Z, Keel SG, Badeck F, Barthel M, Boeckx P, Buchmann N, Brugnoli E, Esperschütz J, *et al.* 2011. Carbon allocation and carbon isotope fluxes in the plant-soil-atmosphere continuum: A review. *Biogeosciences* **8**: 3457–3489.

Brugnoli E, Hubick KT, von Caemmerer S, Wong SC, Farquhar GD. **1988**. Correlation between the Carbon Isotope Discrimination in Leaf Starch and Sugars of C_3 Plants and the Ratio of Intercellular and Atmospheric Partial Pressures of Carbon Dioxide. *Plant physiology* **88**: 1418–24.

Burnell JN, Hatch MD. **1988**. Photosynthesis in Phosphoenolpyruvate Cells of *Urochloa panicoides*. **260**: 187–199.

Cabañero AI, Recio JL, Rupérez M. **2006**. Liquid chromatography coupled to isotope ratio mass spectrometry: A new perspective on honey adulteration detection. *Journal of Agricultural and Food Chemistry* **54**: 9719–9727.

von Caemmerer S. **2000**. *Biochemical models of leaf photosynthesis*. Collingwood, Australia: CSIRO Publishing.

von Caemmerer S, Furbank RT. **1999**. Modeling C4 Photosynthesis. In: Monson R, ed. C_4 Plant Biology. San Diego: Academic Press, 173–211.

von Caemmerer S, Ghannoum O, Pengelly JJL, Cousins AB. **2014**. Carbon isotope discrimination as a tool to explore C_4 photosynthesis. *Journal of Experimental Botany* **65**: 3459–3470.

von Caemmerer S, Lawson T, Oxborough K, Baker NR, Andrews TJ, Raines CA. **2004**. Stomatal conductance does not correlate with photosynthetic capacity in transgenic tobacco with reduced amounts of Rubisco. *Journal of Experimental Botany* **55**: 1157–1166.

von Caemmerer S, Millgate A, Farquhar GD, Furbank RT. **1997**. Reduction of ribulose-1,5-bisphosphate carboxylase/oxygenase by antisense RNA in the C4 plant Flaveria bidentis leads to reduced assimilation rates and increased carbon isotope discrimination. *Plant Physiology* **113**: 469–477.

Cai S, Chen G, Wang Y, Huang Y, Marchant DB, Wang Y, Yang Q, Dai F, Hills A, Franks PJ, *et al.* 2017a. Evolutionary Conservation of ABA Signaling for Stomatal Closure. *Plant*

Physiology **174**: 732–747.

Cai S, Papanatsiou M, Blatt MR, Chen Z. **2017b**. Speedy Grass Stomata : Emerging Molecular and Evolutionary Features. *Molecular Plant* **10**: 912–914.

Caine RS, Yin X, Sloan J, Harrison EL, Mohammed U, Fulton T, Biswal AK, Dionora J, Chater CC, Coe RA, *et al.* 2018. Rice with reduced stomatal density conserves water and has improved drought tolerance under future climate conditions. *New Phytologist*: 371–384.

Cano FJ, Sharwood RE, Cousins AB, Ghannoum O. **2019**. The role of leaf width and conductances to CO_2 in determining water use efficiency in C_4 grasses. *New Phytologist*: 1280–1295.

Carins Murphy MR, Jordan GJ, Brodribb TJ. **2016**. Cell expansion not cell differentiation predominantly co-ordinates veins and stomata within and among herbs and woody angiosperms grown under sun and shade. *Annals of Botany* **118**: 1127–1138.

Cerling TE, Harris JM, MacFadden BJ, Leakey MG, Quade J, Eisenmann V, Ehleringer JR. **1997**. Global vegetation change through the Miocene/Pliocene boundary. *Nature* **389**: 153–158.

Cernusak LA, Tcherkez G, Keitel C, Cornwell WK, Santiago LS, Knohl A, Barbour MM, Williams DG, Reich PB, Ellsworth DS, *et al.* 2009. Why are non-photosynthetic tissues generally ^{13}C enriched compared with leaves in C_3 plants? Review and synthesis of current hypotheses. *Functional Plant Biology*.

Cernusak LA, Ubierna N, Winter K, Holtum JAM, Marshall JD, Farquhar GD. **2013**. Environmental and physiological determinants of carbon isotope discrimination in terrestrial plants. *New Phytologist* **200**: 950–965.

Chapman K, Hatch M. **1981**. Aspartate Decarboxylation in Bundle Sheath Cells of *Zea mays* and Its Possible Contribution to C_3 Photosynthesis. *Functional Plant Biology* **8**: 237.

Chen Z-H, Blatt MR. **2010**. Membrane Transport in Guard Cells. *Encyclodpedia of Life Sciences John Wiley & Sons, Ltd: Chichester.*: 1–13.

Chen Z-H, Chen G, Dai F, Wang Y, Hills A, Ruan Y-L, Zhang G, Franks PJ, Nevo E, Blatt MR. **2017**. Molecular Evolution of Grass Stomata. *Trends in Plant Science* **22**: 124–139.

Chen Z-H, Eisenach C, Xu X-Q, Hills A, Blatt MR. **2012a**. Protocol: optimised electrophyiological analysis of intact guard cells from Arabidopsis. *Plant methods* **8**: 15.

Chen Z-H, Hills A, Batz U, Amtmann A, Lew VL, Blatt MR. **2012b**. Systems Dynamic Modeling of the Stomatal Guard Cell Predicts Emergent Behaviors in Transport, Signaling, and Volume Control. *Plant Physiology* **159**: 1235–1251.

Chen Z-H, Hills A, Lim CK, Blatt MR. **2010a**. Dynamic regulation of guard cell anion channels by cytosolic free Ca^{2+} concentration and protein phosphorylation. *The Plant journal : for cell and molecular biology* **61**: 816–825.

Chen SF, Mowery RA, Sevcik RS, Scarlata CJ, Chambliss CK. **2010b**. Compositional analysis of water-soluble materials in switchgrass. *Journal of Agricultural and Food Chemistry* **58**: 3251–3258.

Chen Z, Newman I, Zhou M, Mendham N, Zhang G, Shabala S. **2005**. Screening plants for salt tolerance by measuring K^+ flux: A case study for barley. *Plant, Cell and Environment* **28**: 1230–1246.

Christie JM. **2007**. Phototropin Blue-Light Receptors. *Annual Review of Plant Biology* **58**: 21–45.

Christin PA, Besnard G, Samaritani E, Duvall MR, Hodkinson TR, Savolainen V, Salamin N. **2008**. Oligocene CO_2 Decline Promoted C_4 Photosynthesis in Grasses. *Current Biology* **18**: 37–43.

Christin PA, Osborne CP, Chatelet DS, Columbus JT, Besnard G, Hodkinson TR, Garrison LM, Vorontsova MS, Edwards EJ. **2013**. Anatomical enablers and the evolution of C_4 photosynthesis in grasses. *Proceedings of the National Academy of Sciences of the United States of America* **110**: 1381–1386.

Condon AG, Richards RA, Rebetzke GJ, Farquhar GD. **2004**. Breeding for high water-use efficiency. *Journal of Experimental Botany* **55**: 2447–2460.

Cousins AB, Badger MR, Von Caemmerer S. **2008**. C_4 photosynthetic isotope exchange in NAD-ME and NADP-ME-type grasses. *Journal of Experimental Botany* **59**: 1695–1703.

Covshoff S, Szecowka M, Hughes TE, Smith-Unna R, Kelly S, Bailey KJ, Sage TL, Pachebat JA, Leegood R, Hibberd JM. **2016**. C4 Photosynthesis in the Rice Paddy: Insights from the Noxious Weed Echinochloa glabrescens. *Plant physiology* **170**: 57–73.

Craig H. **1953**. The geochemistry of the stable carbon isotopes. *Geochimica et Cosmochimica Acta* **3**: 53–92.

Craig H. **1957**. Isotopic standards for carbon and oxygen and correction factors for mass-spectrometric analysis of carbon dioxide. *Geochimica et Cosmochimica Acta* **12**: 133–149.

Cuin TA, Bose J, Stefano G, Jha D, Tester M, Mancuso S, Shabala S. **2011**. Assessing the role of root plasma membrane and tonoplast Na+/H+ exchangers in salinity tolerance in wheat: In planta quantification methods. *Plant, Cell and Environment* **34**: 947–961.

Deans RM, Brodribb TJ, Busch FA, Farquhar GD. **2018**. Plant water-use strategy mediates stomatal effects on the light induction of photosynthesis. *New Phytologist*.

Dethloff F, Orf I, Kopka J. **2017**. Rapid in situ 13 C tracing of sucrose utilization in Arabidopsis sink and source leaves. *Plant Methods* **13**: 1–19.

Doust AN, Mauro-Herrera M, Hodge JG, Stromski J. **2017**. The C_4 model grass setaria is a short day plant with secondary long day genetic regulation. *Frontiers in Plant Science* **8**: 1–10.

Dow GJ, Bergmann DC, Berry JA. **2014a**. An integrated model of stomatal development and leaf physiology. *New Phytologist* **201**: 1218–1226.

Dow GJ, Berry JA, Bergmann DC. **2014b**. The physiological importance of developmental mechanisms that enforce proper stomatal spacing in Arabidopsis thaliana. *New Phytologist* **201**: 1205–1217.

Edwards EJ, Osborne CP, Strömberg CAE, Smith SA, Bond WJ, Christin PA, Cousins AB, Duvall MR, Fox DL, Freckleton RP, *et al.* 2010. The origins of C_4 Grasslands: Integrating evolutionary and ecosystem science. *Science* **328**: 587–591.

Ehleringer J, Björkman O, Bjorkman O. **1977**. Quantum yields for CO_2 uptake in C_3 and C_4 plants. *Plant Physiology* **59**: 86–90.

Ehleringer JR, Cerling TE. **2014**. C_3 and C_4 Photosynthesis. *Encyclopedia of Global Environmental Change*.

Ehleringer JR, Cerling TE, Helliker BR. **1997**. C_4 photosynthesis, atmospheric CO_2, and climate. *Oecologia* **112**: 285–299.

Elliott-Kingston C, Haworth M, Yearsley JM, Batke SP, Lawson T, McElwain JC. **2016**. Does Size Matter? Atmospheric CO_2 May Be a Stronger Driver of Stomatal Closing Rate Than Stomatal Size in Taxa That Diversified under Low CO_2. *Frontiers in Plant Science* **7**: 1–12.

Ellsworth PZ, Cousins AB. **2016**. Carbon isotopes and water use efficiency in C_4 plants. *Current Opinion in Plant Biology* **31**: 155–161.

Ellsworth PZ, Feldman MJ, Baxter I, Cousins AB. **2019**. A genetic link between leaf carbon isotope composition and whole-plant water use efficiency in the C_4 grass *Setaria*. *bioRxiv*: 285676.

Elsner M, Jochmann MA, Hofstetter TB, Hunkeler D, Bernstein A, Schmidt TC, Schimmelmann A. **2012**. Current challenges in compound-specific stable isotope analysis of environmental organic contaminants. *Analytical and Bioanalytical Chemistry*.

Engineer CB, Hashimoto-Sugimoto M, Negi J, Israelsson-Nordstrom M, Azoulay-Shemer T, Rappel WJ, Iba K, Schroeder JI. **2016**. CO_2 Sensing and CO_2 Regulation of Stomatal Conductance: Advances and Open Questions. *Trends in Plant Science* **21**: 16–30.

Evans JR, Sharkey TD, Berry J a., Farquhar GD. **1986**. Carbon isotope discrimination

measured concurrently with gas exchange to investigate CO_2 diffusion in leaves of higher plants. *Australian Journal of Plant Physiology* **13**: 281–292.

FAO. **2017**. *Water for Sustainable Food and Agriculture Water for Sustainable Food and Agriculture*.

FAO. **2019**. FAOSTAT. *http://www.fao.org/faostat/en/#home*.

Faraco M, Fico D, Pennetta A, De Benedetto GE. **2016**. New evidences on efficacy of boronic acid-based derivatization method to identify sugars in plant material by gas chromatography-mass spectrometry. *Talanta* **159**: 40–46.

Farquhar GD. **1983**. On the Nature of Carbon Isotope Discrimination in C_4 Species. *Australian Journal of Plant Physiology* **10**: 205–226.

Farquhar GD, von Caemmerer S. **1981**. Some relationships between the biochemistry of photosynthesis and the gas exchange of leaves. *Planta*: 376–387.

Farquhar GD, Cernusak LA. **2012**. Ternary effects on the gas exchange of isotopologues of carbon dioxide. *Plant, Cell and Environment* **35**: 1221–1231.

Farquhar GD, Ehleringer JR, Hubic KT. **1989**. Carbon Isotope Discrimination and Photosynthesis. *Annu. Rev. Plant Physiol. Plant Mol. Biol.*: 503–537.

Farquhar GD, O'Leary MH, Berry JA. **1982**. On the Relationship Between Carbon Isotope Discrimination and the Intercellular Carbon Dioxide Concentration in Leaves. *Australian Journal of Plant Physiology* **9**: 121.

Farquhar GD, Richards RA. **1984**. Isotopic composition of plant carbon correlates with water-use efficiency of wheat genotypes. *Australian Journal of Plant Physiology* **11**: 539–552.

Farquhar GD, Sharkey TD. **1982**. Stomatal Conductance and Photosynthesis. *Annual Review of Plant Physiology*.

Federherr E, Willach S, Roos N, Lange L, Molt K, Schmidt TC. **2016**. A novel high-temperature combustion interface for compound-specific stable isotope analysis of carbon and nitrogen via high-performance liquid chromatography/isotope ratio mass spectrometry. *Rapid Communications in Mass Spectrometry* **30**: 944–952.

Feldman MJ, Ellsworth PZ, Fahlgren N, Gehan MA, Cousins AB, Baxter I. **2018**. Components of Water Use Efficiency Have Unique Genetic Signatures in the Model C_4 Grass *Setaria*. *Plant physiology* **178**: 699–715.

Fernando N, Manalil S, Florentine SK, Chauhan BS, Seneweera S. **2016**. Glyphosate resistance of C_3 and C_4 weeds under rising atmospheric CO_2. *Frontiers in Plant Science* **7**: 1–11.

Franks PJ, Beerling DJ. **2009**. CO_2-forced evolution of plant gas exchange capacity and water-use efficiency over the Phanerozoic. *Geobiology* **7**: 227–236.

Franks PJ, Farquhar GD. **2007**. The Mechanical Diversity of Stomata and Its Significance in Gas-Exchange Control. *Plant Physiology* **143**: 78–87.

Fravolinil A, Williams DG, Thompson TL. **2002**. Carbon isotope discrimination and bundle sheath leakiness in three C_4 subtypes grown under variable nitrogen, water and atmospheric CO_2 supply. *J Exp Bot* **53**: 2261–2269.

Fry B. **2006**. *Stable Isotope Ecology*. Spring St., New York: Springer Science+Business Media, LLC.

Garcia-Mata C, Gay R, Sokolovski S, Hills A, Lamattina L, Blatt MR. **2003**. Nitric oxide regulates K^+ and Cl^- channels in guard cells through a subset of abscisic acid-evoked signaling pathways. *Proceedings of the National Academy of Sciences of the United States of America* **100**: 11116–11121.

Garcia-Mata C, Lamattina L. **2007**. Abscisic acid (ABA) inhibits light-induced stomatal opening through calcium- and nitric oxide-mediated signaling pathways. *Nitric Oxide - Biology and Chemistry* **17**: 143–151.

Gay AP, Hurd RG. **1975**. The Influence of Light on Stomatal Density in the Tomato. *New Phytologist* **75**: 37–46.

Gerald CE, Porter AS, Yiotis C, Elliott-kingston C, Mcelwain JC, Gerald CE. **2016**. Co-ordination in Morphological Leaf Traits of Early Diverging Angiosperms Is Maintained Following Exposure to Experimental Palaeo-atmospheric Conditions of Sub-ambient O_2 and Elevated CO_2. *Frontiers in Plant Science* **7**: 1–11.

Gerardin T, Douthe C, Flexas J, Brendel O. **2018**. Shade and drought growth conditions strongly impact dynamic responses of stomata to variations in irradiance in *Nicotiana tabacum*. *Environmental and Experimental Botany* **153**: 188–197.

Gessler A, Tcherkez G, Peuke AD, Ghashghaie J, Farquhar GD. **2008**. Experimental evidence for diel variations of the carbon isotope composition in leaf, stem and phloem sap organic matter in *Ricinus communis*. *Plant, Cell and Environment* **31**: 941–953.

Ghannoum O. **2016**. How can we breed for more water use-efficient sugarcane? *Journal of Experimental Botany* **67**: 555–557.

Ghannoum O, von Caemmerer S, Conroy JP. **2001a**. Carbon and water economy of Australian NAD-ME and NADP-ME C_4 grasses. *Functional Plant Biology* **28**: 213–223.

Ghannoum O, von Caemmerer S, Conroy J. **2002**. The effect of drought on plant water use efficiency of nine NAD-ME and nine NADP-ME Australian C4 grasses. *Functional Plant*

Biology **29**: 1337–1348.

Ghannoum O, von Caemmerer S, Conroy JP. **2001b**. Plant water use efficiency of 17 Australian NAD-ME and NADP-ME C4 grasses at ambient and elevated CO2 partial pressure. *Australian Journal of Plant Physiology*.

Ghannoum O, von Caemmerer S, Ziska LH, Conroy JP. **2000**. The growth response of C4 plants to rising atmospheric CO2 partial pressure: A reassessment. *Plant, Cell and Environment*.

Ghannoum O, Evans JR, von Caemmerer S. **2011**. Nitrogen and Water Use Efficiency of C_4 Plants. In: C4 Photosynthesis and Related CO2 Concentrating Mechanisms Photosynthesis and Related CO2 Concentrating Mechanisms. 129–146.

Ghannoum O, Evans J, Chow W, Andrews T, Conroy J, von Caemmerer S. **2005**. Faster Rubisco Is the Key to Superior Nitrogen-Use Efficiency in NADP-Malic Enzyme Relative to NAD-Malic Enzyme C_4 Grasses. *Plant Physiology* **137**: 638–650.

Ghashghaie J, Duranceau M, Badeck FW, Cornic G, Adeline MT, Deleens E. **2001**. δ13C of CO2 respired in the dark in relation to δ13C of leaf metabolites: Comparison between Nicotiana sylvestris and Helianthus annuus under drought. *Plant, Cell and Environment* **24**: 505–515.

Gilbert A, Robins RJ, Remaud GS, Tcherkez GGB. **2012**. Intramolecular ^{13}C pattern in hexoses from autotrophic and heterotrophic C_3 plant tissues. *Proceedings of the National Academy of Sciences of the United States of America* **109**: 18204–18209.

Godin J, Fay L. **2008**. Liquid Chromatography Coupled to Isotope Ratio Mass Spectrometry. *Society* **80**.

Godin JP, McCullagh JSO. **2011**. Review: Current applications and challenges for liquid chromatography coupled to isotope ratio mass spectrometry (LC/IRMS). *Rapid Communications in Mass Spectrometry* **25**: 3019–3028.

Grabov A, Blatt MR. **1998**. Membrane voltage initiates Ca^{2+} waves and potentiates Ca^{2+} increases with abscisic acid in stomatal guard cells. *Proceedings of the National Academy of Sciences of the United States of America* **95**: 4778–4783.

Grass Phylogeny Working Group II. **2012**. New grass phylogeny resolves deep evolutionary relationships and discovers C4 origins. *New Phytologist*: 304–312.

Gross S, Glaser B. **2004**. Minimization of carbon addition during derivatization of monosaccharides for compound-specific $\delta^{13}C$ analysis in environmental research. *Rapid Communications in Mass Spectrometry* **18**: 2753–2764.

Harold Brown R. **1999**. *Agronomic Implications of C_4 Photosynthesis*. Woodhead Publishing

Limited.

Hashimoto M, Negi J, Young J, Israelsson M, Schroeder JI, Iba K. **2006**. Arabidopsis HT1 kinase controls stomatal movements in response to CO2. *Nature Cell Biology*.

Hatch M. **1987**. C_4 Photosynthesis: a unique blend of modified biochemistry, anatomy and ultrastructure. *Biochimica et Biophysica Acta* **895**: 81–106.

Hatch M, Kagawa T, Craig S. **1975**. Subdivision of C_4 Pathway Species Based on Differing C_4 Acid Decarboxylating Systems and Ultrastructural Features. *Australian Journal of Plant Physiology* **2**: 111.

Hattersley P. **1982**. δ13 Values of C_4 Types in Grasses. *Aust. J. Plant Physiol* **9**: 139.

Hattersley PW. **1983**. The distribution of C_3 and C_4 grasses in Australia in relation to climate. *Oecologia* **57**: 113–128.

Hattersley P. **1992**. C_4 photosynthetic pathway variation in grasses (Poaceae): its significance for arid and semi-arid lands. In: Desertified grasslands: their biology and management. Linn. Soc. Symp. ser. 181–212.

Henderson SA, von Caemmerer S, Farqhuar G. **1992a**. Short-term Measurements of Carbon isotope discrimination in Several C_4 Species. *Aust J Plant Physiol* **19**: 263–85.

Henderson SA, von Caemmerer S, Farquhar GD, Hammer GL, Wade LJ. **1998**. Correlation between carbon isotope discrimination and transpiration efficiency in lines of the C4 species Sorghum bicolor in the glasshouse and the field. *Australian Journal of Plant Physiology* **49**: 111–123.

Henderson SA, von Caemmerer S, Griffiths H. **1992b**. Carbon isotope discrimination in several C_4 species. *Aust J Plant Physiol* **19**: 263–85.

Henry C, Watson-Lazowski A, Oszvald M, Griffiths C, Paul MJ, Furbank RT, Ghannoum O. **2020**. Sugar sensing responses to low and high light in leaves of the C4 model grass Setaria viridis. *Journal of Experimental Botany*.

Hetherington AM, Woodward FI. **2003**. The role of stomata in sensing and driving environmental change. *Nature* **424**: 901–908.

Hettmann E, Gleixner G, Juchelka D. **2005**. IRM-LC/MS: δ13C analysis of organic acidsin plants. *Application note 30075, Thermo Fisher Scientific*.

Hills A, Chen ZH, Amtmann A, Blatt MR, Lew VL. **2012**. Onguard, a computational platform for quantitative kinetic modeling of guard cell physiology. *Plant Physiology* **159**: 1026–1042.

Hiyama A, Takemiya A, Munemasa S, Okuma E, Sugiyama N, Tada Y, Murata Y, Shimazaki K. **2017**. Blue light and CO_2 signals converge to regulate light-induced stomatal opening. *Nature Communications* **8**: 1284.

Hobbie EA, Werner RA. **2004**. Intramolecular, compound-specific, and bulk carbon isotope patterns in C3 and C4 plants: A review and synthesis. *New Phytologist* **161**: 371–385.

Hubick KT, Farquhar GD, Shorter R. **1986**. Correlation between Water-use Efficiency and Carbon Isotope Discrimination in Diverse Peanut (*Arachis*) Germplasm. *Aust. J. Plant Physiol* **13**: 803–816.

Hubick KT, Hammer GL, Farquhar GD, Wade LJ, von Caemmerer S, Henderson S a. **1990**. Carbon isotope discrimination varies genetically in C_4 species. *Plant physiology* **92**: 534–537.

Huxman TE, Monson RK. **2003**. Stomatal responses of C_3, C_3-C_4 and C_4 Flaveria species to light and intercellular CO_2 concentration: Implications for the evolution of stomatal behaviour. *Plant, Cell and Environment* **26**: 313–322.

Inoue S, Kinoshita T. **2017**. Blue Light Regulation of Stomatal Opening and the Plasma Membrane H + -ATPase. *Plant Physiology* **174**: 531–538.

IPCC. **2018**. *Global Warming* (V Masson-Delmotte, P Zhai, H. Porter, D Roberts, J Skea, PR Shukla, A Pirani, W Moufouma-Okia, C Pean, R Pidcock, *et al.*, Eds.). In Press.

Isoprime L. **2011**. *Liquiface User Guide*. Cheadle, UK.

James SA, Bell DT. **2000**. Influence of light availability on leaf structure and growth of two Eucalyptus globulus ssp. globulus provenances. *Tree Physiology*: 1007–1018.

Joppa LN, Roberts DL, Pimm SL. **2011**. How many species of flowering plants are there? *Proceedings of the Royal Society B: Biological Sciences* **278**: 554–559.

Kanai R, Edwards GE. **1999**. *The Biochemistry of C_4 Photosynthesis*. Woodhead Publishing Limited.

Kanno Y, Hanada A, Chiba Y, Ichikawa T, Nakazawa M, Matsui M, Koshiba T, Kamiya Y, Seo M. **2012**. Identification of an abscisic acid transporter by functional screening using the receptor complex as a sensor. *Proceedings of the National Academy of Sciences of the United States of America* **109**: 9653–9658.

Kellogg E a. **2001**. Update on Evolution Evolutionary History of the Grasses. *Plant physiology* **125**: 1198–1205.

Kim T-H, Bohmer M, Hu H, Nishimura N, Schroeder JI. **2010**. Guard cells signal transduction network: advances in understanding abscisic acid CO_2, and Ca^{2+} signalling.

Annual Review of Plant Biology **61**: 561–591.

Kirkham MB. **2014**. Stomatal Anatomy and Stomatal Resistance. In: Principles of Soil and Plant Water Relations. 431–451.

Knapp AK, Smith W. 1987. Stomatal and photosynthetic responses during sun/shade transitions in subalpine plants: influence on water use efficiency. *Oecologia* **74**: 62–67.

Kohn MJ. **2010**. Carbon isotope compositions of terrestrial C_3 plants as indicators of (paleo)ecology and (paleo)climate. *Proceedings of the National Academy of Sciences* **107**: 19691–19695.

Kolbe AR, Studer AJ, Cousins AB. **2018**. Biochemical and transcriptomic analysis of maize diversity to elucidate drivers of leaf carbon isotope composition. *Functional Plant Biology*.

Kollist H, Nuhkat M, Roelfsema MRG. **2014a**. Closing gaps: Linking elements that control stomatal movement. *New Phytologist* **203**: 44–62.

Kruger NJ, Ratcliffe RG. **2009**. Insights into plant metabolic networks from steady-state metabolic flux analysis. *Biochimie* **91**: 697–702.

Krummen M, Hilkert AW, Juchelka D, Duhr A, Schlüter HJ, Pesch R. **2004**. A new concept for isotope ratio monitoring liquid chromatography/mass spectrometry. *Rapid Communications in Mass Spectrometry* **18**: 2260–2266.

Krummen M, Hilkert AW, Juchelka D, Duhr A, Schlüter HJ, Pesch R, Morrison DJ, Taylor K, Preston T, Abramson FP, *et al.* 2008. Liquid and gas chromatography coupled to isotope ratio mass spectrometry for the determination of ^{13}C-valine isotopic ratios in complex biological samples. *Rapid Communications in Mass Spectrometry* **913**: 269–273.

Kuromori T, Miyaji T, Yabuuchi H, Shimizu H, Sugimoto E, Kamiya A, Moriyama Y, Shinozaki K. **2010**. ABC transporter AtABCG25 is involved in abscisic acid transport and responses. *Proceedings of the National Academy of Sciences of the United States of America* **107**: 2361–2366.

Laanemets K, Brandt B, Li J, Merilo E, Wang YF, Keshwani MM, Taylor SS, Kollist H, Schroeder JI. **2013a**. Calcium-dependent and - independent stomatal signaling network and compensatory feedback control of stomatal opening via Ca^{2+} sensitivity priming. *Plant Physiology* **163**: 504–513.

Laanemets K, Wang YF, Lindgren O, Wu J, Nishimura N, Lee S, Caddell D, Merilo E, Brosche M, Kilk K, *et al.* 2013b. Mutations in the SLAC1 anion channel slow stomatal opening and severely reduce K+ uptake channel activity via enhanced cytosolic [Ca2+] and increased Ca2+ sensitivity of K+ uptake channels. *New Phytologist* **197**: 88–98.

De Laeter JR, Peiser HS. **2003**. A century of progress in the sciences due to atomic weight

and isotopic composition measurements. *Analytical and Bioanalytical Chemistry* **375**: 62–72.

Lai B, Plan M, Hodson M, Krömer J. **2016**. Simultaneous Determination of Sugars, Carboxylates, Alcohols and Aldehydes from Fermentations by High Performance Liquid Chromatography. *Fermentation* **2**: 6.

Lawson T, Blatt MR. **2014**. Stomatal Size, Speed, and Responsiveness Impact on Photosynthesis and Water Use Efficiency. *Plant Physiology* **164**: 1556–1570.

Lawson T, Caemmerer S Von, Baroli I. **2011**. *Photosynthesis and Stomatal Behaviour*. *Progress in Botany* (U Luttge, W Beyschlag, B Budel, and D Francis, Eds.).

Lawson T, Matthews J. **2020**. Guard Cell Metabolism and Stomatal Function. *Annual Review of Plant Biology*.

Lawson T, Vialet-Chabrand SRM. **2018**. Speedy stomata , photosynthesis and plant water use efficiency. *New Phytologist*.

Lazowski AW, Papanicolaou A, Sharwood R, Ghannoum O. **2018**. Investigating the NAD-ME biochemical pathway within - C_4 grasses using transcript and amino acid variation in - C_4 photosynthetic genes. *Photosynthesis Research* **138**: 233–248.

Leakey ADB. **2009**. Rising atmospheric carbon dioxide concentration and the future of C_4 crops for food and fuel. *Proceedings of the Royal Society B: Biological Sciences* **276**: 2333–2343.

Li C, Jackson P, Lu X, Xu C, Cai Q, Basnayake J, Lakshmanan P, Ghannoum O, Fan Y. **2017**. Genotypic variation in transpiration efficiency due to differences in photosynthetic capacity among sugarcane-related clones. *Journal of Experimental Botany* **68**: 2377–2385.

Li Y, Xu J, Haq NU, Zhang H, Zhu XG. **2014**. Was low CO_2 a driving force of C_4 evolution: Arabidopsis responses to long-term low CO_2 stress. *Journal of Experimental Botany* **65**: 3657–3667.

Lind C, Dreyer I, López-Sanjurjo EJ, Von Meyer K, Ishizaki K, Kohchi T, Lang D, Zhao Y, Kreuzer I, Al-Rasheid KAS, *et al.* 2015. Stomatal guard cells co-opted an ancient ABA-dependent desiccation survival system to regulate stomatal closure. *Plant Physiology* **145**: 1006–1017.

Liu X, Mak M, Babla M, Wang F, Chen G, Veljanoski F, Wang G, Shabala S, Zhou M, Chen Z-H. **2014**. Linking stomatal traits and expression of slow anion channel genes HvSLAH1 and HvSLAC1 with grain yield for increasing salinity tolerance in barley. *Frontiers in plant science* **5**: 634.

Liu H, Osborne CP. **2015**. Water relations traits of C_4 grasses depend on phylogenetic lineage, photosynthetic pathway, and habitat water availability. *Journal of Experimental Botany* **66**:

761–773.

Lloyd J, Farquhar GD. **1994**. ^{13}C discrimination during CO_2 assimilation by the terrestrial biosphere. *Oecologia* **99**: 201–215.

Long SP. **1999**. Environmental responses. In: Sage RF, RK M, eds. C4 plants biology. London: Academic Press, 215–249.

Lunn JE, Furbank RT. **1999**. Sucrose biosynthesis in C4 plants. *New Phytologist* **143**: 221–237.

MacKo SA, Ryan M, Engel MH. **1998**. Stable isotopic analysis of individual carbohydrates by gas chromatographic/combustion/isotope ratio mass spectrometry. *Chemical Geology* **152**: 205–210.

Maherali H, Reid CD, Polley HW, Johnson HB, Jackson RB. **2002**. Stomatal acclimation over a subambient to elevated CO_2 gradient in a C_3/C_4 grassland. *Plant Cell and Environment* **2**: 557–566.

Mak M, Babla M, Xu SC, O'Carrigan A, Liu XH, Gong YM, Holford P, Chen ZH. **2014**. Leaf mesophyll K^+, H^+ and Ca^{2+} fluxes are involved in drought-induced decrease in photosynthesis and stomatal closure in soybean. *Environmental and Experimental Botany* **98**: 1–12.

Malone SR, Mayeux HS, Johnson HB, Wayne H. **2016**. Stomatal Density and Aperture Length in Four Plant Species Grown Across a Subambient CO_2 Gradient. *American Journal of Botany* **80**: 1413–1418.

Marten I, Deeken R, Hedrich R, Roelfsema MRG. **2010**. Light-induced modification of plant plasma membrane ion transport. *Plant Biology* **12**: 64–79.

Martins SCV, Mcadam SAM, Deans RM, Damatta FM, Brodribb TJ. **2016**. Stomatal dynamics are limited by leaf hydraulics in ferns and conifers: Results from simultaneous measurements of liquid and vapour fluxes in leaves. *Plant Cell and Environment* **39**: 694–705.

Matrosova A, Bogireddi H, Mateo-Peñas A, Hashimoto-Sugimoto M, Iba K, Schroeder JI, Israelsson-Nordström M. **2015**. The HT1 protein kinase is essential for red light-induced stomatal opening and genetically interacts with OST1 in red light and CO2-induced stomatal movement responses. *New Phytologist* **208**: 1126–1137.

Mauve C, Bleton J, Bathellier C, Lelarge-Trouverie C, Guérard F, Ghashghaie J, Tchapla A, Tcherkez G. **2010**. Kinetic $^{12}C/^{13}C$ isotope fractionation by invertase: evidence for a small in vitro isotope effect and comparison of two techniques for the isotopic analysis of carbohydrates. *Rapid Communications in Mass Spectrometry*: 511–518.

McAusland L, Vialet-Chabrand SRM, Davey P, Baker NR, Brendel O, Lawson T. **2016**.

Effects of kinetics of light-induced stomatal responses on photosynthesis and water-use efficiency. *New Phytologist*: 1209–1220.

Medlyn BE, Barton CVM, Broadmeadow MSJ, Ceulemans R, Angelis P De, Forstreuter M, Freeman M, Jackson SB, Kellomäki S, Laitat E, *et al.* 2001. Stomatal conductance of forest species after long-term exposure to elevated CO_2 concentration: a synthesis. *New Phytologist* **149**: 247–264.

Medrano H, Tomás M, Martorell S, Flexas J, Hernández E, Rosselló J, Pou A, Escalona J-M, Bota J. **2015**. From leaf to whole-plant water use efficiency (WUE) in complex canopies: Limitations of leaf WUE as a selection target. *The Crop Journal* **3**: 220–228.

Meier-Augenstein W. **2004**. GC and IRMS Technology for ^{13}C and ^{15}N Analysis on Organic Compounds and Related Gases. In: Handbook of Stable Isotope Analytical Techniques.

Meinzer FC, Plaut Z, Saliendra NZ. **1994**. Carbon isotope discrimination, gas exchange, and growth of sugarcane cultivars under salinity. *Plant Physiology* **104**: 521–526.

Merchant A, Peuke AD, Keitel C, MacFarlane C, Warren CR, Adams MA. **2010**. Phloem sap and leaf $\delta^{13}C$, carbohydrates, and amino acid concentrations in *Eucalyptus globulus* change systematically according to flooding and water deficit treatment. *Journal of Experimental Botany* **61**: 1785–1793.

Merilo E, Jõesaar I, Brosché M, Kollist H. **2014**. To open or to close: Species-specific stomatal responses to simultaneously applied opposing environmental factors. *New Phytologist* **202**: 499–508.

Merkle RK, Poppe I. **1994**. Carbohydrate composition analysis of glycoconjugates by gas-liquid chromatography/mass spectrometry. In: Methods in Enzymology. 1–15.

Monneveux P, Sheshshayee MS, Akhter J, Ribaut JM. **2007**. Using carbon isotope discrimination to select maize (*Zea mays* L.) inbred lines and hybrids for drought tolerance. *Plant Science* **173**: 390–396.

Morison JI, Gifford RM. **1983**. Stomatal sensitivity to carbon dioxide and humidity: a comparison of two C3 and two C4 grass species. *Plant Physiology* **71**: 789–796.

Morrison DJ, Taylor K, Preston T. **2010**. Strong anion-exchange liquid chromatography coupled with isotope ratio mass spectrometry using a Liquiface interface. *Rapid Communications in Mass Spectrometry* **24**: 1755–1762.

Mott KA. **1988**. Do Stomata Respond to CO_2 Concentrations Other than Intercellular? *Plant Physiology* **86**: 200–203.

Mumm P, Wolf T, Fromm J, Roelfsema MRG, Marten I. **2011**. Cell type-specific regulation of ion channels within the maize stomatal complex. *Plant and Cell Physiology* **52**: 1365–1375.

Newman IA. **2001**. Ion transport in roots: Measurement of fluxes using ion-selective microelectrodes to characterize transporter function. *Plant, Cell and Environment* **24**: 1–14.

Nobuhito S, Katsuya Y. **2008**. Stomatal density of cowpea correlates with carbon isotope discrimination in different phosphorus, water and CO_2 environments. *New Phytologist* **179**: 799–807.

O'Leary MH. **1981**. Carbon isotope fractionation in plants. *Phytochemistry* **20**: 553–567.

Osborne CP, Sack L. **2012**. Evolution of C_4 plants : a new hypothesis for an interaction of CO_2 and water relations mediated by plant hydraulics. *Phil. Trans. R. Soc. B*: 583–600.

Osmond CB, Winter K, Ziegler H. **1982**. Functional Significance of Different Pathways of CO_2 Fixation in Photosynthesis. In: Physiological Plant Ecology II.

Pallaghy CK. **1971**. Stomatal movement and potassium transport in epidermal strips of *Zea mays*: The effect of CO_2. *Planta* **101**: 287–295.

Papanatsiou M, Amtmann A, Blatt MR. **2017**. Stomatal clustering in Begonia associates with the kinetics of leaf gaseous exchange and influences water use efficiency. *Journal of Experimental Botany* **68**: 2309–2315.

Park R, Epstein S. **1961**. Plants, Metabolic fractionation of ^{13}C and ^{12}C in plants. *Plant Physiology* **36**: 133–138.

Parsons JL, Martin SL, James T, Golenia G, Boudko EA, Hepworth SR. **2019**. Polyploidization for the Genetic Improvement of *Cannabis sativa*. *Frontiers in Plant Science* **10**: 1–12.

Passioura JB. **1977**. Grain yield, harvest index, and water use of wheat. *Journal of the Australian Institute of Agricultural Science* **43**: 117–120.

Pau S, Edwards EJ, Still CJ. **2013**. Improving our understanding of environmental controls on the distribution of C_3 and C_4 grasses. *Global Change Biology* **19**: 184–196.

Paul MJ, Foyer CH. **2001**. Sink regulation of photosynthesis. *Journal of Experimental Botany* **52**: 1383–1400.

Pearcy R, Ehleringer JR. **1984**. Comparative ecophysiology of C_3 and C_4 plants. *Plant, Cell & Environment* **7**: 1–13.

Pearson CJ. **1973**. Daily changes in stomatal aperture and in carbohydrates and malate within epidermis and mesophyll of leaves of *Commelina cyanea* and *Vicia faba*. *Australian Journal of Biological Sciences* **26**: 1035–1044.

Pengelly JJL, Tan J, Furbank RT, von Caemmerer S. **2012**. Antisense reduction of NADP-

malic enzyme in Flaveria bidentis reduces flow of CO_2 through the C_4 cycle. *Plant Physiology* **160**: 1070–1080.

Pinto H, Powell JR, Sharwood RE, Tissue DT, Ghannoum O. **2016**. Variations in nitrogen use efficiency reflect the biochemical subtype while variations in water use efficiency reflect the evolutionary lineage of C_4 grasses at inter-glacial CO_2. : 514–526.

Pinto H, Sharwood RE, Tissue DT, Ghannoum O. **2014**. Photosynthesis of C_3, C_3-C_4, and C_4 grasses at glacial CO_2. *Journal of Experimental Botany* **65**: 3669–3681.

Pompelli M, Martins S, Celin E, Ventrella M, DaMatta F. **2010**. What is the influence of ordinary epidermal cells and stomata on the leaf plasticity of coffee plants grown under full-sun and shady conditions? *Brazilian Journal of Biology* **70**: 1083–1088.

Pornsiriwong W, Estavillo GM, Chan KX, Tee EE, Ganguly D, Crisp PA, Phua SY, Zhao C, Qiu J, Park J, *et al.* 2017. A chloroplast retrograde signal, 3'phosphoadenosine 5'-phosphate, acts as a secondary messenger in abscisic acid signaling in stomatal closure and germination. *eLife* **6**: 1–34.

Qu X, Peterson KM, Torii KU. **2017**. Stomatal development in time: the past and the future. *Current Opinion in Genetics and Development* **45**: 1–9.

R Core Team. **2017**. R: A language and environment for statistical computing. http://www.R-project.org/. *R Foundation for Statistical Computing, Vienna, Austria*.

Raissig MT, Matos JL, Gil MXA, Kornfeld A, Bettadapur A, Abrash E, Allison HR, Badgley G, Vogel JP, Berry JA, *et al.* 2017. Mobile MUTE specifies subsidiary cells to build physiologically improved grass stomata. *Science* **355**: 1215–1218.

Ratcliffe RG, Shachar-Hill Y. **2006**. Measuring multiple fluxes through plant metabolic networks. *Plant Journal* **45**: 490–511.

Raven JA. **2002**. Selection pressures on stomatal evolution. *New Phytologist* **153**: 371–386.

Reeves G, Singh P, Rossberg TA, Sogbohossou EOD, Schranz ME, Hibberd JM. **2018**. Natural Variation within a Species for Traits Underpinning C_4 Photosynthesis. *Plant Physiology* **177**: 504–512.

Richards RA, López-Castañeda C, Gomez-Macpherson H, Condon AG. **1993**. Improving the efficiency of water use by plant breeding and molecular biology. *Irrigation Science*.

Rinne KT, Saurer M, Streit K, Siegwolf RTW. **2012**. Evaluation of a liquid chromatography method for compound-specific $\delta^{13}C$ analysis of plant carbohydrates in alkaline media. *Rapid Communications in Mass Spectrometry* **26**: 2173–2185.

Roelfsema MRG, Hedrich R. **2005**. In the light of stomatal opening: New insights into 'the

Watergate'. *New Phytologist* **167**: 665–691.

Ruan Y-L. **2014**. Sucrose Metabolism: Gateway to Diverse Carbon Use and Sugar Signaling. *Annual Review of Plant Biology* **65**: 33–67.

Rudall PJ, Chen ED, Cullen E. **2017**. Evolution and development of monocot stomata. *American Journal of Botany* **104**: 1122–1141.

Ruggiero A, Punzo P, Landi S, Costa A, Van Oosten M, Grillo S. **2017**. Improving Plant Water Use Efficiency through Molecular Genetics. *Horticulturae* **3**: 31.

Sage RF. **2004**. The evolution of C_4 photosynthesis. *New Phytologist* **161**: 341–370.

Sage RF, Christin PA, Edwards EJ. **2011**. The C_4 plant lineages of planet Earth. *Journal of Experimental Botany* **62**: 3155–3169.

Sage RF, Coleman JR. **2001**. Effects of low atmospheric CO_2 on plants: More than a thing of the past. *Trends in Plant Science* **6**: 18–24.

Sage RF, Kubien DS. **2007**. The temperature response of C_3 and C_4 photosynthesis. *Plant, Cell and Environment* **30**: 1086–1106.

Sage RF, McKown AD. **2006**. Is C_4 photosynthesis less phenotypically plastic than C_3 photosynthesis? *Journal of Experimental Botany* **57**: 303–317.

Sage R, Pearcy RW. **2000**. The Physiological Ecology of C_4 Photosynthesis. In: Leegood RC, Sharkey TD, von Caemmerer S, eds. Advances in Photosynthesis and Respiration. Springer, Dordrecht.

Sage RF, Sage TL, Kocacinar F. **2012**. Photorespiration and the Evolution of C_4 Photosynthesis. *Annual Review of Plant Biology* **63**: 19–47.

Sagun J Ver, Badger MR, Chow WS, Ghannoum O. **2019**. Cyclic electron flow and light partitioning between the two photosystems in leaves of plants with different functional types. *Photosynthesis Research*: 1–14.

Schlüter U, Muschak M, Berger D, Altmann T. **2003**. Photosynthetic performance of an *Arabidopsis* mutant with elevated stomatal density (*sdd1-1*) under different light regimes. *Journal of Experimental Botany* **54**: 867–874.

Schroeder JI, Hagiwara S. **1989**. Cytosolic calcium regulates ion channels in the plasma membrane of *Vicia faba* guard cells. *Nature* **338**: 427–430.

Schroeder JI, Raschke K, Neher E. **1987**. Voltage dependence of K channels in guard-cell protoplasts. *Proceedings of the National Academy of Sciences of the United States of America*.

Sevcik RS, Mowery RA, Becker C, Chambliss CK. **2011**. Rapid analysis of carbohydrates in

aqueous extracts and hydrolysates of biomass using a carbonate-modified anion-exchange column. *Journal of Chromatography A* **1218**: 1236–1243.

Shabala S, Cuin TA, Shabala L, Newman I. **2012**. Quantifying kinetics of net ion fluxes from plant tissues by non-invasive microelectrode measuring MIFE technique. *Methods in Molecular Biology*.

Sharkey TD, Raschke K, Sharkey TD, Raschke K. **1981**. Separation and Measurement of Direct and Indirect Effects of Light on Stomata. *American Society of Plant Biologists* (ASPB) **68**: 33–40.

Sharwood RE. **2017**. Engineering chloroplasts to improve Rubisco catalysis: prospects for translating improvements into food and fiber crops. *New Phytologist* **213**: 494–510.

Sharwood RE, Ghannoum O, Kapralov M V., Gunn LH, Whitney SM. **2016**. Temperature responses of Rubisco from Paniceae grasses provide opportunities for improving C_3 photosynthesis. *Nature Plants*.

Sharwood RE, Sonawane B V., Ghannoum O. **2014**. Photosynthetic flexibility in maize exposed to salinity and shade. *Journal of Experimental Botany* **65**: 3715–3724.

Shimazaki K, Doi M, Assmann SM, Kinoshita T. **2007**. Light regulation of stomatal movement. *Annual review of plant biology* **58**: 219–247.

Skrzypek G, Ford D. **2018**. Reference materials selection for the stable carbon isotope analysis of dissolved carbon using a wet oxidation system. *Rapid Communications in Mass Spectrometry*: 473–481.

Slattery RA, Walker BJ, Weber APM, Ort DR. **2018**. The Impacts of Fluctuating Light on Crop Performance. *Plant Physiology* **176**: 990–1003.

Smith BN. **1972**. Natural Abundance of the Stable Isotopes of Carbon in Biological Systems. *BioScience* **22**: 226–231.

Smith PJS, Trimarchi J. **2001**. Noninvasive measurement of hydrogen and potassium ion flux from single cells and epithelial structures. *American Journal of Cell Physiology*: C1–C11.

Smith M, Wild B, Richter A, Simonin K, Merchant A. **2016**. Carbon Isotope Composition of Carbohydrates and Polyols in Leaf and Phloem Sap of *Phaseolus vulgaris* L. Influences Predictions of Plant Water Use Efficiency. *Plant and Cell Physiology* **57**: 1756–1766.

Sonawane BV., Sharwood RE, von Caemmerer S, Whitney SM, Ghannoum O. **2017**. Short-term thermal photosynthetic responses of C_4 grasses are independent of the biochemical subtype. *Journal of Experimental Botany* **68**: 5583–5597.

Sonawane BV, Sharwood RE, Whitney S, Ghannoum O. **2018**. Shade compromises the

photosynthetic efficiency of NADP-ME less than that of PEP-CK and NAD-ME C_4 grasses. *Journal of Experimental Botany* **69**: 3053–3068.

Sun ZJ, Livingston NJ, Guy RD, Ethier GJ. **1996**. Stable carbon isotopes as indicators of increased water use efficiency and productivity in white spruce (Picea glauca (Moench) Voss) seedlings. *Plant, Cell and Environment* **19**: 887–894.

Sutter JU, Sieben C, Hartel A, Eisenach C, Thiel G, Blatt MR. **2007**. Abscisic Acid Triggers the Endocytosis of the Arabidopsis KAT1 K^+ Channel and Its Recycling to the Plasma Membrane. *Current Biology* **17**: 1396–1402.

Takemiya A, Kinoshita T, Asanuma M, Shimazaki KI. **2006**. Protein phosphatase 1 positively regulates stomatal opening in response to blue light in *Vicia faba*. *Proceedings of the National Academy of Sciences of the United States of America* **103**: 13549–13554.

Takemiya A, Shimazaki Kichiro. **2016**. Arabidopsis phot1 and phot2 phosphorylate BLUS1 kinase with different efficiencies in stomatal opening. *Journal of Plant Research* **129**: 167–174.

Tanaka Y, Sugano SS, Shimada T, Hara-Nishimura I. **2013**. Enhancement of leaf photosynthetic capacity through increased stomatal density in Arabidopsis. *New Phytologist* **198**: 757–764.

Tausz M, Warren CR, Adams MA. **2005**. Dynamic light use and protection from excess light in upper canopy and coppice leaves of *Nothofagus cunninghamii* in an old growth, cool temperate rainforest in Victoria, Australia. *New Phytologist* **165**: 143–156.

Taylor SH, Aspinwall MJ, Blackman CJ, Choat B, Tissue DT, Ghannoum O. **2018**. CO_2 availability influences hydraulic function of C_3 and C_4 grass leaves. *Journal of Experimental Botany* **69**: 2731–2741.

Taylor SH, Franks PJ, Hulme SP, Spriggs E, Christin PA, Edwards EJ, Woodward FI, Osborne CP. **2012**. Photosynthetic pathway and ecological adaptation explain stomatal trait diversity amongst grasses. *New Phytologist* **193**: 387–396.

Taylor SH, Hulme SP, Rees M, Ripley BS, Woodward FI, Osborne CP. **2010**. A phylogenetically controlled comparison of leaf nitrogen content in C_3 and C_4 grasses. *New Phytologist*: 780–791.

Taylor SH, Long SP. **2017**. Slow induction of photosynthesis on shade to sun transitions in wheat may cost at least 21% of productivity. *Philosophical Transactions of the Royal Society B: Biological Sciences* **372**.

Tcherkez G, Farquhar G, Badeck F, Ghashghaie J. **2004**. Theoretical considerations about carbon isotope distribution in glucose of C_3 plants. *Functional Plant Biology* **31**: 857.

Tcherkez G, Mahé A, Hodges M. **2011**. $^{12}C/^{13}C$ fractionations in plant primary metabolism.

Trends in Plant Science **16**: 499–506.

Thomas PW, Woodward FI, Quick WP. **2004**. Systemic irradiance signalling in tobacco. *New Phytologist* **161**: 193–198.

Tilman D, Balzer C, Hill J, Befort B. **2011**. Global food demand and the sustainable intensification of agriculture. *Proceedings of the National Academy of Sciences* **108**: 20260–20264.

Turgeon R. **1989**. The Sink-Source Transition in Leaves. *Annual Review of Plant Physiology and Plant Molecular Biology* **40**: 119–138.

Twohey RJ, Roberts LM, Studer AJ. **2019**. Leaf stable carbon isotope composition reflects transpiration efficiency in Zea mays. *Plant Journal*.

Vadez V, Kholova J, Medina S, Kakkera A, Anderberg H. **2014**. Transpiration efficiency: New insights into an old story. *Journal of Experimental Botany* **65**: 6141–6153.

Varshney RK, Ribaut JM, Buckler ES, Tuberosa R, Rafalski JA, Langridge P. **2012**. Can genomics boost productivity of orphan crops? *Nature Biotechnology* **30**: 1172–1176.

Vavasseur A, Raghavendra AS. **2005**. Guard cell metabolism and CO_2 sensing. *New Phytologist* **165**: 665–682.

Vialet-Chabrand S, Dreyer E, Brendel O. **2013**. Performance of a new dynamic model for predicting diurnal time courses of stomatal conductance at the leaf level. *Plant, Cell and Environment* **36**: 1529–1546.

Vialet-Chabrand SRM, Matthews JSA, McAusland L, Blatt MR, Griffiths H, Lawson T. **2017a**. Temporal Dynamics of Stomatal Behavior: Modeling and Implications for Photosynthesis and Water Use. *Plant Physiology* **174**: 603–613.

Vialet-Chabrand S, Matthews JSA, Simkin AJ, Raines CA, Lawson T. **2017b**. Importance of Fluctuations in Light on Plant Photosynthetic Acclimation. *Plant Physiology* **173**: 2163–2179.

Vico G, Manzoni S, Palmroth S, Katul G. **2011**. Effects of stomatal delays on the economics of leaf gas exchange under intermittent light regimes. *New Phytologist* **192**: 640–652.

Vogan PJ, Sage RF. **2012**. Effects of low atmospheric CO_2 and elevated temperature during growth on the gas exchange responses of C_3, C_3-C_4 intermediate, and C_4 species from three evolutionary lineages of C_4 photosynthesis. *Oecologia* **169**: 341–352.

Vogel JP, Garvin DF, Mockler TC, Schmutz J, Rokhsar D, Bevan MW, Barry K, Lucas S, Harmon-Smith M, Lail K, *et al.* 2010. Genome sequencing and analysis of the model grass *Brachypodium distachyon*. *Nature* **463**: 763–768.

Wang Y, Bräutigam A, Weber APM, Zhu XG. **2014**. Three distinct biochemical subtypes of C_4 photosynthesis? A modelling analysis. *Journal of Experimental Botany* **65**: 3567–3578.

Watson-Lazowski A, Papanicolaou A, Koller F, Ghannoum O. **2019**. The transcriptomic responses of C_4 grasses to sub-ambient CO_2 and low light are largely species-specific and only refined by photosynthetic subtype. *The Plant Journal*.

Watson-Lazowski A, Papanicolaou A, Sharwood R, Ghannoum O. **2018**. Investigating the NAD-ME biochemical pathway within C_4 grasses using transcript and amino acid variation in C_4 photosynthetic genes. *Photosynthesis Research* **138**: 233–248.

Webb A a. R, McAinsh MR, Mansfield T a., Hetherington AM. **1996**. Carbon dioxide induces increases in guard cell cytosolic free calcium. *The Plant Journal* **9**: 297–304.

Webster RJ, Driever SM, Kromdijk J, McGrath J, Leakey ADB, Siebke K, Demetriades-Shah T, Bonnage S, Peloe T, Lawson T, *et al.* 2016. High C_3 photosynthetic capacity and high intrinsic water use efficiency underlies the high productivity of the bioenergy grass *Arundo donax*. *Scientific Reports* **6**: 1–10.

Werner RA, Brand WA. **2001**. Referencing strategies and techniques in stable isotope ratio analysis. *Rapid Communications in Mass Spectrometry* **15**: 501–519.

Werner R, Buchmann N, Siegwolf R. **2011**. Metabolic fluxes, carbon isotope fractionation and respiration – lessons to be learned from plant biochemistry. *New Phytologist* **191**: 10–15.

Werner C, Wegener F, Unger S, Nogués S, Priault P. **2009**. Short-term dynamics of isotopic composition of leaf-respired CO_2 upon darkening: Measurements and implications. In: Rapid Communications in Mass Spectrometry.

Weyers J, Johansen L. **1985**. Accurate estimation of stomatal aperture from silicone rubber impressions. *New Phytologist*.

Wickham H. **2017**. ggplot2: Elegant Graphics for Data Analysis. *Journal of Statistical Software*.

Willmer CM, Sexton R. **1979**. Stomata and plasmodesmata. *Protoplasma* **100**: 113–124.

Wingler A, Walker RP, Chen Z-H, Leegood RC. **1999**. Phospho enol pyruvate Carboxykinase Is Involved in the Decarboxylation of Aspartate in the Bundle Sheath of Maize. *Plant Physiology* **120**: 539–546.

Wong SC, Cowan IR, Farquhar GD. **1979**. Stomatal conductance correlates with photosynthetic capacity. *Nature* **282**: 424–426.

Wood D, Lenné JM. **2018**. A natural adaptive syndrome as a model for the origins of cereal agriculture. *Proceedings of the Royal Society B: Biological Sciences* **285**.

Woodward FI. **1987**. Stomatal numbers are sensitive to increases in CO_2 from pre-industrial levels. *Nature* **327**.

Woodward FI, Kelly CK. **1995**. The influence of CO_2 concentration on stomatal density. *New Phytologist* **131**: 311–327.

Xiong D, Douthe C, Flexas J. **2018**. Differential coordination of stomatal conductance, mesophyll conductance, and leaf hydraulic conductance in response to changing light across species. *Plant Cell and Environment* **41**: 436–450.

Xiong D, Flexas J, Yu T, Peng S, Huang J. **2016**. Leaf anatomy mediates coordination of leaf hydraulic conductance and mesophyll conductance to CO_2 in *Oryza*. *New Phytologist*: 572–583.

Xu LK, Hsiao TC. **2004**. Predicted versus measured photosynthetic water-use efficiency of crop stands under dynamically changing field environments. *Journal of Experimental Botany* **55**: 2395–2411.

Xu Z, Jiang Y, Jia B, Zhou G. **2016**. Elevated-CO_2 Response of Stomata and Its Dependence on Environmental Factors. *Frontiers in Plant Science* **7**: 1–15.

Young JJ, Mehta S, Israelsson M, Godoski J, Grill E, Schroeder JI. **2006**. CO_2 signaling in guard cells: calcium sensitivity response modulation, a Ca^{2+}-independent phase, and CO_2 insensitivity of the gca2 mutant. *Proceedings of the National Academy of Sciences of the United States of America* **103**: 7506–11.

Zhang L. **2013**. Development and Application of Liquid Chromatography Coupled to Isotope Ratio Mass Spectrometry.

Zhao C, Wang Y, Chan KX, Marchant DB, Franks PJ, Randall D, Tee EE, Chen G, Ramesh S, Phua SY, *et al.* 2019. Evolution of chloroplast retrograde signaling facilitates green plant adaptation to land. *Proceedings of the National Academy of Sciences of the United States of America* **116**: 5015–5020.

Zhou Y, Stuart-Williams H, Farquhar GD, Hocart CH. **2010**. The use of natural abundance stable isotopic ratios to indicate the presence of oxygen-containing chemical linkages between cellulose and lignin in plant cell walls. *Phytochemistry* **71**: 982–993.

Zhu J, Qi J, Fang Y, Xiao X, Li J, Lan J, Tang C. **2018**. Characterization of sugar contents and sucrose metabolizing enzymes in developing leaves of Hevea brasiliensis. *Frontiers in Plant Science* **9**: 1–11.